FOOD EMULSIONS STABILISED BY BLENDS OF PLANT AND DAIRY PROTEINS

Emma B.A. Hinderink

Propositions

1. Emulsion characterisation requires considering the dynamics occurring at both short and long time scales. (this thesis)
2. Partial replacement of dairy proteins by plant proteins in emulsions leads to interfacial displacement. (this thesis)
3. Scientific impartiality is impaired when terming results positive or negative.
4. Scientists should be judged on the quality of the knowledge they generate, not the quantity.
5. The energising effect of colleagues surpasses the efficiency of working from home.
6. Global crises need to be solved globally.

Propositions belonging to the thesis entitled

Food emulsions stabilised by blends of plant and dairy proteins

Emma B.A. Hinderink
Wageningen, 1 April 2021

Food emulsions stabilised by blends of plant and dairy proteins

Emma B.A. Hinderink

Thesis committee

Promotor

Prof. Dr C.G.P.H. Schroën

Personal chair at the Laboratory of Food Process Engineering

Wageningen University & Research

Co-promotor

Dr C.C. Berton-Carabin

Associate professor, Laboratory of Food Process Engineering

Wageningen University & Research

Dr L.C.M. Sagis

Associate professor, Laboratory of Physics and Physical Chemistry of Foods

Wageningen University & Research

Other members

Prof. Dr T. Huppertz, Wageningen University & Research

Dr R. Miller, TU Darmstadt, Germany

Prof. Dr B.S. Murray, University of Leeds, United Kingdom

Dr N.J. Zuidam, Unilever, Wageningen

This research was conducted under the auspices of the Graduate School VLAG (Advanced studies in Food Technology, Agrobiotechnology, Nutrition and Health Sciences)

Food emulsions stabilised by blends of plant and dairy proteins

Emma B.A. Hinderink

Thesis

submitted in fulfilment of the requirements for the degree of doctor

at Wageningen University

by the authority of the Rector Magnificus,

Prof. Dr A.P.J. Mol,

in the presence of the

Thesis Committee appointed by the Academic Board

to be defended in public

on Thursday 1 April 2021

at 11 a.m. in the Aula.

Emma B.A. Hinderink

Food emulsions stabilised by blends of plant and dairy proteins

264 pages

PhD thesis, Wageningen University, Wageningen, the Netherlands (2021)

With references, with summaries in English and Dutch

ISBN: 978-94-6395-658-1

DOI: https://doi.org/10.18174/537414

Content

Chapter 1

Introduction and thesis outline

1.1. Emulsions

Many foods contain or consist of emulsions, i.e., small droplets of one liquid finely dispersed in another liquid. In order to be physically stabilised, these droplets need to be covered by emulsifiers. The most widely used food emulsifiers are dairy proteins, which are present in e.g., beverages, infant formula or dressings. However, due to sustainability issues and societal drivers, a transition is currently ongoing towards the use of plant proteins in foods (the so-called protein transition), and thus, in food emulsions. This goes with a number of technological challenges; in general, plant proteins are outperformed by dairy proteins in terms of emulsifying and interfacial properties (Amine et al., 2014). Plant proteins require intensive pre-treatments (Fernandez-Avila et al., 2016; Peng et al., 2016; Shao et al., 2014) and in addition, they may negatively affect the product taste (García Arteaga et al., 2020). To achieve a rational compromise between functionality and product quality, we therefore target partial replacement of dairy proteins by plant proteins.

1.2. Emulsion stability

Emulsions consist of two immiscible liquids, of which one is dispersed in the other as droplets, forming oil-in-water (O/W) or water-in-oil (W/O) systems. Due to the thermodynamic incompatibility between oil and water, the formation of interface leads to a change in Gibbs free energy (ΔG) given by equation 1.1:

$$\Delta G = \gamma \cdot \Delta A \qquad 1.1$$

Here γ is the interfacial tension (mN/m) between the two phases, and ΔA the interfacial area difference between an emulsion and a completely phase-separated system. A reduction of the interface, through e.g., coalescence reduces ΔG *(*Figure 1.1), and is thus beneficial from a thermodynamic point of view. Emulsifiers reduce the interfacial tension, and thus also ΔG.

Prior to complete phase separation, a number of physical destabilisation mechanisms may occur, which may not only be driven by the aforementioned Gibbs free energy minimization, but also by other driving forces. For instance, the density difference between oil and water is a driving force for droplet creaming in emulsions if the droplets have a lower density than the continuous phase, (Figure 1.1) or sedimentation if the density difference is opposite. The parameters involved in creaming are described by Stokes' law (equation 1.2 (McClements, 2005)).

$$v = \frac{2(\rho_d - \rho_c) \cdot g \cdot r^2}{9 \cdot \eta_c} \qquad 1.2$$

where v is the creaming or sedimentation velocity (m/s), ρ_d and ρ_c the densities (kg/m^3) of the dispersed and continuous phase, respectively, g the gravitational constant (m/s^2), r the droplet radius (m) and η the viscosity of the continuous phase (kg/m.s). From this follows that emulsions with a high continuous phase viscosity and small droplet size are more stable against creaming (McClements, 2005). When droplets flocculate, their effective size increases, and so does their creaming/sedimentation velocity. The same holds for larger droplets formed through coalescence, which may ultimately lead to oiling off. Whether these two latter effects occur depends greatly on how the oil-water interface is stabilised, and this is discussed in the next sections.

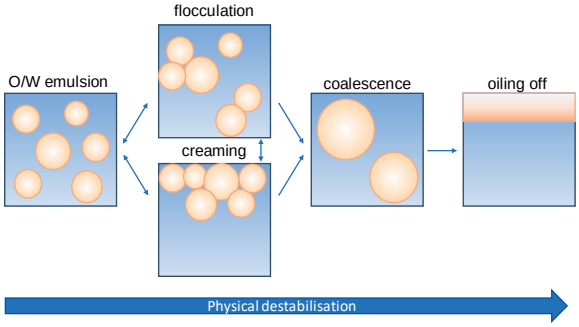

Figure 1.1. Schematic representations of the main physical destabilisation mechanisms in O/W emulsions.

In order to disperse one liquid into another, and obtain physically stable emulsions, emulsifiers are commonly used. Emulsifiers are amphiphilic molecules that adsorb at the oil-water interface to reduce the interfacial tension, and thus, the Gibbs free energy of the emulsion (equation 1.1). Droplet formation in conventional emulsification devices can be divided into three stages; droplet deformation, break-up and possibly re-coalescence. Droplet deformation and break-up are facilitated by a low interfacial tension. If not sufficiently stabilised, the newly formed droplets tend to re-coalesce (Tcholakova et al., 2008), which therewith increases the droplet size and polydispersity (e.g., emulsifier-poor regime, Figure 1.2).

Food emulsions are often formulated with a large excess of emulsifiers compared to the actual amount needed to cover the oil-water interface (Berton-Carabin et al., 2014), which leaves a large fraction of the emulsifier non-adsorbed in the continuous phase. In such an emulsifier-

rich regime, the minimum droplet size which can be achieved is limited by the emulsification procedure (pressure, shear rate, number of passes) (Tcholakova et al., 2003). After emulsion formation emulsifiers have an instrumental role: they should form an interfacial layer that protects the emulsions against long-term physical destabilisation.

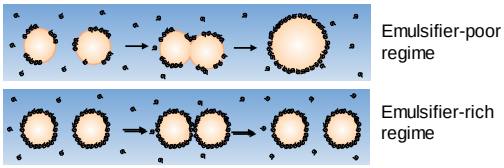

Figure 1.2. Schematic representation of the dynamic evolution of emulsion droplets during emulsification. Depending on the interfacial coverage immediately after droplet formation, droplets may be prone to re-coalescence, leading to emulsions with larger droplet size; alternatively, with rapidly sufficiently covered interfaces, droplet sizes are smaller.

Conventional emulsifiers include low molecular weight components and amphiphilic biopolymers such as polysaccharides and proteins. It is good to mention that colloidal particles can also be used to physically stabilise emulsions, forming so-called Pickering emulsions (Berton-Carabin et al., 2015). Although a lot of early work on this topic was conducted with inorganic particles (e.g., silica), over the past decade food-grade materials such as starch particles, fat crystals or protein particles have become increasingly popular for this purpose (Berton-Carabin et al., 2015; Dickinson, 2013, 2020; Murray, 2019).

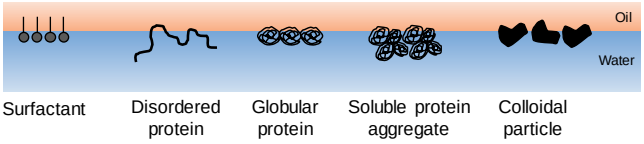

Figure 1.3. Schematic representation of adsorbed surfactants, disordered and globular proteins, soluble protein aggregates and colloidal particles at the oil-water interface (not to scale).

1.2.1. Proteins

For food applications, proteins are often preferred over surfactants, such as polysorbates, as they contribute to the nutritional value of the product and comply with the clean label trend. Interfacial layers made of proteins are usually thin (2-6 nm) and electrically charged (Dickinson, 1994; McClements, 2005). The stability of emulsions is often related to the surface load (mg/m^2), which is a measure of the amount of protein per m^2 of surface area. At low protein concentrations (protein-poor regime; Figure 1.2), the surface load corresponds to

a protein monolayer (Tcholakova et al., 2003) whereas in the protein-rich regime, more proteins may adsorb, leading to denser and thicker layers.

Proteins have either a global positive charge or a global negative charge at pH values below or above their isoelectric point, respectively. At pH values away from the isoelectric point, protein-covered emulsion droplets are protected against flocculation due to electrostatic repulsion, while at pH values close to the isoelectric point, or at high ionic strength (which leads to screening of the charges of proteins), emulsions may become unstable because attractive droplet-droplet interactions predominate. Next to electrostatic interactions, adsorbed proteins provide steric repulsion. In general, electrostatic repulsions are weaker than steric repulsion at short distances, which implies that even if protein-stabilised droplets flocculate due to electrostatic interactions (pH close to isoelectric point, screening of charges), steric interactions can prevent droplets from approaching close enough to coalesce (McClements, 2005). When both electrostatic and steric repulsions are not strong enough, droplets can come into close contact and the interfacial film may rupture, leading to coalescence, which will be discussed further in section 1.3.

1.2.2. Dairy proteins

Dairy proteins have good emulsifying properties and are often used in food emulsions. Dairy proteins are subdivided into caseins (disordered proteins, around 80%) and whey proteins (mostly globular proteins, around 20%). Caseins can be classified into α_{s1}-, α_{s2}-, β- and κ-casein. Whey proteins comprise mainly bovine serum albumin, β-lactoglobulin and α-lactalbumin. In bovine milk, caseins are organised as micelles, but during isolation processes the micelles are disrupted, and the isolated caseins only have a limited tertiary structure. This allows them to adsorb rapidly at the oil-water interface with their hydrophobic parts sticking into the oil phase and their hydrophilic parts protruding into the water phase (Graham et al., 1979b), providing steric repulsion between droplets (Dickinson, 2001). When present in excess, non-adsorbed caseins may destabilise emulsions through depletion flocculation (Dickinson et al., 1997).

The conformation of globular whey proteins changes slowly after adsorption at the oil-water interface, leading to partial unfolding and exposure of amino acids that were initially buried in the hydrophobic core of the molecules. Such unfolding may lead to enhanced protein-protein interactions through hydrophobic bonds or, in the case of β-lactoglobulin, through

covalent disulfide bonds (Dickinson & Matsumura, 1991; Monahan et al., 1993). As a result, a compact and viscoelastic interfacial layer is formed, in contrast to the flexible caseins that form thick but less dense interfacial films (Dickinson, 1992, 2001).

1.2.3. Plant proteins

Due to the environmental impact of animal-derived proteins, plant proteins (e.g., from soy or pea) are gaining interest as more sustainable food alternatives. Traditionally, soy proteins have been the focus of attention (Ji et al., 2015; Li et al., 2016; Tang, 2017); however pea proteins are becoming increasingly popular due to their high nutritional value and lower allergenicity, and have therefore been selected in the present work. Peas contain about 20-30% proteins of which 65-80% are globulins, i.e., storage proteins, and 10-20% are albumins, i.e., water-soluble proteins (Gatehouse et al., 1984). The globulins are composed of legumin (11S), vicilin (7S) and convicilin. Legumin has a hexameric quartenary structure (six subunits) with a molecular size of ~360 kDa, with acidic (~40 kDa) and basic (~20 kDa) subunits linked together by disulfide bonds (Gatehouse et al., 1984). Vicilin is a trimeric protein of ~170 kDa with a large number of subunits of ~50, 33, 31, 19, 16, 13.5 and 12.5kDa (Gatehouse et al., 1984). Convicilin is considered tetrameric, with a molecular weight of 210-290 kDa, and subunits of ~71 kDa (Croy et al., 1980). Due to its smaller size and higher flexibility, vicilin is more surface-active (i.e., able to lower the interfacial tension) than legumin (Dagorn-Scavinier et al., 1986) and has better emulsifying properties (Dagorn-Scavinier et al., 1987). When used in a protein mixture, it was found to dominate the interfacial (Dagorn-Scavinier et al., 1986) and the emulsifying properties (Dagorn-Scavinier et al., 1987).

During isolation processes, plant proteins are exposed to harsh conditions (Chen et al., 2019) that can induce protein denaturation and aggregation, which leads to insolubility of the plant proteins (Wagner et al., 2000) as well as formation of small soluble aggregates (Chen et al., 2019). When using the full fraction of a commercial pea protein isolate that contains soluble and insoluble proteins, polydisperse emulsions are formed (Gumus et al., 2017a; McCarthy et al., 2016), but when using the soluble fraction only (Figure 1.4), monodisperse emulsions can be formed (Gumus et al., 2017a; Ho et al., 2017). The fact that a large fraction (typically 75-90%) is insoluble implies that the proteins exist in a supramolecular, particulate form. Nonetheless, if these structures are partly wetted by the oil and water phases, they could behave as colloidal stabilisers (Figure 1.3), which will be discussed further in Chapter 8. Next

to the solubility issues, harsh processing may lead to protein oxidation which may affect the interfacial properties in a positive (Kong et al., 2013; Liu et al., 2015) or negative way (Berton-Carabin et al., 2016; Muijlwijk et al., 2017); this will be discussed further in Chapter 6.

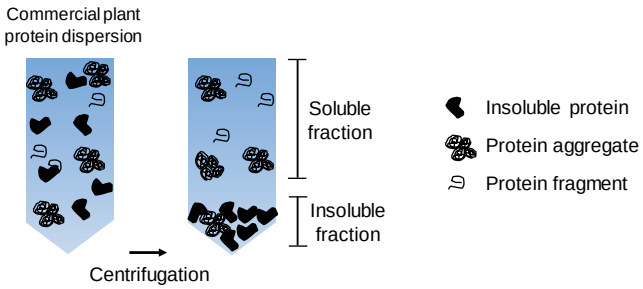

Figure 1.4. Schematic overview of a commercial plant protein dispersion before and after centrifugation. The commercial isolate contains protein fragments, soluble aggregates and insoluble proteins.

1.2.4. Protein blends

When using blends of plant and dairy proteins (or any other protein blend) to stabilise emulsions, it can be hypothesized that the following structural organisations of the interfacial films could be encountered (Figure 1.5):

1. A synergistic blend at the interface, leading to an interconnected and viscoelastic interfacial film, and emulsions with excellent physical stability and high resistance against coalescence;
2. A heterogenous interfacial blend: Both proteins adsorb at the interface but are not compatible and form phase-separated interfacial domains (Dickinson, 2011);
3. Multi-layered films, with one protein dominating the oil-water interface, and the second protein adsorbing onto this primary layer. Due to conformational changes of the first protein after adsorption, interactions with the bulk proteins can occur, that would not occur between both proteins in bulk (Le Floch-Fouéré et al., 2010);
4. Single protein films in case of competitive adsorption. One protein is more surface-active than the other and dominates the interface. The proteins are incompatible and do not interact, leaving the second protein in the bulk.

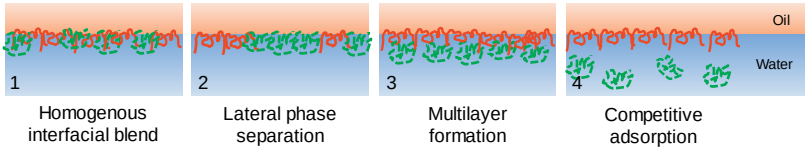

Figure 1.5. Possible interfacial structures formed in emulsions stabilised by plant-dairy protein blends.

The interface is a dynamic region and its composition and structure may change over time (Dickinson, 2011). When using a mixture of proteins, they may compete for adsorption during emulsification (Damodaran, 2004; Euston et al., 1996; Hunt et al., 1994; McClements et al., 2018), and possibly displace each other in time. Therefore, it is not only of importance to characterise the individual protein properties but also when present in a mixture.

The interfacial composition of protein blend-stabilised emulsions is expected to be dependent on the partitioning of the proteins between the bulk and interface, and on the protein concentration used. In the case of a binary mixture of caseins and whey proteins, the caseins were reported to preferentially adsorb in the protein-rich regime (>2 wt.% protein, 30% v/w oil) with whey protein adsorption being sterically hindered by the adsorbed caseins (Britten et al., 1991; Hunt et al., 1994). When using a binary mixture of sodium caseinate and pea protein isolate, it was reported that both proteins adsorb to the oil-water interface (Yerramilli et al., 2017), albeit this was only tested for one protein concentration.

Proteins can displace each other from the interface over time. For example, in exchange experiments where an emulsion was made with one protein, and the second was introduced after emulsification, β- and α-caseins could displace each other (Anand et al., 1996; Dickinson, Rolfe, et al., 1988). The whey protein β-lactoglobulin was able to displace pre-adsorbed α-lactalbumin, but α-lactalbumin could only displace pre-adsorbed β-lactoglobulin when present at a ten-fold higher concentration (Dickinson, Rolfe, et al., 1989). It was suggested that the resistance to displacement is a result of rigidity of the interface (Dalgleish, 1996). Interfaces stabilised by globular whey proteins have a surface shear viscosity that is about 10^3-10^4 times higher than for flexible caseins (Dickinson, 2001; Murray et al., 1996), due to the high packing density of the proteins, and strong protein-protein interactions. Displacement of the globular proteins could be enhanced by increasing the proteins' flexibility or interfacial mobility by using α-lactalbumin in its molten globule state (e.g., by

reducing pH to 7 or by removing calcium ions), leading to displacement of pre-adsorbed β-lactoglobulin (Matsumura et al., 1994).

Competitive adsorption and protein displacement are generally not considered in the design of protein blend-stabilised emulsions, yet are expected to be of great importance for the emulsions' physical stability. Therefore, these aspects are investigated in detail in Chapters 2 and 4.

1.3. Properties of the interfacial layer and its relation to emulsion stability

For droplet coalescence to occur, droplets need to be in close contact and the interfacial film needs to rupture. The sum of the attractive and repulsive interactions (i.e., van der Waals, electrostatic, steric interactions) determines if droplets can come into close contact (McClements, 2005; Walstra, 2003). This has been investigated for colloids in general by Derjaguin, Landau, Verwey, and Overbeek (Derjaguin et al., 1941; Verwey et al., 1955), and their so-called DLVO theory is very commonly applied. It predicts the magnitude of the droplet-droplet interactions as a function of the distance between two droplets (Figure 1.6). If the resulting interaction potential is positive, the repulsive forces dominate, while at negative values the attractive forces dominate. Droplets can come into close contact when their kinetic energy is higher than the potential energy peak between the primary (left) and secondary (right) minimum (Walstra, 2003), e.g., due to a lack of electrostatic repulsion. It is good to point out that steric interactions occur in the primary minimum, when interfacial layers overlap. This stabilisation mechanism is generally not taken into account in the DLVO theory, which assumes that droplets coalesce in the primary minimum (McClements, 2005).

Coalescence of two droplets can be divided into four different stages; approach of two droplets, drainage of the continuous film between them, film rupture and growth of the linkage between the droplets, or neck growth. The rupture of an interfacial film (i.e., coalescence) can be seen as dilatational deformation (Bos et al., 2001; Murray, 2011), and therefore assessing the dilatational rheological properties of interfaces is useful to understand their stability. For instance, the ability of proteins to form thick and viscoelastic interfacial layers is directly linked to coalescence stability (Dickinson, Murray, et al., 1988).

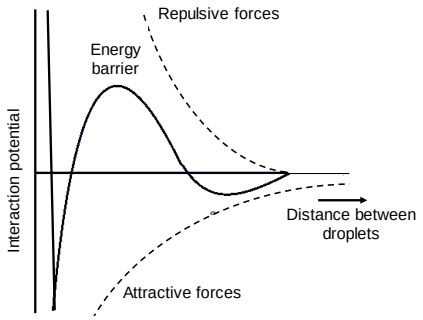

Figure 1.6. Inter-droplet interaction potential plotted as a function of the distance between two droplets. Dashed lines represent the repulsive and attractive forces and the black line the inter-droplet potential including primary and secondary minimum and the energy barrier.

The two most popular devices to perform such measurements are the Langmuir trough and the automated drop tensiometer. In a drop tensiometer, a millimetric droplet of one phase is formed at the tip of a needle and immersed in the other phase. The shape of the droplet is a balance between the gravitational forces and interfacial tension; thus, the latter can be determined from the droplet shape. The dilatational rheological properties of oil-water or air-water interfaces can be accessed by applying sinusoidal area deformation (Sagis & Scholten, 2014). The variation of interfacial tension upon deformation can be used to calculate elastic and loss moduli (E_d' and E_d", respectively) (equations 1.3 and 1.4):

$$E_d' = \Delta\gamma \left(\frac{A_0}{\Delta A}\right) \cos\delta \qquad 1.3$$

$$E_d'' = \Delta\gamma \left(\frac{A_0}{\Delta A}\right) \sin\delta \qquad 1.4$$

Here $\Delta\gamma$ is the difference in interfacial tension, A_0 the initial droplet/bubble area, ΔA the amplitude of change in area, and δ the phase shift of the oscillating interfacial tension signal, compared to the induced area change.

The interfacial dilatational rheology can be related to the interfacial resistance to coalescence but does not consider the contribution of steric and electrostatic repulsions. For example, caseins form interfaces with very low elastic moduli (Dickinson, 2001; Graham et al., 1980) but are able to form stable emulsions because of efficient droplet-droplet repulsion under appropriate solvent conditions. Furthermore, planar model interfaces may not fully represent the interfacial layers present in emulsions (Figure 1.7). In tensiometric devices, emulsifier

adsorption is dominated by diffusion and measurements typically start after one to several seconds. In contrast, droplets produced within a high-pressure homogeniser are small (0.2-10 µm), formed within milliseconds, and emulsifier adsorption is driven by convective mass transport rather than diffusion (Stang et al., 1994). Microfluidic devices can be used to bridge this gap since they involve much faster droplet formation (sub-second scale) compared to the classic tensiometric devices. The former devices are therefore probably more appropriate to understand early droplet formation (Chapters 5 and 6), whereas dilatational rheology is insightful for long-term physical stability of emulsions (Chapter 3).

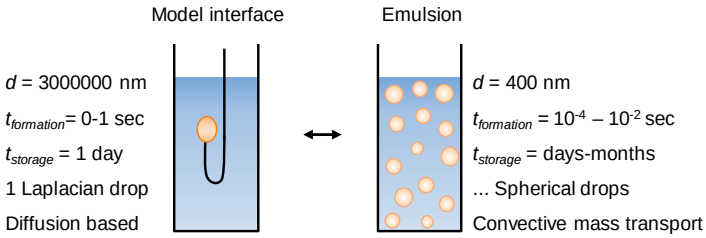

Figure 1.7. Schematic overview of major differences between droplet formation and properties in model interface-based devices (e.g., as illustrated here, using an automated drop tensiometer) or in emulsion systems.

1.4. Research aim and approach

The aim of this thesis is to understand the formation and stability of emulsions stabilised by blends of dairy and plant proteins. We use sodium caseinate and whey protein isolate as dairy proteins, and pea protein isolate as a plant protein source.

The formation and stability of emulsions involve phenomena occurring over a wide range of time (milliseconds for the formation of droplets during emulsification, and hours to days for the stability and interfacial rearrangements) and length scales (proteins' molecular properties, up to large scale emulsion formation). On top of that, the use of protein blends results in complex, non-equilibrated interfacial structures. Therefore, one could see this project as a puzzle that we consider as a whole, and for which various pieces need to be logically assembled in order to obtain the complete image. In other words, to characterise the complex plant-dairy protein blend-stabilised emulsions, a comprehensive range of techniques have to be combined to understand phenomena at different time and length scales (Figure 1.8).

Conventional methods are available to characterise a number of emulsion properties separately; however, innovative methods are needed to probe effects that occur at very short time scales and under conditions that approach the ones occurring in a homogeniser (e.g., convective mass transport, sub-second scale). We use microfluidic tools to probe the interfacial rheological properties of protein stabilised-emulsion droplets within 1 second, and link this to their stability at the same time scale. Model interfaces are used to provide information about long-term stability of the emulsions, and we specifically focus on interfacial rearrangements occurring over time, an aspect that is largely overlooked in protein-stabilised food emulsions. A special point of attention concerns the emulsifying and structural properties of pea proteins. We compare molecular properties of a commercial, industrially-relevant isolate and of lab-purified pea protein isolates by intrinsic fluorescence measurements. By combining all these length and time scales, a thorough understanding is obtained, leading to a solid basis for the design of protein blend-stabilised emulsions.

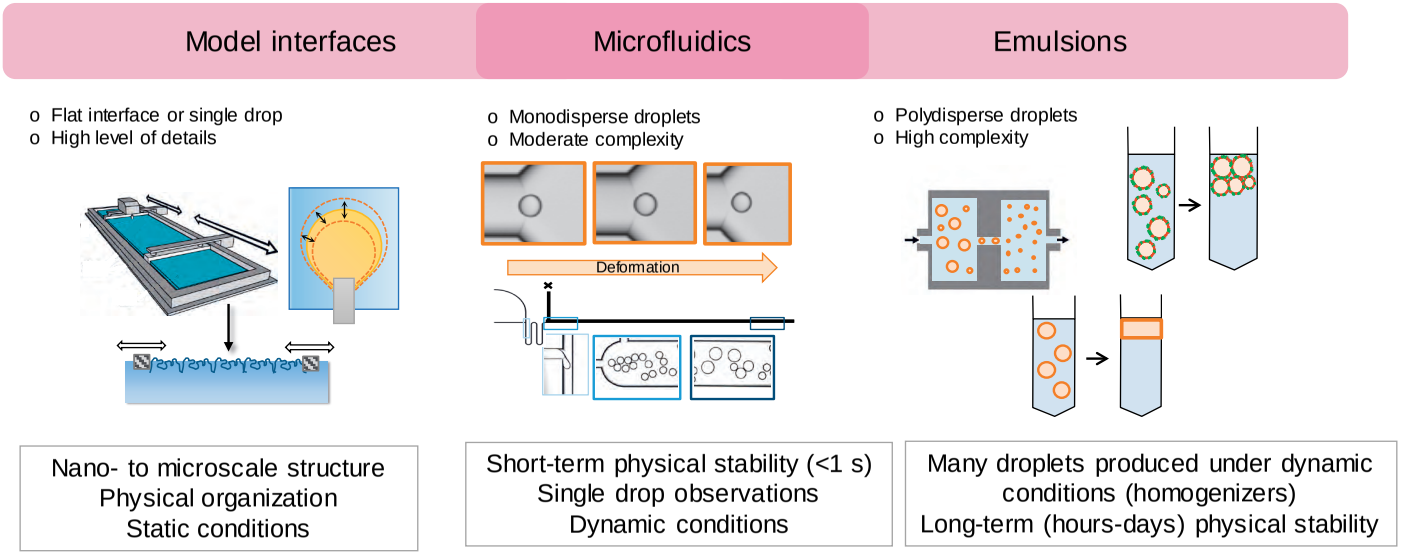

Figure 1.8. Overview of the multi-scale approach involving coupled techniques used in the thesis.

1.5. Thesis outline

The thesis outline is described below per chapter, and a graphical representation is given in Figure 1.9.

In **Chapter 2**, we use blends of plant and dairy proteins to physically stabilise O/W emulsions. For both the blends and the individual proteins, droplet size, emulsion stability, surface load and interfacial composition are determined over time. In the protein-rich regime, we demonstrate a synergistic behaviour in terms of physical stability when using protein blends. Furthermore, we show that compositional rearrangements occur at the interface within days. In parallel, in **Chapter 3**, we characterise the interfacial properties of protein blends and of their individual constituents in more detail, using model air-water and oil-water interfaces. We demonstrate that the rheological response of the blend-stabilised interfaces deviates from what could be expected by averaging those of the individual proteins, and depends on the type of protein blend and interface used.

In order to understand the physical stability of plant-dairy protein blend-stabilised emulsions, it is not only important to characterise their initial interfacial properties, but also to evaluate and understand the interfacial rearrangements over time; an aspect that is largely overlooked for protein-stabilised emulsions in the literature, thus we focused on it in **Chapter 4.** We produce emulsions with WPI and PPI, separately or as a blend, and add extra protein post-emulsification. The surface load and composition are measured over time. We compare these findings with results obtained using an automated drop tensiometer with bulk-phase exchange to highlight the effect of sequential protein adsorption on interfacial tension and dilatational rheology. We demonstrate that in-plane protein interactions are the driving force for this displacement, rather than a decrease in interfacial tension.

In **Chapter 5**, we use microfluidic tools to understand early film formation in protein-stabilised emulsions. We use tailor-made microfluidic chips to characterise the interfacial rheological properties of protein stabilised-droplets at short time scales (<1 second). This technique goes beyond what can be measured using conventional tensiometric devices. The rheological properties are linked to the propensity of freshly prepared droplets to coalesce within the same time scale.

In **Chapter 6** we systematically induce oxidation at various levels to commercial pea proteins, and determine the coalescence stability of emulsions stabilised with these oxidised

proteins using microfluidic techniques. We compare with results obtained with oxidised whey proteins in previous work, and also use Langmuir-Blodgett films to evaluate the homogeneity of films.

From the previous chapters, it was evident that the emulsifying and interfacial properties of dairy and plant proteins are very different. In **Chapter 7**, we zoom into this aspect further, and use right-angle and front surface fluorescence spectroscopy to gain insight in the tertiary structure of the proteins in solution and at the interface. To gain further insight in the behaviour of the commercial isolate, we compare its properties to those of fully denatured pea proteins, and of lab-purified ones.

In **Chapter 8**, we dive deeper into the emulsion stabilisation efficiency of the commercial pea protein isolate in relation to various applications. We evaluate the physical stability of emulsions prepared with full pea protein isolate, or with the insoluble pea protein fraction, and use whey protein-stabilised emulsions for comparison. We consider not only fluid emulsions with a relatively low oil fraction (10 wt.% oil), but also high internal phase emulsions (HIPEs, 70 wt.% oil).

Finally, in **Chapter 9**, we provide a general discussion of the main findings and future directions. We highlight approaches to decipher interfacial phenomena, such as characterising interfacial displacement and the interfacial properties of insoluble matter (e.g., plant proteins).

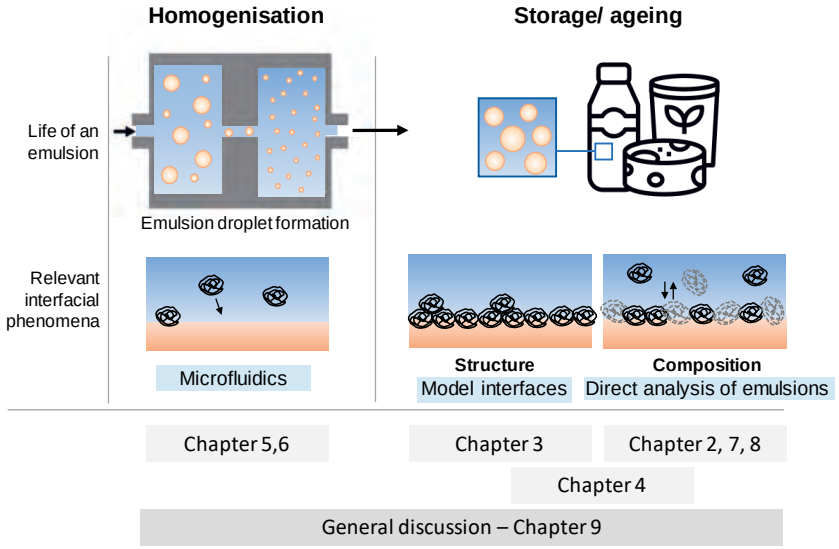

Figure 1.9. Graphical outline of the thesis content and chapter division.

Chapter 2

Synergistic stabilisation of emulsions by blends of dairy and soluble pea proteins: Contribution of the interfacial composition

This chapter has been published as Hinderink, E. B. A., Münch, K., Sagis, L., Schroën, K., Berton-Carabin, C. C. Synergistic stabilisation of emulsions by blends of dairy and soluble pea proteins: Contribution of the interfacial composition. *Food Hydrocolloids.* **2019**, *97*. https://doi.org/10.1016/j.foodhyd.2019.105206

2.1. *Abstract*

Proteins from animal and plant sources are known to be able to physically stabilise emulsions, whereas much less is known about emulsions prepared with blends of proteins of different origin. Here we use blends of pea protein isolate (PPI) with whey protein isolate (WPI) or with sodium caseinate (SC) to physically stabilise emulsions prepared by high-pressure homogenisation. For both the blends and the individual proteins, droplet size, emulsion stability, surface load and interfacial compositions were determined. The droplet size and surface load (measured over a concentration range 0.2-1.6 wt.% protein in the starting aqueous solution) were the lowest for SC- and WPI-stabilised emulsions, and the highest for PPI-stabilised emulsions, whereas emulsions stabilised by the blends (1:1 ratio) had intermediate droplet size values and surface loads. PPI- and SC-stabilised emulsions showed some physical destabilisation (e.g., flocculation and coalescence, respectively) over 14 days of storage, whereas the WPI-PPI or SC-PPI blends formed emulsions that remained stable, suggesting synergistic effects.

When used in blends, both dairy and plant proteins adsorbed at the oil-water interface, but compositional rearrangements at the interface occurred within days. More specifically, whey proteins were able to partly displace pea proteins from the interface, which were themselves able to displace SC. However, such a displacement was only possible when the displacing protein was present in sufficiently high excess. Such considerations are usually not taken into account in food emulsion formulation, even though they are very relevant, as the interfacial layer protects emulsions droplets against physical destabilisation.

Graphical abstract

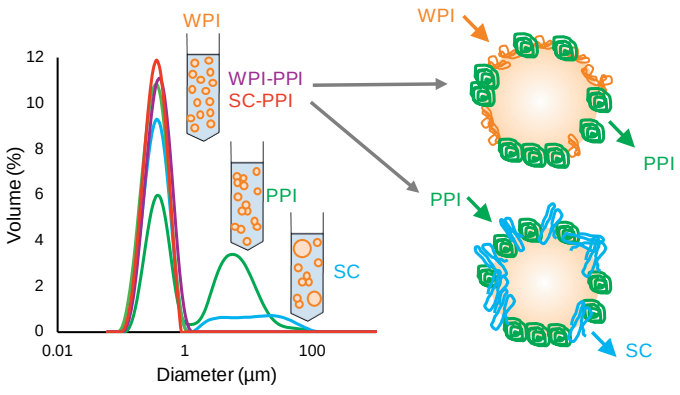

2.2. Introduction

Proteins are widely used in the food industry to stabilise oil-in-water (O/W) emulsions. They are able to adsorb at the oil-water interface, protecting the droplets against physical destabilisation (e.g., coalescence, flocculation) by steric and electrostatic repulsions between the droplets (McClements, 2005) and, for some of them, by formation of a network at the interface. Dairy proteins are widely used as emulsifiers in food emulsions (Dickinson, 2001) and include flexible proteins (caseins) and globular proteins (whey proteins). The flexible caseins rapidly adsorb at the interface with the hydrophobic parts protruding into the oil phase, and the more hydrophilic parts into the water phase, leading to steric repulsion that prevents droplets from approaching each other too closely (Dickinson, 2001). The globular whey proteins undergo conformational changes after adsorption at the interface, exposing, for example, the sulfhydryl groups of β-lactoglobulin, leading to a covalently, highly interconnected and viscoelastic network that protects droplets against coalescence (Dickinson & Matsumura, 1991).

Due to the negative impact of animal-derived proteins on the environment, and to their high cost, plant proteins (e.g., from soy or pea) are gaining interest as more sustainable emulsifiers. Especially pea proteins are becoming popular because of their nutritional value and their lower allergenic potential compared to soy proteins. Pea proteins are composed of the globular proteins 11S legumin, 7S vicilin and convicilin, of which vicilin has the highest emulsifying activity (Barac et al., 2010). The emulsifying properties of a range of plant proteins, including pea proteins, have already been studied (Gumus et al., 2017a; Ho et al., 2017; Karaca et al., 2011; Liang et al., 2013; Tang, 2017) and it is clear that they suffer some drawbacks, such as limited emulsifying capacity and consequences for the product taste. Therefore the full replacement of dairy proteins by plant proteins is challenging, but partial replacement could still be an option.

Using blends of plant and dairy proteins could be a way to integrate functionality, sustainability and product quality. Some work has been done using mixtures of sodium caseinate and soy protein (Ji et al., 2015), and whey protein isolate and pea protein isolate (Ho et al., 2018), both reported synergistic behaviour of the blends with regard to the physical stabilisation of emulsions, which was attributed to the dense interfacial layers formed. Sodium caseinate and pea protein blends were reported to behave either synergistically due to mutual interactions, decreasing depletion flocculation (Yerramilli et al., 2017), or in an

antagonistic manner when mostly SC adsorbed at the interface and the other proteins induced depletion flocculation (Ho et al., 2018). Since there was a notable concentration difference between these two studies, differences in surface coverage and concentration of non-adsorbed proteins may have played a deciding role in the observed effects.

The underlying stabilisation mechanism of plant-dairy protein-based emulsions is clearly not well understood, albeit that it can be expected to be dependent on the partitioning of the proteins between the interface and bulk, and on the protein concentrations used. The concentrations are of importance since too high bulk concentrations may induce depletion flocculation, while too low surface coverage can lead to bridging flocculation and possibly, ultimately to coalescence. The composition of the protein blend-stabilised interfaces is determined by a non-kinetically controlled mechanism within the homogeniser, and is a consequence of the order of protein arrival at the interface (Dickinson, 2011). If both proteins adsorb simultaneously, this could lead to excellent stability when acting synergistically but also destabilise emulsions when the proteins compete for adsorption or form phase-separated interfacial domains. Lateral phase separation may occur when proteins are incompatible or used in high concentrations, leading to a decrease in interfacial viscoelasticity which, in turn, may decrease the physicochemical stability of the emulsion (Sengupta et al., 2000).

Although the adsorption and interfacial behaviour of mixed protein systems, such as blends of dairy and plant proteins, is largely unexplored so far, it should be pointed out that blends of proteins from the same biological origin (e.g., caseins and whey proteins) have been investigated to some extent. Emulsions stabilised by a mixture of whey protein and sodium caseinate showed preferential adsorption of sodium caseinate in the protein-rich regime (>2 wt.% protein, 30 v/w% oil). This was explained by the steric hindrance of the adsorbed sodium caseinate which prevented further whey protein adsorption (Britten et al., 1991; Hunt et al., 1994). Taking this pioneering work as a basis, our study aims at understanding the interfacial and emulsifying behaviour of dairy-plant protein blends. For this purpose, we used whey protein isolate (WPI) and sodium caseinate (SC) as dairy proteins, and pea protein isolate (PPI) as plant protein source.

2.3. Materials and methods

2.3.1. Materials

WPI, purity 94% (BiPro®, Davisco, Switzerland), SC, purity 97% (Excellion™, Sodium Caseinate S, Friesland Campina, the Netherlands), PPI, (NUTRALYS s85F, Roquette, France; see Appendix Table A2.1 for the amino acid composition and content, and protein content), were used as received. The soluble protein concentration was determined using a bicinchoninic acid (BCA) kit (BCA1-1KT, Sigma-Aldrich, Saint Louis, USA). Sunflower oil was purchased from a local supermarket and stripped with Florisil (Sigma-Aldrich, 20281, Supelco, 100-200 mesh) to remove surface-active impurities, as described previously (Berton et al., 2011). Mini-PROTEAN gels (12% Mini-PROTEAN® TGX™ Precast Protein Gels, 10-well comb, 30 µl/well), Bio-safe Coomassie G-250 stain and precision plus protein standard (Bio-Rad, Richmond, CA, USA), were used for SDS-PAGE analysis. Sodium phosphate dibasic, sodium phosphate monobasic, Tris buffer, glycerol, sodium dodecyl sulfate (SDS), glycerol, bromophenol blue R-250 (BPB), and 2-mercaptoethanol were purchased from Sigma Aldrich (Saint Louis, MO, USA) and were of at least of analytical grade. Ultrapure water was obtained from a Milli-Q system (Millipore Corporation, Billerica, Massachusetts, US) and used for all the experiments.

2.3.2. Methods

Preparation of aqueous phases

WPI and SC were dissolved (2 wt.%) in 10 mM phosphate buffer (pH=7.0) and stirred overnight at 4 °C. PPI was dissolved in the same buffer (6 wt.%) and stirred for at least 48 h at 4 °C; the insoluble part was removed by centrifugation (16,000 x *g*, 30 min). The supernatant was centrifuged again under the same conditions to ensure complete removal of the insoluble fraction. The supernatant was collected and its soluble protein content (29 ± 3.0 wt.% of the total protein) was determined with the BCA-assay (Smith et al., 1985) at 562 nm using a DU 720 UV-vis spectrophotometer (Beckman Coulter, Woerden, the Netherlands). At 10 g/L soluble pea proteins, 0.06 wt.% residual fat was present. This supernatant was used for all pea protein-based experiments, and for simplicity is referred to as ‘protein solution’ from now on.

Preparation of emulsions

A coarse emulsion was prepared by mixing 10 wt.% stripped sunflower oil with the protein solutions (0.2-1.6 wt.%) using a high speed blender (S18N-19G, Ultraturrax R, IKA-Werke GmbH & Co., Staufen, Germany) at 11,000 rpm for 1 min. When protein blends were used, both solutions were shortly mixed by hand before adding the oil. The coarse emulsion was then passed five times through a high-pressure M-110Y Microfluidizer (Microfluidics, Massachusetts, USA) at 400 bars to obtain the final emulsion. The emulsions were stored in glass bottles at 4 °C.

Physical stability of emulsions

Droplet size distribution

The droplet size distribution was measured by static light scattering using a Mastersizer 3000 (Malvern Instruments Ltd.; Worcestershire, UK). The refractive index was 1.465 for the dispersed phase (stripped sunflower oil) and 1.330 for the dispersant (water). An absorption index of 0.01 was applied. For emulsions that showed a bimodal distribution, aliquots were diluted (1:1, v/v) in a 1 wt.% SDS solution prior to the measurement, to disrupt possible droplet flocs. Droplet size is reported as the volume weighted mean ($d_{3,2}$) and is the average of at least two independent samples, of which each was measured five times.

Emulsion morphology

Emulsions were visualised using light microscopy (Axioscope, Zeiss, Germany) using 100x magnification, without dilution.

Droplet surface charge

The droplet surface charge (ζ–potential, mV) was determined using dynamic light scattering (Zetasizer Nano ZS, Malvern Instruments, UK). The emulsions were diluted 100 times in ultrapure water prior to the measurement. Measurements were performed at 20 °C after a 2 min equilibration period. The ζ–potential was calculated using the Smoluchowski model with a refractive index of 1.465 for the dispersed phase and 1.330 for the dispersant. ζ–potential values are expressed as the mean of two independent samples, of which each was measured in triplicate.

Adsorption behaviour of proteins

Protein surface load

The continuous phase of the emulsions was separated from the cream phase by centrifugation at 15,000 x *g* for 1.5 hours. The serum phase was collected by cautiously making a hole at the bottom of the tube, and its soluble protein content was determined with the BCA-assay. The surface load was calculated with equation 2.1.

$$\Gamma = \frac{C_s . d_{3,2}}{6\varphi} \qquad 2.1$$

Where C_s is the adsorbed protein concentration calculated, by subtracting the protein concentration in the previously described serum phase from the initial protein concentration of the solution used for emulsion preparation, $d_{3,2}$ the surface weighted mean droplet diameter after dilution of the emulsion in 1 wt.% SDS, and φ the dispersed phase volume fraction.

Protein composition at the interface

The cream phase obtained after centrifugation was re-dispersed into 1 wt.% SDS solution (under agitation), and then re-centrifuged. The subnatant, containing the proteins that were initially adsorbed, was collected, and analysed together with the protein solutions used for emulsion preparation by SDS-PAGE under reducing conditions. All solutions were mixed with a pH 6.8 buffer containing Tris-HCl 0.5 M, glycerol 30% w/v, SDS 10% w/v, bromophenol blue 0.5% w/v and 2-mercaptoethanol, vortexed and heated at 95 °C for 5 min in a heating block. Ten microliters protein standard (Biorad, Precision Plus protein™ Standards, Mw 10-250) and 20 microliters of all protein solutions were loaded on the gel as dependent duplicates. A running buffer of pH 8.3 constituted of Tris-HCl 25 mM, glycerol 192 mM and SDS 0.1 wt.% was used. Electrophoresis was performed in the Mini-PROTEAN Tetra Cell (Bio-rad laboratories, USA) at 200 V. The gels were extensively washed with ultrapure water before staining with Coomassie G-250 for 1 hour. Subsequently, the gels were washed with ultrapure water for 16 hours before analysis. Gels were scanned and analysed using a calibrated densitometer (GS-900™, Bio-rad laboratories, USA) and Image Lab software (Bio-Rad laboratories, USA).

The molecular weights were determined by point to point regression. For WPI solutions, mainly bovine serum albumin (BSA), β-lactoglobulin (β-lg), α-lactalbumin (α-lac), and

traces of immunoglobulins were found. For SC, the major proteins were α-, β- and κ-casein, with traces of whey proteins (ß-lg, α-lac and immunoglobulins). PPI was mainly composed of convicilin (~71 kDa), vicilin subunits (~30, ~34, ~47 and ~50 kDa), α-legumin (38-40 kDa) and β-legumin (19-22 kDa) (Barac et al., 2010). The pea proteins dissociated in the buffer containing SDS solution and 2-mercaptoethanol, leading to multiple bands in SDS-PAGE. The sum of the subunits are reported for the different pea proteins, with a distinction between the vicilin major (45-65 kDa) and minor (25-34 kDa) subunits. SDS-PAGE of the solutions can be found in Appendix Figure A2.1.

2.3.3. Experimental design and data treatment

Each emulsion was characterised for morphology, particle size distribution as function of time (0 to 14 days), surface load and interfacial composition. This was done for at least two independently prepared emulsions, and means and standard deviations were calculated from these replicates. Independent t-tests (SPSS Statistics 20, IBM) were performed, using all experimental values, to determine if differences in surface load and interfacial composition occurring in time were significant.

2.4. Results and discussion

2.4.1. Physical characterisation of fresh emulsions

The average droplet size ($d_{3,2}$) of freshly prepared protein-stabilised emulsions is plotted as a function of protein concentration in the starting aqueous solution, without or with addition of SDS prior to the measurement (Figure 2.1A). For all the emulsions made with individual proteins or 1:1 blends, the droplet size decreased with increasing protein concentration (0.2 to 0.8 wt.%), which is indicative of a protein-poor regime. Above 0.8 wt.%, the droplet size was independent of protein concentration, with an average $d_{3,2}$ of about 0.3-0.5 µm.

The mean droplet size of a freshly prepared emulsion is determined by two processes: droplet break-up, which depends on interfacial tension, energy input and viscosity of the continuous phase, and the subsequent re-coalescence just after droplet break-up (Jafari et al., 2008; Tcholakova et al., 2003). Besides, flocculation may occur, which would also increase the droplet size measured by static light scattering. To check this effect, samples were diluted in a SDS solution, and measured again (Figure 2.1B). At the lowest protein concentrations tested, the WPI- and SC-stabilised emulsions showed $d_{3,2}$ values around 0.7 and 0.6 µm, respectively, which remained the same after SDS addition. This suggests that either re-coalescence after droplet break-up, or higher interfacial tension during formation, was the reason for the larger $d_{3,2}$ compared to the protein-rich regime, rather than droplet flocculation. For the PPI-stabilised emulsions, much larger droplets were found at the lowest protein concentrations, of which the size reduced considerably after addition of SDS (Figure 2.1B), which is indicative of flocculation. Yet, the individual droplet size of the PPI-stabilised emulsions was still larger in the protein-poor regime compared to that of the dairy protein-stabilised emulsions, indicating that either the interfacial tension was less effectively reduced by PPI and/or that more re-coalescence took place during homogenisation.

Emulsions stabilised with 1:1 WPI-PPI and SC-PPI blends showed less flocculation, when made at low concentration, compared to PPI-stabilised emulsions, although the actual droplet sizes were quite similar to that of the PPI-stabilised emulsions (Figure 2.1B). This suggests that protein blends can prevent droplet flocculation, but may still not reduce interfacial tension fast enough during droplet formation or not prevent rapid re-coalescence. Interestingly, replotting the particles sizes for the blend-based emulsions as a function of the dairy protein concentration in the starting aqueous solution (instead of the total protein concentration; Appendix, Figure A2.2) brings the lines in close proximity to those obtained

for emulsions stabilised with only WPI or SC, which could be a first indication that at low concentration, droplet and interface formation is driven by the dairy proteins. At protein concentrations of 0.8 wt.% and higher, small droplets were formed ($d_{3,2}$ <0.4 µm) irrespective of the proteins used. For the chosen homogenisation conditions it can be concluded that all tested individual proteins and blends effectively protect the droplets against re-coalescence at such concentrations.

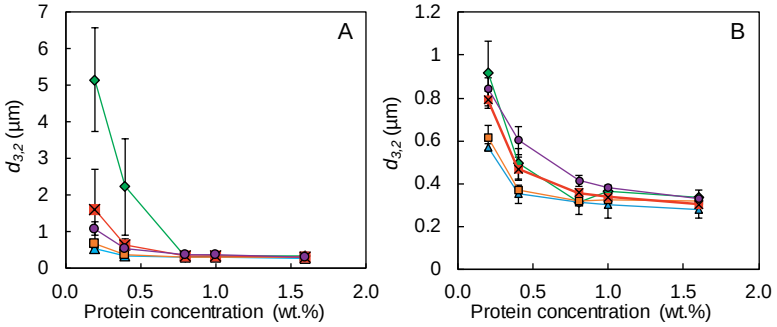

Figure 2.1. A) Surface volume diameter, $d_{3,2}$, as a function of protein concentration in the starting aqueous solutions and B) $d_{3,2}$ measured after twofold dilution with 1 wt.% SDS solution prior to the measurement for emulsions prepared with WPI (■), SC (▲), PPI (◆) 1:1 SC-PPI (☒) and 1:1 WPI-PPI (●). The insert shows

The surface load of the different protein-stabilised emulsions was determined as a function of the protein concentration in the starting aqueous solution (Figure 2.2); the surface load increased with concentration for all emulsions tested. The highest values were found for the PPI-stabilised emulsions, and the lowest for the SC-stabilised emulsions, for all concentrations tested. This is in line with previous studies in which high surface loads were reported for pea proteins (Gumus et al., 2017a; Ladjal Ettoumi et al., 2017) and for plant proteins in general (Gumus et al., 2017a; Ladjal Ettoumi et al., 2017; Shao et al., 2014) compared to dairy proteins. SC-stabilised emulsions had a lower surface load compared to WPI-stabilised emulsions over the whole concentration range, most probably as a result of their disordered structure, which enables them to stabilise a larger interfacial area per gram of protein compared to globular WPI (Hunt et al., 1994).

The highest measured values exceeded the measured saturation surface loads from literature for SC (3 mg/m^2; (Dickinson et al., 1997; Hunt et al., 1994), WPI (2 mg/m^2; (Hunt et al., 1994), and modelled values for PPI (6 mg/m^2; (Gumus et al., 2017a)). Under these conditions, emulsions are made in the protein-rich regime, and surface loads higher than the saturation

surface loads may be related to multilayers and/or protein aggregates at the interface (Graham et al., 1979a; Tcholakova et al., 2003). The small droplet sizes for WPI- and SC-stabilised emulsions (Figure 2.1) and their relatively low surface loads (Figure 2.2) indicate that dairy proteins either more effectively lower the interfacial tension during homogenisation, and/or more efficiently stabilise droplets directly after their formation compared to PPI, also when used in a blend.

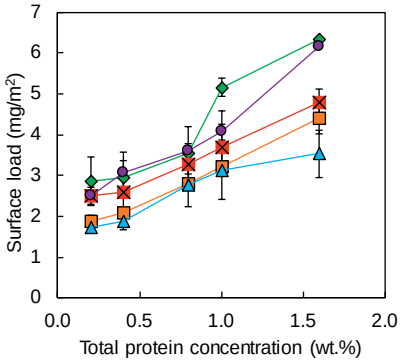

Figure 2.2. Surface load in protein-stabilised emulsions as a function of protein concentration in the starting aqueous solution, for emulsions prepared with WPI (■), SC (▲), PPI (◆), 1:1 WPI-PPI (●) and 1:1 SC-PPI (⊠).

2.4.2. Physical stability

Droplet size distribution

Stability after preparation was investigated using emulsions with 1 wt.% protein, as the droplet size reached a plateau at around 0.8-1 wt.% protein (Figure 2.1). The initial droplet size ($d_{3,2}$) for all emulsions ranged between 0.4-0.5 µm and showed a monomodal distribution (Figure 2.3). A negative ζ–potential was measured for all emulsions over a period of 14 days, with a charge lower than -30 mV (Appendix, Figure A2.3), indicating that electrostatic repulsion was high and most likely not the reason for physical destabilisation.

The WPI-stabilised emulsion was the only individual protein-stabilised emulsion that did not destabilise over the two-week incubation period; for the SC stabilised-emulsion, a bimodal droplet size distribution was found after 14 days (Figure 2.3) which was to a certain extent due to flocculation and partly due to coalescence, as the distribution was still bimodal after dilution with SDS, but shifted to smaller sizes. The relatively high amount of non-adsorbed SC in the continuous phase may have induced depletion flocculation (Britten et al., 1991;

Dickinson et al., 1997; Yerramilli et al., 2017). Furthermore, the low elasticity of the SC-stabilised interfacial layer may not have efficiently protected droplets from coalescing after flocculation (Ho et al., 2017).

PPI-stabilised emulsions were also subjected to substantial destabilisation after 14 days with an additional peak around 6 µm. Addition of SDS solution showed that flocculation was the only mechanism involved, as the droplet size distribution became similar to that of the fresh emulsion after dilution in SDS solution. Yerramilli et al., (2017) reported droplet flocculation due to protein aggregation. Attractive intermolecular interactions between adsorbed proteins may exist due to their hydrophobic nature, which could be strong enough to overcome electrostatic repulsion and therewith lead to flocculation (Berton-Carabin et al., 2018). Despite the occurrence of flocculation, no macroscopic visual effects (e.g., creaming, oiling off) were observed in the PPI-stabilised emulsions.

It is important to mention that no physical destabilisation of PPI- and SC-stabilised emulsions was found by Ho et al. (2018) who used the same conditions (pH, storage temperature) as in the present work, albeit used a higher homogenisation pressure (800 bar, resulting in smaller droplets) and a lower protein concentration (0.7 wt.%). Due to both conditions, less protein would be present in the continuous phase compared to our work, which could result in less or no depletion flocculation (Ho et al., 2018). It is clear that the process conditions (e.g., homogenisation pressure) and protein concentrations used influence emulsion stability greatly, and that small differences may lead to instability by coalescence or flocculation (bridging or depletion) (Guzey et al., 2006).

The emulsions stabilised with 3:1 and 1:1 WPI-PPI blends had a monodisperse droplet size distribution that did not change over 14 days, suggesting excellent physical stability. Minor destabilisation was found for the emulsion stabilised with 1:3 WPI-PPI blend, as shown by the slight right shift of the droplet size distribution, which was due to flocculation (the dilution in SDS gave the same distribution as at day 0). It is good to point out that of three independent replicates the most unstable one (based on change in $d_{3,2}$) is shown in Figure 2.3 for the 1:3 WPI-PPI blend, suggesting that destabilisation was minor. Microscopic observations showed that in the 1:1 WPI-PPI stabilised-emulsion flocculation occurred (Figure 2.4A), which may not have been noted in the static light scattering instrument in which the samples were diluted and analysed under flow, which may have broken down some droplet flocs, especially if depletion flocculation was involved (Dickinson, 2010). The fact

that no coalescence occurred in this emulsion suggest that the interfacial film was strong, which is in line with Ho et al. (2018) who found stable emulsions for 1:3 and 1:1 WPI-PPI blends, for lower protein concentrations and smaller droplets.

Emulsions stabilised with 3:1 and 1:1 SC-PPI blends also showed excellent physical stability, which is in line with findings of Yerramilli et al., 2017 and of Ji et al., 2015, albeit remarkable as both individual proteins led to some emulsion instability under the same conditions. As was the case with the 1:1 WPI-PPI emulsions, light microscopy (Figure 2.4) showed flocculation for 1:1 SC-PPI emulsions which could similarly be explained by de-flocculation in the static light scattering instrument. It is expected that thick mixed protein layers are formed at the interface (Ji et al., 2015) that are strong enough to protect the droplets against coalescence. Emulsions stabilised with 1:3 SC-PPI blends showed some flocculation at day 0 which increased over 14 days (Figure 2.3), but was minor when compared to SC- and PPI-stabilised emulsions.

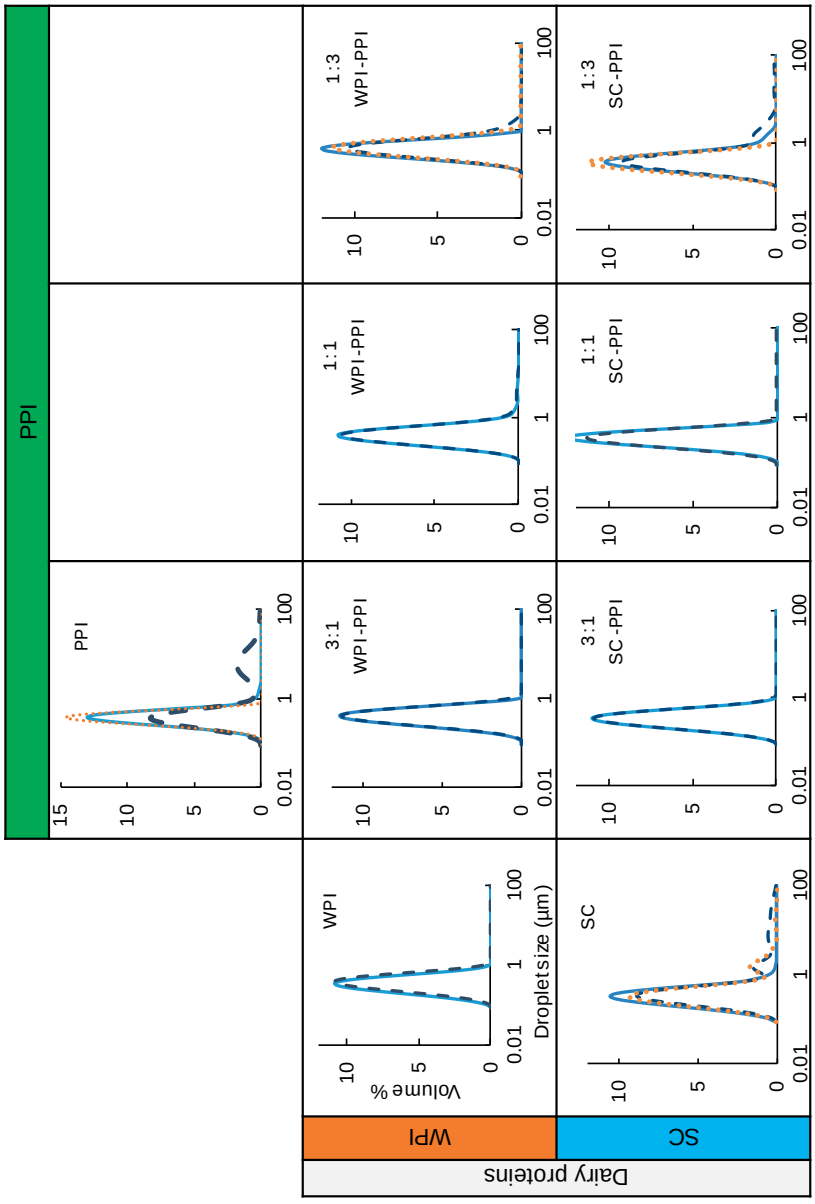

Figure 2.3. Droplet size distribution (volume-based frequency [%] as a function of particle size [µm]) of protein-stabilised emulsions at day 0 (——) and day 14 (– – –). In case of bimodal distribution at day 14, emulsions were diluted twofold with 1 wt.% SDS solution prior to the measurement (▪▪▪▪). For clarity, only one representative sample is shown, but similar trends were obtained for two to three independent replicates.

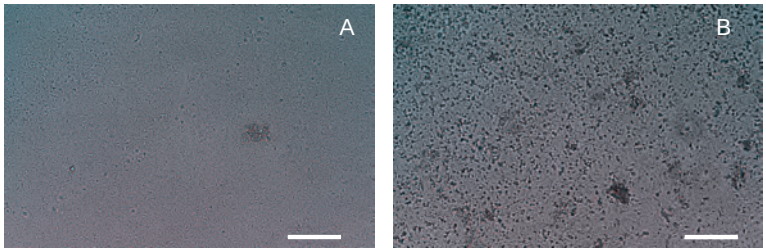

Figure 2.4. Light microscopy images of emulsions stabilised by 1:1 WPI-PPI (A); or 1:1 SC-PPI (B) blend at day 14, 40x magnification. Scale bar represents 50 µm.

2.4.3. Adsorption behaviour

Interfacial composition

To gain insights in the properties of the interfacial films, fresh and after ageing, the surface load and interfacial composition were studied. We focus on 1 wt.% protein-stabilised emulsions and compare results obtained at day 0 and 3 for individual proteins and their 1:1 blends.

Table 2.1. Surface load in emulsions stabilised by the individual proteins and their 1:1 blends at day 0 and day 3. For all samples, no significant difference ($p < 0.05$) was found between day 0 and day 3.

Protein stabilised-emulsions	Surface load (mg/m^2)	
	day 0	day 3
WPI	3.2 ± 0.3	3.0 ± 0.3
1:1 WPI-PPI	3.4 ± 0.4	3.5 ± 0.4
PPI	4.5 ± 0.6	5.0 ± 0.3
1:1 SC-PPI	3.0 ± 0.5	3.1 ± 0.5
SC	3.3 ± 0.5	3.0 ± 0.2

The surface load did not significantly change over three days (Table 2.1, p<0.05). The interfacial film in the WPI-stabilised emulsion at day 0 consisted of ~62% β-lg, 34% α-lac and 3% BSA (Figure 2.5), with β-lg and α-lac dominating as expected from their fractions in the starting aqueous solution (69% and 24%, respectively). The fraction of BSA at the interface was two times lower compared to that in the starting solution, and immunoglobulins could not be detected at the interface. In the SC-stabilised emulsion, the interface was dominated by α-casein (38%) and β-casein (44%), which were the major constituents in the starting SC solution, and some small amounts of κ-casein, BSA, β-lg and α-lac were also

found. The whey proteins detected at the interface in the SC-based emulsions were also found in the initial solutions, and are probably a result of the SC isolation process.

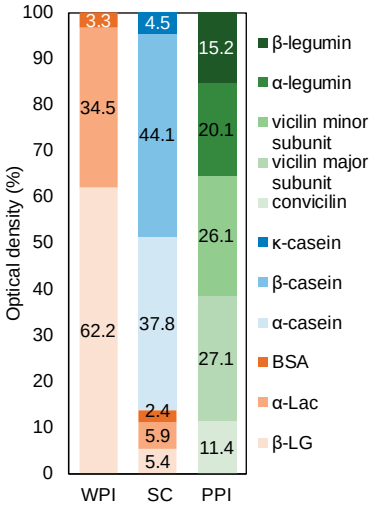

Figure 2.5. Interfacial composition of the emulsions stabilised by WPI, SC and PPI at day 0 determined with SDS-PAGE densitometry. Colours from light to dark indicate for whey proteins (orange): β-Lg, α-Lac, BSA; caseins (blue): α-casein, β-casein and κ-casein; pea proteins (green): convicilin, vicilin major subunit, vicilin minor subunit, α-legumin, β-legumin. Interfacial composition at day 3, and all standard deviations, are reported in Appendix, Table A2.2.

For the PPI-stabilised emulsions, fractions of all subunits were found at the interface; at day 0, 11% convicilin, 54% vicilin subunits and 35% legumin were found. The fraction of vicilin minor subunits was two times lower at the interface compared to its fraction in the starting solution. The other PPI subunits accumulate at the interface (by a factor between 1-1.5) compared to their fraction in the starting solution, which suggests that the vicilin minor subunits did not adsorb rapidly at the interface, due to kinetic or competition effects. It has been described that non-commercial vicilin is more surface-active compared to legumin, but a distinction between the different subunits was not made (Dagorn-Scavinier et al., 1987; Kimura et al., 2008). Ageing of the WPI-, SC-, and PPI-stabilised emulsions over three days did not result in a significant change of the interfacial composition (Appendix, Table A2.2), with the exception of κ-casein, which was not found at the interface of the 3-day aged SC-stabilised emulsion. κ-Casein could also not be detected at the interface in the SC-based blend-stabilised emulsions, although its low concentration in the blends may have made it difficult to measure reliably (Robson et al., 1987).

For the WPI-PPI-stabilised emulsions (Figure 2.6), the major proteins present at the interface were the vicilin minor and major subunits (PPI), and β-lg (WPI), which was expected based on the composition of the individual protein-stabilised interfaces (Figure 2.6). In the fresh WPI-PPI-stabilised emulsions at all ratios tested, the fraction of pea proteins at the interface exceeded that in the starting solution (37% at the interface for WPI-PPI 3:1 ratio, 60% for 1:1 ratio, and 79% for 1:3 ratio). After three days, the amount of adsorbed WPI significantly increased for the 3:1 and 1:1 WPI-PPI-stabilised interfaces (even though the total surface load was constant; Table 2.1), suggesting that some pea proteins were displaced by whey proteins. In the 3:1 WPI-PPI-stabilised emulsion, α-lac and β-lg significantly replaced vicilin major and minor subunits, whereas in the 1:1 emulsion, β-lg significantly replaced the vicilin major subunit at the interface. In general, the overall fraction of adsorbed pea and whey proteins did not significantly change over time in the 1:3 WPI-PPI emulsion, although there was a significant decrease of the vicilin minor subunit at the interface.

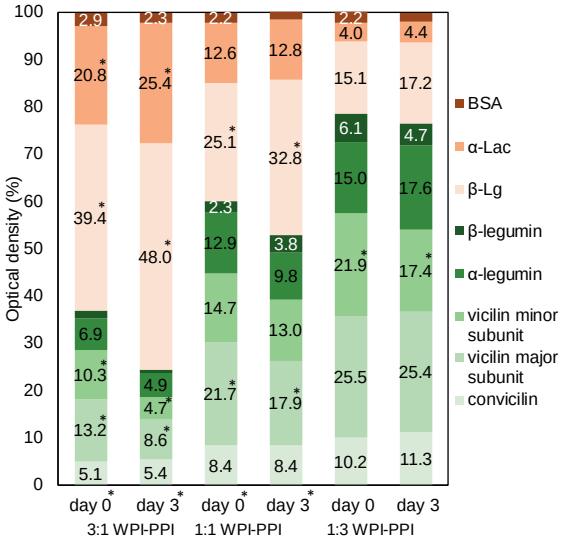

Figure 2.6. Interfacial composition of 3:1, 1:1 and 1:3 WPI-PPI-stabilised emulsions at day 0 and 3 determined with SDS-PAGE densitometry. Colours from light to dark for whey proteins (orange): β-Lg, α-Lac, BSA; For pea proteins (green): convicilin, vicilin major subunit, vicilin minor subunit, α-legumin, β-legumin. A star (*) indicates a significant difference ($p<0.05$) between day 0 and 3 for either the separate fractions or, when indicated at the bottom, for the whole adsorbed WPI or PPI fraction. For clarity, the numerical data corresponding to optical densities lower than 2% are not shown here, but can be found in Appendix, Table A2.3 E, together with the standard deviations for all protein fractions.

For the SC-PPI-stabilised emulsions (Figure 2.7), SC preferentially adsorbed for 1:3 and 1:1 blends (36% and 58% SC at the interface, respectively), but was partially replaced by PPI

over a period of three days. SC is a disordered protein that does not form an interconnected network at the interface, which makes it more prone to displacement compared to globular whey proteins (Dickinson, Rolfe, et al., 1989; Walstra et al., 1993). α- And β-casein can displace each other when adsorbed at an emulsion interface (Dickinson, Rolfe, et al., 1988), and from air-water interfaces in model systems, but they are both unable to displace adsorbed globular proteins (Dickinson, 2011), which is in line with the present findings. Displacement may lead to destabilisation if the pea proteins would be able to completely displace SC, since flocculation is expected to occur (Figure 2.3 and Figure 2.4) as found to a minor extend in the 1:3 SC-PPI-stabilised emulsion over 14-day storage. In the 3:1 SC-PPI-stabilised emulsion, even when not significant, the amount of adsorbed SC seemed to decrease.

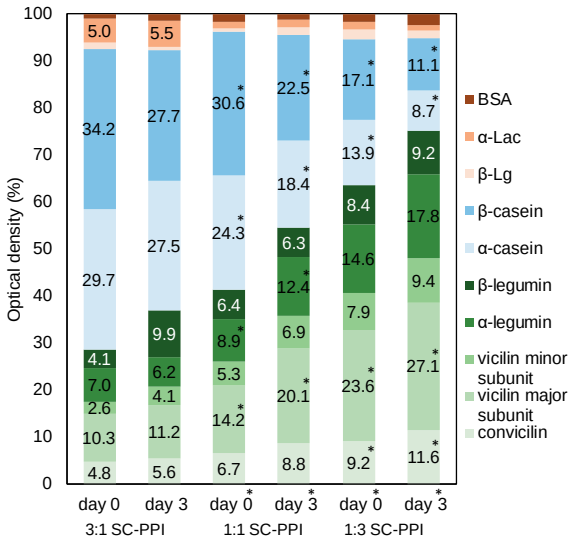

Figure 2.7. Interfacial composition of 3:1, 1:1 and 1:3 SC-PPI-stabilised emulsions at day 0 and 3 determined with SDS-PAGE densitometry. Colour represent from light to dark for caseins (blue): α-casein, β-casein and κ-casein; for pea proteins (green): convicilin, vicilin major subunit, vicilin minor subunit, α-legumin, β-legumin. A star (*) indicates a significant difference ($p<0.05$) between day 0 and 3 for either the separate fractions or when indicated at the bottom, for the whole adsorbed SC or PPI fraction. For clarity, the numerical data corresponding to optical densities lower than 2% are not shown here, but can be found in Appendix, Table A2.4, together with the standard deviations for all protein fractions.

With regard to protein displacement upon emulsion ageing, there were very clear differences between the different ratios of the SC-PPI and WPI-PPI blend-based emulsions. When looking at the interfacial composition in 1:3-WPI-PPI- and 3:1-SC-PPI-stabilised emulsions, the initially predominant proteins at the interface (pea proteins and SC, respectively) were not significantly displaced over time, suggesting that substantial displacement can only take

place under certain conditions. Using model interfaces, it was found that displacement of proteins by surfactants is initiated at defects in the protein network were surfactants can adsorb, referred to as nucleation sites (Mackie et al., 1999). For the protein-stabilised emulsions investigated in the present work it seems that the displacing protein has to be present at the interface in a high enough fraction, which could be related to the nucleation site hypothesis described earlier. Furthermore, the continuous phase concentration of the displacing protein may play a role and would depend on the protein ratio used. Dickinson et al. (1989) found that a β-lg-covered interface did not change when adding α-lac to the continuous phase with the same concentration, but when α-lac was added with a 10-fold higher concentration, β-lg was readily displaced from the interface (Dickinson, Rolfe, et al., 1989) For the 1:3 WPI-PPI and 3:1 SC-PPI-stabilised emulsions, whey or pea proteins, respectively, may not have been present at high enough concentrations for substantial displacement to occur.

Based on these results, one could conclude that whey proteins (β-lg) are able to displace pea proteins (vicilins), and vicilin is able to displace caseins, which could logically imply that whey proteins would displace caseins in a SC-WPI-stabilised emulsion. This was tested by preparing a 1:1 SC-WPI-stabilised emulsion, but the tested hypothesis was not confirmed; the interface consisted of equivalent amounts of both proteins (Figure 2.8), and its composition did not significantly change over a three-day period. Although in previous research a large preferential adsorption of SC (66%) over whey proteins (33%) was reported (Hunt et al., 1994), these authors mention that competitive displacement of SC by whey proteins could not occur due to the steric hindrance by adsorbed SC. The validity of this argument in the present case is, however, questionable, as PPI could readily displace part of the SC from the interface. In addition, displacement in SC-WPI-stabilised emulsions is probably also dependent on the ratio's used and in the present work only a 1:1 blend was tested. Alternatively, the fact that already 50% of the interface consisted of WPI (in contrast to 40% in the WPI-PPI-stabilised emulsion, could indicate that rapid rearrangement occurred directly after homogenisation. Interfacial displacement at such time scales thus seems to be typical for emulsions made with PPI blends, and we expect this to be specific for plant proteins due to their big quaternary structures that are composed of subunits that can exist as monomers, trimers (vicilin ~180 kDa) and hexamers (legumin ~260 kDa) (Barac et al., 2010; Dagorn-Scavinier et al., 1987; Klost et al., 2019; Lam et al., 2018) and may contain process

induced aggregates. The degree of association can unfortunately not be determined by SDS-PAGE in which only the dissociated subunits are detected.

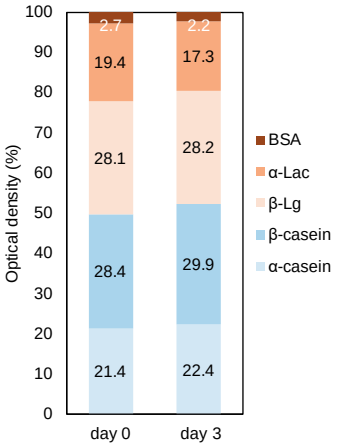

Figure 2.8. Interfacial composition of SC-WPI-stabilised emulsions at day 0 and 3 determined with SDS-PAGE densitometry. Colour represent from light to dark for whey proteins (orange): β-Lg, α-Lac, BSA; for caseins (blue): α-casein and β-casein. The adsorbed protein fractions at day 0 and 3 were not significantly different, the standard deviations are reported in Appendix, Table A2.5.

From the results presented here, it is clear that dairy proteins can be replaced to some extent by pea proteins and improving the physical stability of the emulsions, but displacement of adsorbed proteins occurs over time. This implies that when designing emulsions made with such protein blends, it is necessary to not only take the overall protein concentrations into account as would be the case for any emulsion, but to also consider displacement effects that can lead to synergistic or antagonistic effects, that may in turn enhance or reduce emulsion stability.

2.5. Conclusions

Our findings show that blends of PPI with SC or WPI can be used to produce emulsions with a physical stability that is superior compared to emulsions prepared with the individual proteins, suggesting synergistic effects. Such effects can be linked to the ability of the dairy proteins to prevent droplet flocculation, whereas in the SC-PPI-stabilised emulsions, pea proteins are expected to be efficient at preventing droplet coalescence. By interfacial composition analysis, we could confirm that both proteins co-exist at the interface in all blend-stabilised emulsions. However, the interfacial composition was possibly subjected to changes post-emulsification, depending on which proteins initially dominated the interface, and the concentrations in the continuous phase. When present in sufficiently high amount, whey proteins are able to displace pea proteins from the interface, and in turn, the latter are able to displace adsorbed caseins. Although, in the present conditions, such a compositional ageing of the interface was not adverse with regard to emulsion stability, it needs to be taken into account to understand the properties of such plant protein-based emulsions. This work illustrates the beneficial effects of using protein blends from a techno-functionality point of view, which is of great relevance for the current transition towards more plant-based foods.

2.6. Appendix

Table A2.1. The amino-acid and nitrogen content in the commercial pea protein isolate. The nitrogen conversion factor is calculated by dividing the total amino acid residues (g/100 g DM) by the nitrogen content in the amino acid residues (g/100 g DM) and used to calculate the protein concentration based on the nitrogen content as measured by Dumas (Flash EA 1112 series Dumas (Interscience, Breda, The Netherlands).

Total amino acid residues (g/100 g DM.)	61.3
Nitrogen content in the amino acid residues (g/100 g DM.)	10.9
Total nitrogen content by Dumas (g/100 g DM)	12.6 ± 0.75
Nitrogen conversion factor	5.6
Protein concentration (g/100 g DM.)	70.6 ± 4.2

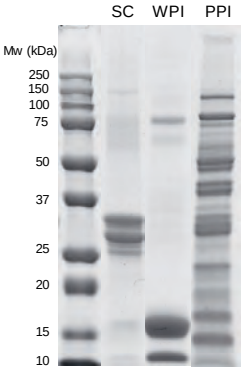

Figure A2.1. SDS-PAGE profiles under reducing conditions of SC, WPI and PPI solutions. The first lane on the left represents the molecular weight markers.

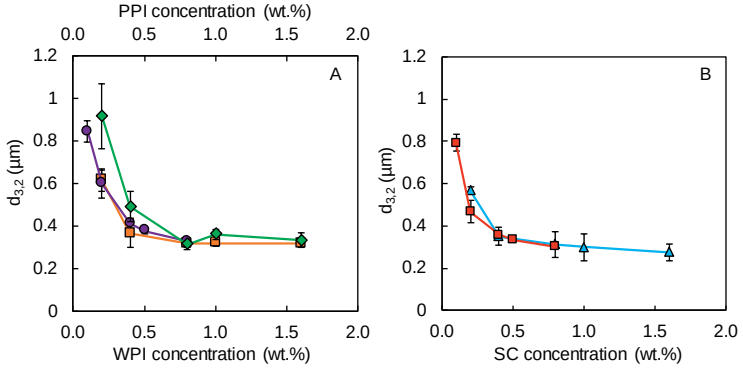

Figure A2.2. Surface volume diameter, $d_{3,2}$, after a twofold dilution in 1 wt.% SDS solution prior to the measurement as a function of A) WPI concentration in the starting aqueous solution for emulsions prepared with WPI (■) and 1:1 WPI-PPI (●), or pea protein concentration for the PPI-stabilised reference emulsion (◆); or B) SC concentration for emulsions prepared with SC (▲) and 1:1 SC-PPI (✖).

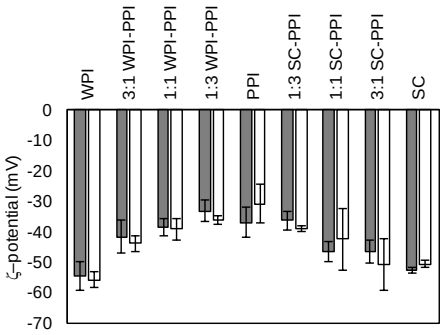

Figure A2.3. ζ–potential of the protein-stabilised emulsions at day 0 (grey bars) and day 14 (white bars)

Table A2.2. Interfacial composition of WPI-, SC- and PPI-stabilised emulsions at day 0 and day 3. κ-casein was not found at the interface in the SC-stabilised emulsions at day 3.

		Day 0		Day 3	
		optical density (%)	St dev.	Optical density (%)	St dev.
WPI	β-Lg	62.2	3.1	65.2	6.2
	α-Lac	34.5	1.9	33.2	5.9
	BSA	3.3	0.4	1.6	0.0
SC	α-casein	37.8	0.1	41.4	1.3
	β-casein	44.1	4.6	45.9	2.8
	κ-casein	4.5	0.8	-	-
	β-Lg	2.3	1.0	6.3	0.6
	α-Lac	5.4	1.0	1.8	0.5
	BSA	5.9	1.7	4.6	0.5
PPI	convicilin	11.4	1.0	10.7	0.3
	vicilin major subunit	27.1	1.6	28.5	3.0
	vicilin minor subunit	26.1	1.9	26.4	2.2
	α-legumin	20.1	1.6	18.7	2.4
	β-legumin	15.2	0.9	15.8	3.5

Table A2.3. Interfacial composition of WPI-PPI-stabilised emulsions at day 0 and day 3. A star (*) indicates a significant difference between day 0 and day 3 in the different fractions or, if indicated at the days, for the whole WPI and PPI fraction.

	3:1 WPI-PPI				1:1 WPI-PPI				1:3 WPI-PPI			
	day 0*		day 3*		day 0*		day 3*		day 0		day 3	
	optical density (%)	St dev.	optical density (%)	St dev.	optical density (%)	St dev.	optical density (%)	St dev.	optical density (%)	St dev.	optical density (%)	St dev
convicilin	5.1	0.3	5.4	0.0	8.4	1.2	8.4	1.7	10.2	0.5	11.3	0.9
vicilin major subunit	13.2*	0.5	8.6*	1.9	21.7*	1.7	17.9*	2.6	25.5	1.0	25.4	0.6
vicilin minor subunit	10.3*	1.9	4.7*	2.0	14.7	3.0	13.0	1.0	21.9*	1.6	17.4*	1.0
α-legumin	6.9	1.4	4.9	0.4	12.9	1.0	9.8	3.1	15.0	2.6	17.6	0.7
β-legumin	1.5	0.3	0.7	0.1	2.3	0.5	3.8	1.1	6.1	1.4	4.7	0.8
β-Lg	39.4*	3.8	48.0*	4.4	25.1*	2.6	32.8*	3.5	15.1	4.1	17.2	0.2
α-Lac	20.8*	0.5	25.4*	0.3	12.6	0.8	12.8	1.3	4.0	0.6	4.4	0.3
BSA	2.9	0.1	2.3	0.4	2.2	0.0	1.6	0.2	2.2	0.4	1.9	0.3

Table A2.4. Interfacial composition of SC-PPI-stabilised emulsions at day 0 and day 3. A star (*) indicates a significant difference between day 0 and day 3 in the different fractions or, if indicated at the days, for the whole SC and PPI fraction.

	3:1 SC-PPI				1:1 SC-PPI				1:3 SC-PPI			
	day 0*		day 3*		day 0*		day 3*		day 0		day 3	
	optical density (%)	St dev.	optical density (%)	St dev.	optical density (%)	St dev.	optical density (%)	St dev.	optical density (%)	St dev.	optical density (%)	St dev
convicilin	4.8	0.5	5.6	2.9	6.7	0.5	8.8	2.9	9.2*	0.3	11.6*	0.6
vicilin major subunit	10.3	2.2	11.2	0.2	14.2*	2.5	20.1*	3.8	23.6*	1.2	27.1*	0.1
vicilin minor subunit	2.6	1.2	4.1	1.3	5.3	1.2	6.9	0.9	7.9	0.8	9.4	0.5
α-legumin	7.0	0.4	6.2	2.2	8.9*	1.4	12.4*	1.7	14.6	0.2	17.8	0.5
β-legumin	4.1	3.4	9.9	2.1	6.4	0.2	6.3	0.8	8.4	0.3	9.2	0.6
β-Lg	29.7	2.1	27.5	5.3	24.3*	2.4	18.4*	4.1	13.9*	0.3	8.7*	0.0
α-Lac	34.2	3.0	27.7	5.8	30.6*	2.7	22.5*	4.1	17.1*	0.3	11.1*	0.4
BSA	1.3	0.2	0.8	0.9	0.5	0.6	1.7	0.1	2.2	0.2	1.6	0.1

Table A2.5. Interfacial composition of SC-WPI-stabilised emulsions at day 0 and day 3. No significant difference was found between the interfacial composition at day 0 and day 3.

	1:1 SC-WPI			
	day 0		day 3	
	optical density (%)	St dev.	optical density (%)	St dev.
α-casein	21.4	2.5	22.4	1.3
β-casein	28.4	3.9	29.9	1.6
β-Lg	28.1	3.2	28.2	0.6
α-Lac	19.4	3.0	17.3	0.6
BSA	2.7	1.1	2.2	0.7

Chapter 3

Behaviour of plant-dairy protein-blends at air-water and oil-water interfaces

This chapter has been published as Hinderink, E.B.A., Sagis, L., Schroën, K., Berton-Carabin, C.C. Behaviour of plant-dairy protein blends at air-water and oil-water interfaces. *Colloids Surfaces B Biointerfaces* **2020**, *192* (April), 111015. https://doi.org/10.1016/j.colsurfb.2020.111015.

3.1. Abstract

Recent work suggests that using blends of dairy and plant proteins could be a promising way to mitigate sustainability and functionality concerns. Many proteins form viscoelastic layers at fluid interfaces and provide physical stabilisation to emulsion droplets; yet, the interfacial behaviour of animal-plant protein blends is greatly underexplored. In the present work, we considered pea protein isolate (PPI) as a model legume protein, which was blended with well-studied dairy proteins (whey protein isolate (WPI) or sodium caseinate (SC)). We performed dilatational rheology at the air-water and oil-water interface using an automated drop tensiometer to chart the behaviour and structure of the interfacial films, and to highlight differences between films made with either blends, or their constituting components only.

The rheological response of the blend-stabilised interfaces deviated from what could be expected from averaging those of the individual proteins and depended on the proteins used; e.g. at the air-water interface, the response of the caseinate-pea protein blend was similar to that of PPI only. At the oil-water interface, the PPI and WPI-PPI interfaces gave comparable responses upon deformation and formed less elastic layers compared to the WPI-stabilised interface. Blending SC with PPI gave stronger interfacial layers compared to SC alone, but the layers were less stiff compared to the layers formed with WPI, PPI and WPI-PPI. In general, higher elastic moduli and more rigid interfacial layers were formed at the air-water interface, compared to the oil-water interface, except for PPI.

Graphical abstract

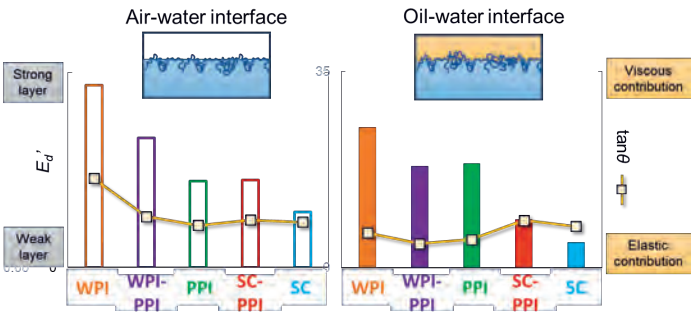

3.2. Introduction

Many food products are multiphase systems, such as foams and emulsions. These products often contain proteins, which are amphiphilic molecules that adsorb at the air-water or oil-water interface, and thereby play a crucial role in the formation and stability of the systems. Protein adsorption reduces the surface free energy, which facilitates small bubble and droplet formation during homogenisation; and next, proteins form an interfacial layer that protects bubbles and droplets against physical destabilisation, either by inducing steric/electrostatic repulsion, or by forming viscoelastic layers that mechanically prevent coalescence (Bos et al., 2001; Dickinson, 1999; McClements, 2004b). Foams and emulsions have a high specific surface area (i.e., are interface-dominated systems) and therefore their stability strongly depends on the protein's interfacial properties (Berton-Carabin et al., 2018; Sagis, 2011).

Surface activity (i.e., ability to increase surface pressure, or decrease interfacial tension) of the proteins is an important attribute in the droplet formation process but does not explain bubble and droplet stability over time. For this, dilatational rheological properties are relevant, as they directly affect the propensity of droplets to resist coalescence (Bos et al., 2001; Murray, 2011). The interfacial properties of dairy proteins (i.e., caseins and whey proteins) have already been widely studied. The flexible caseins tend to adsorb rapidly at the interface but the resulting film elasticity is low due to the lack of intermolecular protein interactions (Dickinson, 2001; Graham et al., 1979a, 1980). In comparison, globular dairy proteins such as bovine serum albumin (BSA), lysozyme and β-lactoglobulin (β-lg) adsorb slower but form stronger viscoelastic films, which is attributed to their ability to form densely packed monolayers with in-plane protein-protein interactions at both the air- and oil-water interface (Dickinson, 2011; Williams et al., 1996).

Proteins from legume plants such as soy and pea are gaining interest as more sustainable protein sources, and the interfacial properties of their main constituents have also been investigated. For soy, that is glycinin and β-conglycinin (Keerati-u-rai et al., 2012; Martin et al., 2003; Ruíz-Henestrosa et al., 2007; Wagner et al., 1999); and for pea, vicilin and legumin (Dagorn-Scavinier et al., 1986, 1987). Soy proteins have been shown to adsorb slowly at the air- and oil-water interface due to their compact and large structure, as a result of hydrophobic intermolecular interactions (Santiago et al., 2008). Recent work also showed that the soluble fraction of soy or pea proteins forms interfacial layers with an elasticity close to that of whey protein-based films, at a stripped oil-water interface, but the layers were less interconnected

and less stretchable (Ho et al., 2017). Yet, when used in emulsions, soluble pea proteins were outperformed by dairy proteins, i.e., the former lead to larger and less physically stable droplets (Hinderink et al., 2019).

Using blends of plant and dairy proteins might be the solution to strive for sustainability while not compromising technological functionality. In contrast to mixtures of proteins from the same biological origin (e.g., casein and whey protein), the interfacial behaviour of plant-dairy proteins has been studied only scarcely. Blending soy or pea proteins with whey proteins or sodium caseinate led to interfacial elasticities at the stripped oil-water interface between those of the individual proteins, suggesting that both proteins contributed to the elasticity of the interfacial film (Ho et al., 2018). However, the underlying film structure and protein interactions are not yet understood.

Interfacial behaviour is often characterised with a Langmuir trough or an automated drop tensiometer (Sagis & Fischer, 2014) that both allow for surface pressure to be followed over time, as well as for interfacial dilatational rheology to be studied. A Langmuir trough can also be combined with ellipsometry to record film thickness (Möbius et al., 1998; Wilde et al., 2004), and to construct Langmuir-Blodgett (LB)-films of which the structural heterogeneity can be assessed by atomic force microscopy (AFM) (Sagis et al., 2019). The advantage of LB-films in combination with AFM is the length scale at which the interfaces are studied, typically the nanometer scale (Bernardini et al., 2013; Dickinson, 2011), which is relevant to the size of protein molecules and small supramolecular structures.

The range of available techniques to study the oil-water interface is more limited than for the air-water interface, and consequently, emulsifying properties are often related to air-water interface measurements. Protein adsorption and interfacial rheology have already been compared for air- and oil-water interfaces, leading to contradictory conclusions. Williams & Prins (1996) reported no difference in the elastic moduli for β-casein and β-lg at the oil- or air-water interface. Krägel et al. (2003) (for β-lg) and Santiago et al. (2008) (for soy proteins) found a faster increase of the surface pressure at the oil-water interface compared to the air-water interface, which they linked to facilitated protrusion of the hydrophobic parts of the protein into the oil phase. As a result, thicker adsorbed layers were formed compared to the air-water interface, onto which proteins spread more which led to thinner layers showing smaller changes in surface pressure (Krägel et al., 2003). The difference between data recorded at air- or oil-water interfaces is not surprising, when considering the fact that protein

adsorption at the oil-water interface already varies for different oil types, with more polar oils inducing less protein unfolding, which results in lower surface pressures and slower interfacial network formation (Bergfreund et al., 2018).

Herein, we aim to understand the protein-protein interactions at the interface, and the interactions of the proteins with the adjoining bulk phases to design well-defined plant-dairy protein films. We considered whey protein isolate (WPI) and sodium caseinate (SC) as dairy proteins, and the soluble fraction of pea protein isolate (PPI) as plant protein source. The individual proteins and their 1:1 (w/w) blends were extensively studied at the air-water interface (Langmuir trough, LB-films + AFM, ellipsometry, automated drop tensiometer) and at the stripped sunflower oil-water interface (automated drop tensiometer).

3.3. Materials and methods

3.3.1. Materials

WPI, purity 94% (BiPro®, Davisco, Switzerland), SC, purity 97% (Excellion™, Sodium Caseinate S, Friesland Campina, the Netherlands), PPI, (NUTRALYS s85F, Roquette, France; see Appendix Table A2.1, Chapter 2 for the amino acid composition and content, and protein content), were used as received. Sodium phosphate dibasic (Na_2HPO_4), sodium phosphate monobasic (NaH_2PO_4) were purchased from Sigma Aldric (Saint Louis, USA). The soluble protein concentration was determined using a bicinchoninic acid (BCA) kit (BCA1-1 KT, Sigma- Aldrich, Saint Louis, USA). Sunflower oil was purchased from a local supermarket and stripped with Florisil (Sigma-Aldrich, 20,281, Supelco, 100–200 mesh) to remove surface-active impurities, as described previously (Berton et al., 2011). Ultrapure water was obtained from a Milli-Q system (Millipore Corporation, Billerica, Massachusetts, US) and used for all the experiments.

3.3.2. Preparation of aqueous phases

WPI and SC (1 wt.%) were dissolved in a 10 mM phosphate buffer (pH=7.0) and stirred overnight at 4 °C. PPI was dispersed in the same buffer (6 wt.%) and stirred for at least 48 h at 4 °C. The insoluble part was removed by centrifugation (16,000 x *g*, 30 min), and the supernatant was re-centrifuged in similar conditions, after which the second supernatant was collected and used for the experiments. A BCA assay (Smith et al., 1985) was used to determine the protein content of the supernatant, as described previously (Hinderink et al., 2019). The protein solutions were diluted to 1 g/L for air-water measurements, or 0.1 g/L for oil-water measurements.

3.3.3. Automated drop tensiometer measurements

The interfacial tension between air or stripped sunflower oil and the protein solutions in 10 mM phosphate buffer was measured with an automated drop tensiometer (Tracker, Teclis, Longessaigne, France). A pendant drop was used for the air-water measurements, a rising drop for the oil-water experiments (i.e., a drop of oil was immersed in a cuvette filled with the protein solution) using 20-gauge needles. SC, WPI, and PPI were tested individually as well as 1:1 (w/w) plant-dairy protein blends. The interfacial tension was recorded for 3.5 h at 20 °C, using a drop area of 15 mm^2 for the air-water experiments, and 30 mm^2 for the oil-

water experiments. The interfacial tension was calculated based on the shape of the droplet using the Laplace equation (Benjamins et al., 1996).

After 3.5 h, amplitude sweeps were performed with a constant frequency of 0.1 Hz. The droplet interface was compressed and expanded in a sinusoidal way, ranging from 5 to 30% deformation. In the frequency sweep experiments, the oscillation frequency was varied from 0.002 to 0.1 Hz, while the amplitude was kept constant (5%). For both the amplitude and frequency sweeps, 5 deformation cycles were done, after which 5 rest cycles were applied before the next deformation started. The oscillating surface tension signal was analysed with a Fast Fourier transform, and the intensity and phase of the first harmonic was used to calculate the dilatational elastic modulus (E_d') and the dilatational viscous modulus (E_d") according to equations 3.1 and 3.2.

$$E_d' = \Delta\gamma \left(\frac{A_0}{\Delta A}\right) \cos\delta \qquad 3.1$$

$$E_d'' = \Delta\gamma \left(\frac{A_0}{\Delta A}\right) \sin\delta \qquad 3.2$$

Here $\Delta\gamma$ is the difference in interfacial tension, A_0 the initial droplet/bubble area, ΔA the amplitude of change in area, and δ the phase shift of the oscillating interfacial tension signal, compared to the induced area change. This first harmonic-based analysis is accurate in the linear response regime. Outside this regime, higher harmonics are present that can be analysed by Lissajous plots in which the change in surface pressure ($\pi=\gamma-\gamma_0$) is plotted against the oscillating deformation signal (30%) (Sagis & Scholten, 2014).

3.3.4. Structural organization of interfacial films

Langmuir isotherms and Langmuir Blodgett films were made at the air-water interface using a KSV NIMA Langmuir trough (medium size, 364 x 76 mm, Biolin Scientific, Espoo, Finland). Buffer was used as substrate and 34 µL of 1 g/L protein solution were spread on the surface. The interfacial layer was equilibrated for 30 min before barriers were closed at a speed of 5 mm/min. Langmuir-Blodgett (LB) films were deposited on a freshly cleaved mica plate that was immersed into the sub phase before the proteins were spread. The films were loaded at a surface pressure of 20 mN/m, with an upward speed of 1 mm/min. They were next dried in a desiccator at least overnight prior to analysis with an atomic force microscope (AFM; MultiMode 8-HRTM, Bruker, Billerica, US). Images were recorded in the tapping

mode using non-conductive pyramidal silicon nitride probes with a nominal spring constant of 0.40 N/m (Bruker, Billerica, US). A lateral scan frequency of 0.977 Hz was used, and the resolution was set at 512 x 512 pixels in a scan area of 2 x 2 μm^2. The AFM images were analysed with NanoScope Analysis 1.5 software.

Film thickness at the air-water interface was measured using an imaging ellipsometer nanofilm EP4 (Accurion GmbH, Goettingen, Germany) in combination with a KSV NIMA Langmuir trough (size, 580 x 145 mm, Biolin Scientific, Espoo, Finland). The trough was filled with phosphate buffer (10 mM) and 200 µL of 1 g/L protein solution were spread on the surface. The interfacial layer was equilibrated for 30 min before barriers were closed at a speed of 5 mm/min until the desired surface pressure was reached. The ellipsometric angles Ψ and Δ were measured at different wavelengths using a filter wheel from 499.8-739.8 nm, and an exposure time of $1.5 \cdot 10^5$ ms. Buffer without proteins was measured five times and used to determine the refractive index, n and extinction coefficient, k, and a Cauchy distribution was used to calculate the film thickness.

3.3.5. Experimental design

All measurements were performed in at least independent duplicates. The LB-films were imaged at least at two locations per film.

3.4. Results and discussion

3.4.1. Air-water interface

Adsorption kinetics and surface activity

The increase in air-water surface pressure for the individual proteins and protein blends was monitored in time using an automated drop tensiometer (Figure 3.1A). The surface pressure first rapidly increased, followed by a phase of slower increase, and subsequently even slower increase, which has be linked to binding, unfolding and reorganization of proteins at the interface, respectively (Beverung et al., 1999). Clear differences were found between the individual proteins; at the end of the experiment, PPI-stabilised interfaces showed the highest surface pressure of 28.8 ± 0.8 mN/m, SC was at 25.9 ± 0.8 mN/m, and WPI was the lowest at 23.3 ± 1.3 mN/m. However, initially SC increased the surface pressure the fastest (Appendix, Figure A3.1), followed by PPI and WPI. WPI consists of the globular proteins α-lactalbumin (α-lac) and β-lactoglobulin (β-lg), whereas caseins have no secondary or tertiary structure and therefore adsorb and spread fast at the interface because less rearrangements occur (Maldonado-Valderrama et al., 2005). Pea proteins adsorbed rapidly and increased the surface pressure the most over the measured time scale, which is probably related to their greater hydrophobicity compared to dairy proteins, imparting them with a higher driving force for adsorption (Wierenga et al., 2003). The WPI-PPI blend-stabilised interface followed the surface pressure curve of the PPI-stabilised interface until a surface pressure of 29.0 ± 1.3, which could be indicative of a preferential adsorption of pea proteins. For the SC-PPI blend-stabilised interface, the surface pressure increased faster compared to PPI and SC alone, and (30.1 ± 0.8 mN/m) than SC only, indicating that protein adsorption seems to be accelerated and enhanced in the blend.

In the Langmuir trough, proteins were spread at the interface and subsequently compressed, which opposes the previously described experiments where film formation was driven by protein diffusion. The surface pressure isotherms differed for the individual proteins (Figure 3.1B). Upon compression of the whey protein monolayer, the surface pressure first increased linearly (looking from right to left, i.e., while decreasing surface area), after which the increase levelled off, indicating that the adsorbed proteins interacted and changed conformation. In contrast, the pea protein film gave a linear response upon compression, indicating no specific interaction between proteins. For SC, the lowest surface pressure

values were obtained; the surface pressure levelled off at 20 mN/m and only further increased to 21.7 ± 0.1 mN/m, which is close to the equilibrium spreading pressure of 22 mN/m for β-casein (Graham et al., 1979b).

The isotherm for the WPI-PPI blend showed a lower increase in surface pressure compared to the one for WPI, but both were similar in shape, which suggests that whey proteins dominate the film behaviour. The isotherm for SC-PPI first showed a linear increase in surface pressure, after which a plateau was reached at a surface pressure around 21 mN/m, followed by a second linear increase when compressing further, which makes this isotherm rather different from those of the individual constituent proteins. The plateau value was comparable to that of SC, which makes us believe that the surface pressure response of this blend was initially dominated by SC up to a value of 21 mN/m, after which the contribution of pea proteins became more prominent.

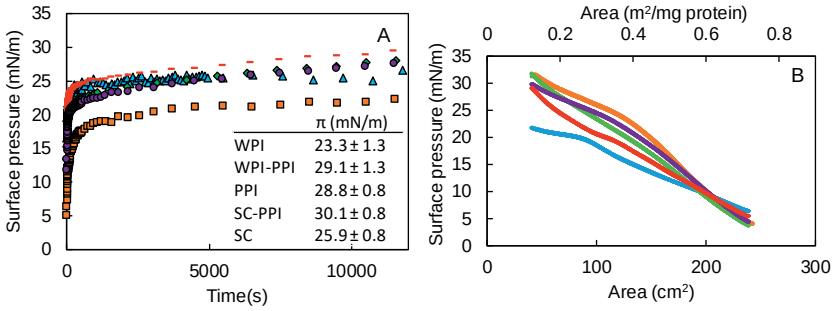

Figure 3.1. A) Surface pressure using a pendant drop in an automated drop tensiometer at protein concentration 1g/L at the air-water interface over time measured for WPI (■), SC (▲), PPI (◆) 1:1 SC-PPI (▬) and 1:1 WPI-PPI (●), the table reports the 'equilibrium' interfacial tension and B) Surface pressure isotherm of the individual proteins and their blends at the air-water interface measured by Langmuir trough for WPI (orange), SC (blue), PPI (green), 1:1 WPI-PPI (purple) and 1:1 SC-PPI (red). For clarity, one representative curve is shown per sample, but similar results were obtained on multiple independent replicates.

Interface structural organization

To further characterise the physical properties of the protein films involved in the surface pressure isotherm experiments, film thickness as a function of surface pressure was determined using an ellipsometer in combination with a Langmuir trough. At a surface pressure of 20 mN/m, SC formed the thickest layer (3.7 ± 0.15 nm), followed by SC-PPI (3.4 ± 0.28 nm), PPI (3.1 ± 0.14 nm), WPI-PPI (2.9 ± 0.07nm) and WPI (2.1 ± 0.07). Compression of the interfacial layer led to an increase in film thickness, along with the previously described increase in surface pressure, for all systems tested. For SC, even though the surface pressure

levelled off from a certain compression level, the film thickness may have increased due to molecules stacking below the primary monolayer (Graham et al., 1979b), albeit rather loosely due to the disordered structure of the caseins. Interestingly, the SC-PPI-stabilised interface was able to reach a surface pressure of 26 mN/m and was thicker (5.5 ± 0.71 nm) compared to the PPI-based layer (4.8 ± 0.64 nm). This suggests that when present in this blend, SC remains at the interface together with the pea proteins, which is also confirmed by the high surface pressures reported in Figure 3.1A, and linked to faster increase of the surface pressure, which has been related to thicker interfacial layers (Benjamins, 2000; Krägel et al., 2003).

It should be pointed out that ellipsometer data reflect an average film thickness; when looking at the LB films constructed at 20 mN/m (Figure 3.3) it is clear that all films are structurally heterogenous. In these LB films, a noticeable difference occurs between WPI, PPI or WPI-PPI (both globular proteins) and SC or SC-PPI (containing disordered SC); films containing SC show some large clusters, whereas in all other films the clusters are smaller. At low surface pressures, caseins spread at the interface (< 20 mN/m) but upon compression loops are formed in the aqueous phase (Graham et al., 1979b; MacRitchie, 1998). The large clusters in the SC-containing LB films may thus correspond to protein material protruding into the aqueous phase as induced by the compression process. Structural heterogeneity is common in protein films, as found for e.g., β-lg (Rühs et al., 2013), β-casein (Berton-Carabin et al., 2013) and WPI (Yang et al., 2020) and oxidative modified PPI (Hinderink, Kaade, et al., 2020).

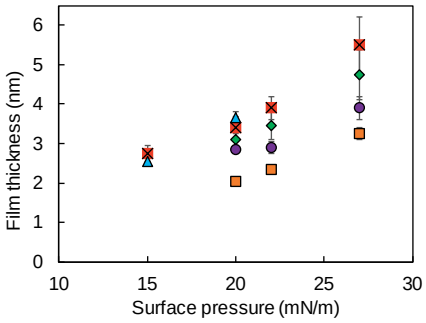

Figure 3.2. Film thickness for WPI (■), SC (▲), PPI (◆) 1:1 SC-PPI (⊠) and 1:1 WPI-PPI (●) at the air-water interface as function of the surface pressure. Error bars represent the standard deviation of multiple measurements on at least two independent replicates.

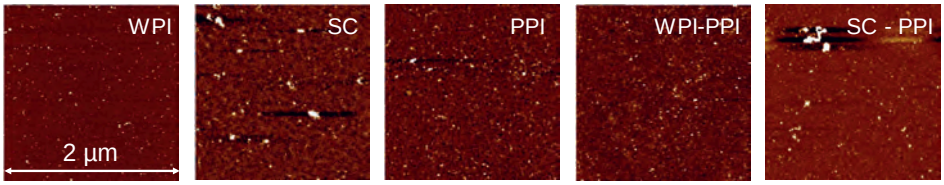

Figure 3.3. AFM images of LB films prepared with the individual proteins (WPI, SC, PPI) and their blends. LB films are constructed at the air-water interface at a surface pressure of 20 mN/m, and imaged after drying at room temperature. The overall layer height is up to 5.3 nm, with black representing the lowest areas and white the highest ones. For clarity, one representative image is shown per sample, but similar results were obtained on multiple independent replicates.

Interface rheological properties

Oscillatory dilatational amplitude sweeps (sinusoidal deformation 5-30%) at a frequency of 0.01 Hz were performed after an adsorption and equilibration time of 3.5 h. Elastic (E_d') and viscous (E_d") moduli were calculated from the oscillatory data and plotted as function of the applied deformation amplitude. For all proteins tested, elastic moduli (Figure 3.4A) were substantially higher than viscous moduli (Appendix, Figure A3.2).

The elastic moduli of the WPI-stabilised air-water interface decreased from 56 mN/m at 5% deformation to 21 mN/m at 30% deformation (Figure 3.4A). This strain dependence of the elastic modulus indicates that the interfacial network weakened upon deformation, which can be attributed to the ability of β-lactoglobulin to form disulphide linkages in a highly interconnected network, that weakens upon deformation (Dickinson et al., 1990). The strain dependence was less for WPI-PPI- (E_d' only varied from 25 to 20 mN/m) and not present in PPI-, SC-, and SC-PPI-stabilised interfaces. The elastic moduli of the SC-stabilised interface were below 10 mN/m, which made them the weakest among all proteins tested. This can be explained by the fact that casein monolayers are loosely packed with weak protein-protein interactions (Dickinson, 2001). However, when SC was combined with PPI, the values for E_d' were similar to those recorded for interfaces with PPI only, which implies that either PPI dominates the SC-PPI-stabilised interface, or interactions occur between the PPI and SC, leading to a response similar to that of PPI. For WPI-PPI-stabilised interfaces, the elastic moduli are in between those of WPI- and PPI-based layers, suggesting the presence of both proteins at the interface.

Oscillatory dilatational frequency sweeps (0.002-0.05 Hz) were performed at fixed amplitude of 5%. Again, elastic moduli were higher than viscous moduli, and only the elastic moduli are reported as function of frequency, on a double logarithmic scale (Figure 3.4B). WPI

formed the most elastic layer (highest E_d') followed by WPI-PPI, SC-PPI and PPI, whereas SC formed the layer with the lowest E_d', which is in line with the amplitude sweep results. The slope of the double logarithmic plot of elastic moduli as function of frequency was around 0.1, which is typical for soft glassy interfaces, and implies that the contribution of diffusional exchange of protein between the bulk and the interface to the response is negligible (van Kempen et al., 2013).

To understand these effects in a more detailed way, Lissajous plots were used, that show the surface pressure as a function of the deformation during oscillatory dilatational experiments, and thus provide information about the interfacial network behaviour in extension and compression. The advantage of Lissajous plots is that nonlinear effects are not neglected, and they thus give a richer impression of surface behaviour, as compared to simply calculating moduli. In brief, a linear shape of the Lissajous plot indicates a purely elastic behaviour, and a spherical shape a viscous behaviour of the interface. Linear viscoelastic responses result in an ellipse-shaped plot, and non-linear behaviour leads to asymmetric shapes (Sagis & Scholten, 2014), as shown in Figure 5 top left. All systems tested gave predominantly elastic responses upon 30% deformation i.e., $\Delta A/A_0$=0.3 (Figure 5) but also showed asymmetries that are indicative of a nonlinear response, even when the apparent modulus appeared to be strain independent. This clearly indicates the benefit of Lissajous plots over the first harmonics approach.

SC, PPI, and SC-PPI-stabilised interfaces gave a nonlinear viscoelastic response, dominated by elasticity (narrow ellipse). At the start of extension (the lower left corner of the plot, at $\Delta A/A_0$= -0.3) the surface pressure first increased, after which it levelled off towards maximum extension ($\Delta A/A_0$= +0.3). This is a signature of interfacial strain softening in extension, due to disruption of the interfacial microstructure. Upon compression the reverse phenomenon happened, which indicates strain stiffening due to increased surface density of clustered protein regions, approaching a jammed state (Sagis & Fischer, 2014). This strain softening in extension and strain hardening upon compression is typical for protein-stabilised interfaces. For the SC-stabilised interface, lower surface pressures compared to PPI- and SC-PPI-stabilised interfaces were found at maximum extension, but similar surface pressures at maximum compression. We reported earlier a thicker interfacial layer (Figure 3.2), and higher surface pressure (Figure 3.1A) for the SC-PPI blend compared to its individual counterparts. Combining this with the Lissajous plot results allows us to conclude that

enhanced protein adsorption in this specific blend has led to the improved dilatational elasticity compared to SC only, that does however not surpass that of PPI only.

WPI-stabilised interfaces are more viscous than the others (also seen in the loss moduli in Appendix, Figure A3.2), and the plot is relatively wide at the lower left part as a result of yielding of the surface microstructure upon the start of the extension. It is clear from the apparent moduli reported in Figure 4A that the WPI-stabilised interfaces are the stiffest (due to stronger in-plane protein-protein interactions). When a certain surface stress is exceeded the microstructure yields, and starts to flow towards maximum extension when the slope approaches almost zero, indicating a predominantly viscous response. The shape of the Lissajous plot is typical for WPI-stabilised air-water interfaces as recently reported by (Yang et al., 2020). The interface based on the WPI-PPI blend showed a more elastic response compared to PPI alone, with strain softening in extension and strain stiffening in compression, and a less viscous behaviour compared to WPI. The plot suggests that both proteins were present at the interface, which could not be that clearly concluded from Figure 3.1A.

To conclude, blending PPI with SC gave a synergistic behaviour at the air-water interface, in the sense that PPI helped retaining SC at the interface upon compression, and increased the interfacial elasticity compared to SC alone. In contrast blending PPI with WPI hindered the formation of an interconnected network, typical for WPI-stabilised interfaces.

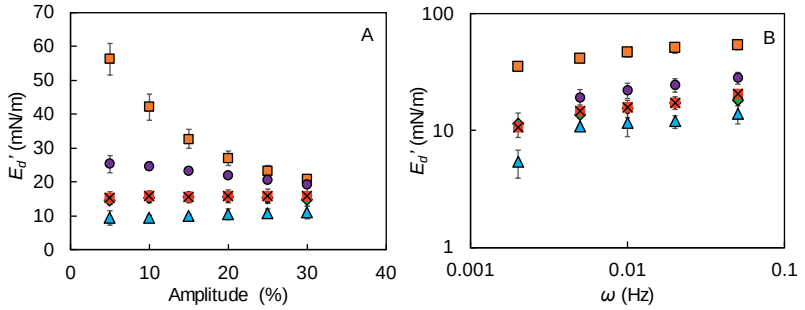

Figure 3.4. Apparent dilatational elastic moduli (Ed') at the air-water interfaces stabilised by WPI (■), SC (▲), PPI (◆) 1:1 SC-PPI (☒), and 1:1 WPI-PPI (●) blend A) as a function the applied deformation (frequency, 0.01 Hz) and B) as a function of the applied frequency (amplitude, 5%). Error bars represent the standard deviation of multiple measurements on at least two independent replicates.

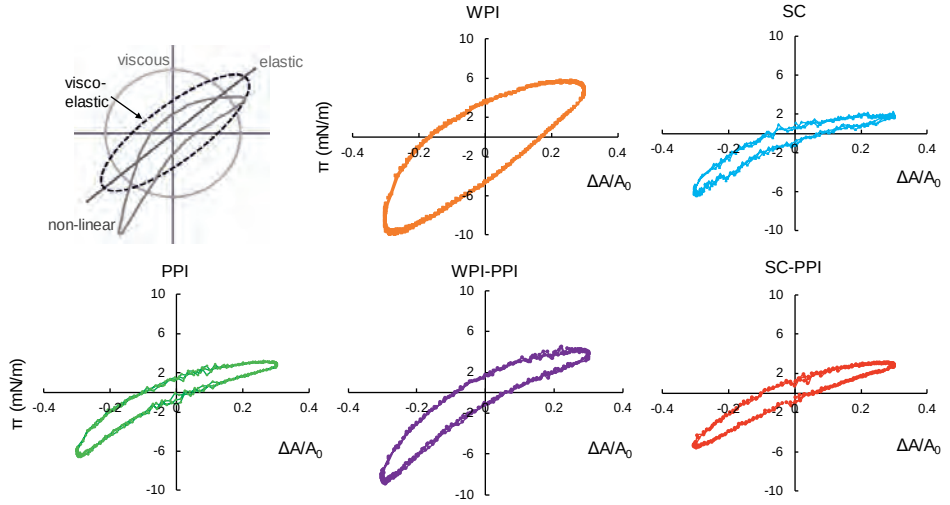

Figure 3.5. Example of Lissajous plots depicting viscous, elastic, viscoelastic and non-linear viscoelastic interfaces in top left; and Lissajous plots at 30% dilatational deformation and oscillation frequency at 0.01 Hz at the air-water interface for WPI (orange), SC (blue), PPI (green), 1:1 WPI-PPI (purple) and 1:1 SC-PPI (red). For clarity only one replicate is shown, but similar results were obtained for at least independent duplicates.

3.4.2. Oil-water interface

Adsorption kinetics and interfacial activity

At the oil-water interface, layers made of pure PPI or SC led to the highest surface pressure (~18 mN/m), and WPI to the lowest (~17 mN/m) (Figure 3.6), with SC increasing surface pressure the fastest (Figure 3.6). The curve corresponding to the WPI-PPI-stabilised interface was initially between those of the WPI- and PPI-stabilised interfaces, and towards the end of the measurement, closer to that of pure WPI. The curve corresponding to the SC-PPI-stabilised interface was in between those of the SC and PPI-stabilised interfaces, but eventually a similar pseudo-equilibrium surface pressure was reached for PPI, SC and SC-PPI-stabilised interfaces. For all protein systems tested, the surface pressure increased less at the oil-water interface than at the air-water interface (Figure 3.1A). Please keep in mind that oil-water interface experiments were performed at 0.1 g/L protein solution whereas for the air-water it was 1 g/L, which implies that the local protein concentration in the immediate vicinity of the interface differed by one order of magnitude.

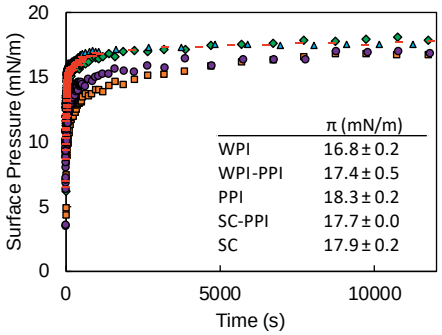

Figure 3.6. Surface pressure over 3.5 hours (the insert table gives pseudo-equilibrium interfacial tension, i.e., the average of the last 20 points) for whey protein (WPI, ■), sodium caseinate (SC, ▲), pea protein (PPI, ◆), 1:1 whey protein-pea protein blend (WPI-PPI, ●) and 1:1 sodium caseinate-pea protein blend (SC-PPI, –) at the stripped sunflower oil-water interface. For clarity, one representative curve is shown per sample, but similar results were obtained on multiple independent replicates.

Interface rheological properties

At the oil-water interface, the apparent elastic moduli of the WPI-, PPI- and WPI-PPI-stabilised layers decreased upon deformation (Figure 3.7). This strain dependence was the strongest for the WPI-based layer, which showed a decrease from 32 to 18 mN/m, and the lowest for PPI and WPI-PPI (i.e., decrease from 20 to 16 mN/m for both). The SC-PPI- and SC-stabilised interfaces were the weakest with elastic moduli of 8.5 and 4.5 mN/m, respectively, and no strain dependence, indicating weaker in-plane protein interactions for these systems. The elastic moduli of all interfaces were lower at the oil-water interface compared to the air-water interface (Figure 3.4) except for the PPI-stabilised interface, which had an elastic modulus of 15 mN/m and no strain-dependence at the air-water interface. Remarkably, the WPI-PPI-stabilised layers exhibited the same moduli as the PPI-stabilised ones, which was not the case at the air-water interface, and indicates that either only pea proteins adsorbed, or the structure and interactions within the film are similar with the blend or PPI alone.

Oscillatory dilatational frequency sweeps (0.002-0.05 Hz) were performed at a fixed amplitude of 5%, and the elastic moduli were plotted as function of applied frequency on a double logarithmic scale (Figure 7B). Whey proteins formed the most elastic layer (highest E_d'), followed by WPI-PPI and PPI, SC-PPI, and SC as the lowest, which is in line with the amplitude sweep results. For WPI-, PPI- and WPI-PPI-stabilised interfaces a slope close to 0.1 was found, which implies that the contribution of diffusion from the bulk to the interface was negligible, as explained earlier (van Kempen et al., 2013). For the SC- and SC-PPI-

stabilised interfaces, the slope was 0.25, indicating that diffusion-controlled processes may have contributed to the response to deformations, which is different from the findings at the air-water interface. It was reported that β-casein increased the surface pressure faster at the oil-water interface compared to the air-water interface, which was related to the possibility of the protein to penetrate into the oil phase with its longer hydrophobic chain, leaving only a short hydrophilic tail interacting with the water phase (Kotsmar et al., 2010).

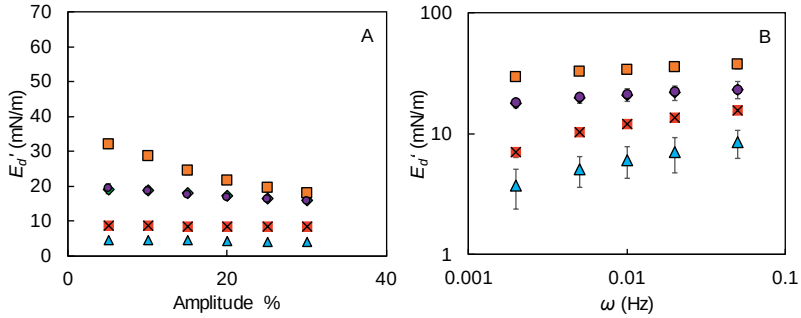

Figure 3.7. Apparent dilatational elastic moduli (E_d') at the oil-water interfaces stabilised by WPI (■), SC (▲), PPI (◆) 1:1 SC-PPI (⊠) and 1:1 WPI-PPI (●) blend A) as a function of the applied deformation (frequency, 0.01 Hz) and B) as a function of the applied frequency (amplitude, 5%). Error bars represent the standard deviation of multiple measurements on at least two independent replicates.

The surface pressure as a function of the deformation (amplitude equal to 30%) was plotted in Lissajous plots for all systems tested (Figure 3.8), and showed strain softening in extension and strain hardening upon compression, with clear differences between the interfaces. The WPI-stabilised interface was predominantly elastic, as seen from the narrow shape of the plot, and the Lissajous plot was similar to previous ones reported in literature (Berton-Carabin et al., 2016; Ho et al., 2018). For the PPI-stabilised interface, the lower left part of the graph has a pointy shape, which means that upon compression and subsequent extension a similar response in surface pressure was measured, indicative of weak in-plane attractive interactions. When such interactions are strong, the densification induced by the compression can lead to a significant increase in the stiffness of the structure, which then results in a steep slope of the Lissajous plot upon extension of the interface (compare to WPI at the air-water interface, which shows strong protein-protein interaction, in Figure 5). The Lissajous plot of the WPI-PPI-stabilised interface showed the same response upon deformation, which may be interpreted as PPI dominating the interface, although that is not that likely since the surface pressure of WPI-PPI is very close to that of WPI (Figure 3.6). Most likely, both proteins are

at the interface, with pea proteins hindering whey protein network formation, resulting in a less interconnected and less elastic interface compared to whey protein-based layer with dilatational properties similar to those found for PPI only.

The SC-stabilised oil-water interface gave an almost linear viscoelastic response with almost no strain softening nor hardening in extension and compression. This, together with the relatively high exponent found in the frequency dependence, indicates that the in-plane interactions are too weak to induce network formation, and that the response is dominated by exchange of SC between bulk and interface. For the SC-PPI-stabilised interface, an extremely narrow plot was obtained, for which the slope levels off in extension, and increases in compression. As observed for the air-water interface, in-plane network formation did not occur, and the surface concentration of the proteins merely increases upon compression and decreases upon extension. The resulting changes in the surface tension led to a plot resembling a curved line.

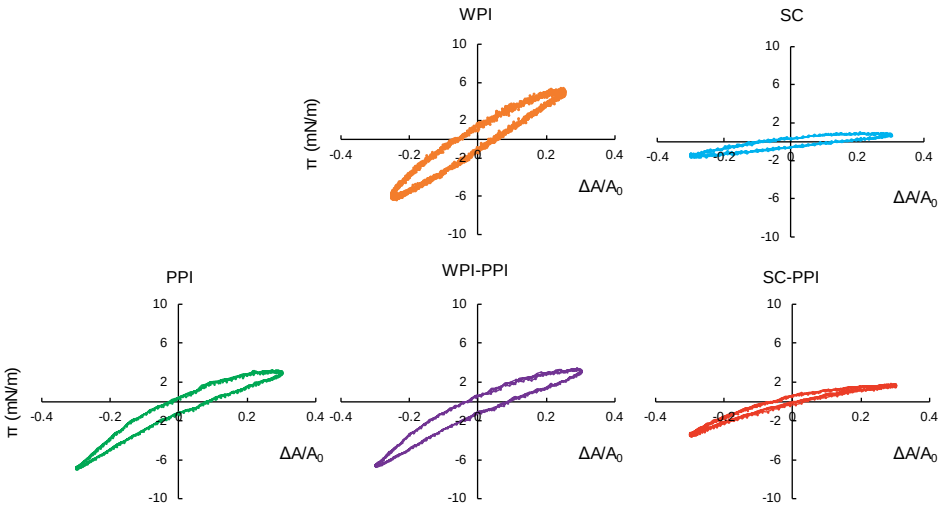

Figure 3.8. Lissajous plots at 30% dilatational deformation and oscillation frequency at 0.01 Hz at the oil-water interface for WPI (orange), SC (blue), PPI (green), 1:1 WPI-PPI (purple) and 1:1 SC-PPI (red). For clarity only one replicate is shown, but similar results were obtained for at least independent duplicates.

Our results put in a wider perspective

In literature, various effects have been described regarding protein adsorption and network formation at the oil- or air-water interfaces, and here we summarise them and use them to put into perspective the results that are reported herein. In general, it is assumed that globular proteins unfold at the interface with the oil-phase acting as a solvent for the hydrophobic

segments, which reduces the van der Waals cohesion between the apolar side chains of the proteins (Graham et al., 1979b). This also implies that globular proteins can unfold more at the oil-water compared to the air-water interface (Mitropoulos et al., 2014; Murray et al., 1996; Wüstneck et al., 1999). In the present study, elastic moduli were higher, except for PPI-stabilised interfaces, at the air-water interface, which may be explained by hydrophobic intra-protein interactions that are hindered by solvation in the oil phase (Wüstneck et al., 1999). Furthermore, it has been suggested that the solvent quality affects interfacial viscoelastic moduli. Benjamins et al. (2006) compared the interfacial elastic modulus of ovalbumin and β-lactoglobulin adsorbed at triacylglycerol-, hydrocarbon- or air-water interfaces, and found that triacylglycerol was the best solvent and air the worst. A strong correlation between the interfacial tension of the bare interface and interfacial elastic moduli was reported (Benjamins et al., 2006). It has to be noted that in that respect, an oil phase is not always a better solvent phase compared to air; higher elastic moduli of β-lg were found at the *n*-tetradecane interface compared to the air-water interface (Murray et al., 1998), and we also found that PPI gave higher moduli at the oil-water interface.

It has been suggested that the polarity of the oil is a good indication for the extent of protein unfolding, with more polar oils leading to less protein unfolding and less surface pressure changes (Bergfreund et al., 2018). Next to the decrease of hydrophobic interactions by solvation in the oil phase, there are also differences in the in-plane electrostatic repulsion between proteins for the two interfaces. The dielectric constant of air is approximately 1 (Benjamins et al., 2006), and that of sunflower oil about 3 (Prevc et al., 2013). That means that the electrostatic repulsion between the proteins (which has the nature of a dipole-dipole interaction because of the asymmetry in the counter-ion distribution) is shorter-ranged for the oil-water interface. This would result in increased attractive protein interactions, possibly leading to a higher modulus if this effect is larger than the reduction of attractive interactions due to improved solvent quality.

It is clear that in the tested blends, PPI hinders the formation of elastic WPI-layers at both interfaces, whereas it improved the elasticity of the SC-stabilised interface at both interfaces. When blending WPI with soy protein isolate (SPI), that by itself produces interfaces with lower moduli than WPI, this leads to interfaces that closely resemble those of pure WPI (Ho et al., 2018). This suggests that the interactions between SPI and WPI are stronger compared

to those between WPI and PPI reported herein, and that such interactions are highly protein- and blend-specific.

3.5. Conclusions

We investigated the interfacial properties of dairy proteins (WPI, SC), plant protein (PPI) and their 1:1 blends (WPI-PPI, SC-PPI) at the air- and oil-water interfaces (Appendix, Figure A3.3). At the air-water interface, WPI formed the thinnest layer that consists of an interconnected network with superior stiffness compared to all the other systems tested. Blending WPI with PPI decreased the layer elasticity compared to WPI alone, but gave a stronger layer compared to PPI alone. SC formed the weakest interfacial layer, and blending it with PPI improved the layer's mechanical strength. The SC-PPI interfacial layer had the same strength as the PPI-stabilised interface, and PPI was able to retain SC at the interface, therewith forming thicker layers compared to layers made of the individual counterparts. At the oil-water interface, PPI and WPI-PPI had a similar behaviour when subjected to dilatational deformation, and formed weaker layers compared to WPI. Blending SC with PPI gave stronger interfacial layers compared to SC alone, but the layers were inferior in stiffness compared to the layers formed with WPI, PPI and WPI-PPI.

Overall, lower elastic moduli were found at the oil-water interface compared to the air-water interface, due to the ability of the oil phase to interact with the hydrophobic parts of the proteins, therewith acting as a solvent. This solvation hindered the inter-protein hydrophobic interactions and, as a result, interfacial layers with lower connectivity were formed, which led to lower elastic moduli. We concluded that the interfacial properties of individual proteins are not additive and highly depend on the interface used, which should be considered when attempting to explain the performance of food dispersions based on the involved interfacial properties.

3.6. Acknowledgements

The authors wish to thank Regina Giovani for performing preliminary experiments.

3.7. Appendix

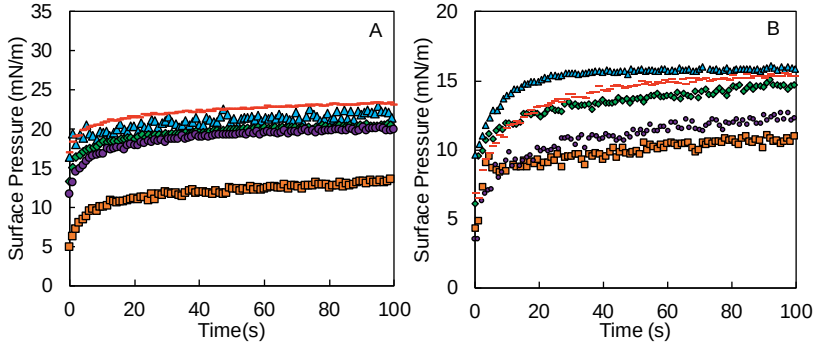

Figure A3.1. A) Surface pressure using a pendant drop in the automated drop tensiometer of 1g/L protein B) surface pressure using a rising drop in the automated drop tensiometer at 0.1g/L protein in the first 100 seconds of protein adsorption

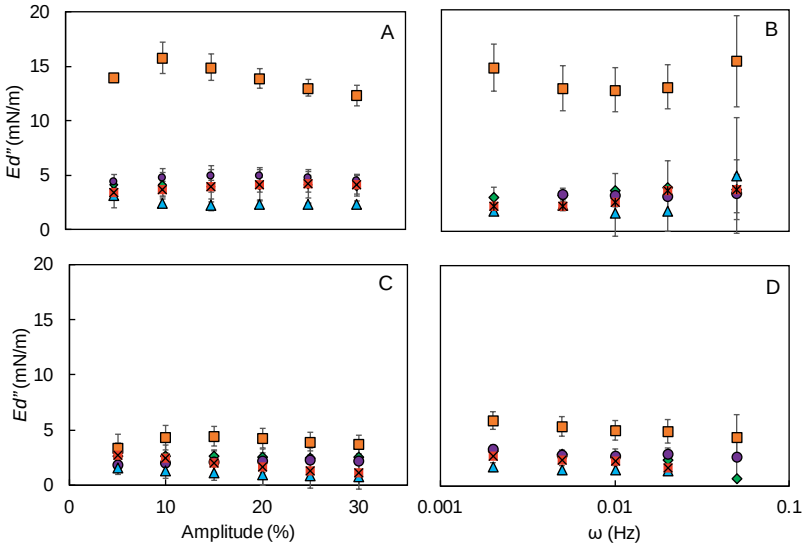

Figure A3.2. Dilatational loss moduli (E_d') of interfaces stabilised by WPI (■), SC (▲), PPI (◆) 1:1 SC-PPI (☒) and 1:1 WPI-PPI (●) blend as A-C) a function the applied deformation (frequency, 0.01 Hz) and B-D) a function of the applied frequency (amplitude, 5%) at the air-water (A,B) or oil-water interface (C,D). Error bars represent the standard deviation of at least two independent replicates.

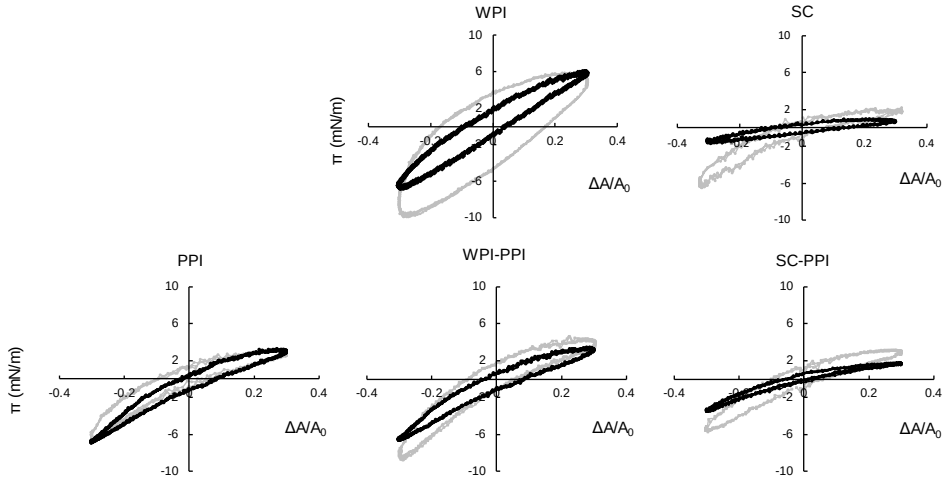

Figure A3.3. Lissajous plots at the air-water interface (grey) and oil-water interface (black) at 30% deformation

Chapter 4

Sequential adsorption and interfacial displacement in emulsions stabilised with plant-dairy protein blends

This chapter has been published as Hinderink, E.B.A., Sagis, L., Schroën, K., Berton-Carabin, C.C. Sequential adsorption and interfacial displacement in emulsions stabilised with plant-dairy protein blends. *Journal of Colloid and Interface Science*. **2021**, *583*, 704–713. https://doi.org/10.1016/j.jcis.2020.09.066.

4.1. Abstract

Hypothesis: Many traditional or emergent emulsion products contain mixtures of proteins, resulting in complex, non-equilibrated interfacial structures. It is expected that protein displacement at oil-water interfaces depends on the sequence in which proteins are introduced during emulsion preparation, and on its initial interfacial composition.

Experiments: We produced emulsions with whey, pea or a whey-pea protein blend and added extra protein post-emulsification. The surface load was measured indirectly via the continuous phase, or directly via the creamed phase. The interfacial composition was monitored over a three-day period using SDS-PAGE densitometry. We compared these findings with results obtained using an automated drop tensiometer with bulk-phase exchange to highlight the effect of sequential protein adsorption on interfacial tension and dilatational rheology.

Findings: Addition of a second protein increased the surface load; especially pea proteins adsorbed to pre-adsorbed whey proteins, leading to thick interfacial layers. The addition of whey proteins to a pea protein- or whey-pea protein blend-stabilised emulsion led to significant displacement of the pea proteins by β-lactoglobulin. We determined that protein-protein interactions were the driving force for this displacement, rather than a decrease in interfacial tension. These outcomes could be instrumental in defining new strategies for plant-animal protein hybrid products.

Graphical abstract

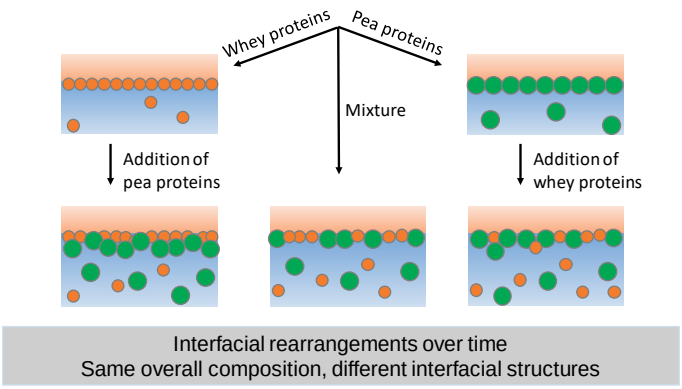

4.2. Introduction

Proteins are commonly used to stabilise food emulsions. After adsorption at the oil-water interface, proteins provide steric and electrostatic repulsion that prevents droplets from approaching each other too closely (McClements, 2005). Protein ingredients used for food applications are never pure from a molecular composition perspective, e.g., whey protein isolate contains mostly bovine serum albumin (BSA), α-lactalbumin (α-lac) and β-lactoglobulin (β-lg); or caseinates contain mostly α-, β- and κ-caseins. As a consequence, when applied in emulsions, mixtures of proteins adsorb at the oil-water interface and contribute to emulsion stability (Morris et al., 2008). Different proteins may compete for adsorption during emulsification (Damodaran, 2004; Euston et al., 1996; Hunt et al., 1994; McClements et al., 2018), and possibly displace each other over time.

Displacement of proteins adsorbed at an oil-water interface by surfactants has been studied extensively, for which the orogenic displacement theory has been suggested. According to this theory, displacement of a pre-adsorbed protein film starts at a so-called nucleation site where surfactants can adsorb, and displacement then proceeds from this site (Mackie, Gunning, Wilde, & Morris, 1999). Whether this mechanism also applies to protein displacement by another protein is not known, yet it is highly relevant to understand the mechanisms underlying protein interfacial rearrangements. Several studies were conducted using model interfaces and/or emulsions to characterise protein partitioning between the interface and the aqueous phase, and also to investigate protein-protein interactions. For example, at model interfaces, in a system consisting of a mixture of α-casein and β-casein, the latter predominated at the air-water interface after spontaneous adsorption, but over time the proteins were able to displace each other (Anand et al., 1996). When using the egg white proteins ovalbumin and lysozyme, ovalbumin adsorbed at the air-water interface with lysozyme being present as a second layer, independently of the order of addition (e.g., sequentially or as mixture) (Le Floch-Fouéré et al., 2010). The predominant adsorption of ovalbumin was attributed to its higher surface activity, and the interaction of ovalbumin and lysozyme in the interfacial region led to the formation of additional layers. This interaction is fascinating, since the proteins did not interact in the bulk: it therefore implies that the protein conformational changes induced by interfacial adsorption are a pre-requisite for the interaction.

Exchange experiments in emulsions where one protein was adsorbed first, and the second protein added post-emulsification, indicated that α-casein and β-casein were able to displace each other from the interface (Dickinson, Rolfe, et al., 1988), which is in line with to the findings at model interfaces (Anand et al., 1996). When using a 1:1 mixture of α-lac and β-lg for emulsification, no preferential adsorption was reported (Dalgleish et al., 1991; Dickinson, Flint, et al., 1989; Euston et al., 1996), which would be expected for proteins with similar propensity to adsorb on oil droplets under convective flow. However, in emulsion exchange experiments, pre-adsorbed α-lac was readily displaced by added β-lg, but pre-adsorbed β-lg was displaced only when ten times as much α-lac was added to the continuous phase (Dickinson, Rolfe, et al., 1989).

It was suggested that the resistance to displacement may be linked to the mechanical properties of the protein layer (Dalgleish, 1996), which can be quantified through parameters such as the interfacial shear viscosity. For instance, interfacial films made of globular whey proteins have a surface shear viscosity that is about 10^3-10^4 times higher than that of flexible casein films (Dickinson, 2001; Murray et al., 1996). Moreover, the relative importance of the elastic and viscous contributions is probably also instrumental: intermolecular attraction between adsorbed proteins, leading to an interconnected solid-like elastic film at the interface (Bos et al., 2001; Murray, 2011), could be particularly effective at preventing protein displacement, whereas a predominantly viscous behaviour would not be able to do so. Therefore, it is important to characterise in depth the rheological properties of protein-based interfacial layers, which can be performed by oscillatory dilatational deformation experiments. Whey protein stabilised-interfaces have an elastic dilatational modulus (E_d') that is around 10-fold higher than for caseins (Hinderink, Sagis, et al., 2020), which could explain the resistance of adsorbed whey proteins to displacement. Yet, displacement of such globular proteins can be facilitated by increasing the interfacial mobility, or the flexibility of the displacing protein (Matsumura et al., 1994).

In another study, adsorbed egg yolk phosvitin could be displaced from the interface by β-casein and also, but to a lesser extent, by β-lg. Displacement of phosvitin was facilitated by repulsive forces existing within the adsorbed layer, as phosvitin has a strong negative charge density at neutral pH (Dickinson, Hunt, et al., 1991). A special case are emulsions stabilised by ovalbumin that, after addition of β-lg, did not show displacement over 48 hours nor extra

adsorption of β-lg, whereas when both were present during emulsification, β-lg dominated the interfacial composition, showing its higher interfacial activity (Dalgleish et al., 1991).

For sustainability reasons, mixtures of animal and plant-derived proteins have recently gained a lot of interest as emulsion stabilisers (Hinderink et al., 2019; Ho et al., 2018; Ji et al., 2015; Yerramilli et al., 2017). There is limited work available on this topic, and on the properties of the compositionally complex interfaces that are formed. When using a binary mixture of sodium caseinate and pea protein isolate, it was reported that both proteins adsorb at the oil-water interface (Yerramilli et al., 2017), albeit the interfacial composition was not measured over time and only one concentration was considered. In previous work, we found a synergistic behaviour in terms of emulsion stability when blending sodium caseinate or whey proteins with soluble pea proteins (Hinderink et al., 2019). Ageing of the blend-stabilised interfaces led to interfacial rearrangements, and protein displacement. Whey proteins were able to displace pea proteins, which were themselves able to displace caseins. However, this displacement only took place when the displacing protein was present at equal or higher concentration in the continuous phase of the emulsion than the displaced protein. Since both proteins were present at the interface and in the continuous phase, it could not be distinguished if the displacement was driven by the initial interfacial composition, or by the continuous phase concentration of the displacing protein.

To address this gap, the present study aims at understanding protein displacement at plant-dairy protein stabilised oil-water interfaces, by varying the order of addition of different proteins in emulsion systems. We investigated protein interfacial displacement in 10 wt.% oil-in-water (O/W) emulsions with different interfacial composition and continuous phase protein concentrations. Displacement, as measured in the emulsions systems, is linked to the interface rheological properties before and after displacement which enables us to determine the driving forces for the displacement. As dairy protein source we used whey protein isolate (WPI), and as plant protein source, pea protein isolate (PPI).

4.3. Materials and methods

4.3.1. Materials

WPI, purity 94% (BiPro®, Davisco, Switzerland), SC, purity 97% (Excellion™, Sodium Caseinate S, Friesland Campina, the Netherlands), PPI, (NUTRALYS s85F, Roquette, France; see Appendix Table A2.1, Chapter 2 for the amino acid composition and content, and protein content). The compositional analysis of the non-protein material present in the commercial PPI is reported in Kornet et al., 2020. The soluble protein concentration was determined using a bicinchoninic acid (BCA) kit with a standard bovine serum albumin (BSA) solution. (Thermo Fisher Scientific, Massachusetts, US). Sunflower oil was purchased from a local supermarket and stripped with Florisil (Sigma-Aldrich, Saint Louis, MO, USA, 20281, Supelco, 100-200 mesh) to remove surface-active impurities, as described previously (Berton, Genot, & Ropers, 2011). Mini-PROTEAN gels (12% Mini-PROTEAN® TGX™ Precast Protein Gels, 10-well comb, 30 µl/well), Bio-safe Coomassie G-250 stain, Laemmli sample buffer, Tris/Glycine/SDS-buffer (running buffer) and precision plus protein standard (Bio-Rad, Richmond, CA, US), were used for SDS-PAGE analysis. Sodium phosphate dibasic, sodium phosphate monobasic, sodium dodecyl sulfate (SDS) and 2-mercaptoethanol were purchased from Sigma Aldrich and were at least of analytical grade. Ultrapure water was obtained from a Milli-Q system (Millipore Corporation, Billerica, Massachusetts, US) and used for all the experiments.

4.3.2. Preparation of aqueous phases

WPI (1 or 10 wt.%) was dissolved in 10 mM phosphate buffer (pH 7.0) and stirred overnight at 4 °C. PPI was dispersed in the same buffer (6 wt.%) and stirred for at least 48 h at 4 °C; the insoluble part was removed by centrifugation (16,000 x *g*, 30 min) and the supernatant was collected and centrifuged again under the same conditions to ensure complete removal of the insoluble fraction. The second supernatant was collected, and its protein content was determined with the BCA-assay (Smith et al., 1985) at 562 nm using a DU 720 UV-vis spectrophotometer (Beckman Coulter, Woerden, the Netherlands), which was about 25% of the total proteins present in the starting suspension. At 10 g/L soluble pea proteins, 0.06 wt.% residual fat was present (Hinderink et al., 2019). This supernatant was used for all pea protein-based experiments, and for simplicity is referred to as ‘pea protein solution’ from now on.

4.3.3. Preparation of emulsions

A coarse emulsion was prepared by mixing 10 wt.% stripped sunflower oil with the protein solutions (1 wt.%) using a high-speed blender (S18N-19G, Ultraturrax R, IKA-Werke GmbH & Co., Staufen, Germany) at 11,000 rpm for 1 min. When protein blends were used, both solutions were shortly mixed by hand before adding the oil. The coarse emulsion was then passed five times through a high-pressure M-110Y Microfluidizer (Microfluidics, Massachusetts, USA) at 400 bars to obtain the final emulsion. The emulsions were diluted with a second protein solution (1 or 10 wt.% protein) to obtain a 5 wt.% O/W emulsion (Table 1). The emulsions were stored in glass bottles at 4 °C.

Table 4.1. Overview of the protein solutions used for emulsification and for post-emulsification addition

Initial protein solution (emulsification)	Second protein solution (post-emulsification)
1 wt.% PPI	1 wt.% WPI
	10 wt.% WPI
1 wt.% WPI	1 wt.% PPI
1 wt.% WPI-PPI	1 wt.% PPI
	1 wt.% WPI
	10 wt.% WPI

4.3.4. Droplet size distribution

The droplet size distribution of the initial emulsions was measured by static light scattering using a Mastersizer 3000 (Malvern Instruments Ltd.; Worcestershire, UK). The refractive index was 1.465 for the dispersed phase (stripped sunflower oil) and 1.330 for the dispersant (water). An absorption index of 0.01 was applied. All emulsions were diluted (1:1, v/v) in a 1 wt.% SDS solution prior to the measurement, to de-flocculate any flocs present and thereby measure the individual droplet size.

4.3.5. Determination of surface load and interfacial composition

The surface load in emulsions, i.e., the mass of adsorbed proteins per unit of interfacial area, was determined via three different methods (Figure 4.1): via determination of the non-adsorbed protein amount in the continuous phase (method 1), or of the adsorbed protein amount in the creamed phase (method 2) and in the washed creamed phase (method 3).

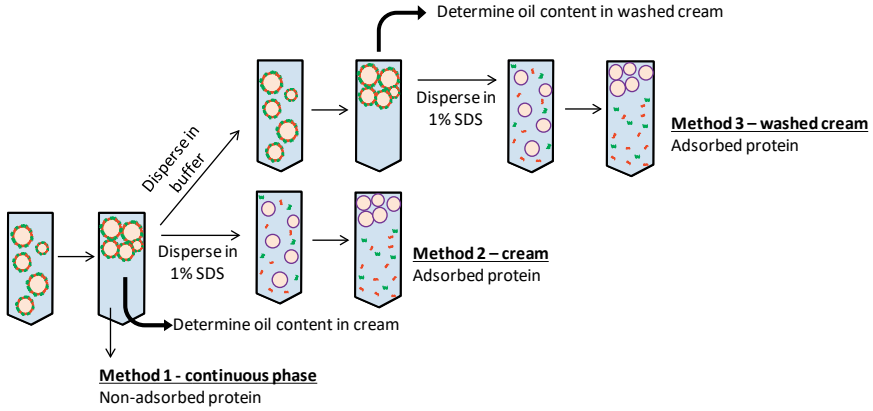

Figure 4.1. Overview of the methods applied to determine the protein surface load in emulsions: 1) via the continuous phase 2) via the cream and 3) via the washed cream. The oil content was determined by hexane:isopropanol (3:2 v/v) extractions, and protein content using the BCA-assay.

The continuous phase of the emulsions was separated from the creamed phase by centrifugation at 15,000 x g for 1 hour. The serum phase was collected by making a hole at the bottom of the tube, and its soluble protein content was determined with the BCA-assay. The surface load Γ (mg/m^2) was calculated with equation 4.1.

$$\Gamma = \frac{C_s . d_{3,2}}{6\varphi} \qquad 4.1$$

Where C_s (mg/L) is the adsorbed protein concentration calculated by subtracting the protein concentration in the serum phase from the initial protein concentration of the solution used for emulsion preparation, $d_{3,2}$ the surface-weighed mean droplet diameter after dilution of the emulsion in 1 wt.% SDS, and φ the dispersed phase volume fraction. The calculated surface load corresponds to method 1.

For the surface load determination via the creamed phase (method 2), the amount of adsorbed proteins and the oil content in the cream were determined. The creamed phase obtained after centrifugation was re-dispersed in 1 wt.% SDS solution (mass ratio 0.06:1). The resulting mixture was agitated under slow rotation for at least 1 hour and then re-centrifuged at 15,000 x g for 1 hour. The aqueous subnatant, containing the proteins that were initially adsorbed, was collected, and protein content determined by the BCA assay. The oil content in the creams was determined by mixing an aliquot of the cream with hexane:isopropanol (3/2 v/v) and water in a mass ratio of 0.02 (sample):1 (organic phase):0.2 (water). The obtained tubes were vortexed three times for 1 min, then agitated under slow rotation for at least one hour

before centrifugation (3000 x *g*, 5 min). The upper phase was carefully taken out and collected in Eppendorf tubes. Tubes were placed in the fume hood overnight at 40 °C for the hexane to evaporate and weighed subsequently. Eppendorf tubes had preliminary been weighed to determine the amount of extracted oil. The total surface area of the emulsion was calculated based on the oil content and $d_{3,2}$, and surface load (mg/m^2) was calculated from the amount of adsorbed protein and total surface area. For the washed surface load (method 3) the cream was first dispersed in buffer (0.05:1 mass ratio) and agitated under slow rotation for 1 hour before the surface load was determined as described before.

The protein interfacial composition in the washed cream was determined by SDS-PAGE under reducing conditions. The final subnatant obtained via method 3 (Figure 1) was mixed (0.75:1 v/v) with a pH 6.8 buffer containing Tris-HCl 0.5 M, glycerol 30% w/v, SDS 10% w/v, bromophenol blue 0.5% w/v and 2-mercaptoethanol, vortexed and heated at 95 °C for 5 min in a heating block. Ten microliters protein standard (Biorad, Precision Plus protein™ Standards, Mw 10-250) and 20 µL of the diluted samples in sample buffer were loaded on the gel as dependent duplicates. A running buffer of pH 8.3 consisting of Tris-HCl 25 mM, glycerol 192 mM and SDS 0.1 wt.% was used. Electrophoresis was performed in the Mini-PROTEAN Tetra Cell (Bio-rad laboratories, USA) at 200 V. After electrophoresis the gels were extensively washed with ultrapure water before staining with Coomassie G-250 for 1 hour. Subsequently, the gels were washed with ultrapure water for 12 hours before analysis. Gels were scanned and analysed using a calibrated densitometer (GS-900™, Bio-rad laboratories, USA) and Image Lab software (Bio-Rad laboratories, USA). The molecular weights were determined by point to point regression. For WPI solutions, mainly bovine serum albumin, β-lactoglobulin, α-lactalbumin, and traces of immunoglobulins were found. PPI mainly consisted of convicilin (~71 kDa), vicilin subunits (~30, ~34, ~47 and ~50 kDa), α-legumin (38-40 kDa) and β-legumin (19-22 kDa) (Barac et al., 2010). The pea proteins dissociated in the buffer containing SDS solution and 2-mercaptoethanol, leading to multiple bands in SDS-PAGE. The sum of the subunits is reported for the different pea proteins.

4.3.6. Automated drop tensiometer measurements

The interfacial tension between stripped sunflower oil and the protein solutions in 10 mM phosphate buffer (pH 7.0) was measured with an automated drop tensiometer (ADT, Tracker, Teclis, Longessaigne, France) at 20 °C. The ADT was equipped with a single-phase exchange device for the continuous phase. We used a rising drop with an area of 30 mm^2 (i.e., a drop

of oil was immersed in a 25-mL glass cuvette filled with the protein solution) using 20-gauge needles. We started with a 0.01 wt.% WPI or PPI solution as the continuous phase, and after a first adsorption phase, the continuous phase was exchanged with 0.01 wt.% solution of the other protein (experimental details are given below). The interfacial tension was calculated using the Windrop software, based on the shape of the droplet using the Laplace equation (Benjamins et al., 1996).

After 3.25 hours, one oscillatory measurement (amplitude $\Delta A/A_0$=0.05) was performed with a frequency of 0.1 Hz with five active and one passive cycle, after which the phase exchange was started. A total of 125 mL of the second protein solution was rinsed through the cuvette (25 mL) with a flow rate of 10 mL/min, to ensure complete refreshment of the continuous phase. The second protein was allowed to adsorb for one hour before amplitude sweeps with $\Delta A/A_0$ in the range of 0.05-0.3 and a frequency 0.1 Hz, started. Five deformation cycles were applied, after which five rest cycles were applied before the next deformation started. The oscillating surface tension signal was analysed with a Fast Fourier transform, and the intensity and phase of the first harmonic was used to calculate the dilatational elastic modulus (E_d') and the dilatational viscous modulus (E_d") according to equations 4.2 and 4.3.

$$E_d' = \Delta\gamma \left(\frac{A_0}{\Delta A}\right) \cos\delta \qquad 4.2$$

$$E_d'' = \Delta\gamma \left(\frac{A_0}{\Delta A}\right) \sin\delta \qquad 4.3$$

Here $\Delta\gamma$ is the amplitude of the change in interfacial tension, A_0 the initial droplet area, ΔA the amplitude of change in droplet area, and δ the phase shift of the oscillating interfacial tension signal, compared to the induced area change. This first harmonic-based analysis is accurate in the linear response regime. For the higher deformation amplitudes, the response enters the nonlinear viscoelastic regime, in which higher harmonics are present in the surface tension signal. As an alternative, measurements in the nonlinear regime were analysed by Lissajous plots in which the change in surface pressure ($\pi=\gamma-\gamma_0$) is plotted against the oscillating deformation signal (Sagis & Scholten, 2014) to compare the behaviour of the various interfaces.

4.3.7. Experimental design and data treatment

Each emulsion was characterised for particle size distribution, surface load and interfacial composition at day 0, 1 and 3. This was done for at least two independently prepared emulsions, and means, and standard deviations were calculated from these replicates. Independent t-tests (SPSS Statistics 20, IBM) were performed, using all experimental values, to determine if differences in surface load and interfacial composition occurring in time were significant ($p<0.05$).

4.4. Results and discussion

4.4.1. Surface load

We determined the surface load of the initial emulsions via the continuous phase, the cream and the washed cream (Figure 4.2). For all tested proteins, the three methods gave the same trends, with the continuous phase method leading to higher surface loads then those determined from the cream, and from the washed cream. The latter method gave the lowest surface loads: 2.5, 1.4 and 1.5 mg/m^2 for PPI-, WPI- and WPI-PPI-stabilised emulsions, respectively. These values are in good agreement with values reported for washed creams of WPI-stabilised emulsions, around 1.5-3.2 mg/m^2 (Hunt et al., 1994). Although widely used, the surface load determined via the continuous phase is an indirect method (McClements, 2005), and may be overestimated due to the presence of small oil droplets in the continuous phase or to protein precipitation upon centrifugation (Hunt et al., 1994). Regarding method 2 (analysis of the creamed phase as such), proteins that may be loosely attached to the interface or captured between the oil droplets in the creamed phase would erroneously be considered as adsorbed. Washing of the cream is expected to remove loosely bound proteins, and possibly even those that are present as a secondary layer at the interface. Also, proteins captured in the void fraction of the cream would be removed and thus the lowest values were expected for this technique.

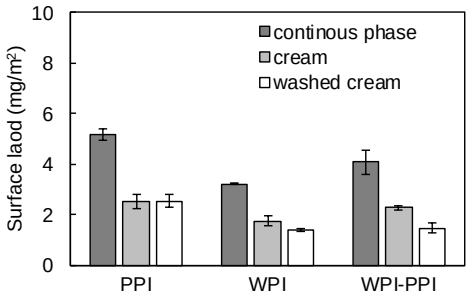

Figure 4.2. Surface load in 1 wt.% WPI, PPI or WPI-PPI-blend stabilised emulsions determined via the continuous phase, cream and washed cream at day 0.

When adding the second protein to the initial emulsions, an increase in surface load was observed for all systems tested (Figure 4.3A) which suggests additional association of proteins to the pre-formed interfacial layer; more details on the composition of the interfaces will be given in the next section. As a control experiment, we also measured the surface load

of WPI, PPI and WPI-PPI stabilised-emulsions after addition of more of the same protein post-emulsification (Appendix, Figure A4.1) and also found an increase in the surface load compared to the initial emulsions, both via the cream and washed cream methods. An exception to this trend is the surface load in the WPI-stabilised emulsion with added WPI post-emulsification, determined via the washed cream method (method 3), which perfectly matched the surface load determined in the starting WPI-based emulsion (Appendix, Figure A4.1). In exchange experiments carried out by others, the surface load of a β-casein-stabilised emulsion increased by about one third after addition of 1 wt.% β-lg, as determined via the continuous phase analysis after centrifugation. This increase was explained by multilayer formation and/or by adsorption of the second protein in gaps present in the original interfacial layer (Dalgleish et al., 1991). The presence of non-adsorbed proteins in the void fraction of the cream could lead to an overestimation of the surface load. This effect probably explains the lower surface loads determined via the washed cream method, compared to the cream method.

Only a few methods are available to determine the surface load in protein-stabilised emulsions without physical separation of the serum and creamed phases. For example, Granger and co-workers used front-surface fluorescence to determine protein partitioning between the interface and the continuous phase (Granger et al., 2005). The location of the proteins could be determined due to the sensitivity of the intrinsic fluorescence of the tryptophanyl residues to aqueous or hydrophobic environments. However, the change in fluorescence emission spectra between adsorbed and non-adsorbed proteins is small for proteins such as β-lg and casein, and this method is therefore not applicable for all proteins (Rampon, Genot, et al., 2003).

Based on these initial results, we concluded that the surface load determined via the washed cream is the most accurate to quantify the adsorbed protein amount at the oil-water interface (e.g., not present as loosely bound or interstitial proteins), and will therefore be used for the displacement study. It is good to note that over the three-day period, the surface load as determined from the washed cream did not significantly change (Figure 4.3B, $p < 0.05$); more details on the implications in terms of interface composition follow in the next section.

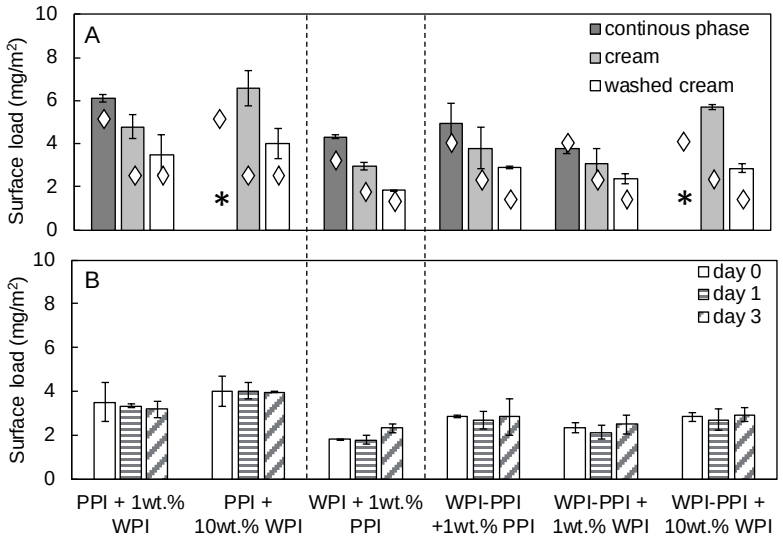

Figure 4.3. A) Surface load in emulsions after addition of the second protein determined via the continuous phase, cream and washed cream at day 0. The star (*) indicates that the surface load was not measured via the continuous phase for the sample. The white diamonds correspond to the surface loads of the initial emulsions (from Figure 4.2); and B) surface load determined via the washed cream at day 0, 1 and 3.

4.4.2. Interfacial composition

For the PPI-stabilised emulsions, all protein species initially present in the solution were found at the interface (Figure 4.4A). The addition of 1 wt.% PPI-solution to the PPI-stabilised emulsion led to an increase of all proteins at the interface. Extra adsorption was also found for the other tested systems, e.g., WPI- or WPI-PPI-stabilised emulsion after addition of 1 wt.% WPI or 1 wt.% WPI-PPI, respectively (Figure 4.4B and C). The pea protein-stabilised interface is dominated by the vicilin, as described in detail earlier (Hinderink et al., 2019). Directly after the addition (day 0) of 1 or 10 wt.% WPI solution, whey proteins adsorbed at the PPI-stabilised interface (Figure 4.4A). Over the three-day period, the adsorbed amount of β-lg significantly increased at the expense of the pea proteins, and at the expense of α-lac that was yet added simultaneously.

In the WPI-stabilised emulsion (Figure 4.4B), β-lg was the major protein dominating the interface with 0.99 mg/m^2. After addition of PPI, almost half of the surface load consisted out of pea proteins, which shows that pea proteins partly displaced the pre-adsorbed whey proteins and adhered to the interface. This is remarkable since proteins did not show specific interactions in bulk, as measured by asymmetric flow field flow fractionation (AF4,

Appendix, Figure A4.2). In a previous study on ovalbumin and lysozyme, lysozyme was found to adsorb at an ovalbumin-based interfacial layer as a consequence of interfacial electrostatic complexation, yet without interfacial displacement (Le Floch-Fouéré et al., 2010). However, in contrast to ovalbumin and lysozyme, whey and pea proteins have similar overall charges and electrostatic complexation is thus probably not the reason for the interfacial accumulation of pea proteins. Over time, the concentration of adsorbed β-lg significantly increased 0.74 to 1.10 mg/m^2, as well as that of adsorbed legumin (0.24 to 0.31 mg/m^2).

In the WPI-PPI blend-stabilised emulsions, proteins from both sources initially co-located at the interface (Figure 4.4C). Upon addition of a 1 wt.% WPI-PPI solution, the surface load increased mainly due to extra adsorption of pea proteins. This confirms their high affinity for the pre-adsorbed protein layer, as was also found for the addition of pea proteins to a WPI-stabilised emulsion (Figure 4.4B) or to a PPI-stabilised emulsion (see also Appendix, Figure A4.1). When adding pea proteins to the WPI-PPI blend-stabilised emulsion, the interface composition was clearly dominated by pea proteins and no significant changes in interface composition occurred over the three-day period (Figure 4.4C). The addition of 1 or 10 wt.% WPI solutions also increased the surface load of the WPI-PPI blend-stabilised emulsions however, to a lower extent compared to the system where PPI was added. Remarkably, this higher surface load was a result of extra adsorption of pea proteins. This shows the lower affinity of whey proteins for the pre-adsorbed WPI-PPI-layer, compared to pea proteins. After addition of whey proteins (1 or 10 wt.%) to the WPI-PPI blend-stabilised emulsions, the β-lg concentration significantly increased at the expense of all other adsorbed proteins (pea proteins and α-lac).

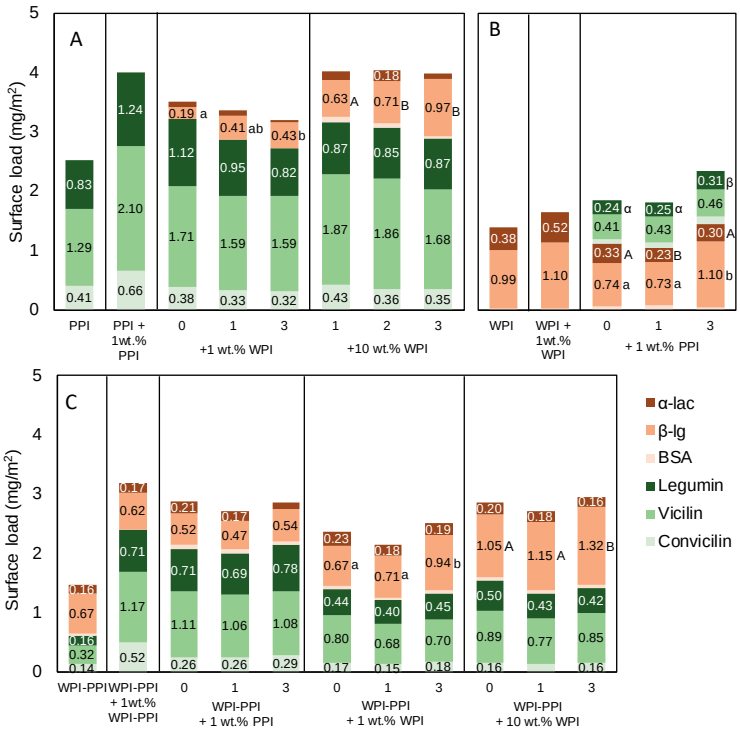

Figure 4.4. Interfacial composition measured in the washed cream (method 3) of A) PPI-stabilised emulsion with no addition, addition of PPI at day 0 and with addition of 1 wt.% WPI or 10 wt.% WPI at day 0, 1, and 3. B) WPI-stabilised emulsion without addition, with addition of 1 wt.% WPI at day 0 and 1 wt.% PPI at day 0, 1 and 3. C) WPI-PPI-stabilised emulsion with no addition, with addition of 1 wt.% WPI-PPI at day 0 and with addition of 1 wt.% PPI, 1 wt.% WPI or 10 wt.% WPI at day 0, 1 and 3. Significance in surface composition changes over time within the sample is indicated by different letters.

To summarise, we determined that β-lg is able to induce interfacial displacement for the following systems: PPI-stabilised emulsions after addition of 1 and 10 wt.% WPI; WPI-stabilised emulsion after addition of 1 wt.% PPI; and WPI-PPI-stabilised emulsions after addition of 1 and 10 wt.% WPI. We estimated the amount of whey proteins present in the continuous phase of our emulsions immediately after addition of the second protein using the protein concentration as measured in the continuous phase (method 1). A continuous phase whey protein concentration of ~1 g/L was determined for the WPI-PPI-stabilised emulsion after addition of 1 wt.% PPI; whereas the WPI-stabilised emulsion after addition of 1 wt.% PPI, had ~2.2 g/L whey proteins in the continuous phase. In the former case, β-lg did not displace pea proteins over the three-day period, whereas in the latter case, it did. When comparing with previous work (1:3 w/w WPI-PPI blend-stabilised emulsion) in which no

displacement was measured in similar storage conditions, ~0.9 g/L whey proteins was present in the continuous phase (Hinderink et al., 2019).

Due to the limited solubility of the commercial pea proteins, the addition of 10 wt.% PPI to the WPI-stabilised emulsion could not be tested and we can only speculate about the outcome. It is expected that at higher pea protein concentrations, higher amounts will adsorb at the WPI-stabilised interface. However, it is unlikely that pea proteins would be able to displace the whey proteins. When adsorbed at the oil-water interface, whey proteins are known to form a viscoelastic network linked by intermolecular disulfide bridges involving the free thiol groups of β-lg (Dickinson & Matsumura, 1991). Because of this, displacement studies on model interfaces using surfactants showed that β-lg resisted interfacial displacement by Tween 20 better than β-casein, which does not establish such covalent protein-protein interactions (Mackie, Gunning, Ridout, Wilde, & Morris, 2001). In line with this, it was found that when β-casein was added to a freshly prepared β-lg-stabilised emulsion, it was able to displace 0.5 mg/m^2 β-lg within 1 hour (Dalgleish et al., 1991), whereas β-casein added to a β-lg-stabilised emulsion preliminary aged for 3 days could not displace the adsorbed β-lg anymore (Dalgleish, 1996). When adding β-lg to a β-casein-stabilised emulsion, extra adsorption of the β-lg took place, but no casein displacement was measured (Dalgleish et al., 1991). For the two major whey proteins it was found that α-lac was only able to displace ~15% of pre-adsorbed β-lg, when added at a concentration of 10 wt.% whereas 1 wt.% β-lg could displace ~30% α-lac of a pre-adsorbed film (Dickinson, Rolfe, et al., 1989). In general, whey proteins have low interfacial mobility and form layers with high viscoelastic moduli (Dalgleish, 1996; Dickinson, Rolfe, et al., 1989), making the protein layer more resistant to displacement compared to other proteins (e.g., pea proteins). This aspect was next further investigated by performing interfacial rheology measurements.

4.4.3. Interface rheological measurements

Whey protein films have a higher resistance against dilatational deformation compared to pea protein films (Hinderink, Sagis, et al., 2020; Ho et al., 2018). Since interfacial dilatational rheology (i) is a direct consequence of the interface composition and structure and (ii) is related to emulsion stability (Bos et al., 2001), it is interesting to probe possible changes in interface rheological properties after addition of the second protein. For this, we used an automated drop tensiometer with external phase exchange.

For the interfacial layer initially formed with WPI the interfacial tension was 15.9±0.1 mN/m and decreased to 14.1±0.1 mN/m after the phase exchange with the PPI solution (Figure 4.5A, the interfacial tension during exchange is reported in the Appendix, Figure A4.3). The opposite effect was found for the interface initially covered with PPI with an interfacial tension of 13.5±0.1 mN/m, where the interfacial tension increased after the phase exchange with the WPI solution to 14.1±0.1 mN/m. The fact that the same interfacial tension was obtained is certainly worth noticing, but does not necessarily mean that the same interfacial structures were formed. In order to investigate the structural properties of the involved interfacial films further, oscillatory dilatational deformation was applied. The resistance to dilatational deformation is quantified through the elastic (E_d') and viscous moduli (E_d"), calculated from the dynamic interfacial tension response.

Before phase exchange, the elastic modulus of the WPI-stabilised interface was the highest (30 mN/m at $\Delta A/A_0$=0.05, Figure 4.5B), in accordance with previous results (Hinderink, Sagis, et al., 2020). Interfaces stabilised by WPI tend to have high moduli, an indicator of relatively strong in-plane interactions between the adsorbed protein molecules. After addition of PPI to the pre-adsorbed WPI, the elastic modulus decreased (16 mN/m at $\Delta A/A_0$=0.05), indicating that the film became less stiff. Upon increased deformation amplitude, the elastic moduli decreased to 13 mN/m ($\Delta A/A_0$=0.3), showing a low strain dependency. The PPI-stabilised interface had an elastic modulus of 20 mN/m at $\Delta A/A_0$=0.05 before phase exchange. So, the layer formed by adding PPI to a pre-adsorbed WPI-stabilised interface had a lower elastic modulus compared to both layers made of the individual proteins. A lower value for E_d' and a weak strain dependency of that modulus show that the connectivity typically found for whey protein-stabilised interfaces was decreased by the adsorption of the pea proteins. Addition of WPI to the pre-adsorbed PPI-stabilised interface increased the interfacial elastic modulus. Upon increasing the deformation amplitude, the elastic modulus decreased from 24 mN/m 0.05 to 18 mN/m at $\Delta A/A_0$=0.05 and 0.3, respectively. Such a strain dependency and increase in elastic modulus indicate that whey proteins contributed to the in plane-protein interactions, leading to a stiffer interface. The same was reported for mixtures of β-lg and β-casein at the air-water interface, that are able to displace each other: when adding a low concentration of β-lg to a β-casein solution, the viscoelastic moduli was ten times higher compared to that measured for the β-casein-stabilised interface alone (Fainerman et al., 2020).

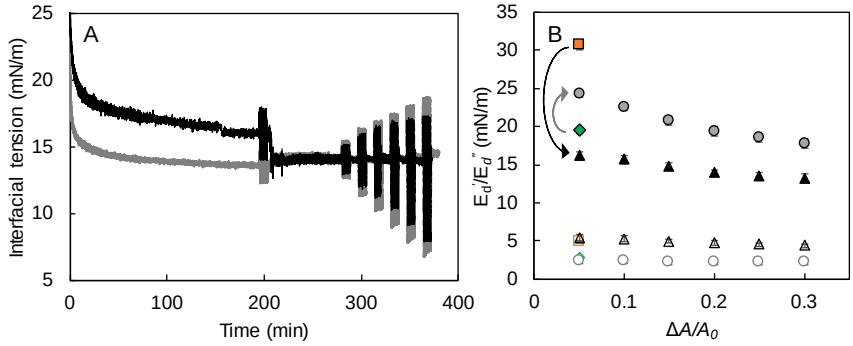

Figure 4.5. A) Interfacial tension (γ) during equilibration and amplitude sweeps ($\Delta A/A_0$=0.05-0.30) for a PPI-based interface followed by exchange with WPI (grey) and a WPI-based interface followed by exchange with PPI (black), B) the dilatational elastic (E_d' closed symbols) and viscous (E_d" open symbols) moduli as a function of the applied deformation before and after the phase exchange. Adsorbed PPI (0.01 wt.%, green diamond) followed by exchange with WPI (0.01 wt.%, grey circle); and adsorbed WPI (0.01 wt.%, orange square) followed by exchange with PPI (0.01 wt.%, black triangle).

To characterise the interfacial structure in more detail, the surface pressure as a function of the deformation ($\Delta A/A_0$=0.3) was plotted for both phase exchange systems and for the individual proteins (Figure 4.6). The so-called Lissajous plots obtained provide information about the interfacial network behaviour in dilatational expansion and compression. Furthermore, the plots include possible nonlinear effects, which are otherwise neglected when only calculating the dilatational moduli (E_d' and E_d"). A linear shape of the plot indicates an elastic behaviour of the interfacial layer, whereas a spherical shape indicates a viscous behaviour. A linear viscoelastic response results in an ellipse-shaped plot, whereas non-linear responses result in asymmetric shapes that may give information regarding jamming, buckling, yielding, etc. of the interfacial film (Sagis & Scholten, 2014).

All systems tested gave a predominantly elastic and non-linear response upon 30% deformation (Figure 4.6). At the start of expansion ($\Delta A/A_0$=-0.3) the surface pressure first increased, after which it levelled off towards maximum expansion ($\Delta A/A_0$=0.3), upon compression the reverse phenomenon happened, i.e., the surface pressure decreased strongly. This is indicative of interface strain softening in expansion and strain hardening in compression, which is typical for globular protein-stabilised interfaces (Sagis & Fischer, 2014). The Lissajous plots of individual whey and pea protein-stabilised interfaces have been extensively described elsewhere (Hinderink, Sagis, et al., 2020). In brief, the pointy shape of the plot obtained for the pea protein-based interface when approaching maximum compression (lower left part of the plot) shows that the surface pressure change is the same

in compression and subsequent expansion, meaning that only weak in-plane protein interactions are present. Upon expansion, strain softening occurs meaning that the interfacial structure is disrupted. In contrast, the plot obtained for the whey protein-stabilised interface showed a steeper slope upon expansion, which is a result of protein interactions leading to a stiff structure which is gradually, and to a lesser extend compared to the PPI-stabilised interface, disrupted upon expansion.

The interface formed with pre-adsorbed whey proteins, followed by introduction of pea proteins, showed the most viscous response compared to the other interfaces, as concluded from the open shape of the Lissajous plot (Figure 4.6), and confirmed by the higher loss moduli E_d" (Figure 4.5B). Upon compression, the density of adsorbed proteins increased, which led to an increase in the interactions between the proteins. At the start of the subsequent expansion (lower left corner of the plot), we observe that the slope of the tangent to the plot is significantly lower compared to the interface stabilised by WPI. This indicates that pea proteins adsorbed to the pre-adsorbed whey protein interface, as was also found in the emulsion systems (Figure 4.4) and disrupted the pre-adsorbed whey protein network. Although having an increased surface load, the resulting interfacial film is less stiff, and has relatively a more viscous response compared to the individual protein-stabilised interfaces. The strain softening in expansion can be explained by the disruption of the interfacial microstructure. Such a strain softening is also found for the control pea protein-stabilised interface (Figure 4.6A), but to a much lesser extent than for the whey protein-stabilised interfaces (Figure 4.6C). Taking into account (i) the adsorption of pea proteins to a pre-adsorbed whey protein-stabilised droplet (Figure 4.4), (ii) the fact that the interfacial tension decreased upon introducing the pea protein solution in the cuvette and (iii) the changes in the surface rheological behaviour, it is presumable that pea proteins adsorb in the interfacial layer, thereby decreasing the connectivity and hence the stiffness of the interfacial network.

The interface formed with pre-adsorbed pea proteins, followed by introduction of whey proteins, gave a predominantly elastic response, as seen by the narrow shape of the Lissajous plot (Figure 4.6B). The slope of the plot is steeper compared to the control pea protein-stabilised interface (Figure 4.6A) and it reached higher surface pressures in expansion. This leads to a higher elastic modulus E_d' in the first harmonic analysis (Figure 4.5B) and points to a somewhat more cohesive structure which shows less softening in expansion. This shows that whey proteins were located at the interface and reinforced the interfacial elasticity.

Because pea proteins alone did not form a strong interconnected network, it may be possible for whey proteins to squeeze into holes/defects in the interfacial layer. However, compared to the whey protein-stabilised interface, lower surface pressures were reached and relatively low interactions between the proteins occurred as seen by the pointy shape of the Lissajous-plot upon compression and subsequent expansion (lower left part of the plot). Furthermore, the 'equilibrium' interfacial tension increases, but did not reach the same interfacial tension as the whey protein-stabilised interface (Figure 4.5A). This suggests that pea proteins still largely contributed to the interfacial structure and, when viewed from a different angle, did not allow whey proteins to form a cohesive film. Whey proteins adsorbed slightly after addition to the pea protein-stabilised emulsion droplets (Figure 4.4, day 0) and displaced the adsorbed pea proteins over time. Whey proteins are probably not present at high enough concentrations to allow the formation of an interconnected stiff whey protein network (i.e., lower elastic moduli compared to whey protein alone). The rate of displacement will be enhanced at higher concentrations of added whey proteins (i.e., addition of 10wt.% WPI) as this will enhance protein adsorption (Miller et al., 2005).

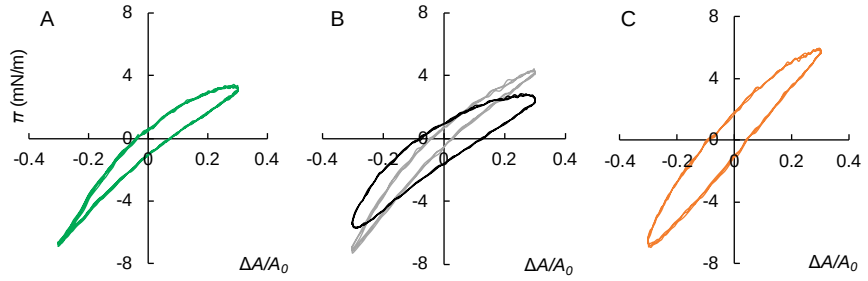

Figure 4.6. Lissajous plots of surface pressure versus applied deformation ($\Delta A/A_0$=0.30) for A) PPI-stabilised interface, B) PPI-based interface followed by exchange with WPI (grey), WPI-based interface followed by exchange with PPI (black) or C) WPI-stabilised interface.

Surfactants are known to displace adsorbed proteins since they are more effective in interfacial tension reduction (Wilde et al., 2004). However, the exact same mechanism cannot be considered to explain the current data, since added whey proteins displace pea proteins (Figure 4.4) while leading to an *increase* in interfacial tension (Figure 4.5A, Appendix, Figure A4.3). Other things being equal, an increase in interfacial tension is not thermodynamically favourable, so this effect is counterintuitive at first sight. Yet, in view of all thermodynamic driving forces in the system, an increase in interfacial tension may be compensated by thermodynamically favourable conformational protein rearrangements

including interactions with the interface and in-plane protein interactions. The energy barrier for adsorption is related to the interactions of the proteins with the interface molecules rather than surface pressure (Sengupta et al., 1998). The interactions may be more favourable for the whey proteins compared to the pea proteins. Furthermore, after adsorbing at the interface, the surface pressure increases. From a critical adsorbed protein concentration on, the surface pressure only increases slightly although the adsorbed amount still increases (Fainerman et al., 2020). At the interface, a concentration dependent two-dimensional aggregation of the protein starts. Interfacial protein aggregation has been described to reduce the interfacial tension due to displacement of water molecules at the interface and/or inclusion of the water molecules in the protein aggregates (Rao et al., 2000). Due to protein aggregation, the interfacial region behaves as a disordered viscoelastic solid (Sagis et al., 2019). One could hypothesize that in case of β-lg and therefore also, whey proteins, the formation of the highly elastic interfacial layer may not only remove water from the interface but also from the hydrophobic parts of the adsorbed proteins, which would be thermodynamically favourable.

The present results show that oil-water interfaces stabilised by protein blends can be structured and tuned based on the order of addition of the proteins. Interfacial proteins can interact with bulk proteins, leading to thick, viscous interfaces. If the initial layer is stiff enough, no protein displacement is expected and only add-on layers with minimal in-depth insertion are formed. In the case of an initially weak interfacial film, protein displacement may occur, which eventually results in a mixed interface with non-additive rheological characteristics.

4.5. Conclusions

Plant-dairy protein blend-stabilised emulsions have been gaining interest as both sustainable and functional alternatives to emulsions stabilised by their individual counterparts (Hinderink et al., 2019; Ho et al., 2018; Ji et al., 2015; Yerramilli et al., 2017). However, in protein blend-stabilised emulsions, complex and non-equilibrated interfacial structures are formed and interfacial displacement occurs (Hinderink et al., 2019). The current study focused on whey-pea protein blend-stabilised emulsions. Pea proteins were able to adsorb to the oil-water interface after introduction to a pre-adsorbed whey protein interface, but did not displace the pre-adsorbed proteins over time. We found that the whey proteins, and more specifically β-lactoglobulin, were able to displace pre-adsorbed pea proteins from the oil-water interface. Displacement seemed to be driven by an increased interfacial elasticity rather than a decrease in the interfacial tension. This may be explained by the removal of water from the adsorbed proteins and interfacial protein-protein interactions that would be thermodynamically more favourable compared to interfacial tension changes. Our results match previous results showing that β-lactoglobulin is able to displace pre-adsorbed proteins but is not itself displaced easily after adsorption at the oil-water interface (Dalgleish et al., 1991; Dickinson, Rolfe, et al., 1989). A highlight of the current work is that we were able to understand displacement in mixed protein-based systems by combining displacement studies in emulsions and interfacial rheology. Interfacial displacement was measured at relatively low continuous phase whey protein concentrations (>1 g/L), which is much lower that the protein concentrations typically used to stabilise emulsions. As such rearrangements are even more likely to occur with higher protein concentrations in the continuous phase, this implies that the present outcomes are highly relevant when formulating protein blend-stabilised emulsions. Our results therefore highlight the importance of protein dynamics in complex emulsion systems, and thereby open perspectives for the rational structuring of plant-dairy protein blend-stabilised emulsions.

4.6. Acknowledgements

Authors would like to thank Veronique Solé for helping with the AF4 experiments and Esther van Osta for performing preliminary experiments.

4.7. Appendix

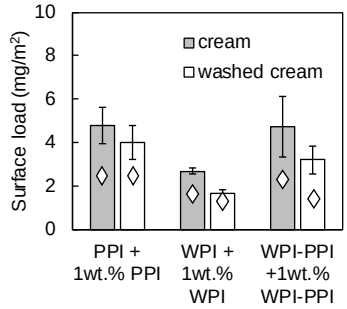

Figure A4.1. Surface loads determined in the cream or washed cream of emulsions diluted to 5 wt.% oil with more of the same protein added post-emulsification. The white diamonds correspond to the surface loads of the initial emulsions as measured via the cream and washed cream (from Figure 2).

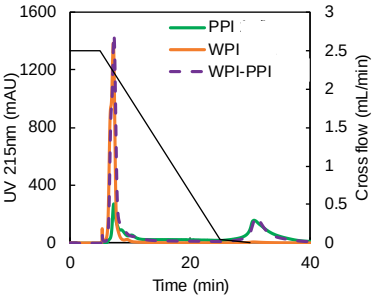

Figure A4.2. WPI and PPI (1 g/L) and WPI-PPI mixture (2 g/L) in 10 mM phosphate buffer were separated using an Asymetricla Flow Field Flow Fractionation instrument equipped with a trapezoidal channel using a regenerated cellulose membrane with a cut-off of 10 kDa and 350 µm spacer (Dualtec, Wyatt Technology Corporation Santa Barbara, USA). Phosphate buffer 10mM filtered through 0.1µm membrane (Durapore, Millipore, France) was used as liquid carrier. The samples (100 µL) were introduced into the channel at 0.20 mL/min with a crossflow flow rate of 2.5 mL/min during 3 min. They were eluted with a crossflow flow rate of 2.5 mL/min for 20 minutes. Then, the cross flow was gradually reduced from 2.5 to 0.05 mL/min in 5 min and it was maintained at 0.05ml/min during 20min as shown by the black line. Proteins were detected at 215 nm (Agilent technologies, Santa Clara, USA).

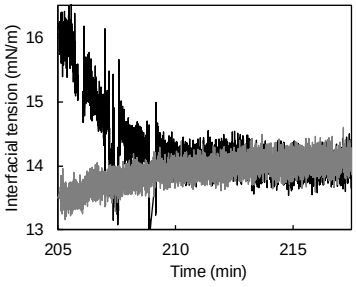

Figure A4.3. Interfacial tension during phase exchange 205-217.5 min up to 250 min, for a PPI-based interface followed by exchange with WPI (grey) and a WPI-based interface followed by exchange with PPI (black).

Chapter 5

Early film formation in protein-stabilised emulsions: Insights from a microfluidic approach

This chapter has been submitted as Hinderink, E.B.A., de Ruiter, J., de Leeuw, J., Sagis, L.C.M., Schroën, K., Berton-Carabin, C.C. Early film formation in protein-stabilised emulsions: Insights from a microfluidic approach

5.1. Abstract

Hypothesis: In conventional emulsification devices, interface formation and stabilisation occur within milliseconds. Such time scales can be accessed using microfluidic devices. Protein network formation at liquid-liquid interfaces starts at time scales similar to those of droplet formation in conventional emulsification devices (i.e., in milliseconds). It is expected that protein adsorption is followed by rearrangements resulting in a viscoelastic network.

Experiments: Using a tailor-made microchip, we probed droplet deformation to study the interfacial rheological properties of droplets, within time scales ranging from 0.16 - 1 s. We further investigated the coalescence stability of droplets at the same time scales. Whey protein isolate (WPI), pea protein isolate (PPI), or their blends were used as emulsifiers at 0.01-1 g/L.

Findings: The rheological properties of the protein-interfaces showed that early network formation takes place. WPI-stabilised interfaces were mechanically stronger compared to PPI-stabilised interfaces, and WPI-stabilised droplets were much less prone to coalescence than their PPI counterparts. Although the blend-stabilised films showed high interconnectivity, this did not prevent droplet coalescence, probably due to structural heterogeneity. The insights obtained with the tailor-made microfluidic devices help to capture effects at short time scales and are relevant to unravel phenomena occurring in large scale processing.

Graphical abstract

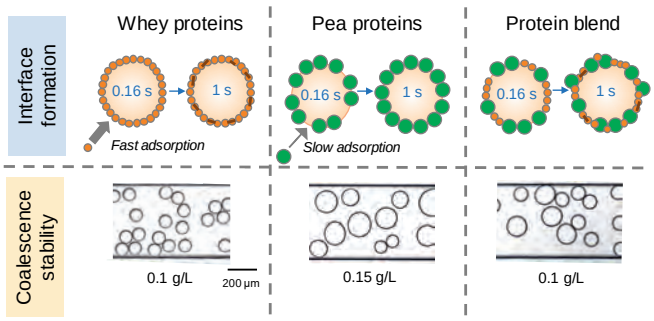

5.2. Introduction

The structure and properties of fluid interfaces have been characterised at many different time and length scales. For instance, second-to-hour time scales can be studied in a Langmuir-trough or in a drop tensiometer (Sagis & Scholten, 2014). Within these time scales, interfacial tension and rheology have been investigated in great detail for many low molecular weight emulsifiers. Proteins, the focus of the present study, show more complex interfacial behaviour due to post-adsorption rearrangements and interactions taking place at the interface that are generally observed at relatively long time scales (Berton-Carabin et al., 2018; Murray, 2011; Wilde et al., 2004). Although these measurements can be insightful for long-term stability of interfaces and of interface-dominated colloidal systems, such as emulsions (Bos et al., 2001; Murray, 2011), the conditions used are very different from those occurring during droplet formation in large scale emulsification processes. The latter involve short time scales and convective mass transport of emulsifiers towards the interface, which hampers the translation of results obtained with the previously mentioned methods that are diffusion-based and at longer time scales. To understand the phenomena occurring during emulsification, effects that take place at very small scale and extremely short time scales need to be investigated, and for that microfluidic techniques are particularly suited.

Microfluidic techniques may be applied for the preparation of some emulsions as reviewed in Schroën, Bliznyuk, et al., (2015). In such devices, convection is largely responsible for the mass transport of surfactants and hence interfacial film formation within the chips (Muijlwijk, Huang, et al., 2016). Microfluidic tools can also be used as analytical tools, e.g., to perform dynamic interfacial tension measurements at the sub-second scale (Muijlwijk, Hinderink, et al., 2016; Schroën et al., 2020; Steegmans et al., 2009; Wang et al., 2009; Xu et al., 2012) or to investigate the physical stability of emulsion droplets to coalescence in time scales relevant to processing, both for surfactant-stabilised systems (Baret et al., 2009; Krebs et al., 2012) and for protein-based ones (Hinderink, Kaade, et al., 2020; Muijlwijk et al., 2017). In a few cases, microfluidic setups have been applied to probe the rheological properties of interfacial films covering emulsion droplets (Pipe et al., 2009; Trégouët et al., 2019; Zhao et al., 2012), within the millisecond to second range.

Subjecting emulsion droplets to deformation is a commonly used principle to assess interfacial tension and/or rheology. In that respect, the behaviour of liquid droplets in simple shear flow, without the presence of emulsifiers, is well understood. For such systems, droplet

deformation (D) depends on the viscosities of the dispersed (η_d) and continuous (η_c) phases, their ratio $\lambda = \eta_d/\eta_c$, the interfacial tension (γ), the droplet radius (r), and the shear stress (σ), and is given by $D = Ca\frac{(19\lambda-16)}{(16\lambda+16)}$ with $Ca = \frac{\sigma r}{\gamma}$ the capillary number. At uniform flow velocity or quiescent conditions, the subsequent droplet shape relaxation after maximum deformation (D_{max}) can be described by a single exponential decay $D = D_{max} * e^{\frac{-t}{\tau}}$, where t is the time and τ the characteristic relaxation time (Cabral et al., 2006).

The droplet deformation patterns become more complex when emulsifiers are present in the system. Emulsifiers adsorb at the oil-water interface, therewith reducing the interfacial tension of the system, depending on the time allowed, concentrations used, and the applied mass transfer conditions. When emulsifiers are present, the capillary number fails to describe the deformation (Erni et al., 2005; Zhao et al., 2012). Upon deformation of emulsifier-based interfaces, the dilated regions of the interface have a lower interfacial surfactant concentration, resulting in an interfacial tension gradient, which is not taken into account in the capillary number. Furthermore, if complex viscoelastic interfaces are formed, the degree of deformation is restricted (Jones et al., 2003), which, in case of high interfacial shear stresses, may lead to oscillation upon relaxation (Erni et al., 2005). From the droplet deformation patterns over time, rheological parameters can be extracted. The maximum deformation is related to the stiffness of the interface and the relaxation time provides information about the relative importance of the viscous and elastic contributions to the response of the interfacial layer. Highly elastic interfaces relax immediately back to their original shape, whereas viscoelastic fluid-like interfaces tend to have a (multi-) exponential decay. Viscoelastic solid-like interfaces can display exponential decays with superimposed oscillations (Sagis, 2009). These can be particularly important in fast deformations, where elastic effects couple to inertial effects.

Often, viscoelastic interfaces display more than one relaxation time, and a simple exponential decay is not able to capture this complexity. In recent work we showed that protein-based interfaces display dynamic heterogeneity in response to sudden amplitude deformations, which is the result of local variations in the relaxation kinetics (Sagis et al., 2019). For these types of interfaces, a stretched exponential decay, $D = D_{max} * e^{\frac{-t^{\beta}}{\tau}}$ with a parameter β typically between 0.4 and 0.6 (Sagis et al., 2019), would be more appropriate to describe the deformation relaxation pattern.

Since proteins are widely used emulsifiers in the food industry (Dickinson, 1994), it is highly relevant to understand the formation of related interfacial films at short time scales. To the best of our knowledge, it is the very first time that such a protein film formation is scrutinised at sub-second time scales; in previous work on protein-based droplets (Erni et al., 2005, 2011), this was addressed at rather long time scales (~2 hours). It is well-known that many proteins are subject to conformational rearrangements, such as partial unfolding, after adsorption (Beverung et al., 1999); and some, such as the whey protein β-lactoglobulin, can form interconnected interfacial layers (Dickinson & Matsumura, 1991; Hinderink, Sagis, et al., 2020; Monahan et al., 1993; Murray, 2011) that protect droplets against coalescence during the emulsion's lifespan (Berton-Carabin et al., 2018; Dickinson, Murray, et al., 1988). The question is whether such a network, or at least its initial states, are already formed at very short time scales, which may thus be instrumental in the subsequent droplet stabilisation.

In the current study, we considered, as protein emulsifiers, whey protein isolate (WPI), which is known to form interconnected, strong interfacial films within hours-days, and pea protein isolate (PPI) as a typical plant protein alternative, which contains native and process-induced supramolecular structures (multimers, aggregates). We tested both proteins individually, and also mixtures of the two, in tailor-made microfluidic chips that allow for probing the rheological properties of protein films covering emulsion droplets, at short time scales ranging from 0.16 s to 1 s. The rheological properties were linked to the propensity of freshly prepared droplets to coalescence, within the same time scale, which was also investigated with microfluidic tools.

5.3. Materials and methods

5.3.1. Materials

WPI, (97.0-98.4% purity BiPro®, Davisco, Switzerland) and PPI (NUTRALYS s85F, Roquette, France, see Appendix Table A2.1, Chapter 2 for the amino acid composition and content, and protein content) were used. The compositional analysis of the non-protein material present in the commercial PPI is reported in Kornet et al., (2020). The soluble protein content was determined using a bicinchoninic acid (BCA) kit with a standard bovine serum albumin (BSA) solution (Thermo Fisher Scientific, Massachusetts, US). Hexadecane (>99% pure), sodium dodecyl sulfate (SDS), sodium phosphate dibasic and sodium phosphate monobasic were purchased from Sigma Aldrich and were at least of analytical grade. Ultrapure water was obtained from a Milli-Q system (Millipore Corporation, Billerica, Massachusetts, US) and used for all the experiments.

5.3.2. Preparation of protein solutions

WPI (1 wt.%) was dissolved in 10 mM phosphate buffer (pH 7.0) and stirred overnight at 4 °C. PPI was dispersed in the same buffer (6 wt.%) and stirred for at least 48 h at 4 °C; the insoluble part was removed by centrifugation (16,000 x *g*, 30 min) and the supernatant was collected and centrifuged again under the same conditions to ensure complete removal of the insoluble fraction. The second supernatant was collected, and its protein content was determined with the BCA-assay (Smith et al., 1985) at 562 nm using a DU 720 UV-vis spectrophotometer (Beckman Coulter, Woerden, the Netherlands); typically 25% of the total proteins present in the starting suspension are present in this supernatant. At 10 g/L soluble pea proteins, 0.06 wt.% residual fat was present (Hinderink et al., 2019). This supernatant was used for all the pea protein-based experiments, and for simplicity is referred to as ‘pea protein solution’ from now on. A 1:1 weight ratio of the individual proteins was used for the protein blends.

5.3.3. Microfluidic experiments

Custom-designed borosilicate glass microfluidic chips (Figure 5.1A and B) were produced by Micronit Microtechnologies B.V. (Enschede, The Netherlands). The chips were placed in a chip holder (Fluidic Connect 4515, Micronit Microfluidics) and connected with PEEK tubing (0.75 mm, BGB Analytik). The continuous and dispersed phase were pressurised into the microfluidic device using a pressure system (OB1, Elveflow, France), and controlled with

mini CORI-Flow sensors (Bronkhorst B.V., Netherlands). The protein solutions and hexadecane were filtered (0.22 µm PES filters, Merck, Germany) before the experiments. A high-speed camera (MotionPro Y4-A2) was connected to a light microscope (Axiovert 200 MAT, Carl Zeiss B.V.), and used to record the images.

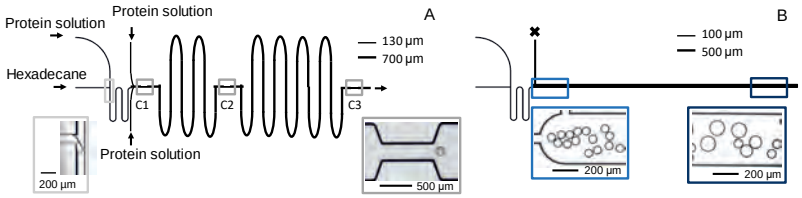

Figure 5.1. Layout of the microfluidic rheology chip (A) and coalescence chip (B), (Hinderink, Kaade, et al., 2020)). The channel widths in the rheology chip are 130 µm in the T-junction and subsequent meandering channel, 700µm in the main channel and 225 µm in the three constrictions. The channels have a depth of 45 and 110 µm at the T-junction and in the main channel, respectively. The three constrictions have a 70° angle (C1, C2 and C3). The extra inlets into the main channel are used to accelerate the droplets after formation. The coalescence chip has channel widths of 100 and 500 µm, and a uniform channel depth of 45 µm. The extra inlet of the coalescence channel is not used and closed, as indicated by the cross.

Rheology chips

In this microfluidic set-up (Figure 5.1A), oil droplets were formed at the T-junction connecting the continuous and dispersed phase channels (width = 130 µm), and next flowed through a meandering channel of the same width (length = 14.8 mm) and a uniform depth of 45 µm, that allows for adsorption of proteins. The continuous phase (protein solution) was pressurised into the chip at a flow rate of 20-30 µL/min, and the dispersed phase (hexadecane) at a flow rate of 1.5 µL/min. To accelerate the droplets in the main channel, two extra flows were added in the beginning of the channel to reach a droplet velocity of 0.2 m/s. The two extra flows were generated by the same syringe pump (NE-300, Prosense, Oosterhout, The Netherlands), and monitored with a third flow sensor (capacity 0.03-1mL/min, Elveflow, Paris, France). A PEEK Y-connector (P512, Idex health & Science) was used to split the flow. The main channel had a width of 700 µm and a depth of 110 µm and three constrictions (named C1, C2 and C3 in the downstream direction) with a width of 225 µm, a length of 600 µm, and an opening angle into the main channel of 70°. The length of the meandering channel was 14.8 mm and the channel length between C1 and C2 was 68.3 mm, and between C2 and C3, 119.9 mm. Images were recorded at the outlet of each constriction at 17,000 frames per second (fps) for 10,000 frames and a pixel resolution of 0.655 µm/pixel. The images were analysed with a custom-written script in Matlab R2018b. Deformation was expressed as

D=(*a*-*b*)/(*a*+*b*); with *a* and *b* the dimensions of the droplet perpendicular and parallel to the flow, respectively.

Coalescence chips

In this microfluidic set-up (Figure 5.1B), oil droplets were formed at the T-junction connecting the continuous and dispersed phase channels (width = 100 µm), and next flowed through a meandering channel of 14.8 mm, after which they entered the coalescence channel (width = 500 µm, length = 26.2 mm) where they may collide. All channels had a uniform depth of 45 µm. The chips were placed in a chip holder and connected to the continuous phase and dispersed phase using PEEK tubing. The continuous phase (protein solution) was pressurised into the chip to obtain a flow rate of 40 µL/min, and the dispersed phase (hexadecane) at a flow rate of 2 µL/min. Using these flow rates, the total residence time in the chips was 2 s. The extra channel connected to the coalescence channel was not used and hence closed during the experiment. Images were recorded at the outlet of the coalescence channel, 1000 frames at 30 fps and a pixel resolution of 1.321 µm/pixel. The two-dimensional area of each droplet was determined using a custom-made ImageJ macro (Muijlwijk et al., 2017). From the mean droplet area (A_f) at a certain position in the coalescence channel, and the mean initial droplet area (A_i), the mean number of coalescence events (N_{coal}) was calculated.

Data treatment

The maximum deformation is reported as the average of 5-30 individual droplets. Fitting of the stretched exponential decay to the relaxation patterns was done with MATLAB R2018b, utilizing the curve fitting tool. Fitting was performed on data from at least 3 droplets. An independent t-test (SPSS Statistics 20, IBM) was performed to determine if differences in relaxation time for different protein concentrations and constrictions (C1-C3) were significant ($p < 0.05$).

5.4. Results and discussion

5.4.1. Validation of the microfluidic rheology chips with SDS-based droplets

As a reference system, we first investigated SDS-based droplets. Under the current convective mass transport conditions, the minimum interfacial tension can be reached in about 10 ms at 10 g/L SDS (Muijlwijk, Hinderink, et al., 2016). Since the first constriction is positioned at 160 ms after droplet formation, it is expected that the equilibrium interfacial tension has been reached (Muijlwijk, Hinderink, et al., 2016). However, during passage through the constriction (typically <1 ms), the interface is dilated and dynamic interfacial phenomena may occur. Therefore, we used a stretched exponential fit; $D = D_{max} * e^{\frac{-t^{\beta}}{\tau}}$ (Sagis et al., 2019) to determine the relaxation time of droplets, and thereby detect possible structural heterogeneity. The stretched exponential gives a good fit of the experimental data (Figure 5.2).

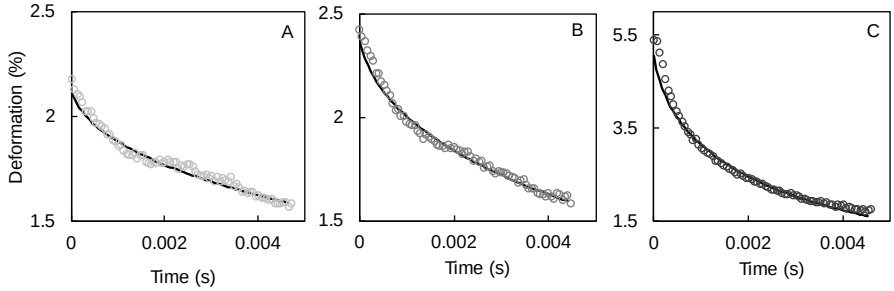

Figure 5.2. Droplet deformation over time with the corresponding stretched exponential fit (solid line) for A) 0.1, B) 1 and C) 10 g/L SDS in C1.

The droplet deformation increased with SDS concentration (Table 5.1), which is interesting since the same equilibrium interfacial tension (γ_{eq}) was expected for the 1 g/L and 10 g/L SDS-based droplets after 160 ms, albeit not necessarily during the dynamic deformation process. Droplet deformation is directly related to the capillary number and to the dynamic interfacial tension (Brosseau et al., 2014). This highlights that dynamic effects introduced by the interface dilatation (<1 ms) in the constriction are playing a crucial role. At 10 g/L SDS, far above the CMC of SDS (2.4 g/L), SDS molecules are expected to rapidly adsorb at the dilated interface, decreasing the dynamic interfacial tension: this could thus result in higher deformations. Conversely, 1 g/L SDS is below the CMC and the adsorption at the dilated interface is slower, resulting in a higher dynamic interfacial tension and smaller

deformations. For all concentrations, the stretch exponent β of ~0.5 (Table 5.1) reveals dynamic heterogeneity (β<1) during relaxation, which suggests that the interface is not homogeneously covered by the SDS-molecules as a result of deformation, and concentration gradients have developed on the surface. At 10 g/L SDS concentration, the relaxation time is significantly lower. It could be that the initially lower surface tension leads to more deformation of the droplet, which results in a higher dynamic surface tension (when diffusion is too slow to compensate for the dilation) (Jones et al., 2003). A higher surface tension implies a higher driving force for the droplet to relax back to its spherical shape.

For the droplets formed with 0.1 g/L SDS, the relaxation time was significantly lower at C3 compared to C1. Although the difference in relaxation time is still relatively small, and no difference in the maximum deformation was found, this could indicate that this droplet was not yet at a steady state when passing through the first constriction.

To conclude, for SDS-based droplets, rapid adsorption from the bulk phase increases the maximum droplet deformation. However, within the short deformation time involved, adsorption of SDS molecules cannot fully compensate the interfacial surfactant concentration gradient which develops, resulting in dynamic heterogeneity upon relaxation.

Table 5.1. Experimentally determined maximum droplet deformation D_{max} and fitted β and τ parameters for interfacial films stabilised by SDS (0.1-10 g/L). The averages were obtained from at least five replicates. The standard deviations of the fitted parameters are smaller than the variation between replicates. Significant differences are indicated by different letters ($p<0.05$).

	D_{max} (%)		β		τ (s)	
SDS concentration (g/L)	C1	C3	C1	C3	C1	C3
10	5.4±0.14	4.7±0.04	0.49^{A}	0.50^{A}	0.003^{a}	0.003^{a}
1	2.4±0.02	2.5±0.02	0.49^{A}	0.48^{A}	0.023^{b}	0.023^{b}
0.1	2.2±0.01	2.2±0.02	0.49^{A}	0.51^{A}	0.048^{c}	0.036^{d}

5.4.2. Maximum deformation of protein-stabilised droplets

For protein-based droplets, we first discuss their maximum deformation patterns in this section; droplet relaxation is then discussed in the next section. In the first constriction, the maximum deformation of protein-based droplets was between 2 and 3% (Figure 5.3). For the WPI-based droplets, the maximum deformation increased slightly when increasing the protein concentration from 0.01 to 0.1 g/L, after which it decreased to a constant value (~2%) at 0.5 and 1 g/L WPI. This can be interpreted as follows: a lower interfacial tension at 0.1

g/L compared to 0.01 g/L enables a higher deformation; then, at higher concentrations, the interfacial protein concentration is higher, giving a higher resistance to deformation due to in-plane interactions.

The same trend is found for PPI-based systems, although with a shift to higher concentrations. Again, this suggests a reduction of the interfacial tension for 0.5 g/L PPI compared to 0.1 g/L PPI, and an increased resistance of the interfacial film against deformation at higher protein concentration. For all concentrations tested, the maximum deformation is lower for WPI- compared to PPI-based droplets. This suggests that either the interfacial tension was lower for the PPI-based interfaces, or a less stiff interface was formed. For the droplets formed with a WPI-PPI blend, the maximum deformation decreased upon increasing protein concentration.

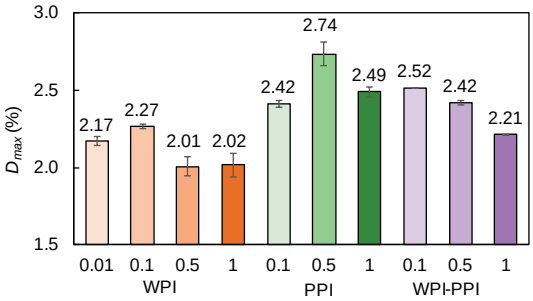

Figure 5.3. Maximum deformation (%) of emulsion droplets at the first constriction (i.e., 0.16 s after droplet formation at the T-junction) of the microfluidic rheology chip, with WPI, PPI or blends of WPI-PPI at various concentrations in the aqueous phase.

Based on the flow rate and the length of the channels, the droplets pass the first constriction after 0.16 s, the second one after 0.5 s and the third one after 1 s. For the WPI-based droplets, the maximum deformation remained constant (Figure 5.4A) throughout these successive constrictions. This suggests that a metastable interface was formed within 0.16 s, and that extra protein adsorption, or further interactions/rearrangements at the interface during this time frame did not occur, or at least did not increase its stiffness. In all constrictions, the maximum deformation was slightly higher at 0.1 g/L compared to 0.5 and 1 g/L (Figure 5.4A). However, at C3, the maximum deformation was similar for 0.1 and 0.01 g/L WPI (Appendix B, Figure B1), which could mean that the protein layer was formed in a different way depending on whether low (0.01, 0.1 g/L) or high (0.5, 1 g/L) whey protein concentrations were used. For conventional emulsification, it is assumed that at higher

protein concentrations, a closer packing of proteins may occur (Hunt et al., 1994; Tcholakova et al., 2003), and different interfacial compositions are present (Ye, 2008). If this also holds for our microfluidic experiments, this could imply that at low concentrations, multiple protein species were present at the interface (e.g., α-lactalbumin, β-lactoglobulin and bovine serum albumin), whereas at higher concentrations, one protein tends to dominate the interfacial composition.

For PPI and WPI-PPI (Figure 5.4B, C), at the lowest concentration tested (0.1 g/L), the maximum droplet deformation increased at C2, which could be due to a moderate decrease of the interfacial tension, as compared to the situation in C1. The maximum deformation then decreased again at C3, probably due to further protein adsorption in the C2-C3 interval, and to in-plane interactions between adsorbed proteins resulting in a stiffer interface. At higher concentrations (0.5 and 1 g/L), the maximum deformation decreased monotonously going from C1-C2-C3 (Figure 5.4B and C). At 1 g/L and long adsorption time (1 s, C3), the PPI-based interfacial layer resists deformation to the same extent as whey protein-based layers; in both cases this is probably due to lateral inter-protein interactions that result in a rigid interfacial network (Williams et al., 1997).

The maximum droplet deformation was overall higher for pea protein-based interfaces compared to whey protein-based ones. Based on the aforementioned findings and explanations, a higher droplet deformation may be explained by two factors: a lower dynamic interfacial tension, or a less stiff and interconnected interfacial film. The former factor is difficult to assess in the time scale and hydrodynamic conditions encountered here; however, using an automated drop tensiometer, we previously found relatively similar - and high - interfacial tensions at the oil-water interface for WPI and PPI solutions, at the first measurable time point, i.e., slightly below 1 s (Hinderink, Sagis, et al., 2020; Ho et al., 2017). The second factor, related to the structural organisation of the interface, is likely to have played a role either through weaker protein-protein interactions or due to a lower adsorbed amount. For emulsions prepared by conventional homogenisation techniques, it was found that pea proteins have a higher surface coverage (i.e., mg protein per m^2 interface), compared to whey proteins (Hinderink et al., 2019). Therefore, to form such an interfacial film, more protein material would need to accumulate at the interface, and thus a longer time would be required, which matches the outcomes of the present work. Whether inter-protein interactions

may have played a role is discussed further in section 3.3; in the following lines, we first discuss the role of protein adsorption and surface load of the droplets.

Emulsifier adsorption can be divided into three steps: 1) transport of the molecules to the interfacial sub-layer by diffusion or convection, 2) diffusion through the sub-interface and 3) kinetic adsorption at the interface (Brösel et al., 1999). To verify if convection or diffusion was dominating mass transport, the Péclet number was calculated (Appendix A). A Péclet number below 1 indicates that diffusion is dominating, whereas a value above 1 indicates that convective mass transport is dominating (Baroud et al., 2008). The Péclet number (~ 10^3 – 10^4) confirms convective mass transport throughout the whole chip. Nonetheless, proteins must next diffuse through the sub-interface. The diffusion coefficient is inversely proportional to the particle radius (r) and, for macromolecules this is related to their molecular weight (Friedman et al., 1986). The major whey proteins have a relatively low molecular weight: bovine serum albumin (66.5 kDa), β-lactoglobulin (18 kDa) and α-lactalbumin (14 kDa), whereas the main pea proteins are legumin, a hexamer with a molecular weight of 360 kDa and vicilin, a trimer with a molecular weight of 170 kDa (Gatehouse et al., 1984). The diffusion coefficients were estimated from their molecular weight according to the Stokes-Einstein equation, and are typically more than two times lower for the components in pea protein (Appendix A). Besides the native molecules and supramolecular assemblies, it is good to point out that as a result of the harsh extraction processes (heat, solvents and pH-shifts) applied to produce commercial plant protein isolates, structural changes may occur including extensive aggregation (Amagliani & Schmitt, 2017; Chen, Zhao, & Sun, 2013; van der Goot et al., 2016). The diffusion coefficient of such aggregates will be extremely low. Overall, the diffusion of pea proteins components through the sub-interface is expected to be lower compared to whey proteins, which could explain the slower network formation. In a drop tensiometer, where the highest frequency achieved for oscillatory dilatational deformation is ~0.1 Hz, the maximum interfacial expansion rate (~0.005 s^{-1}) is already too high for significant re-adsorption of proteins to occur (Hinderink, Sagis, et al., 2020). In our microfluidic chips, the expansion rate is orders of magnitude higher (~20 s^{-1}), so it is clear that in the present work, protein re-adsorption during droplet deformation did not play a substantial role.

When both proteins were used together at 0.1 g/L, the maximum deformation of the droplets remained constant (2.5-2.6%) over the first two constrictions, after which it decreased in the

third constriction (2.3%). Thus, at 0.1 g/L, the maximum droplet deformation at C1 and C2 resembles the deformation of the PPI-based droplets, suggesting low interactions between the adsorbed proteins and/or low interfacial coverage (see also Appendix B, Figure B2). At higher concentrations (0.5 and 1 g/L), the maximum deformation decreased from C1-C2-C3. This may be due to enhanced protein adsorption when using blends (Hinderink et al., 2021), leading to higher surface loads and thicker interfacial layers compared to the individual proteins.

The fact that the maximum droplet deformation decreased over time and with increasing protein concentration clearly indicates different behaviour compared to SDS-based interfaces. For protein-based interfaces, the adsorption and in-plane protein interactions are responsible for the maximum deformation whereas for surfactants the transfer between the bulk and interface plays a major role. The fact that this already occurs at the very short time scales used here is remarkable; until now, this had only been described after 2 hours for surfactant- and protein-stabilised (lysozyme, β-lactoglobulin) droplets (Erni et al., 2005).

Overall, the WPI-based droplets were able to resist the bulk shear stress to a higher degree compared to the PPI- or blend-based droplets, leading to a lower deformation. For whey proteins, and especially its main component β-lactoglobulin, it is known that interfacial polymerisation due to intermolecular disulfide bonds (Dickinson & Matsumura, 1991; Monahan et al., 1993) results in viscoelastic layers with a high resistance against deformation when given sufficient time to develop (Hinderink, Sagis, et al., 2020; Schröder, Berton-Carabin, et al., 2017; Yang et al., 2021), i.e., within at least hours. In the microfluidic devices, the involved time scales are orders of magnitude lower, and thus the high resistance against deformation is most likely an effect of surface coverage and of non-covalent, in-plane protein interactions such as hydrogen bonds and van der Waals interactions, causing significant viscoelastic surface stresses, that are expectedly the basis for further network formation.

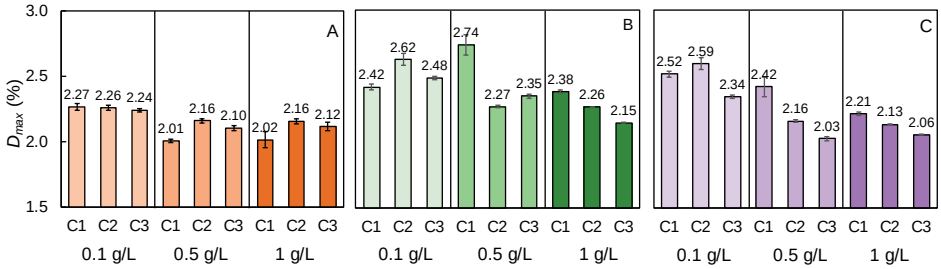

Figure 5.4. Maximum deformation (%) of emulsion droplets at constrictions C1, C2 and C3 of the microfluidic rheology chip, with (A) WPI, (B) PPI or (C) blends of WPI-PPI at various concentrations (0.1-1 g/L) in the aqueous phase.

5

5.4.3. Relaxation behaviour of protein-stabilised droplets

While the maximum deformation gives insight into the stiffness of the interfacial layer, the relaxation time gives information about the relative importance of the viscous and elastic contributions. We plotted the stretched exponential fit in Figure 5.5A-C for the 1 g/L protein-based droplets (see Appendix B, Figure B3 for the other concentrations). The relaxation times for the WPI-, PPI- and WPI-PPI-based droplets are reported in Figure 5.5D, and the stretch exponent β in Appendix B, Table B1. The protein-based interfaces exhibited β values in the range of 0.4-0.7, which is similar to values obtained for protein-stabilised interfaces after 3 hours ageing (Sagis et al., 2019; Yang et al., 2020, 2021); it is thus worth noticing that a similar degree of interfacial heterogeneity -as indicated by this parameter- is already found within 1 s of droplet lifespan.

In general, when increasing protein concentration and adsorption time, the relaxation time increased (Figure 5.5D). Interestingly, at the first constriction, the relaxation times for 0.1 g/L WPI- and 0.5 g/L PPI-based droplets were shorter compared to 0.01 g/L WPI- and 0.1 g/L PPI-based ones, respectively. These systems also had a higher maximum deformation (Figure 5.4), probably due to a higher surface coverage (i.e., lower dynamic interfacial tension without restricting deformation). At higher concentrations and/or longer adsorption times, the relaxation times increase (Figure 5.5) indicating that in-plane protein interactions start playing a role in the relaxation pattern of the interfacial film, resulting in an increase in the viscous contribution to the response. We did not observe any superimposed oscillations in the decay, which implies that the response at these time scales is dominated by the viscous contributions.

The WPI-based droplets had longer relaxation times compared to the PPI-based ones, at the same concentration and adsorption time (Figure 5.5D). This suggests a relatively higher viscous contribution in the WPI protein-based interfaces compared to PPI. It is clear that in-plane protein interactions already play a role in the probed time scales (0.16 s - 1 s), and increase over time. Work of Erni and co-workers (Erni et al., 2005), involving much longer time scales, showed oscillations in the relaxation pattern due to formation of interfacial stresses of the viscoelastic protein network. We did not observe such oscillations, probably due to the shorter time scales used in our work that only allowed very early network formation.

In the first constriction, there is no significant difference in relaxation time between the WPI-PPI-based droplets and the droplets stabilised by the individual components. From C1 to C3, the relaxation times become significantly longer for the blend-based droplets at 0.5 and 1 g/L; more proteins adsorb at the interface, leading to a relatively higher viscous contribution (Figure 5.5D), and reduced maximum deformation (Figure 5.4).

The 1 g/L WPI-PPI blend solution contains 0.5 g/L WPI, and 0.5 g/L PPI. When comparing with the same concentrations of the individual proteins, the maximum deformation obtained with 1 g/L WPI-PPI (D_{max}= 2.2%) was similar to that found for 0.5 g/L WPI (D_{max}= 2.0%), but considerably lower than that found for 0.5 g/L PPI (D_{max}= 2.7%), which may be interpreted as dominant effects from WPI. Furthermore, the relaxation times obtained for the 1 g/L WPI-PPI- and 0.5 g/L WPI-based droplets were similar in the first constriction, whereas the 0.5 g/L PPI-based droplets had a significantly lower relaxation time. After 1 s, the maximum droplet deformation with 1 g/L WPI-PPI was the same as with 0.5 or 1 g/L WPI, with, however, a significantly longer relaxation time. This shows that there is also a synergistic contribution of the pea proteins, leading to a relatively more viscous network over time.

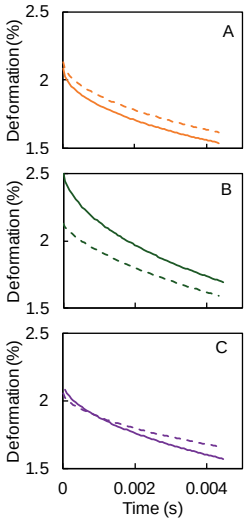

D

Protein concentration (g/L)		τ (s) C1	τ (s) C3
1	WPI	0.041^{e-i}	0.045^{f-i}
	PPI	0.021^{a-b}	0.025^{a-d}
	WPI-PPI	0.034^{c-g}	0.059^{j-k}
0.5	WPI	0.031^{b-e}	0.049^{i}
	PPI	0.017^{a}	0.033^{b-g}
	WPI-PPI	0.021^{a-b}	0.063^{k}
0.1	WPI	0.039^{e-i}	0.049^{h-j}
	PPI	0.024^{a-d}	0.015^{a}
	WPI-PPI	0.020^{a-n}	0.033^{d-g}
0.01	WPI	0.044^{f-i}	0.033^{b-f}

Figure 5.5. Relaxation patterns of the stretched exponential fit for (A) WPI-, (B) PPI- and (C) WPI-PPI-based droplets at a concentration 1 g/L in the aqueous phase. Solid lines represent the relaxation patterns in C1, and dashed lines in C3. The relaxation patterns of droplets stabilised by 0.01, 0.1 and 0.5 g/L proteins are reported in Appendix B, Figure B3 (D) Relaxation time (τ) for droplets stabilised by WPI, PPI or WPI-PPI blends with various continuous phase concentrations. The averages were obtained from at least three droplets. Significant difference between the parameters is indicated by different letters ($p<0.05$). The standard deviations of the fitted parameters are smaller than the variation between replicates.

5.4.4. Coalescence stability of protein-based droplets, and relation with interface rheological properties

The coalescence stability of droplets was tested in another so-called coalescence chip. In this device, after allowing protein adsorption onto individual droplets for 100 ms (i.e., time spent in the meandering channel), droplets are allowed to interact over a time span of 2 s. The number of coalescence events is depicted as a function of protein concentration in Figure 5.6A. As expected, the coalescence occurrence decreased with increasing protein concentration for all proteins tested. When using PPI, a higher protein concentration was needed to fully stabilise the droplets against coalescence compared to WPI (0.5 g/L vs 0.1 g/L, respectively). The difference between the coalescence stability of whey and pea protein-stabilised emulsions has been extensively described in previous work, and it was concluded that droplet-droplet bridging by pea protein aggregates induced coalescence (Hinderink, Kaade, et al., 2020). In the present work, we attempt to combine these insights with the observed short-term rheological properties of the droplet interfaces.

To understand the effect of the interfacial layer on droplet coalescence, it is useful to shortly recall the coalescence mechanism. Droplet coalescence can be divided into three different

stages: approach of the two droplets, drainage of the continuous phase film, and film rupture (McClements, 2005). Here the term 'film' refers to the continuous phase between the droplets, and in absence of emulsifiers, this process can be described adequately using the previously mentioned stages. However, in the presence of emulsifiers, interfacial viscoelasticity comes into play (Dickinson, Murray, et al., 1988). Many proteins are extremely effective in preventing coalescence under quiescent conditions (Dickinson, 1992; Van Aken et al., 2000). They provide strong electrostatic and steric interactions depending on the environmental conditions (e.g., ionic strength and pH) and may form an interfacial layer with high resistance against interfacial film rupture.

The local rupture of the interfacial film (i.e., moment when the liquid interior of both involved droplets gets in contact) can be seen as a dilatational deformation (Bos et al., 2001; Murray, 2011), which is why the dilatational rheological properties of interfaces are considered relevant parameters to understand emulsions stability. This property is usually measured using drop tensiometry, thus at comparatively long time scale (as would occur during storage). During emulsion formation, relevant processes would occur at much shorter time scale; therefore, we believe that the insights that are obtained with our microfluidic tools are relevant for re-coalescence processes as they would occur in large scale processing equipment.

Whey protein-stabilised droplets had a higher resistance against deformation compared to pea protein-stabilised-droplets (Figure 5.3). This suggests the formation of a stiffer interfacial layer that is expected to be more resistant to rupture compared to the pea protein-stabilised interface. Furthermore, we did not observe changes in the maximum deformation of WPI-stabilised droplets over time (Figure 5.4) which suggests the fast formation (<0.16 s) of a stiff interfacial film, leading to lower coalescence occurrence. For pea proteins, higher concentrations (1 g/L) and long residence times in the microchip (1 s) were needed to reach the same interfacial stiffness. Furthermore, for all concentrations tested in the rheology chip, the relaxation times of the pea protein-stabilised droplets were shorter compared to those of the whey protein-stabilised droplets, and the pea protein layer needed more time to develop. We think that this very early interfacial stiffness provided by WPI is instrumental in preventing coalescence, together with the absence of protein aggregates in WPI. Conversely, the aggregates present in PPI (even in its 'soluble' fraction, as presently used) probably promote droplet coalescence (Hinderink, Kaade, et al., 2020).

Compared to WPI, higher concentrations of PPI were needed to keep the droplets completely stable to coalescence (Figure 5.6A). To visualise the respective contribution of each protein to the propensity of droplets to coalesce when blends were used, we determined the protein concentration needed to reach a coalescence occurrence of 0.4 (Figure 5.6B), and plotted it as a function of the WPI mass ratio in the blend (Figure 5.6C). For droplets stabilised by only PPI or WPI, concentrations of ~0.25 and 0.03 g/L were required, respectively. For the blends, higher protein concentrations were needed compared to the values calculated by expecting an equal contribution of both proteins (represented by the dashed line on Figure 5.6C). For example, in a blend with 75 wt.% WPI (3:1 WPI-PPI) the protein concentration needed to reach coalescence occurrence of 0.4 was 0.16 g/L, compared to 0.1 g/L for the calculated values. For the blends with lower fractions of WPI (25 or 33 wt.%), the total protein concentration needed to stabilise the droplets was as high as with PPI alone. These results show that pea proteins hamper the droplet stabilisation effect of whey proteins, and play an active destabilising role in that respect.

The deformation experiments suggested that the WPI-PPI blends led to substantial adsorption and network formation, forming an interface with good resistance against deformation and long relaxation time (e.g., at C3 and 1 g/L). However, this film did not form fast enough (e.g., at C1) to lead to a positive effect in the coalescence chip. It is expected that at the time scales that were investigated bridging of droplets by adsorbed small pea protein aggregates may have occurred, which would be favoured by an incompletely covered interfaces, leading to enhanced coalescence (Hinderink, Kaade, et al., 2020; Nagarkar et al., 2012; Schröder et al., 2018).

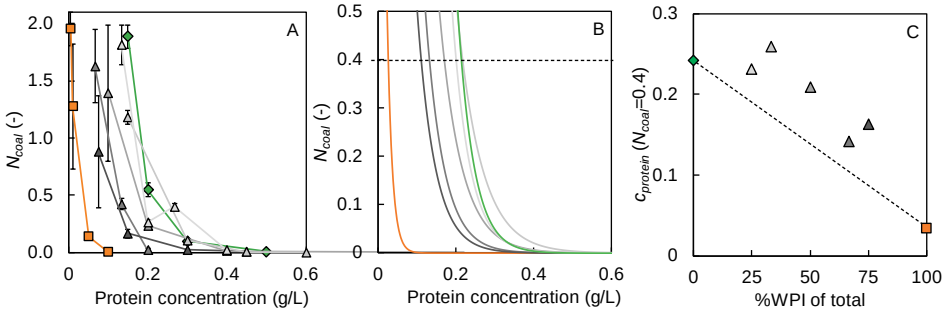

Figure 5.6. (A) Mean coalescence occurrence at the end of the coalescence channel with different total protein concentrations (0.01-0.6 g/L) of WPI (■), PPI (◆), or blends of WPI-PPI in different mass ratios 3:1 (▲), 2:1 (▲), 1:1 (▲), 1:2 (▲), 1:3 (▲); (B) Fit of the coalescence occurrence at the end of the coalescence channel for WPI (—), PPI (—), or blends of WPI-PPI in different mass ratios 3:1 (—), 2:1 (—), 1:1 (—), 1:2 (—), 1:3 (—); The dashed line represents the coalescence occurrence of 0.4. (C) Protein concentration needed to have a coalescence occurrence of 0.4 as a function of the % of WPI in the sample. In panel B, the dashed line represents the values that would be obtained for emulsions stabilised with the blends, if the coalescence propensity was strictly proportional to the protein ratio used.

5.5. Conclusion

In this work, we used tailor-made microfluidic chips to understand the phenomena involved in the early interfacial film formation in protein-stabilised emulsions. In the so-called rheology chip, we investigated rheological properties upon droplet deformation upon passage through successive constrictions (i.e., 0.16 -1 s after their formation) for different protein concentrations in the aqueous phase (0.01-1 g/L). In the so-called coalescence chip, we characterised the propensity of similarly prepared droplets to coalescence. Whey proteins adsorbed immediately and formed interfacial layers resistant to deformation over the whole concentration range tested (0.1-1 g/L), and thereby, droplets that were immediately stable against coalescence. With pea proteins, higher concentrations (1 g/L) and longer adsorption times (1 s) were needed to reach the same resistance to deformation, and stability against coalescence. The slower adsorption of pea proteins is a result of their higher molecular weight and the presence of native and/or processed-induced supramolecular structures (Amagliani, O'Regan, et al., 2017; Chen, Zhao, & Sun, 2013), and higher concentrations were needed for full surface coverage. When both proteins were used as a blend, pea proteins hindered the stabilisation properties of whey proteins. Yet, over time, blend-based interfacial films with high interfacial connectivity were formed, that resisted deformation well, had a relatively high viscous contribution compared to films stabilised with their individual counterparts, and were stable against coalescence when used at sufficiently high concentration.

We showed that both SDS- and protein-based droplets were characterised by dynamic interfacial heterogeneity during the dilatation-relaxation process. Dynamic heterogeneity in protein-stabilised interfaces was reported after 2 hours (Sagis et al., 2019; Yang et al., 2020, 2021), but never at sub-second scale. For protein-based interfaces, in-plane intermolecular interactions are particularly relevant, whereas for surfactants the transfer between the bulk and interface plays a major role. Until now, such effects had only been described after several hours (Erni et al., 2005), but we showed herein that they are already present at very short times after droplet formation (0.16 s), which is an important step toward unravelling the early stages of interfacial protein arrangements and structure formation. We specifically note that sub-second network formation at the interface results in an increase of the viscous contribution, which will be the start of the interconnected film, typical for protein-stabilised interfaces. In a previous study, we produced emulsions using the same proteins, via conventional high-pressure homogenisation, and found larger droplets and higher surface

loads for PPI- and WPI-PPI blend-stabilised emulsions compared to WPI-stabilised emulsions, in the protein-poor regime (Hinderink et al., 2019), which is in line with the results obtained with the microfluidic techniques. Tailor-made microfluidic devices allow us to understand interfacial phenomena at short time scales, which can be instrumental for the rational design of protein-stabilised emulsions, and even more generally, of emulsions with complex interfacial structures.

5.6. *Appendix*

Appendix A

The Péclet number was calculated using: $P\acute{e} = \frac{v_c L}{D}$

Where v_c is the continuous phase velocity, L the characteristic length scale (the channel depth), and D the diffusion coefficient of the protein. The diffusion coefficient was calculated using Stokes-Einstein $D = \frac{kT}{6\pi\eta r}$, with k=1.38x10^{-23} J K^{-1}, T=293 K, η=9.08x10^{-5} kg m^{-1} s^{-1} and it's minimum droplet radius r (m) calculated using $r = 0.066M^{1/3}$x 10^{-9}, with M de molecular weight in Daltons (Erickson, 2009). The velocity in the meandering channel is 0.09 m/s, during maximum deformation just after the constriction 0.25 m/s and in the main channel 0.06 m/s. The characteristic length is 4.5x10^{-6} m for the meandering channel and 1.1x10^{-7} m for the constriction and the main channel. See Table A1 for the calculations.

Table A1. Molecular weight of the proteins, estimated protein radius, diffusion coefficient (D) and Péclet number in the meandering channel, at maximum deformation just after the constrictions and in the main channel.

	MW (kDa)	r (nm)	D (m^2/s)	Pé meandering	Pé constriction	Pé main
α-lac	14.2	1.6	1.48x10^{-9}	2.77x10^3	1.86x10^4	4.46x10^3
BSA	66.5	2.7	8.84x10^{-10}	4.64x10^3	3.11x10^4	7.47x10^3
β-lg	18	1.7	1.37x10^{-9}	3.00x10^3	2.01x10^4	4.83x10^3
Legumin	360	4.7	5.03x10^{-10}	8.15x10^3	5.46x10^4	1.31x10^4
Vicilin	170	3.7	6.46x10^{-10}	6.35x10^3	4.25x10^4	1.02x10^4

Appendix B

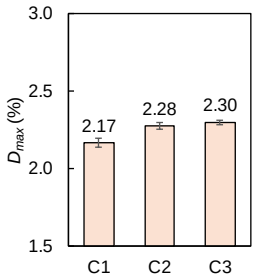

Figure B1. Maximum deformation at the three constrictions for 0.01 g/L WPI.

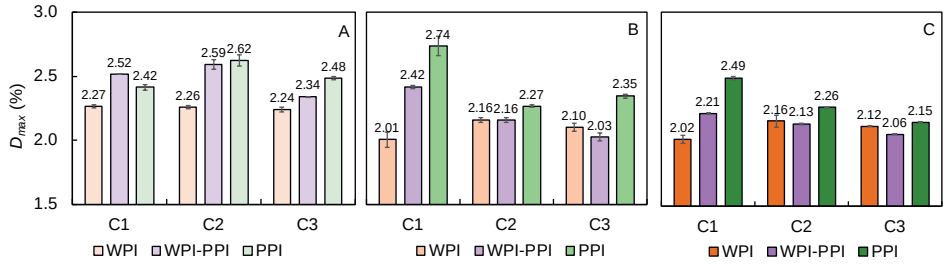

Figure B2. Maximum deformation (%) at C1, C2 and C3 for a protein concentration of; A) 0.1 g/L, B) 0.5 g/L and C) 1 g/L.

Table B1. Heterogeneity parameter (β) for droplets stabilised by whey protein isolate (WPI), pea protein isolate (PPI) or WPI-PPI blends with various continuous phase concentrations. The averages were obtained from at least three droplets. Significant difference between the parameters is indicated by different letters ($p<0.05$). The standard deviations of the fitted parameters are smaller than the variation between replicates.

Protein concentration		β		
(g/L)		C1	C2	C3
WPI	1	0.532^{B-I}	0.555^{E-J}	0.551^{D-J}
	0.5	0.535^{B-I}	0.577^{G-J}	0.551^{D-J}
	0.1	0.482^{A-E}	0.539^{C-I}	0.463^{A-B}
	0.01	0.506^{A-G}	0.500^{A-F}	0.483^{A-E}
PPI	1	0.595^{I-K}	0.582^{H-J}	0.709^{M-N}
	0.5	0.522^{A-I}	0.662^{K-M}	0.561^{G-J}
	0.1	0.480^{A-D}	0.615^{J-L}	0.754^{N}
WPI-PPI	1	0.588^{H-J}	0.671^{LM}	0.590^{I-K}
	0.5	0.514^{A-H}	0.592^{I-K}	0.580^{H-J}
	0.1	0.5178^{A-H}	0.458^{A}	0.480^{A-C}

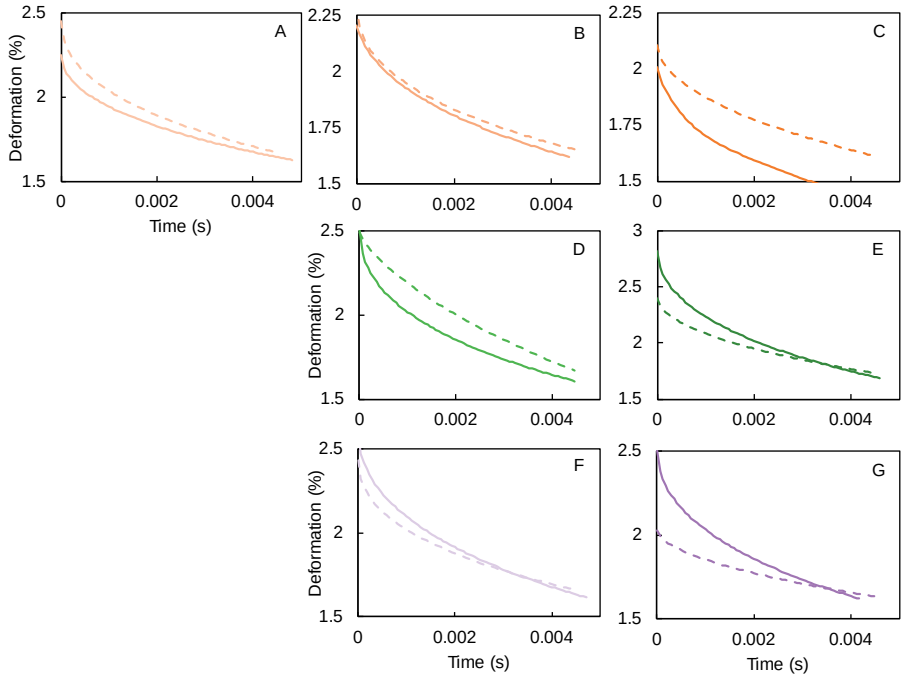

Figure B3 Relaxation patterns of the stretched exponential fit for (A) 0.01 g/L WPI-, (B) 0.1 g/L WPI-, (C) 0.5 g/L WPI-, (D) 0.1 g/L PPI-, (E) 0.5 g/L PPI, (F) 0.1 g/L WPI-PPI- and (G) 0.5 g/L WPI-PPI-stabilised droplets at a concentration 1 g/L in the aqueous phase. Solid lines represent the relaxation patterns in C1, and dashed lines in C3.

Chapter 6

Microfluidic investigation of the coalescence susceptibility of pea protein-stabilised emulsions: Effect of protein oxidation level

This chapter has been published as Hinderink, E.B.A., Kaade, W., Sagis, L., Schroën, K., Berton-Carabin, C.C. Microfluidic investigation of the coalescence susceptibility of pea protein-stabilised emulsions : Effect of protein oxidation level. *Food Hydrocolloids.* **2020**, *102* (102). https://doi.org/10.1016/j.foodhyd.2019.105610.

6.1. *Abstract*

Proteins are used to stabilise oil-in-water (O/W) emulsions, and plant proteins are gaining interest as functional ingredients due to their higher sustainability potential compared to e.g., dairy proteins. However, their emulsifying properties are not that well understood, and depend on how their production process affects their physicochemical status. In the present work, we use the soluble fraction of commercial pea protein isolate to stabilise O/W emulsion droplets formed in a microfluidic device, and record coalescence stability after droplet formation (11-173 ms) for different protein concentrations (0.1-1 g/L). For the shortest adsorption times (11- 65 ms) droplets were unstable, whereas for longer adsorption times differences in coalescence stability could be charted. Metal-catalysed oxidation of pea proteins performed for up to 24-h, prior to emulsion formation and analysis, increased the coalescence stability of the droplets, compared to fresh pea proteins. This may be explained by oxidation-induced protein fragmentation, leading to low molecular weight products. The Langmuir-Blodgett films looked highly heterogeneous for films prepared with fresh or mildly oxidised (3-h) proteins, and was more homogenous for 24-h oxidised proteins. This could be the cause for the observed differences in emulsion coalescence stability, structurally heterogeneous films being more prone to rupture.

From this work, it is clear that the emulsifying properties of pea are strongly dependent on their chemical status, and associated structural properties at the molecular and supramolecular levels. The present microfluidic device is an efficient tool to capture such effects, at time scales that are relevant to industrial emulsification.

Graphical abstract

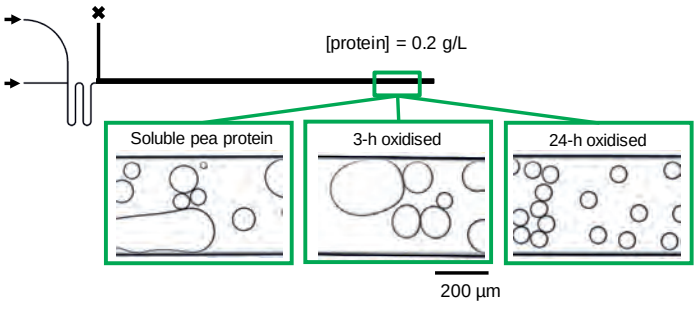

6.2. Introduction

Many food products such as dressings, mayonnaises, ice creams, and soups are oil-in-water (O/W) emulsions, i.e., dispersions of oil droplets in an aqueous phase. Emulsions are standardly made with large-scale homogenisers that disperse the oil phase into the continuous water phase, at the expense of considerable energy. Often, industrial homogenisation processes involve a combination of droplet break-up and rapid droplet recoalescence, with both phenomena taking place at very short time scales (Walstra, 2003). How droplet formation and recoalescence are related is not well understood, because it is highly challenging to do quantifiable measurements under these conditions. If information on these typical time scales was obtained, this would open new routes for emulsification, which could facilitate the development of innovative emulsions based on different raw materials. This is especially relevant for the so-called protein transition that promotes the use of plant proteins, of which the functionality is not well-characterised yet.

Dairy proteins are often used as emulsifiers as they are able to adequately stabilise emulsion droplets (Dickinson, 1997; McClements, 2004b) and add to the nutritional quality of the product. However, due to their high cost and environmental impact, plant proteins, e.g., from soy and pea, are gaining interest as more sustainable alternatives. The advantage of pea over soy proteins is their lower allergenic potential and higher nutritional value, as they are rich in the essential amino acids tryptophan and lysine (Roy et al., 2010). Although pea proteins may be used to make small and stable droplets in the protein-rich regime (Can Karaca, Low, & Nickerson, 2011; Gumus, Decker, & McClements, 2017; Ho, Schroën, Martín-González, & Berton-Carabin, 2017; Hinderink et al., 2019), when used at lower concentrations their functionality is considerably less compared to that of dairy proteins, such as whey proteins and sodium caseinate. For example, a recent study reported a droplet size ($d_{3,2}$) of 0.7 µm for a soluble pea protein-stabilised emulsion, compared to 0.4 µm for whey protein- or sodium caseinate-stabilised emulsions. The size difference is probably caused by slow adsorption of pea proteins and rapid droplet recoalescence during homogenisation (Hinderink et al., 2019). Plant protein isolation processes often involve heat, pH changes and different solvents (van der Goot et al., 2016), which may induce protein aggregation and possibly also changes in the protein's chemical status, such as oxidation.

Protein oxidation leads to amino acid side chain modifications, fragmentation and protein cross linking (Lund et al., 2011), and is normally undesirable in foods as it decreases protein

digestibility. In emulsion systems, protein oxidation is interrelated with lipid oxidation (Berton, Ropers, et al., 2012), which subsequently negatively affects the sensory and nutritional quality of the food products (Jacobsen, 1999). Protein oxidation has also been reported to affect the emulsifying and interfacial properties of proteins: for instance, highly oxidised whey protein formed less elastic interfacial layers compared to the non-oxidised material (Berton-Carabin et al., 2016), resulting in lower emulsion droplet coalescence stability (Muijlwijk et al., 2017). In contrast, when exposed to low concentrations of pro-oxidant (H_2O_2) for short times, an increase in the emulsifying activity and emulsion stability indices was observed for whey protein (Kong et al., 2013). Improved emulsifying properties were also reported for soy proteins that were moderately oxidised, which was attributed to structural changes in the proteins such as partial unfolding, thereby increasing the electrostatic repulsion between emulsion droplets (Liu et al., 2015). Despite these few specific examples, protein oxidation is generally considered an adverse alteration that can modify the interfacial and emulsifying properties of proteins in many ways, given the varied and often substantial changes in protein structure and supramolecular structures that are involved. Other chemical modifications, such as succinylation, glycosylation, phosphorylation or hydrolysis can also modify proteins interfacial and emulsifying properties (Achouri, Zhang, & Shiying, 1998; Can Karaca, Low, & Nickerson, 2015; Malabat, Sánchez-Vioque, Rabiller, & Gueguen, 2001; Vioque, Sánchez-Vioque, Clemente, Pedroche, & Millán, 2000).

Emulsion droplet formation and possible recoalescence take place within the millisecond to second range, but conventional size measurements are, at the earliest, performed only a few minutes after emulsion preparation (Håkansson, 2016), which makes it rather impossible to distinguish both effects. Microfluidics can be used to measure coalescence stability of the droplets directly after formation (Krebs et al., 2012, 2013), allowing observation in the sub-second range. The microfluidic set-up developed by Krebs et al. contains a T-shaped junction at which oil droplets are formed in a continuous water phase, a meandering channel where emulsifier adsorption continues, followed by a coalescence channel where droplets may collide, and are subject to coalescence if not sufficiently stabilised. This method was already used to study the coalescence stability of low molecular weight surfactant-stabilised droplets (sodium dodecyl sulphate) (Krebs et al., 2012) and dairy protein-stabilised droplets (β-lactoglobulin, whey protein and oxidised whey protein) (Muijlwijk et al., 2017). In the latter

study, the length of the meandering channel was varied, allowing for variation in adsorption time and thus droplet coverage, while making droplets interact under similar flow conditions. This work demonstrated that it is possible to quantify the effect of protein adsorption time on droplet coalescence, and to distinguish between different proteins. For example, when using an adsorption time of 100 ms, about 2 times more whey protein (0.01 wt.%) than pure β-lactoglobulin were needed to stabilise the same oil volume fraction (25% v/v). Compared to their structurally heterogeneous counterparts, homogenous interfaces were found to be more stable against coalescence stability observed with microfluidics (Muijlwijk et al., 2017), and this effect may also apply for pea protein-based interfaces.

Taking that work as a basis, our study aims at understanding the coalescence stability of pea protein-stabilised droplets when made at different protein concentrations, protein adsorption times, and degree of protein oxidation. The observed behaviour is linked to interface structural heterogeneity through Langmuir-Blodgett films analysed by atomic force microscopy (AFM). The combination of these techniques allows us to link the chemical properties of pea protein, the coalescence stability of emulsion droplets, and the formed interfacial structures. This is an important step towards the rational design of plant protein-stabilised emulsions based on typical time scales relevant to emulsification processes.

6.3. Materials and methods

6.3.1. Materials

PPI was obtained from Roquette, France (NUTRALYS s85F, See Appendix Table A2.1, Chapter 2 for the amino acid composition and content, and protein content). The soluble protein concentration was determined using a bicinchoninic acid (BCA) assay (BCA1-1KT, Sigma-Aldrich, Saint Louis, USA). Sodium phosphate dibasic (Na_2HPO_4), sodium phosphate monobasic (NaH_2PO_4), hexadecane, iron (II) sulphate ($FeSO_4$), hydrogen peroxide (H_2O_2), sodium ascorbate ($C_6H_7NaO_6$), hydrochloric acid (HCl), 2,4-dinitrophenyl hydrazine (DNPH) ($C_6H_6N_4O_4$), trichloroacetic acid (TCA) ($C_2HCl_3O_2$), guanidine (CH_5N_3), Tris buffer, glycerol, sodium dodecyl sulphate (SDS), glycerol, bromophenol blue R-250 (BPB), 2-β-mercaptoethanol, and solvents (ethanol, ethyl acetate, 2-propanol) were all purchased from Sigma Aldrich (Saint Louis, Missouri, USA) and were of analytical grade. Mini-PROTEAN gels (12% min i-PROTEAN® TGX™ Precast Protein Gels, 10-well comb, 30 µl/well), Bio-safe Coomassie G-250 stain, and precision plus protein standard (Bio-Rad, Richmond, CA, USA), were used for SDS-PAGE analysis. Ultrapure water was obtained from a Milli-Q system (Millipore Corporation, Billerica, Massachusetts, US), and used for all the experiments.

6.3.2. Preparation of protein samples

PPI (6 wt.%) was dispersed in a 10 mM phosphate buffer (pH 7.0) and stirred for at least 24-h at 4 ºC. The insoluble part was removed by centrifugation (16,000 x *g*, 30 min) and the supernatant was centrifuged again under the same conditions. The protein content of the supernatant was determined with the BCA assay (Smith et al., 1985) at 562 nm using a DU 720 UV-vis spectrophotometer (Beckman Coulter, Woerden, the Netherlands). This supernatant was used for all pea protein-based experiments, and is for simplicity referred to as ‘protein solution’ from now on.

Pro-oxidant solutions, i.e., $FeSO_4$ 600 µM; H_2O_2 150 mM; and sodium ascorbate 150 mM, were prepared separately in 10 mM phosphate buffer (pH 7.0). To catalyse the production of hydroxyl radical through the Fenton reaction, equal amounts of each solution were added to the protein solution to reach final pro-oxidant concentrations of 100 µM; 25 mM; and 25 mM, respectively, and a final protein concentration of 5 g/L. The mixture was rotated at 25 °C in the dark for 48 h (SB3 rotator, Stuart, Staffordshire, UK).

Aliquots were taken in time (1, 3, 6, 24, and 48 h), of which the oxidising agents were immediately removed by ultrafiltration-centrifugation (Amicon cells, cutoff 10 kDa, Sigma-Aldrich) at 4,000 x *g*, for 30 min at 20 °C, to prevent further metal-catalysed oxidation to take place (Chao et al., 1997). Ultrafiltration-centrifugation was performed three times. After each step, the filtrate was discarded and the retentate brought back to the initial volume by adding fresh buffer. The final retentate, containing the oxidised proteins, was re-suspended in a volume of fresh buffer equivalent to the volume of filtrate discarded. The exact protein concentration was then determined with the BCA assay, after which the protein solutions were stored at -20 °C until further use.

6.3.3. Characterisation of protein samples

Determination of protein-bound carbonyls

Protein-bound carbonyls were determined according to the procedure of Levine et al. (1990). Briefly, aliquots of 200 µL PPI solution were mixed with 2-propanol (ratio 1:10 v/v) and centrifuged at 15,000 x *g* for 5 min at 20 °C. The supernatant was discarded, and the protein pellet dispersed in 500 µL 10 mM DNPH solution (2,4-dinitrophenylhydrazine) in 2N HCl and kept for 60 min at 20 °C in the dark; 500 µL of 2 M HCl solution received the same treatment and used as blank. The tubes were placed on ice and 500 µL of 400 g/L TCA solution was added to precipitate the proteins. Subsequently the tubes were centrifuged (15,000 x *g*, 5 min, 20 °C) and the supernatants were discarded. The pellets were washed twice with 1 mL of ethanol/ethyl acetate (1/1 v/v), once with 1 mL of 2-propanol, and finally dissolved in 1 mL guanidine chloride 6 M at 37 °C, followed by centrifugation (15,000 x *g*, 5 min, 20 °C) to remove any insoluble matter. The absorbance of the supernatant was measured at 370 nm using samples without DNPH as blanks. The protein-bound carbonyl content was calculated using 22,000 M^{-1} cm^{-1} as molar absorption coefficient, and the soluble protein content was determined through the BCA assay. The results were express in mmol carbonyl per kg of soluble protein.

Tryptophan fluorescence

The intensity of tryptophan fluorescence emission in the protein solutions was determined between 300-380 nm with a step size of 1 nm, at a scan rate of 60 nm/min using a RF-6000 fluorescence spectrophotometer (Shimadzu, Kyoto, Japan). The excitation wavelength was

set at 290 nm. The maximum peak intensity was determined for the oxidised pea protein solution and compared to that of the non-oxidised solution.

Surface exposed hydrophobicity

The anionic fluorescent probe ANSA (8-anilo-1-naphtalensulfonic acid ammonium salt) was used to quantify the exposed hydrophobicity of the fresh and oxidised pea proteins. Aliquots of 10 µL ANSA solution (2.4 mM in 10 mM phosphate buffer at pH 7.0) were added to 1 mL of protein solution (0.12 g/L). After each addition, the emission spectrum was recorded between 400 and 650 nm using an RF-6000 fluorescence spectrophotometer. An excitation wavelength of 385 nm and scan rate of 200 nm/min were chosen, with both excitation and emission bandwidths at 5.0 nm. The relative exposed hydrophobicity was expressed as increase or decrease in the integrated titration curve between 400-600 nm after blank subtraction with respect to the non-oxidised pea protein solution.

High performance size-exclusion chromatography (HP-SEC)

High performance size-exclusion chromatography (HP-SEC) was performed using a Dionex UltiMate 3000 Rapid Separation Liquid Chromatography system (Thermo Scientific) to identify the size of soluble and oxidised PPI. Before separation, the solutions were filtered using a mini spike syringe filter with a pore size of 0.2 µm. Proteins were separated on a TSK (Gel-G3000SWXL+G2000SWXL 5 µm 300x7.8 mm) column. The temperature of the column was set to 30 °C. The proteins were eluted with a buffer containing 30% acetonitrile (ACN) in ultrapure water containing 0.1% trifluoroacetic acid (TFA) at 1.5 mL/min flow rate. The HP-SEC column was used in line with a UV detector (214 nm). To relate the retention time to the molecular weight of the proteins, a calibration curve was generated with the following protein standards: Thyroglobulin, 670 kDa; g-Globulin, 158 kDa; Ovalbumin, 44.3 kDa; α-Lactalbumin, 14 kDa; Aprotinin, 6.51 kDa; Bacitracin, 1420 Da and Phenylalanine 165 Da (Sigma-Aldrich, Saint Louis, USA).

Sodium dodecylsulphate polyacrylamide gel electrophoresis (SDS-PAGE)

SDS-PAGE was performed under reducing conditions for the fresh, 3- and 24-h oxidised pea proteins. Proteins were diluted to 2 g/L in a pH 6.8 buffer containing Tris-HCl (0.5 M), glycerol (30% w/v), SDS (10% w/v), chromophenol blue (0.5 % w/v), and 2-β-mercaptoethanol (5% v/v), and next mixed for 5 min in a heating block at 95 °C. Next, 25 µLs of the protein samples, and 10 µL of the protein standard (Biorad, Precision Plus

protein™ Standards, MW 10-250) were loaded onto the gel. A running buffer of pH 8.3 containing Tris-HCl 25 mM, glycerol 192 mM, and SDS 0.1 wt.% was used. Electrophoresis was performed in the mini-PROTEAN Tetra Cell (Bio-rad laboratories, USA) at 200 V. The gels were washed with ultrapure water before staining with Coomassie G-250 for 1 hour, which in turn was followed by extensive washing with ultrapure water.

Protein ζ-potential measurement

The ζ-potential of the protein samples was measured using dynamic light scattering (Zetasizer Ultra, Malvern Instruments, UK). A protein concentration of 1 g/L was used. Measurements were performed at 25 °C after a 2-min equilibration period. The ζ–potential was calculated using the Smoluchowski model and is expressed as the mean of two independent samples, of which each was measured in triplicate.

6.3.4. Microfluidic experiments

Microfluidic chips and connectors

Custom-designed borosilicate glass microfluidic chips (Figure 6.1) were produced by Micronit Microtechnologies B.V. (Enschede, The Netherlands). In this set-up, oil droplets were formed at the T-junction connecting the continuous and dispersed phase channels (width = 100 µm) and next flow through a meandering channel of the same width, after which they enter the coalescence channel (width = 500 µm, length = 26.2 mm). All channels have a uniform depth of 45 µm. The length of the meandering channel was varied to alter the adsorption time (from 11 to 173 ms), i.e., the time between the formation of oil droplets at the T-junction, and their entering in the coalescence channel. This was systematically investigated for the non-oxidised pea protein solution; for the oxidised pea proteins, only the chip with an adsorption time of 100 ms was used (Figure 6.1).

The chips were placed in a chip holder and connected with glass capillaries to the continuous phase (protein solution) that was pressurised into the chip at a flow rate of 40 µL/min, and to the dispersed phase hexadecane (flow rate of 2 µL/min). The phases were dosed into the microfluidic device using a pressure system (OB1, Elveflow, France), and controlled with mini CORI-Flow sensors (Bronkhorst B.V., Netherlands). The continuous phase was filtered (0.22 µm PES filter, Merck, Germany) before the experiments.

Imaging and analysis

A high-speed camera (MotionPro Y4-A2) was connected to a light microscope (Axiovert 200 MAT, Carl Zeiss B.V.), Images were recorded at the inlet and outlet of the coalescence channel, 1000 frames at 30 fps and a pixel resolution of 1.321 µm/pixel). The two dimensional area of each droplet was determined using a custom-made ImageJ macro (Muijlwijk et al., 2017). From the mean droplet area (A_f) at a certain position in the coalescence channel, and the mean initial droplet area (A_i), the mean number of coalescence events (N_{coal}) was calculated. The coalescence frequency (f_{coal}) was then calculated based on a residence time of 2 seconds at a total flow rate of 42 µL/min (Krebs et al., 2012; Muijlwijk et al., 2017), as shown in equation 6.1:

$$f_{coal} = \frac{N_{coal}}{t_{res}} \qquad 6.1$$

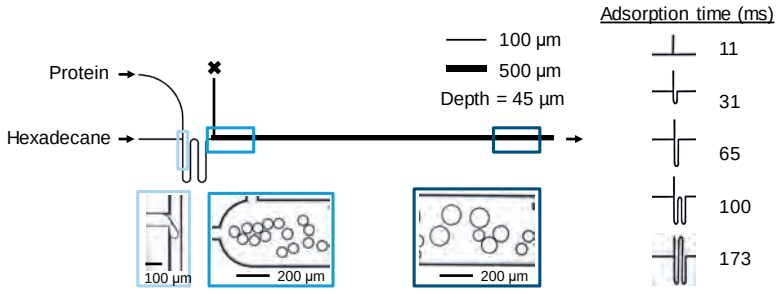

Figure 6.1. Layout of the microfluidic coalescence chip with an adsorption time of 100 ms (left). The channel widths are 100 and 500 µm as indicated by the thickness of the lines, and have a uniform depth of 45 µm. The length of the coalescence channel is 26.2 mm. The extra inlet in the coalescence channel is closed as indicated by ***x****. On the right side an overview of the different meandering channels and the corresponding adsorption times is given, when used at a total flow rate of 42 µL/min.*

6.3.5. Structural organisation of the interface

Langmuir-Blodgett (LB) films were constructed at the air-water interface using a medium KSV NIMA Langmuir trough (364 x 76 mm, Biolin Scientific, Espoo, Finland). Phosphate buffer (10 mM, pH 7.0) was used as subphase, onto which 34 µL of 1 g/L of fresh or 3-h oxidised protein solution; or 48 µL of 0.7 g/L of 24-h oxidised protein solution were spread. The interfacial layer was equilibrated for 30 min before compression, induced by slowly moving the barriers at a speed of 5 mm/min, took place. LB films were constructed on a freshly cleaved mica plate that had been immersed in the subphase before the protein solution was spread. The films were loaded at a surface pressure of 20 mN/m (fresh, and 3-h oxidised protein) or 15 mN/m (24-h oxidised protein) with an upward speed of 1 mm/min. The films

were dried in a desiccator before analysis with an atomic force microscope (AFM). The surface pressure isotherms of the proteins are reported in the appendix (Figure A6.1).

AFM images were acquired using a MultiMode 8-HRTM, Bruker AFM (Billerica, US) in tapping mode using non-conductive pyramidal silicon nitride probes with a nominal spring constant of 0.40 N/m (Bruker, Billerica, US). A lateral scan frequency of 0.977 Hz was used and the resolution was set at 512 x 512 pixels in a scan area of 2 x 2 μm^2. The AFM images were analysed with the NanoScope Analysis 1.5 software.

6.4. Results and discussion

6.4.1. Coalescence stability of emulsions stabilised with non-oxidised pea proteins

The coalescence stability of emulsion droplets stabilised by the soluble fraction of fresh pea protein (PPI) was studied for a protein concentration range of 0.1-1 g/L. It is important to mention that the initial droplet size is independent of the protein concentration used, for all concentrations tested; this indicates that the interfacial tension at the moment of droplet formation is constant over the concentration range used (Appendix, Figure A6.2).

We start by discussing the results obtained when using an adsorption time of 100 ms (Figure 2). For all concentrations used the coalescence frequency was lower (but nonzero) in the beginning of the coalescence channel compared to the end of the coalescence channel. This shows that coalescence occurred quite immediately for the low concentrations used, and continued over the coalescence channel, and protein adsorption in the coalescence channel itself could not prevent further coalescence (Figure 6.2). For protein concentrations over 0.5 g/L, the droplets were effectively stabilised. This indicates that the interface became sufficiently covered during passage of the meandering channel (100 ms), therewith protecting the droplets against coalescence (as also discussed further in Figure 3).

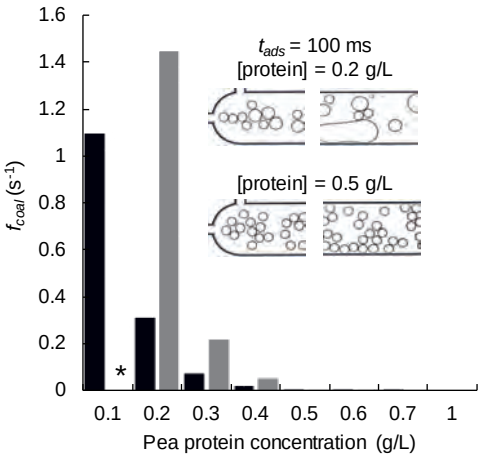

*Figure 6.2. Mean coalescence frequency at the outlet of the coalescence channel measured in the chip with 100 ms adsorption time for different concentrations (0.1-1 g/L) of the soluble pea protein in the front (black) and the end (grey) of the coalescence channel, * indicates that the coalesced droplets were too large to measure.*

When using meandering channels corresponding to adsorption times of 11 to 173 ms, the coalescence frequency decreased upon increasing protein concentration, as was also expected from the results in Figure 2, and upon increasing adsorption time (Figure 3). It should be noted that for adsorption times of 11 and 31 ms, the droplets almost immediately coalesced, for all tested protein concentrations. In contrast, from literature (Muijlwijk et al., 2017) it is known that 0.2 g/L WPI was enough to fully stabilise hexadecane droplets within 31 ms (f_{coal} < 0.02 s^{-1}). With pea protein, this was possible only at 0.5 g/L PPI using an adsorption time of 100 ms, which again was considerably higher compared to previous research in which 0.1 g/L was needed for WPI, and 0.05 g/L for β-lactoglobulin, respectively. A small overview of obtained results is shown in Table 6.1. From this it is clear that pea proteins require either a higher concentration, or a longer adsorption time to make stable emulsion droplets, as compared to whey proteins.

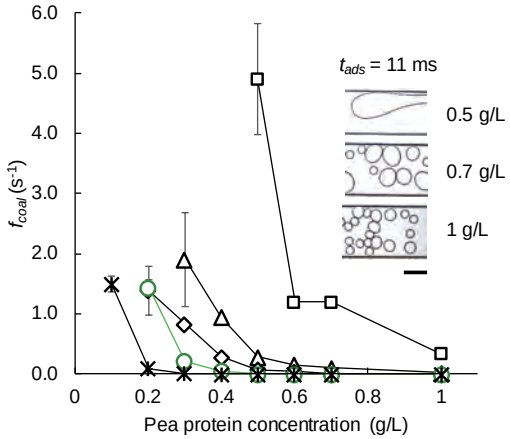

Figure 6.3. Mean coalescence frequency at the outlet of the coalescence channel measured in chips with different adsorption times 11(□), 31 (△), 65 (◊), 100 (○) and 173 (∗) ms and protein concentrations (0.1-1 g/L). The lines between the markers guides the eye. Microscopy images are taken at the outlet of the coalescence channel. The scale bare represents 200 µm.

Table 6.1. Overview of the concentrations needed to obtain stable emulsions (f_{coal} < 0.02 s^{-1}) with PPI, WPI, oxidised WPI and β-Lg after different adsorption times (t_{ads} 11-173 ms) and total flow rate of 42 µL/min. A dash indicates that no stable emulsion droplets were formed within the tested concentration range.

		t_{ads} (ms)				
		11	31	65	100	173
	Concentrations tested (g/L)	*Protein concentration (g/L) for f_{coal} < 0.02 s^{-1})*				
PPI	0.1-0.7, 1	-	-	0.7	0.5	0.3
β-Lg*	0.005, 0.01, 0.05, 0.1	-	0.05	0.05	0.05	0.005
WPI*	0.01, 0.02, 0.1, 0.2	-	0.2	0.2	0.1	0.1
Oxidised WPI*	0.02, 0.1, 0.2	-	-	-	-	0.2

* (Muijlwijk et al., 2017); in the first line results from the current paper are summarised.

It can also be interesting to compare these findings with observations for emulsions made using conventional emulsification devices, which we produced in an earlier study using the same proteins in the protein-poor regime, where PPI-stabilised droplets were considerably larger than WPI-stabilised droplets (0.7 and 0.4 µm, respectively). We proposed that this could be due to enhanced recoalescence of the droplets in the homogeniser, or to a higher interfacial tension, when pea proteins are used, compared to whey proteins (Hinderink et al., 2019). From the present study we can conclude that enhanced recoalescence is probably the main reason. In this previous study, we also found that PPI-stabilised emulsions had higher surface loads compared to WPI-stabilised ones. This could be a result of the quaternary structure of the pea proteins containing legumin (hexameric structure, 330-410 kDa), and vicilin (trimeric structure, 180-210 kDa (Mession et al., 2015)), and possibly the presence of soluble aggregates in solution due to their association behaviour at neutral pH and ionic strength below 0.1 M (Gueguen et al., 1988), or as a consequence of processing (Amagliani & Schmitt, 2017). In general, aggregated protein-stabilised emulsions have a higher surface load compared their non-aggregated counterparts, as was found for emulsions stabilised with aggregated soy protein (Cui et al., 2014), aggregated caseinate (Mulvihill et al., 1991) and aggregated whey-casein blends (Chevallier et al., 2016).

Emulsifying properties are often related to protein hydrophobicity (Wierenga et al., 2003). Soluble pea proteins are about 1.5 times more hydrophobic compared to whey proteins, which rules out the possibility that with pea proteins, the slower formation of an interfacial film which can efficiently prevent rapid recoalescence would be due to insufficient surface-

exposed hydrophobicity. Instead, the high molecular weight and aggregated state of pea proteins are probably the main reasons for the high pea protein concentrations needed to prevent recoalescence. As mentioned before, protein aggregation may result from the processing conditions applied to yield plant protein ingredients (concentrates, isolates) (Amagliani & Schmitt, 2017; van der Goot et al., 2016). These processes often involve harsh conditions (temperature, solvents, pH), leading to substantial physicochemical changes. Among such changes, protein oxidation may lead to protein cross-linking, as well as to amino acid side chain modifications, and protein fragmentation. The oxidative state of plant proteins is, however, not often considered with regard to possible consequences on emulsion stability, whereas various effects have been described, as illustrated in the introduction; therefore, next we investigate this systematically.

6.4.2. Oxidised pea proteins: characterisation and consequences on emulsion stabilisation

Physicochemical characterisation of oxidised pea proteins

In order to evaluate the effect of protein oxidation on the functional properties of pea proteins, samples were purposely oxidised, and first characterised with regard to their physicochemical properties. Their overall oxidative state was assessed through the measurement of protein-bound carbonyls (Figure 6.4A). In the initial pea protein solution, protein-bound carbonyls were detected (7 mmol/kg soluble protein), possibly as a result of the processing or storage of the pea protein isolate. Protein-bound carbonyls increased rapidly up to a plateau of around 33.5 mmol/kg soluble protein after 6 hours. The relative tryptophan intensity decreased rapidly to 0.4 after 6 hours. As shown in Figure 6.4A, the loss in tryptophan fluorescence intensity is well correlated with the formation of protein bound carbonyls. Changes in intrinsic tryptophan fluorescence upon oxidation can occur through changes in the protein tertiary structure (Liu et al., 2015), or through oxidative damage to the tryptophan due to its high susceptibility to reactive oxygen species (Utrera et al., 2012), which is probably the main reason for the loss of tryptophan fluorescence here.

Surface exposed hydrophobicity of pea proteins decreased upon oxidation (Figure 6.4B); amino acids were directly oxidised resulting in amino acid side chain modifications, and protein backbone fragmentation due to α-amidation or glutamyl residue oxidation. Consequently, the proteins aggregated which led to a decrease in the relative hydrophobicity

in the first 3-h after which a plateau was reached; further oxidation did not further decrease hydrophobicity, as was also reported for oxidised WPI (Berton-Carabin et al., 2016). The charge of the pea proteins was altered upon oxidation from 21.3 ± 0.4, 20.9 ± 0.8 to -34.2 ± 0.7 mV for PPI, 3- and 24-h oxidised pea proteins, respectively. The surface charge can change upon oxidation due to the exposure of buried amino acids and disturbance of the acid to basic amino acid proportion (Chen, Zhao, Sun, Ren, & Cui, 2013)

SDS-PAGE analysis confirmed that the protein composition changed upon oxidation (Figure 6.5A). In the first lane, the major pea proteins can be identified: convicilin (~71 kDa), vicilin subunits (~30, ~34, ~47 and ~50 kDa), α-legumin (38-40 kDa) and β-legumin (19-22 kDa) (Barac et al., 2010). Upon protein oxidation, the bands became less clearly separated, and after 24-h of oxidation, a continuous band covering a broad range of molecular weights was formed similar to previous observations for other proteins (Berton-Carabin et al., 2016; Berton, Genot, et al., 2012). When looking closely at the lanes for oxidised samples under reducing conditions, stains corresponding to higher molecular weights can be observed, which corresponds to aggregates that were not broken down in the reducing buffer. HP-SEC revealed the formation of lower MW compounds upon oxidation and confirmed a decrease in the peaks corresponding to the major components and aggregates initially present (Figure 5B). Microscopy showed the formation of insoluble protein aggregates in the 24-h oxidised sample (Appendix, Figure A6.3), these aggregates were removed before analysis (0.2 µm) and measurements. Oxidation led to a protein solubility of 52 and 26% for 3- and 24-h oxidised pea proteins, respectively (Appendix, Figure A6.4)

Overall, we conclude that upon incubation of the pea protein solution under oxidative conditions, a number of chemical reactions occurred simultaneously or sequentially, which led to the formation of protein-bound carbonyls, to oxidative damage of certain amino acids (e.g., tryptophan), to conformational changes, fragmentation and aggregation. This resulted in a highly heterogeneous protein mixture of various molecular weights and supramolecular structures, and in an overall decreased surface exposed hydrophobicity.

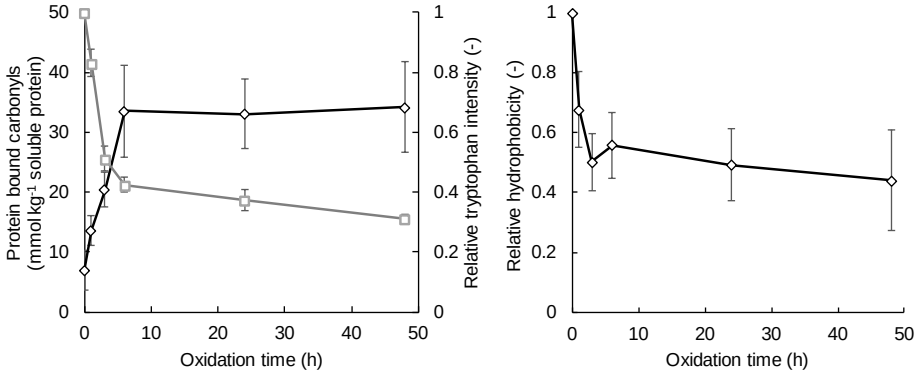

Figure 6.4. A) Formation of protein-bound carbonyls (◊) and change in relative tryptophan fluorescence (□) in pea protein solution incubated in oxidative conditions. B) Relative surface exposed hydrophobicity of soluble pea protein, fresh and under oxidative conditions. Error bars represent the standard deviation of at least 4 independent replicates, measured in triplicate.

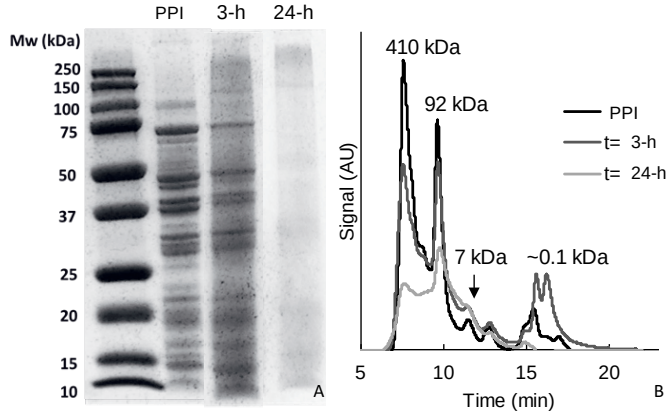

Figure 6.5. A) SDS-PAGE profiles under reducing conditions of soluble pea protein, fresh, and after 3- and 24-h incubation under oxidative conditions. The first lane on the left represents the molecular weight markers. B) HP-SEC profiles of the soluble pea protein, fresh and after 3 and 24-h incubation under oxidative conditions.

Coalescence stability of emulsions stabilised with oxidised pea proteins

Coalescence stability of emulsion droplets stabilised by fresh, 3- and 24-h oxidised pea protein was tested in the microfluidic chip with the meandering channel corresponding to an adsorption time of 100 ms. A similar coalescence stability was found for the fresh and 3-h oxidised pea protein solutions, i.e., droplets became stable at protein concentrations around 0.4-0.5 g/L (Figure 6.6). The 24-h oxidised pea protein solution formed stable droplets already at a concentration of 0.3 g/L. Interestingly, the surface exposed hydrophobicity

values were similar for the 3- and 24-h oxidised samples, and therefore probably not the reason for the improved droplet stability with the 24-h oxidised samples. The net surface charge of the 24-h oxidised samples was larger which, for long-term stability, may lead to more stable droplets, due to enhanced repulsion. Yet all samples were largely negatively charged (below -20 mV) and therefore this parameter is probably not the main reason for the distinct stabilisation mechanism of the 24-h oxidised sample. Upon oxidation protein tertiary structure can change; for example, in soy protein isolate it was reported that soluble protein aggregates with more flexible structures were formed upon moderate oxidation (Chen, Zhao, Sun, et al., 2013), and those could easily adsorb at the interface and enhance the emulsifying properties.

Next to the protein's secondary structure changes, the heterogeneity of the mixture increased upon oxidation. After 24-h the pea proteins were largely converted into protein oxidation products: peptides and aggregates (as detailed earlier). This may result in heterogeneous interfacial structures, which, in turn, may affect droplet stability (Sagis et al., 2019; Wilde, 2000). The structural heterogeneity of the interfacial layers has been studied with Langmuir-Blodgett (LB) films formed with fresh, 3- and 24-h oxidised pea protein, spread at the air-water interface, and analysed with AFM. For the fresh (Figure 6.7A) and 3-h oxidised PPI (Figure 6.7B), a heterogeneous, coarse-grained interfacial film was observed. Such a structure suggests the presence of protein aggregates at the interface, which as mentioned before could be a consequence of the isolation process and hydrophobic nature of the pea proteins. Alternatively, the heterogeneous structure could also be formed by in-plane aggregation of the proteins, leading to a jammed or quasi gelled 2-dimensional structure (Sagis et al., 2019). In the film made with 3-h oxidised pea protein, large aggregates were detected, whereas for the 24-h oxidised pea protein (Figure 6.7C), a more structurally homogenous interface was observed, with only a few small protein clusters present. This may seem to contradict the aforementioned description of this sample, in which large aggregates could be seen by optical microscopy (Appendix, Figure A6.3). However, the largest ones were removed by the filtration step (0.22 µm) prior to the experiment, and other large aggregates may have desorbed from the monolayer due to gravitational forces, or have been pushed out upon compression (Figure 6.7D).

It is interesting to speculate on the components present, their effect on the interfacial films, and how that may affect emulsion stability. For this, it seems useful to first recall some factors

that prevent or promote coalescence. Coalescence can be prevented by steric and/or electrostatic repulsion between droplets, which depend on the interfacial layer formed by emulsifiers (McClements, 2005). When steric or electrostatic repulsions are not strong enough, droplets can approach to very short distances and, if not sufficiently stabilised, coalesce. During the onset of coalescence, the interfaces are subjected to large dilatational deformation, and interfaces with a high resistance to such deformations (e.g., stabilised by a viscoelastic protein network) are protected against film rupture and subsequent coalescence (Berton-Carabin et al., 2018). Alternatively, having highly mobile surface-active molecules (e.g., low molecular weight surfactants) is also advantageous, as they can rapidly compensate an interfacial gradient and induce surface flow (Levich et al., 1969) leading to high stability through the Gibbs-Marangoni mechanism. Particles, which include protein aggregates, may lead to droplet-droplet bridging at low particle concentrations (Chevallier et al., 2019), leaving the non-bridging region particle free. The surface next to the particle is susceptible to disturbances leading to film rupture and droplet coalescence (Nagarkar et al., 2012; Schröder et al., 2018); the latter authors used the same microfluidic chips as in the current study and found that colloidal lipid particles induced coalescence due to droplet-droplet bridging at low surface coverage. At higher surface coverage, the droplets were protected against bridging and coalescence (Schröder et al., 2018).

Taking all of this into consideration, it is likely that the pea protein aggregates in the fresh and 3-h oxidised pea proteins act as particles and bridge droplets at low concentrations, therewith inducing coalescence. At higher concentrations, and higher surface loads, droplets do not share pea protein aggregates anymore and densely packed interfacial layers are formed, that protect the droplets against coalescence. In case of the 24-h oxidised pea proteins, protein fragments may predominantly adsorb at the droplets' surface, leading to rapid formation of a thin and mobile interfacial film.

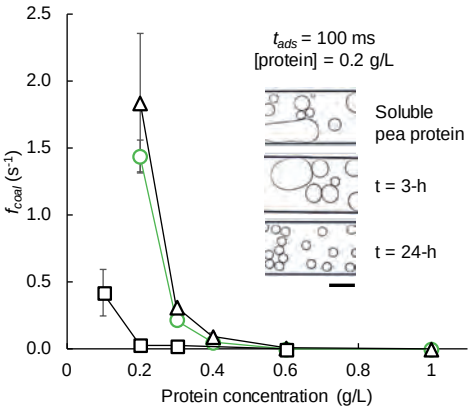

Figure 6.6. Mean coalescence frequency at the outlet of the coalescence channel measured with an adsorption time of 100 ms for different concentrations (0.1-1 g/L) of the soluble pea protein, fresh (○) and after 3-h (△) and 24-h (□) incubation in oxidative conditions. The insert shows microscopic pictures taken at the outlet of the channel, the scale bar representing 200 µm.

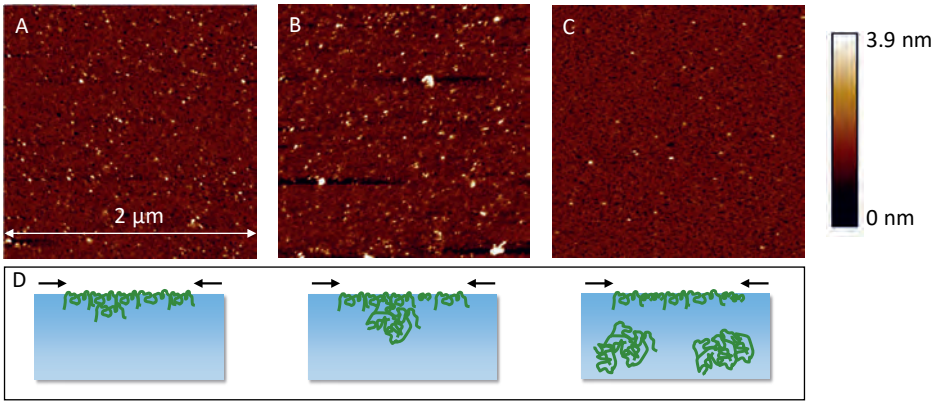

Figure 6.7. Atomic force microscopy images of dried Langmuir-Blodgett films prepared at the air-water interface with soluble pea protein, fresh (A) and after 3-h (B) and 24-h (C) incubation in oxidative conditions. D) schematic representation of interfacial layer and the subphase. The films were loaded onto freshly cleaved mica at a surface pressure of 15-20 mN/m.

6.4.3. Critical reflection on the interfacial and emulsifying properties of oxidised pea proteins

From these results, we can conclude that upon oxidation, fragmentation and aggregation of pea proteins occurs. Perhaps counterintuitively, extended oxidation leads to structurally more homogenous interfacial films, and to high coalescence stability of emulsion droplets, at least at the short time scales used in our microfluidic devices. This is probably due to a more abundant presence of low molecular weight species, which allows for faster completion of

interfacial layers that also require lower surface loads. Droplet-droplet bridging by protein aggregates also does not take place. Please keep in mind that these measurements were done over a 2-second time interval, and are thus relevant with regard to the rapid recoalescence within homogenisation devices, but not necessarily with regard to long-term emulsion stability. The latter is for proteins often related to the formation of thick viscoelastic layers (Bos et al., 2001), and it is not expected that the 24-h oxidised pea protein will form such layers.

One of the major drawbacks of pea proteins is their low solubility in neutral aqueous solutions (Klost et al., 2019). In the present work, the so-called soluble fraction was used, which represents about 25% of the total protein present in the starting ingredient. It thus implies that pea proteins are used less effectively than the completely soluble dairy-based proteins. Upon oxidation, pea protein solubility decreases even further due to extensive aggregation (Appendix, Figure A6.4), therewith reducing the usable part of pea proteins further, assuming that only the soluble part is effective in emulsion stabilisation. Furthermore, oxidation of proteins leads to loss of nutritional value, and formation of compounds with questionable health effects, and is thus undesirable (Estévez et al., 2019).

Our results suggest that the improved coalescence stability is mainly due to protein fragmentation, and therefore, other fragmentation methods, such as hydrolysis, can be considered to improve the emulsifying properties of pea proteins and mitigate the previously mentioned negative effects. It has been shown that whey protein hydrolysates can be used to stabilise emulsions at a lower surface load (Schröder, Berton-Carabin, et al., 2017), although this did not lead to higher emulsion stability compared to whey protein-stabilised emulsions. For rapeseed and pea protein it has been reported that hydrolysis can improve the emulsifying activity index and emulsion stability (Barać et al., 2011; Vioque et al., 2000). In addition, spray-dried emulsions stabilised by trypsin-hydrolysed pea proteins showed lower lipid oxidation compared to non-hydrolysed pea proteins, which was explained by the exposure of amino acids that possess antioxidant activity (Tamm et al., 2016). To generalise, protein hydrolysis can improve the emulsion formation and short-term stability due to a fast adsorption of proteinaceous material at the interface. However, for long-term stability, moderate hydrolysis of plant proteins should be preferred, as such moderately hydrolysed proteins form stronger elastic films compared to the smaller peptides (Wouters et al., 2016).

6.5. *Conclusions*

In the present work, the short-term coalescence stability of emulsion droplets stabilised by the soluble fraction of pea proteins, that was oxidised to different extents. We found that higher concentrations of pea proteins were needed to prevent rapid recoalescence of oil droplets compared to whey proteins, which is considered a reference protein emulsifier. Extensive protein oxidation led to an increase in recoalescence stability, which was related to protein fragmentation, forming low molecular weight compounds. Protein oxidation also resulted in a structurally more homogenous interfaces, compared to non-oxidised proteins, which could explain the improved emulsion stability to recoalescence. Protein oxidation is a phenomenon that may occur during production and storage of plant protein isolates. Upon oxidation protein solubility decreased and large aggregates were formed which negatively affects the valorisation of pea proteins. From our work, it is clear that the oxidative state is very relevant for plant protein functionality, which should not be overlooked in product design.

6.6. *Acknowledgments*

The authors wish to thank Jeffrey Essers and Francesca Allevi for performing preliminary experiments.

6.7. *Appendix*

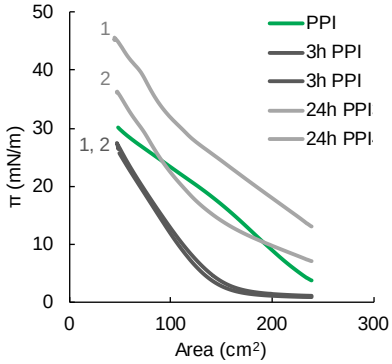

Figure A6.1. Surface pressure isotherms of soluble pea protein (PPI), fresh and after 3 and 24-h incubation in oxidative conditions. Every line represents a dependent duplicate, and for the oxidised samples, the independent duplicates are both plotted.

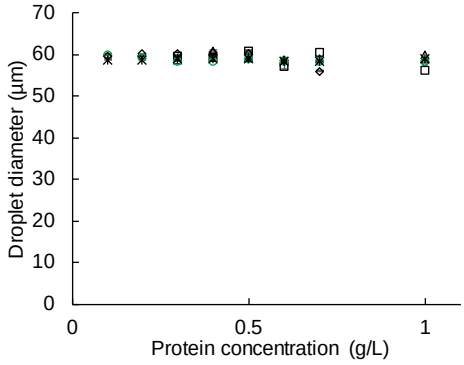

Figure A6.2. Droplet diameter at the inlet of the coalescence channel measured in microfluidic chips with different adsorption times 11(□), 31 (△), 65 (◊), 100 (○) and 173 (∗) ms and protein concentrations (0.1-1 g/L).

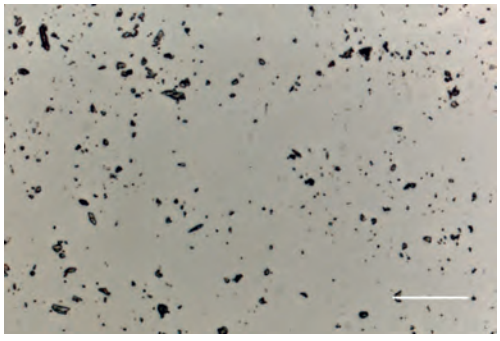

Figure A6.3. Optical microscopy image of 24-h oxidised pea protein (40x magnification), revealing the presence of large aggregates. Scale bar represents 50 µm.

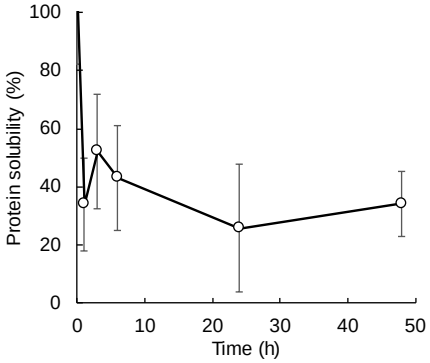

Figure A6.4. Protein solubility under oxidative conditions as percentage of the soluble (non-oxidised) pea protein solution. Error bars represent the standard deviation of at least 3 independent replicates, measured in triplicate.

Chapter 7

Conformational changes of whey and pea proteins upon emulsification approached by front-surface fluorescence

This chapter is submitted as Conformational changes of whey and pea proteins upon emulsification approached by front-surface fluorescence, Hinderink E.B.A, Berton-Carabin, C.C., Schroën, K., Riaublanc, A., Houinsou-Houssou, B., Boire, A., Genot, C.

7.1. *Abstract*

Proteins are widely used to stabilise emulsions, and plant proteins have raised increasing interest for this purpose. The interfacial and emulsifying properties of proteins depend largely on their molecular properties. We used fluorescence spectroscopy to characterise the conformation of food proteins from different biological origins (dairy or pea), and transformation processes (commercial or lab-made isolates), in solution and at the oil-water interface. The fourth derivative of fluorescence spectra provided insights in the local environment of tryptophan (Trp) residues, and thus in the protein structure. In emulsions, whey proteins adsorbed with their Trp-rich region at the oil-water interface. Proteins in the commercial pea isolate were present as soluble aggregates, and no changes in the local environment of the Trp residues were detected upon emulsification, suggesting that these structures adsorb without conformational changes. The lab-purified pea proteins were less aggregated, and a Trp-free region of the vicilin adsorbed at the oil-water interface.

Graphical abstract

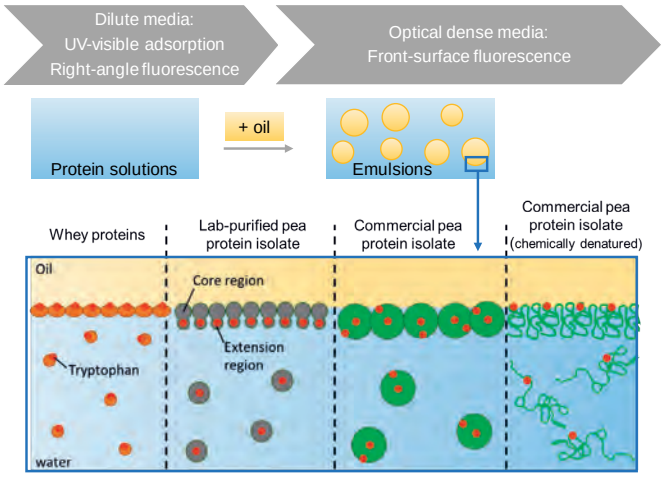

7.2. Introduction

Proteins are widely used to stabilise food oil-in-water (O/W) emulsions, i.e., dispersions of oil droplets in an aqueous phase. Dairy proteins (typically, whey or casein fractions) are excellent emulsifiers and widely used in the food industry (Dickinson, 1997, 2001). They adsorb at the oil-water interface and stabilise the droplets by steric and electrostatic repulsions (McClements, 2004a). Furthermore, whey proteins undergo conformational changes after adsorption (Dickinson & Matsumura, 1991; Monahan et al., 1993) and form a viscoelastic layer (Hinderink, Sagis, et al., 2020; Murray, 2011), which has been related to a high stability of emulsion droplets to coalescence (Dickinson, Murray, et al., 1988).

Over the past decades, plant proteins such as soy, lentil, and pea proteins have gained interest as more sustainable emulsifiers (Gumus et al., 2017a; Ho et al., 2017; Ladjal Ettoumi et al., 2017; Yerramilli et al., 2017). Pea proteins are particularly popular due to their ability to grow in Europe and to their low allergenic potential (Roy et al., 2010). During the production of commercial pea protein isolates, heat, solvents and pH-shifts are applied, which results in substantial chemical and structural changes of the proteins (Duque Estrada et al., 2018; Hinderink, Kaade, et al., 2020), and consequently to decreased protein solubility. The emulsifying properties of commercial pea proteins have already been studied, and it is clear that they suffer some drawbacks, such as limited emulsifying capacity due to their low solubility at food-relevant pHs (Gumus et al., 2017b; McCarthy et al., 2016). Therefore, the use of pea protein concentrates and isolates obtained from milder processes have recently gained interest (Geerts et al., 2017; Sridharan et al., 2020). The resulting isolates contain non-denatured proteins which are less aggregated compared to commercial isolates, but also more non-proteinaceous components such as polyphenols and lipids, due to the lower extent of purification involved.

Fluorescence spectroscopy is a classical method to characterise the structural conformation of proteins (Genot et al., 1984; Lakowicz, 2007). An advantage of fluorescence spectroscopy is the lack of extrinsic probes, and of complex sample preparation which may modify the protein structure (e.g., denaturation, new interactions). The method relies on the intrinsic fluorescence properties of the three aromatic amino acid residues in the protein: phenylalanyl, tyrosinyl, and tryptophanyl. Emission spectra of most proteins are typically dominated by the contribution of tryptophan (Trp) which emits at the longest wavelengths, has the largest extinction coefficient and the highest quantum yield. Furthermore, the excitation energy of

tyrosine (Tyr) residues can be transferred to the Trp residues. An interesting property is the sensitivity of Trp fluorescence to its local environment. Consequently, changes in the Trp emission spectra can be related to changes in the tertiary protein structure e.g., conformational changes, subunit association, substrate binding, or denaturation (Lakowicz, 2007). In classical fluorescence spectroscopy, experiments are done in right-angle mode using dilute solutions with absorbances below 0.1. At absorbances higher than 0.1, the inner filter effect induces absorption of the exciting radiation, or re-absorption of the emitted light. To overcome this problem, front-surface fluorescence spectroscopy can be used to characterise turbid samples such as suspensions and emulsions (Castelain et al., 1994; Granger et al., 2005; Rampon et al., 2001; Rampon, Genot, et al., 2003). The shape of the spectra and maximum emission wavelength provide information regarding the overall location of the Trp residues. In addition, by calculating the fourth-derivative of the emission spectra, it is possible to distinguish the partitioning of Trp residues between hydrophobic and hydrophilic environments (Granger et al., 2005; Rampon et al., 2001).

In this work, we aimed to investigate the conformational changes induced upon emulsification of proteins present in food ingredients arising from different biological origins and transformation processes: whey protein isolate, commercial pea protein isolate, and mildly purified pea proteins. We chose to tackle this question by deploying a comprehensive array of fluorescence spectroscopic characterisations.

We used UV-visible absorption and emission fluorescence spectroscopy to gain insight into the tertiary structure of the proteins. We focussed on the fluorescence of Trp residues as affected by their environment, and we also took the contribution of the Tyr residues' fluorescence into account, which can give information about the energy transfer from Tyr to Trp and thus, about interactions occurring within the peptide chain. In that respect, we compared in-house purified pea proteins with commercial pea proteins and chemically denatured commercial pea proteins (using 6 M guanidine hydrochloride), to obtain insights in their quaternary and tertiary structure change as a result of processing. Furthermore, we studied the structural changes of the proteins when present at the oil-water interface in emulsions using front-surface fluorescence. The fourth derivative spectra were calculated to deconvolute the contribution of Trp residues present in hydrophilic and hydrophobic environments, making this work an original and important step to unravel the interfacial behaviour and emulsifying properties of plant proteins.

7.3. Material and methods

7.3.1. Materials

Sodium phosphate dibasic, sodium phosphate monobasic, sodium dodecyl sulfate (SDS), Tween 20 and guanidine hydrochloride were purchased from Sigma Aldrich (Saint Louis, MO, US) and were at least of analytical grade. A bicinchoninic acid kit including a standard bovine serum albumin (BSA) solution was purchased from Thermo Fisher Scientific (Massachusetts, US). Mini protean gels (BOLT, Tris-Bis 4-12%, precast polyacrylamide gels, 10-wells), NuPAGE MES SDS (running buffer), and SeeBlue Prestained standard (Novex), were used for SDS-PAGE analysis and purchased from Thermo Fischer Scientific. Instant Blue protein stain was purchased from Sigma aldrich. Sunflower oil was purchased from a local supermarket and stripped with alumina powder (MP Alumina N-Super I, MP Biomedicals, France) to remove surface-active impurities and tocopherols, as described previously (Berton et al., 2011). Ultrapure water was obtained from a Milli-Q Reference A+ system (Millipore Corporation, Billerica, Massachusetts, US) and used for all the experiments.

Whey protein isolate (WPI, BiPro®, Davisco, Switzerland), pea protein isolate (cPPI, NUTRALYS s85 F, Roquette, France) were used as commercial protein ingredients. To prepare the in-house extracted pea protein isolate (iePPI), pea seeds (Alimex Europe BV, Sint Kruis, The Netherlands) were milled (Hosokawa-Alpine, Augsburg, Germany) to obtain the yellow pea flour. The flour (average particle size of 100 µm) was first dispersed in distilled water (1:9 w/w) at 4 °C for 2 hours. The pH was set and maintained at 8.0 by progressive addition of 0.5 M NaOH solution, using a pH-stat, and maintained at this pH. The suspension was then centrifuged at 17,000 x *g* for 20 minutes at 4 °C. The supernatant was filtered using a filter paper (5951/2, Whatman). The pH of the filtered supernatant was lowered to 4.5 using 1 M HCl, and stirred overnight at 4 °C. The obtained mixture was centrifuged at 17,000 x *g* for 20 minutes at 4 °C, and the pellet was resuspended in ultrapure water (1:9 w/w) for one hour at 20 °C before adjustment to pH 8. The mixture was stirred overnight at pH 8.0. The suspension was centrifuged at 17,000 x *g* for 20 minutes at 4 °C and the supernatant was collected and centrifuged again using the same conditions. The obtained protein solution (final supernatant) was dialysed (5 kDa, Hydrosart, Sartorius) against ultrapure water until the conductivity of the external liquid did not decrease anymore (38 µS/cm). Subsequently, the dialysed solution was freeze-dried and stored at -20 °C until

further use. The legumin (11S) and vicilin (7S) were produced using the protocol previously established and described by (Gueguen et al., 1984).

The amino acid composition and protein content of WPI, cPPI (commercial), and iePPI (in-house extracted) were analysed by Triskelion (Utrecht, The Netherlands) and are reported in Table 7.1. The water content was measured using the Karl-Fisher method and the total nitrogen content was measured using a Flash EA 1112 series Dumas analyser (Interscience, Breda, The Netherlands).

Table 7.1. Amino acid composition in g/100 g dry matter (DM) of the WPI, iePPI, and cPPI powders.

Amino acid	Amino acid content			Amino acid residue* content		
g/ 100 g DM	WPI	iePPI	cPPI	WPI	iePPI	cPPI
Alanine	4.7	3.3	3.1	3.8	2.6	2.5
Arginine	2.4	7.4	6.4	2.2	6.6	5.7
Aspartic acid	11.0	9.9	8.3	9.5	8.6	7.2
Cysteine	2.9	0.6	0.7	2.5	0.5	0.6
Glutamic acid	16.0	15.0	13.0	14.0	13.2	11.4
Glycine	1.5	3.1	2.9	1.1	2.4	2.2
Histidine	1.2	1.7	1.5	1.1	1.5	1.3
Isoleucine	5.4	4.0	3.5	4.7	3.5	3.0
Leucine	12.0	7.0	5.9	10.4	6.0	5.1
Lysine	9.5	6.4	5.2	8.3	5.6	4.6
Methionine	2.1	0.7	0.7	1.8	0.6	0.7
Proline	3.6	3.3	2.9	3.0	2.8	2.4
Serine	3.4	4.1	3.5	2.8	3.4	2.9
Threonine	4.4	2.7	2.6	3.7	2.3	2.2
Valine	4.9	4.1	3.8	4.1	3.5	3.2
Tryptophan	2.3	0.6	0.7	2.1	0.6	0.6
Tyrosine	3.3	2.9	2.4	3.0	2.6	2.2
Phenylalanine	3.1	4.4	3.9	2.8	3.9	3.5
Total amino acid residues (g/100 g DM)				80.9	70.1	61.3
Nitrogen content in the amino acid residues (g/100 g DM)				12.8	12.6	10.9
Total nitrogen content by Dumas (g/100 g DM)				14.9	14.7	12.6
Nitrogen-to-protein conversion factor				6.31	5.58	5.60

* *Amino acid residue results from the removal of the H_2O molecule upon formation of the polypeptide bond*

7.3.2. Preparation of aqueous phases

WPI (1 wt.%) was dissolved in 10 mM phosphate buffer (pH 7.0) and stirred overnight at 4 °C. For the pea protein ingredients, cPPI (6 wt.%) and iePPI (2 wt.%) were dispersed in that same buffer and stirred for at least 48 h at 4 °C; the insoluble part was removed by centrifugation (12,000 x *g*, 40 min) and the supernatant was collected and centrifuged again under the same conditions to ensure complete removal of the insoluble fraction. The second supernatant was collected, and its protein content was determined with the BCA assay (Smith et al., 1985) at 562 nm using a UV-visible spectrophotometer (lambda, 12, Perkin-Elmer, Norwalk, USA), leading to 25% and 60% of the total proteins present in the starting dispersion for cPPI and iePPI, respectively. For front-surface fluorescence experiments, the solutions were diluted to 1 wt.% protein using the same phosphate buffer, and for right-angle fluorescence measurements, they were diluted to 0.1 wt.% and 0.025 wt.% for iePPI and cPPI, respectively. Furthermore, an 8 wt.% cPPI dispersion was prepared in the same phosphate buffer and stirred for at least 48 h at 4 °C; the insoluble part was removed by centrifugation (12,000 x *g*, 40 min). Guanidine hydrochloride salt was added to the supernatant (concentrated cPPI-solution), to reach a concentration of 6 M, forming a cPPI solution in 6 M guanidine hydrochloride referred to as cPPI*. Guanidine hydrochloride is a chaotropic agent that chemically denatures the protein by binding to the hydrophobic patches, resulting in a loss of the tertiary structure and exposure of the amino acids initially buried in the protein core (Mason et al., 2003). The soluble protein content was measured, and the cPPI* solution was further diluted with 6 M guanidine hydrochloride in 10 mM phosphate buffer to reach 0.1 or 1 wt.% protein. The WPI was directly dispersed (1 wt.%) in the 6M guanidine hydrochloride buffer, stirred overnight at 4 °C and subsequently diluted to 0.1 wt.% protein using the same buffer.

7.3.3. Preparation and characterisation of emulsions

Coarse emulsions were prepared by mixing 10 wt.% stripped sunflower oil with each of the protein solutions (1 wt.%) using a high-speed blender (Heidolph Silent Crusher, Schwabach, Germany) at 20,000 rpm for 30 sec. The coarse emulsion was passed through a high pressure homogeniser (Panda plus 1000; GEA Niro Saovi, Italy) at 200 bars for 3 min.

The droplet size distribution was measured by static light scattering using a Horiba LA-960 laser particle size analyser (Horiba Scientific, Jobin Yvon, France). The refractive indices were set at 1.465 and 1.330 for the dispersed and continuous phases, respectively. Emulsions

were diluted in 1 wt.% SDS solution prior to the measurement, or, in the case of the cPPI*-stabilised emulsions, in 1 wt.% Tween 20 solution, to disrupt possible droplet flocs and measure the individual droplet sizes.

Fresh emulsions were centrifuged at 15,000 x *g* for 1 hour to separate the cream phase from the serum. The serum phase was collected by cautiously making a hole at the bottom of the tube, and filtered with a 0.2 µm filter (Minisart High-Flow, Sartorius Stedim Biotech GmbH, Goettingen, Germany). The soluble protein content was determined with the BCA assay. The surface load was calculated with equation (7.1).

$$\Gamma = \frac{C_s \cdot d_{3,2}}{6\phi} \qquad 7.1$$

Where C_s is the adsorbed protein concentration calculated by subtracting the protein concentration in the serum phase from the initial protein concentration of the solution used for emulsion preparation, $d_{3,2}$ the surface weighted mean droplet diameter of the emulsion (diluted in 1 wt.% SDS or 1 wt.% Tween-20), and ϕ the dispersed phase volume fraction (10 wt.%).

The creamed phase (iePPI, cPPI and WPI) obtained after centrifugation was re-dispersed into 1 wt.% SDS and then re-centrifuged. The supernatant, containing the initially adsorbed proteins, was collected and analysed together with the starting solution and serum phase by SDS-PAGE under reducing conditions. The samples were mixed (1:1 v/v) with a pH 6.8 buffer containing Tris-HCl 0.5 M, glycerol 30% w/v, SDS 10% w/v, bromophenol blue 0.5% w/v and 2-mercaptoethanol, vortexed and heated at 95 °C for 5 min in a heating block. Five microliters protein standard (SeeBlue Prestained, Novex, LC5625, Mw 3-109 kDa) and 20 µL of the diluted samples in sample buffer were loaded on the gel. A MES running buffer of pH 7.3 consisting of was used. Electrophoresis was performed in a Mini Gel Tank (ThermoFischer Scientific, USA) at 150 V for 45 minutes. After electrophoresis the gels were stained with Instant Blue for 1 h. Subsequently, the gels were washed with ultrapure water for 12 h before analysis. Gels were scanned and analysed using a calibrated densitometer (GS-900TM, Bio-rad laboratories, USA) and Image Lab software (Bio-Rad laboratories, USA). The molecular weights were determined by point to point regression. For WPI solutions, mainly bovine serum albumin (BSA), β-lactoglobulin (β-lg), α-lactalbumin (α-lac), and traces of immunoglobulins were found. PPI containing samples mainly consisted of convicilin (~71 kDa), vicilin subunits (~30, ~34, ~47 and ~50 kDa), α-legumin (38–40 kDa)

and β-legumin (19–22 kDa) (Barac et al., 2010); and vicilin fragments (~12.5-19, (Gatehouse et al., 1982)).The pea proteins dissociated in the buffer containing SDS solution and 2-mercaptoethanol, leading to multiple bands in SDS-PAGE. The sum of the subunits is reported for the different pea proteins.

7.3.4. Absorption spectra

Absorption spectra of protein solutions were recorded with a UV-visible spectrophotometer (Shimadzu UV1800, Shimadzu corportaion, Kyoto, Japan) coupled with the UV probe software (v2.30). UV-visible spectra were recorded for solutions at 1 g/L for WPI and iePPI, and at 0.25 g/L for cPPI, to have absorbances of ~1 at 280 nm. The spectra were acquired between 200 and 650 nm with a scan speed of 360 nm/min and a sampling interval of 0.5 nm. Ultrapure water was used for setting the baseline.

The theoretical UV-visible absorbance spectra of each protein dispersion were calculated for 1 g/L of protein. Experimental reference spectra of Trp, Tyr and Phe were obtained from the PhotochemCAD database (Taniguchi, Du, et al., 2018; Taniguchi & Lindsey, 2018). The theoretical spectra were calculated as a linear combination of each reference spectrum based on the respective content of Trp, Tyr and Phe of the protein isolate.

7.3.5. Fluorescence measurements

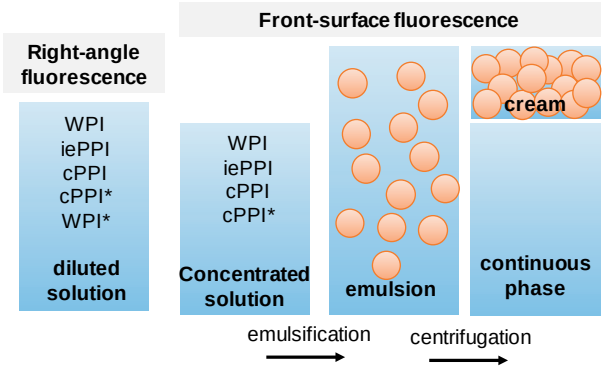

Figure 7.1. Schematic overview of the samples on which right-angle or front-surface fluorescence measurements were performed. For the right-angle fluorescence measurements, the solutions were diluted in order to have absorbances ~0.1 at 280 nm.

Emission spectra were recorded using a double-monochromator single-photon counting spectrofluorimeter (FLSP920, Edinburgh Instruments, UK) equipped with a 450 W Xenon lamp (Xe900) as light source and either a front-surface (FF) accessory (concentrated

solutions, emulsions, and creams) or a classical temperature-controlled right-angle (RA) accessory (diluted solutions). The spectra were automatically corrected in excitation and emission from instrument distortions. Figure 7.1 shows a schematic overview of the experimental design applied. In the RA-configuration, the temperature was controlled and set at 20 °C. For FF measurements, the temperature of the room was controlled (set at 20 °C) and, in practice, varied between 18-20 °C.

RA fluorescence emission spectra were recorded for diluted protein solutions. The protein solutions were diluted such that the total absorbance at 280 nm was ~ 0.1 (as determined using the above-described UV-visible spectrophotometer) to minimise the inner filter effect. WPI and iePPI solutions were accordingly used at 0.1 g/L, and cPPI and cPPI* solutions at 0.025 g/L. The diluted samples were placed in a 10-mm pathway quartz cell. RA-fluorescence emission spectra were recorded from 260, 275, or 290 nm to 450 nm (step 1 nm, dwell time = 0.3 s) with excitation wavelengths of 260, 275, or 290 nm, respectively. The slit widths were set at 4 and 2 nm for excitation and emission pathways, respectively. The background intensities of the buffer solutions (10 mM phosphate buffer, or 6 M guanidine hydrochloride) were subtracted from the protein emission spectra. To compare the shapes of the emission spectra among the different samples, all measured emission intensities were normalised (divided by the maximum absorbance of the sample). The fluorescence spectra recorded with excitation wavelengths of 275 and 290 nm were normalised at the signal at 365 nm, where only Trp emits. The difference between both normalised spectra represents the Tyr contribution to the spectrum with an excitation wavelength of 275 nm (Genot et al., 1984).

Fluorescence emission spectra of emulsions, creamed phases, serum phases, and 1 wt.% starting solutions were recorded in FF mode. Before analysis, the serum phases were filtered through a 0.2 µm filter, and the creamed phases were gently placed on filter paper to remove loosely bound water. Samples were measured in an 0.5-mm pathway quartz cell. FF fluorescence emission spectra were recorded from 275 or 290 nm to 450 nm (step 0.5 nm, dwell time = 0.3 s) with excitation wavelengths of 275 or 290 nm, respectively. The slit widths were set at 2 nm in both excitation and emission pathways. FF emission spectra were normalised to a maximum intensity of 1, and the normalised spectra were used for fourth-derivative calculations. The spectra were smoothed by the Savitsky-Golay procedure (polynomic order 2, width 21 points) and fourth derivatives were calculated according to the

Savitzky-Golay procedure (width 40 points). The data sets were analysed with Unscrambler x10.2 (CAMO Software, Oslo, Norway).

7.3.6. Statistical analysis

Each measurement was performed in at least independent duplicates. Two independently prepared emulsions were used for the FF measurements and surface load determination. IBM SPSS statistics software was used for statistical analysis with one-way ANOVA and to compare means post-hoc with the Tukey method. Significance was established with $p<0.05$.

7.4. Results and discussion

7.4.1. Absorption spectra

The absorption spectra measured for WPI, iePPI and cPPI solutions are reported in Figure 7.2. The theoretical spectra were calculated using the amino acid composition of the protein powders (Table 7.1), assuming that the extinction coefficients and the absorption spectra of the residues in the proteins are similar to those of the free aromatic amino acids (Figure 7.2, insert).

The wavelength of maximum absorbance in the absorption spectrum of the WPI solution was 280 nm, which is typical for proteins (Layne, 1957). At 289 nm, a shoulder was present in the spectrum, which is characteristic for the absorption of Trp residues. No apparent contribution of the Phe residues to the spectra was observed, due to the low molecular concentration in the sample (17.0 μM, Appendix, Appendix A7.1) and the low extinction coefficient of Phe (ε =191 cm^{-1} M^{-1} at 257 nm). The similar shape of the theoretical absorbance spectrum (Figure 7.2, insert) confirms that the aromatic amino acids are solely responsible for the absorption spectrum of the WPI solution.

For the iePPI solution, the maximum absorbance was at 270 nm, which is thus shorter than typical maxima for Trp (280 nm) and Tyr (275.5 nm) residues. The shoulders between 250 and 270 nm correspond to the absorption of Phe residues. The occurrence of these peaks confirms the high molar concentration in Phe residues (27.0 μM) compared to Trp and Tyr residues (3.1 and 26.6 μM, respectively (Appendix, Appendix A7.1)). The non-zero absorption above 320 nm can be attributed to the turbidity of the sample due to the presence of non-protein compounds and/or protein aggregates (Oreskes et al., 1979). At neutral pH and low ionic strength (<0.1 M), legumin aggregates into supramolecular protein structures (Gueguen et al., 1988), therewith contributing to the turbidity of the sample. The theoretical iePPI absorbance spectrum has a maximum absorbance at 275 nm, with a lower total absorbance compared to the experimental spectra. The blue-shifted maximum wavelength and the higher total absorbance of the experimental spectrum suggests the presence of other, non-protein absorbing species (e.g., polyphenols).

The absorbance spectrum for the cPPI solution was recorded at a protein concentration of 0.25 g/L due to the high absorption of the sample. The maximum absorbance was at 258 nm, which is a shorter wavelength than as found for the iePPI solution (275 nm) and of proteins

in general (280 nm). Commercial plant protein isolation processes involve heat, pH changes and different solvents (van der Goot et al., 2016). As a result, proteins are oxidised (Duque Estrada et al., 2018), denatured (no endothermic peak in DSC measurements) and highly aggregated (Geerts et al., 2017). It should be noted that such a process-induced aggregation is more extensive than the aggregation related to the quaternary structure of native legumin at low ionic strength and neutral pH. The theoretical spectrum (at 1 g/L, Figure 7.2, insert) has a maximum wavelength at 275 nm and a lower total adsorption compared to the experimental spectra. This suggests that the experimental spectrum was largely modified by non-protein compounds and aggregates resulting from the process applied to produce the ingredient.

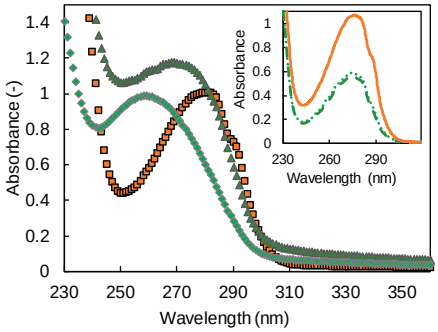

Figure 7.2. Absorption spectra of 1 g/L WPI (■), 1 g/L iePPI (▲) and 0.25 g/L cPPI (◆) solutions in 10 mM phosphate buffer, pH 7.0. The insert shows the theoretical spectra of 1 g/L WPI (___), iePPI (_ _) and cPPI (.....) as calculated from their amino acid composition (Table 7.1).

7.4.2. Right-angle fluorescence emission spectra

Emission spectra of N-acetyl-L-tryptophan amide and of N-acetyl-L-tyrosine at λ_{ex}=290 and 275 nm, respectively, were recorded (Figure 7.3). The maximum absorbance of N-acetyl-L-tyrosine was recorded at 303 nm, and that of N-acetyl-L-tryptophan amide at 353 nm. The latter value corresponds to Trp in contact with mobile water (Vivian et al., 2001); when exposed to locally more hydrophobic environments, λ_{max} is at shorter wavelengths (i.e., blue shifted (Lakowicz, 2007)).

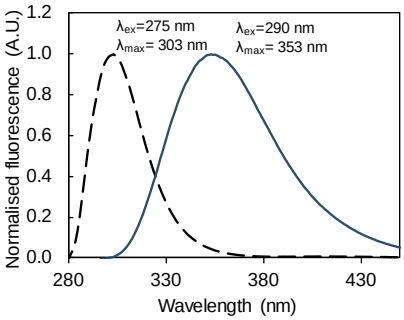

Figure 7.3. Emission spectra of N-acetyl-L-tryptophan amide with λ_{ex}=290 nm (solid line), and of N-acetyl-L-tyrosine at λ_{ex}=275 nm (dashed line) in 6 M guanidine hydrochloride.

In right-angle fluorescence spectroscopy, the total absorbance of the sample should not exceed 0.1 (at ~280 nm) to avoid as much as possible the inner filter effect. Without the inner filter effect, the emission intensities reflect the actual emission properties of the fluorophores. To comply with this requirement, the iePPI- and WPI solutions were diluted to a final protein concentration of 0.1 g/L, and the cPPI-solution to 0.025 g/L.

The complexity of the interpretation of protein fluorescence results from the presence of multiple fluorophores, including primarily the three aromatic amino acids – Phe, Tyr, and Trp, whose location may be distributed between different local environments. Yet, Trp largely dominates the fluorescence signal in Trp-containing proteins, and is the only amino acid with a high sensitivity to its local environment (Lakowicz, 2007). Furthermore, at excitation wavelengths above 290 nm, Trp is the only emitting amino acid. Therefore, a blue- or red-shift of the emission spectra recorded at λ_{ex} >290 nm can be interpreted as a more hydrophilic or hydrophobic local environment of Trp residues, respectively, and is assumed to be a result of conformational changes, subunit association, substrate binding or denaturation (Lakowicz, 2007). The spectral bandwidth (i.e., the width of the spectrum at half maximum intensity (I_{max}/2)), gives an impression of how broadly Trp residues are distributed over different environments (e.g., 62 nm for of N-acetyl-L-tryptophan amide at λ_{ex}=290 nm, Figure 7.3).

For the WPI solution, the maximum emission wavelength (λ_{max}) was at 331 nm (Figure 7.4) and the spectral bandwidth 53 nm (Appendix, Appendix A7.2). The λ_{max}, corresponds to Trp residues that are not directly accessible to water molecules (Burstein et al., 1973; Vivian et al., 2001), which is in line with previous data reported for WPI (λ_{max}=333, pH 7.1, (Xiang et

al., 2011)), and for pure β-lactoglobulin representing ~70% of the protein in WPI (λ_{max}=332, pH 6-8, (Burstein et al., 1973). After denaturing whey proteins in 6 M guanidine hydrochloride (sample referred to as WPI*), a red shift (9 nm) of λ_{max} was observed, indicating that the local environment of Trp became more hydrophilic (340 nm). According to the classification of Burstein, this corresponds to Trp molecules in contact with bound water at the surface of the protein molecule (Burstein et al., 1973). The λ_{max} recorded for WPI* (340 nm) was shorter compared to that of N-acetyl-L-tryptophan amide (λ_{max}=353 nm), which could indicate that the proteins did not denature fully.

For the iePPI solution, λ_{max} was at 328 nm with a spectral bandwidth of 59 nm. This suggests that the Trp residues are distributed between more contrasted local environments compared to WPI, and in an overall more hydrophobic environment. Pea protein isolates are composed of two major proteins, legumin and vicilin in a mass ratio of 1:2 (as determined by SDS-PAGE densitometry). At pH 7.0 the legumin is a hexamer with a molecular weight of 360 kDa and the vicilin a trimer with a molecular weight of (170 kDa) (Gatehouse et al., 1984). Since both proteins co-exist in the iePPI solution, we recorded the emission spectra of native legumin and vicilin (Gueguen, Vu, & Schaeffer, 1984) for comparison purposes Figure 7.4C. The legumin had a λ_{max} at 321 nm, and the vicilin solution at 336 nm, suggesting that the Trp residues are in a more hydrophilic environment in the legumin solution. However, the spectral bandwidth recorded for the vicilin (74 nm) was much broader compared to the legumin solution (52 nm), which indicates a broader range of local environments of the Trp residues in the vicilin solution.

The cPPI solution showed a λ_{max} at 334 nm with a shoulder at 321 nm, which is probably a result of the wide distribution of local environments of the Trp residues in the protein, as also indicated by the broad bandwidth (70.5 nm). It is most probably not the vicilin (λ_{max}= *321 nm*), since no native proteins remain in the commercial isolate, as suggested by the loss of denaturation peak in DSC profiles of such samples (Geerts et al., 2017), and the aggregated state of the sample (Figure 7.2). The λ_{max} is red-shifted after denaturation with guanidine hydrochloride to 344 nm. The fact that the λ_{max} of the cPPI* is further red-shifted compared to WPI* (340 nm), suggests extensive protein unfolding, or lower interactions of the peptide backbone of the protein with the Trp residues, and higher exposure of the latter to free/unbound water molecules.

Overall, the emission spectrum for WPI in phosphate buffer had the smallest bandwidth (53 nm), which represents the smallest spread of Trp residues between different local environments, followed by iePPI (59 nm) and cPPI (70.5 nm). The shortest λ_{max} recorded for the iePPI solution indicates that this is the sample in which Trp residues were least able to interact with water molecules, and therefore, the most buried with the protein structure's core (Meagher et al., 1998).

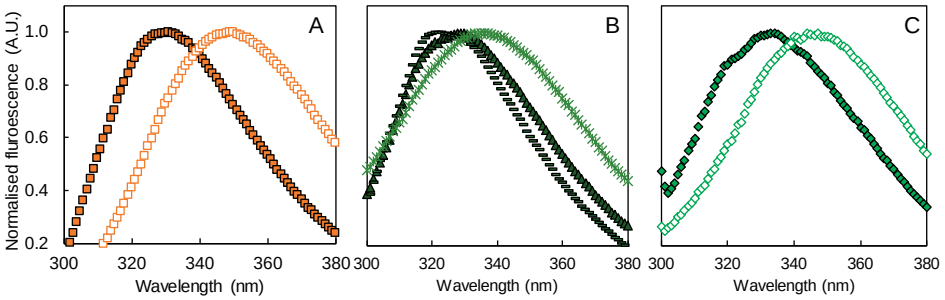

Figure 7.4. Emission spectra (recorded at λ_{ex}=290 nm) normalised at their maximum intensity (A) 1 g/L WPI (■), 1 g/L WPI (□), (B) 1 g/L iePPI (▲), vicilin (*), legumin (-), and (C) 0.25 g/L cPPI (◆), 0.25 g/L cPPI* (◇). Detailed information about λ_{max} and bandwidths are reported in supporting information, Table S2.*

To compare the Trp fluorescence emission intensity (i.e., the quantum yield) of the protein solutions, the emission spectra (λ_{ex}=290 nm) were normalised based on their Trp content (Figure 7.5). The tryptophan quantum yields of proteins is variable due to the presence of other amino acids that may act as quencher, such as lysine and histidine, and of the amide groups in the peptide backbone (Lakowicz, 2007; Pajot, 1976). The fluorescence intensities of cPPI* and WPI* solutions were higher compared to those of the cPPI and WPI solutions, which can be related to the loss of tertiary protein structure and the subsequent decreased quenching. The iePPI solution showed a higher fluorescence intensity compared to the cPPI-solution, whereas both protein ingredients differ only slightly in their amino acid composition (Table 7.1, Appendix A7.1). The absorption spectra (Figure 7.2) were indicative of the presence of non-protein absorbing species in the cPPI sample, and e.g., interaction of the aromatic ring of flavonoids or phenolic acids with the aromatic residues may be responsible for quenching of the system (Rawel et al., 2002). Besides, due to the extensive aggregated state of the proteins the Trp residues may be more quenched, due to the close proximity of other residues and functional groups, compared to the iePPI-solution. Finally, protein

oxidation may have occurred during the cPPI isolation, which could lead to Trp degradation and thus decrease of the fluorescence signal (Estévez et al., 2008; Hellwig, 2020).

The WPI sample showed the lowest fluorescence intensity per mass of Trp (Figure 7.5). β-Lactoglobulin, the main protein in WPI, contains 2 Trp residues; the first one, Trp19, is buried within the hydrophobic binding pocket of the protein, and displays fluorescence. The second, Trp 61, is present at the surface of the protein, in the vicinity of a disulfide bond (Cys66–Cys160), a strong quencher (Qin et al., 1998; Uhrínová et al., 2000) that is not reduced by guanidine hydrochloride, and therefore, the quenching effect is probably still applying in the WPI* samples, at least to some extent.

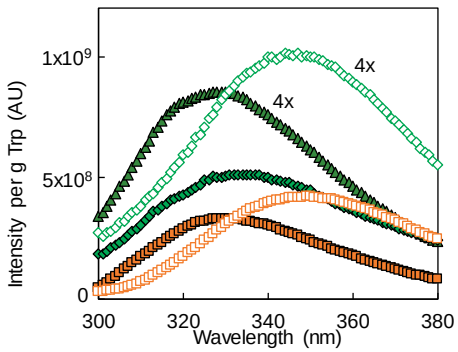

Figure 7.5. Maximum emission intensity per gram of tryptophan for WPI (■), WPI (□), iePPI (▲), cPPI 4x (◆) and, CPPI* 4x (◇). Detailed information about λ_{max}, bandwidth and emission intensity are reported in supporting information, Table S2.*

We recorded fluorescence emission spectra at excitation wavelengths (λ_{ex}) of 275 and 290 nm. At λ_{ex} of 275 nm, both Tyr and Trp residues emit, whereas at λ_{ex} of 290 nm, only Trp residues do so. To determine the Tyr contribution to the emission spectra, spectra recorded at λ_{ex}=275 and 290 nm were normalised by their emission intensity at 365 nm (where only Trp residues emit, Figure 7.3). The difference between both spectra is the Tyr contribution to the total fluorescence recorded at λ_{ex}=275 nm (Figure 7.6).

In the difference spectra (Figure 7.6, black markers) of the pea protein samples (iePPI, cPPI and cPPI*), λ_{max} was at 305 nm, which is close to the value determined for N-acetyl-L-tyrosine (λ_{max}=303 nm, Figure 7.3) and to the theoretical value for Tyr in proteins (λ_{max}=305±2 nm, (Castelain et al., 1994; Lakowicz, 2007)). No fluorescence was detected above 350 nm in the difference spectra. For cPPI* solution, in the emission spectra with λ_{ex}=275 nm, two peaks were observed at 305 and 340 nm, corresponding to Tyr and Trp

residues in hydrophilic environment, respectively. The peak at 305 nm was less pronounced in the spectrum for the cPPI solution (λ_{ex}=275 nm). To quantify this, the ratio (R) between the intensity of the difference peak (Tyr) and of the total peak (Tyr + Trp) at 305 nm was calculated. This ratio was 0.55 for cPPI and 0.75 for cPPI*, confirming the higher Tyr contribution in the former sample. When Tyr residues are within the Förster distance of Trp residues (9-18 *Å* for Tyr-to-Trp (Lakowicz, 2007)) they can transfer their energy to the Trp residues, reducing the Tyr residue emission. The fact that the Tyr residue had a higher emission in the cPPI* solution compared to the cPPI-solution may indicate that in the unfolded protein, the amino acids are further apart than the Förster distance, or that Tyr is less quenched in the cPPI* solution.

In contrast to the pea protein solutions, we did not observe any Tyr contribution in the emission spectrum of the WPI solution. This may indicate that the Tyr signal is efficiently quenched, or energy is transferred from the Tyr residues to the Trp residues due to a distance shorter than the Förster distance. In fact, one Tyr residue is just next to Trp19 in the primary structure (Appendix B). It can also be related to the high Trp/Tyr ratio in whey proteins (0.55) compared to the cPPI (0.25) and iePPI (0.20) samples (Appendix, Appendix A7.1). The contribution of the Tyr residues increased in the WPI* solution compared to the regular WPI one (R_{WPI*}=0.71), for the same reasons as explained for the cPPI samples, i.e., less quenching or reduced energy transfer.

It is often assumed that emission spectra recorded at 270-280 nm are dominated by the fluorescence of Trp residues. The current work shows that, for pea proteins, the Tyr contribution should actually not be neglected.

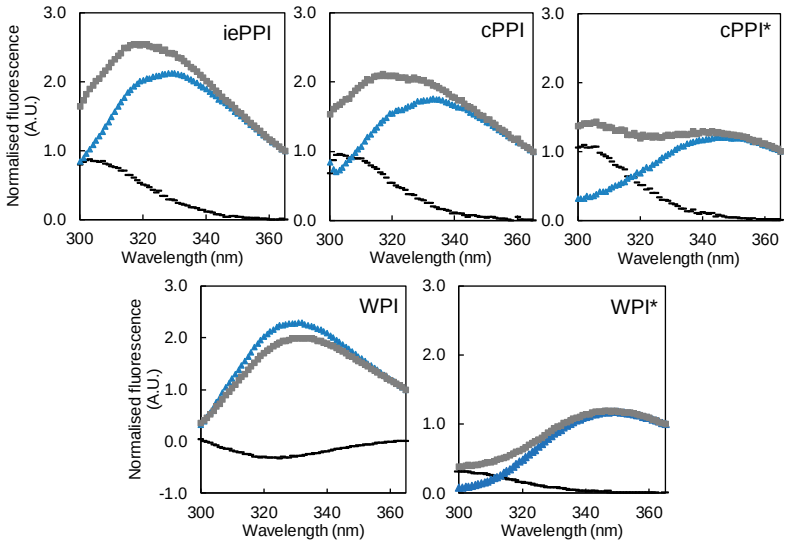

Figure 7.6. Emission spectra normalised at 365 nm, for spectra recorded at λ_{ex}=290 nm (▲) or λ_{ex}=275 nm (■), and the difference spectrum, i.e., normalised spectrum [λ_{ex}=275 nm] – normalised spectrum [λ_{ex}=290 nm] (-).

7.4.3. Front-surface fluorescence spectra

To study the intrinsic fluorescence of molecules in turbid samples, such as concentrated protein solutions (above ~1 g/L) and emulsions, front-surface or front-face mode is required. The front-surface fluorescence emission spectra were normalised based on their maximum intensity, and λ_{max} and spectral bandwidths were compared. .

Normalised emission spectra (λ_{ex} =290 nm)

Normalised front-surface emission spectra, recorded at λ_{ex}= 290 nm, for emulsions, creamed and serum phases, and starting solutions prepared with WPI, cPPI, iePPI, and cPPI* are reported in Figure 7.7.

For the WPI-based creamed phase, the λ_{max} was red-shifted (2 nm) compared to the aqueous samples (solution and serum phase) (Table 7.2), which indicates an overall slightly more hydrophilic environment of the Trp residues. The bandwidth was significantly broader (5 nm) compared to those for the aqueous samples, suggesting more different local environments. As expected, the bandwidth and λ_{max} of the WPI-stabilised emulsions were in between the values of the creamed and aqueous phases, since the proteins partitioned between the oil-water interface (cream) and the water-phase (serum).

For the iePPI samples, the λ_{max} for the creamed phase was also red-shifted and broader compared to serum (8 nm and 4 nm, respectively) and solution (6 nm and 2 nm, respectively). This suggests that the overall environment of the Trp residues after adsorption was more hydrophilic and a greater variety of local environments. The λ_{max} of the serum phase was blue-shifted (2.5 nm) compared to the solution, and the spectrum had a smaller bandwidth (2 nm). The homogenisation process leads to Trp residues being present in a locally more hydrophobic environment, which suggests that protein structure was affected. High pressure homogenisation may induce modifications and rearrangements in the supramolecular structures of proteins (Keerati-U-Rai et al., 2009; Rampon, Riaublanc, et al., 2003). For example, a faba bean protein solution showed a red shift (3 nm) after high pressure homogenisation, which was related to aggregate breakup (Yang et al., 2018).

For the cPPI-samples, λ_{max} was at the same position (332 nm) for the homogenised samples (i.e., emulsion, serum and cream) which shows that the Trp is in the overall the same environment. However, the spectral bandwidth for the cPPI samples was significantly smaller for the solution, compared to the other samples (2.5-3 nm), which shows that upon homogenisation, the Trp residues were more spread between different environments probably due to break up of the aggregates within the homogeniser.

The spectrum for the cPPI* solution had a blue-shifted λ_{max} (14 nm) and broader bandwidth (4 nm) compared to that for the cPPI solution, due to the more hydrophilic environment of the Trp residue after denaturation, which is in line with the results of the diluted solutions. For the cPPI* creamed phase, λ_{max} was blue-shifted by 6-8 nm compared to the solution and serum phase, respectively, which indicates a more hydrophobic environment of the Trp residues and suggests the presence of Trp residues at the oil-water interface after adsorption at the sunflower oil-water interface.

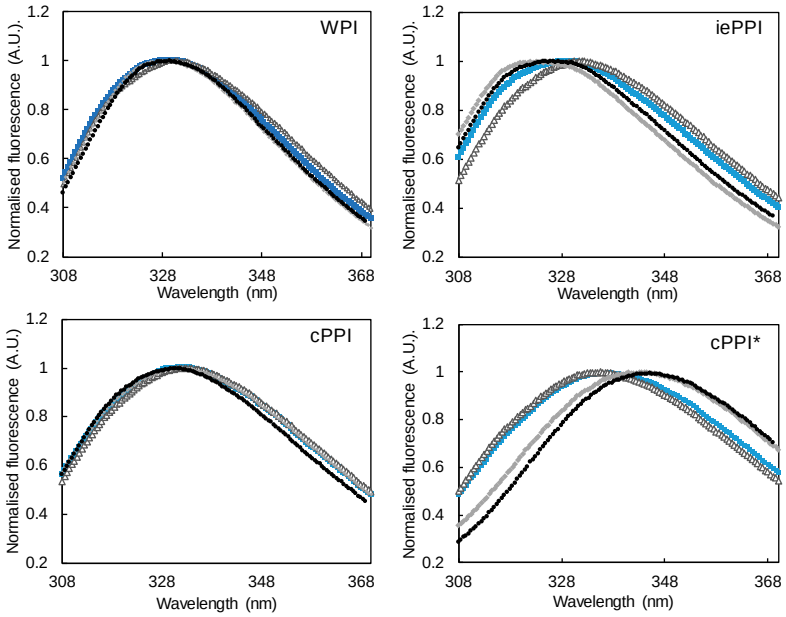

Figure 7.7. Normalised fluorescence emission spectra of emulsion (■), creamed (△) and serum (◆) phases, and initial solutions (●) of WPI, iePPI, cPPI, or cPPI (i.e., cPPI in 6 M guanidine)-containing samples. For clarity, only one representative spectrum is shown per sample, but similar trends were obtained for dependent and independent replicates.*

Table 7.2. Maximum emission wavelength (λ_{max}) and bandwidth of the spectra recorded with an excitation wavelength (λ_{ex}) of 290 nm. Superscript letters denote values that are significantly different ($p<0.05$, $n=4$). Standard deviations are reported in supporting information, Table S4.

Initial fluorescence	λ_{max}^{290} (nm)				Bandwidth^{290} (nm)			
spectra	WPI	iePPI	cPPI	cPPI*	WPI	iePPI	cPPI	cPPI*
Emulsion	329.5^{cd}	329.0^{c}	332.0^{efg}	337.0^{i}	53.5^{B}	58.5^{E}	62.5^{G}	65.5^{J}
Cream	330.5^{de}	332.0^{fg}	332.5^{g}	334.0^{h}	55.5^{C}	59.0^{E}	62.5^{G}	64.5^{HI}
Serum	328.5^{c}	323.5^{a}	332.0^{fg}	343.5^{j}	51.0^{A}	55.0^{C}	63.0^{G}	65.5^{IJ}
Solution	328.5^{c}	326.0^{b}	331.0^{ef}	345.0^{k}	51.0^{A}	57.0^{D}	60.0^{F}	64.0^{H}

Fourth derivative spectra (λ_{ex} =290 nm)

From the normalised emission spectra (λ_{ex}=290 nm, Figure 7.7), fourth derivatives were calculated to deconvolute the respective contributions of Trp residues located in hydrophobic or hydrophilic environments (Granger et al., 2005; Rampon et al., 2001). Derivative spectra exhibited two maximums near 315 and 331 nm, that are attributed to Trp residues in hydrophilic and hydrophobic environments, respectively, as previously reported for BSA (316 and 332 nm, (Rampon et al., 2001)) and skim milk powder (319 and 333 nm, (Granger et al., 2005)).

The fourth derivative spectra of the WPI-based serum phase and solution showed a peak around 336 nm, which is related to a hydrophilic environment (hydrophilic peak) of the Trp residues, and no peak at ~315 nm (hydrophobic peak, Figure 7.8, Table 7.3). The derivative spectra of the creamed phase exhibited two maximums at 315.5 and 331 nm, respectively. The first one can be attributed to Trp residues in hydrophobic environment, due to the adsorption of the proteins at the sunflower oil-water interface. All constituent proteins (BSA, β-lg, α-lac) adsorbed at the interface (Figure 7.9) with an accumulation of α-lactalbumin compared to the composition of the aqueous phase. It was reported that upon adsorption, the proteins' secondary and tertiary structures change, and Trp residues encounter a more hydrophobic environment for β-lactoglobulin (Sakuno et al., 2008) and more hydrophilic environment of the α-lactalbumin (Zhai et al., 2012). In our case, the overall more hydrophobic environment of the Trp residues (Figure 7.8, Table 7.3) thus suggests a strong contribution of the β-lactoglobulin residues to the total spectra. The peak near 331 nm, attributed to Trp in hydrophilic environment, was blue-shifted (2 nm) compared to the serum phase and solution, which may indicate a slightly less hydrophilic location of Trp residues in the cream. The fourth derivative spectrum of the WPI-emulsion was, as expected, in between those of the creamed and serum phases. Our results are in line with previous results obtained on BSA-stabilised sunflower O/W emulsions (Rampon et al., 2004) and confirms the reproducibility of the method.

We extended this approach to pea protein-stabilised emulsions, for which, to the best of our knowledge, no fourth derivative of fluorescence spectra have been reported so far.

The fourth derivative spectra of the iePPI aqueous phases had a hydrophobic peak near 316 nm and a hydrophilic peak near 332 nm. As detailed earlier, pea proteins, and plant proteins in general, have a greater molecular weight and a more complex tertiary and quaternary structure compared to dairy proteins. It is expected that the Trp residues are buried in the interior of the pea proteins' structures, and hence in a relatively hydrophobic environment. The derivative spectrum for the iePPI-based creamed phase exhibited the same two peaks as the aqueous samples (316 and 332 nm) although, the relative intensity of the hydrophilic peak was higher for the creamed phase compared to the aqueous phases, 0.5 vs 0.3 (ratio $I_{max}^{332}/I_{max}^{316}$), respectively, as was also concluded from the non-derivated spectra (Figure 7.7, Table 7.2). A more hydrophilic environment of Trp after adsorption may seem counterintuitive, as adsorbed proteins are, per definition, located in close proximity to the oil phase; and this

finding also opposes the result found for whey proteins. There is a slight accumulation of vicilin at the interface (Figure 7.9), which is in line with previous research that reported higher surface activity of native vicilin compared to legumin (Dagorn-Scavinier et al., 1986, 1987). Our results are also in line with previous findings reported for soy protein-stabilised emulsions: the emission spectra of soy proteins adsorbed at the oil-water interface were found to be red shifted (4-7 nm) compared to the emission spectra of proteins in solution (Miriani et al., 2011). The Trp residues are only present in the 7S soy protein (conglycinin) in the extension region of the α, α' subunit (Miriani et al., 2011) and it was hypothesised that after adsorption at the oil-water interface, the Trp residues are located in a more hydrophilic environment due to protruding of the extension region in the water phase and adsorption of the core region (where no Trp is present) at the oil-water interface (Keerati-u-rai et al., 2012; Miriani et al., 2011). Accumulation of the vicilin and the protruding of its extension region in the water phase thus probably explain the overall more hydrophilic environment of the Trp residues in the creamed phase of the emulsion prepared with iePPI.

The fourth derivative spectra of the cPPI sample also exhibited a hydrophobic and hydrophilic peak at ~316 and ~334 nm, respectively. The ratio between the peaks is the same for all samples (Table 7.3) which shows that, the overall local environment of the Trp residues in cPPI did not change after protein adsorption at the oil-water interface. Legumin preferentially adsorbed at the oil-water interface (Figure 7.9), which confirms the presence of non-native protein structures in the sample; in fact, for native pea proteins, a preferential adsorption of vicilin would be expected (Dagorn-Scavinier, Gueguen, & Lefebvre, 1986, 1987). The so-called soluble fraction consists of non-precipitated soluble aggregates that may adsorb at the oil-water interface as aggregated protein structures (Hinderink, Kaade, et al., 2020), with Trp residues buried within the aggregates, and not exposed to the oil phase. When dissolving cPPI in 6 M guanidine hydrochloride, most of the quaternary and tertiary structure is lost and Trp residues become exposed to the aqueous environment (Figure 7.4). For the cPPI* solution and serum phase, the fourth derivative spectra exhibited a hydrophilic peak at 334 and 335 nm, respectively, and no hydrophobic peak. The absence of the hydrophobic peak in the water phases (Figure 7.8) confirms that substantial protein unfolding occurred, as was before concluded from the red shift in the initial spectra (Figure 7.7, Table 7.2), and from the right-angle fluorescence data in Figure 7.4. The creamed phase exhibited a hydrophobic and hydrophilic peak with maxima at 315 and 331 nm, respectively. The location of the peaks

is the same (p<0.05) as for the WPI-stabilised creamed phase but their ratio is higher for cPPI*, suggesting a higher hydrophilic contribution. For both cPPI and cPPI* the fourth derivative spectra of the emulsions lay, as expected, between those for water phase and cream.

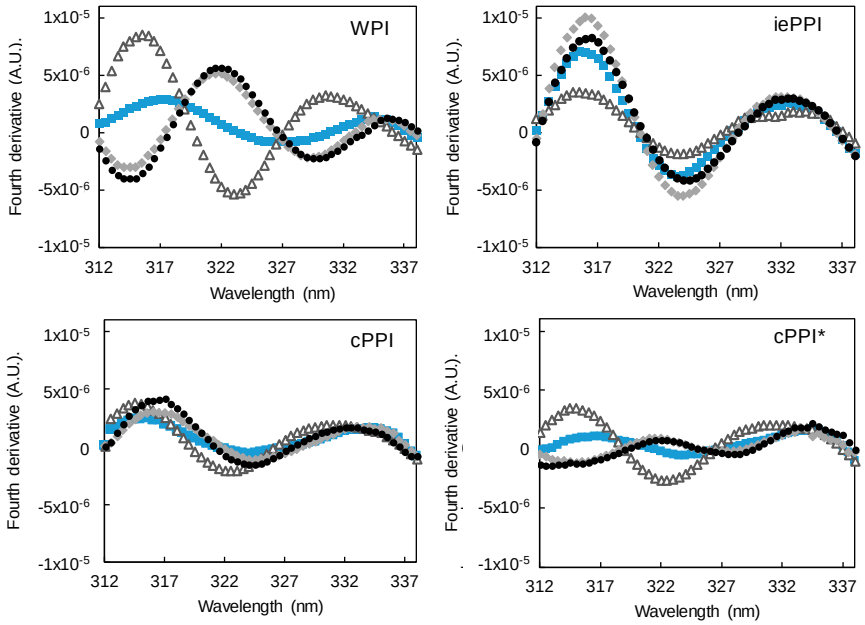

Figure 7.8. Fourth derivative fluorescence spectra of emulsion (■), creamed (△) and serum (◆) phases, and initial solutions (●) of WPI, iePPI, cPPI, or cPPI (cPPI in 6 M guanidine)-containing samples. For clarity, only one representative spectrum is shown for each sample, but similar trends were obtained for dependent and independent replicates*

Table 7.3. Wavelength (nm) of maximum and minimum of the fourth derivative and the ratio between the height of the two peaks (I_{max}^{332}/ I_{max}^{316}). Values presented in italics correspond to a minimum in the fourth derivative spectra. Standard deviations are reported in supporting information, Table S5.

Fourth derivative spectra		$\lambda_{max}/\lambda_{min}$ (312-322 nm)	λ_{max} (317-337 nm)	$I_{max}^{332}/ I_{max}^{316}$
emulsion	WPI	317.5^{g}	334.5^{klmn}	0.4^{qrs}
	iePPI	316.0^{cdefg}	332.0^{hi}	0.4^{qrs}
	cPPI	316.5^{fg}	333.5^{ijklm}	0.7^{s}
	cPPI*	317.0^{g}	334.0^{ijklm}	1.5^{t}
cream	WPI	315.5^{bcdef}	331.0^{h}	0.4^{qr}
	iePPI	316.0^{cdefg}	332.5^{hijk}	0.5^{qrs}
	cPPI	315.0^{bcd}	331.0^{h}	0.6^{qrs}
	cPPI*	315.0^{bc}	331.0^{h}	0.7^{s}
serum	WPI	-	335.5^{mn}	-
	iePPI	316.0^{cdefg}	332.5^{hijk}	0.3^{q}
	cPPI	316.5^{defg}	334.0^{jklm}	0.6^{rs}
	cPPI*	-	334.5^{klmn}	-
solution	WPI	-	336.5^{n}	-
	iePPI	316.5^{defg}	332.0^{hij}	0.3^{qr}
	cPPI	316.5^{efg}	333.5^{ijkl}	0.5^{qrs}
	cPPI*	-	335.0^{lmn}	-

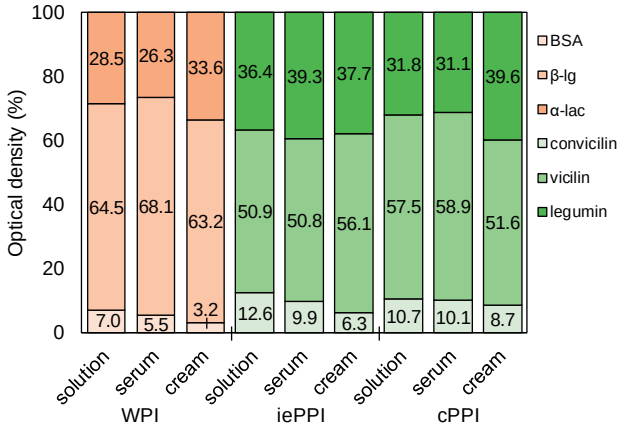

Figure 7.9. Protein composition measured in the solution, serum and creamed phase for WPI-, iePPI- and cPPI- based emulsions. Colours from light to dark indicate for whey proteins (orange); BSA, β-lg and α-lac, and for pea proteins (green); convicilin, vicilin and legumin. Standard deviations are reported in Appendix, Appendix A7.6.

Tyrosine contribution

The Tyr contribution to the fluorescence spectra with λ_{ex}=275 nm was determined according to the previously described procedure for the right-angle fluorescence spectra (see also Appendix, Appendix A7.1). We found a small Tyr contribution in the WPI-based samples (emulsion, creamed and serum phases, R=0.1, 0.2 and 0.1, respectively), and no contribution in the solution. This is in line with the right-angle fluorescence experiments (Figure 7.6), and confirms that the Trp residues dominate the fluorescence of whey proteins, for spectra recorded at λ_{ex} of 275 nm. The highest ratio for the creamed phase (R=0.2), suggests less quenching of Tyr after adsorption at the oil-water interface, due to conformational changes or environmental factors.

The pea protein-containing samples (iePPI, cPPI, and cPPI*) had a Tyr contribution at 305 nm (Appendix, Appendix A7.1). For cPPI and iePPI, the Tyr contribution to the total signal was the same in the different samples i.e., solution, serum, cream and emulsions (R=0.4 and 0.5 for iePPI and cPPI samples, respectively; See also Appendix, Appendix A7.7). For the cPPI* samples, the Tyr contribution was the lowest in the creamed phase (R=0.5), and the highest in the solution (R=0.8). A lower Tyr contribution may be related to increased quenching of the Tyr fluorescence signal, or to increased energy transfer from Tyr to Trp due to protein conformational changes.

7.5. *Conclusions*

Right-angle and front-surface fluorescence provide useful information about the structure of proteins in colloidal systems, from solutions, to aggregate dispersions, and emulsions. In contrast to WPI, the Tyr contribution to the total signal (λ_{ex}=275 nm) was not negligible for the pea protein samples, and has thus to be considered in future research. Furthermore, the fourth derivative spectra provided useful insights in the structure of pea proteins; they notably confirmed that the Trp residues are buried in the hydrophobic core of pea protein structures. The commercial pea proteins are present as soluble aggregates, and adsorb as such (Figure 7.10), accounting for no changes in the local environment of the Trp residues. For the mildly purified pea proteins, it is presumable that a Trp-free region adsorbed at the oil-water interface, and that the Trp-rich region remained in the aqueous phase. This only led to a very small shift compared to dairy proteins (BSA showed a 15-nm shift in λ_{max} upon adsorption, (Rampon et al., 2001)). For pea proteins, the Tyr contribution did not change upon adsorption at the oil-water interface, which suggests that the Förster distance between the Trp and Tyr residues remained unchanged. Further research using different techniques to study protein structure, such as Fourier-transform infrared spectroscopy (FTIR) would be useful to confirm and deepen the current findings.

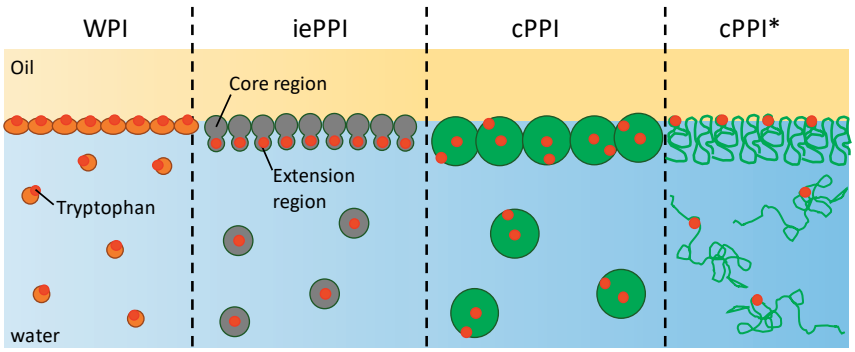

Figure 7.10. Schematic overview of the presumed location of Trp residues in the investigated proteins in solution and after adsorption at the oil-water interface. The illustrated molecules/structures are not to scale, and the red spheres represent the overall environment of the Trp residues.

7.6. *Acknowledgements*

We would like to thank Lucie Ribourg for technical assistance and Véronique Solé-Jamault for the purification of legumin (11S) and vicilin (7S) at lab scale.

7.7. Appendix

Appendix A

Table A7.1. Protein concentration used in right-angle configuration and corresponding Trp, Tyr and Phe concentrations in g/L and μM and the molar ratio: Trp/Tyr.

Protein concentration (g/L)		g/L			uM			Trp/Tyr
		Trp	Tyr	Phe	Trp	Tyr	Phe	
WPI	0.09	0.0019	0.0030	0.0028	9.2	16.4	16.9	0.56
iePPI	0.1	0.0006	0.0029	0.0044	3.1	16.0	26.6	0.20
PPI	0.025	0.0002	0.0006	0.0010	0.8	3.3	5.9	0.24

Table A7.2. Maximum intensities of right-angle fluorescence emission spectra for a normalised protein concentration of 0.1 g/L ($I_{max}^{0.1g/L\ protein}$), or a normalised Trp content (I_{max}^{Trp}). Maximum wavelengths of the right-angle fluorescence spectra and bandwidth were recorded at an excitation wavelength of 290 nm (n=2).

λ_{ex} =290 nm

	Average				SD			
	$I_{max}^{0.1g/L\ protein}$ (A.U.)	I_{max}^{Trp} (A.U.)	λ_{max} (nm)	Bandwidth (nm)	$I_{max}^{0.1g/L\ protein}$ (A.U.)	I_{max}^{Trp} (A.U.)	λ_{max} (nm)	Bandwidth (nm)
iePPI	6.92×10^5	8.5×10^7	328	59	1.2×10^4	2.0×10^5	1.5	0
WPI	5.43×10^5	3.0×10^7	331	53	5.8×10^3	3.2×10^5	0	1.5
cPPI	4.2×10^5	1.6×10^7	334	70.5	1.2×10^5	1.2×10^6	1.5	2.0
cPPI*	4.9×10^5	2.7×10^7	344	67.5	2.5×10^5	4.9×10^5	0	1.0
WPI*	8.8×10^5	4.2×10^7	340	67.5	-	-	-	1.0
vicilin			336	74			-	-
legumin			321	52			-	-

Table A7.3. Surface load (Γ) in protein-stabilised emulsions calculated using the serum protein concentration and $d_{3,2}$. Superscript letters denote values that are significantly different ($p<0.05$).

Γ (mg/m2)	Average	SD
WPI	2.6a	0.0
iePPI	2.9a	0.4
cPPI	3.4ab	0.1
cPPI*	4.1b	0.4

Table A7.4. Standard deviation of λ_{max}^{290} (nm) and bandwidth^{290} (nm) reported in Table 7.2.

Initial fluorescence	λ_{max}^{290} (nm)				Bandwidth^{290} (nm)			
spectra SD	WPI	iePPI	cPPI	cPPI*	WPI	iePPI	cPPI	cPPI*
emulsion	0.5	0.5	0.5	0.0	0.0	0.5	0	0.0
cream	0.5	0.5	0.5	0.5	0.5	0.5	0.5	0.5
serum	0.5	0.5	0.5	0.5	0.5	1.0	0	0.5
solution	0.5	1	0.5	0.5	0.5	0.5	0	0.5

Table A7.5. The standard deviation of wavelength (nm) of maximum and minimum of the fourth derivative and the ratio between the height of the two peaks reported in Table 7.3.

Fourth derivative SD		$\lambda_{max}/\lambda_{min}$ (312-322 nm)	λ_{max} (317-337 nm)	ratio max
emulsion	WPI	0.5	0.5	0.1
	iePPI	0.5	0.5	0.0
	cPPI	1	1	0.1
	cPPI*	0.5	0.4	0.2
cream	WPI	0.0	0.5	0.0
	iePPI	0.5	1.5	0.0
	cPPI	0.5	1	0.1
	cPPI*	0.5	1	0.1
serum	WPI	-	0.5	-
	iePPI	0.5	1	0.0
	cPPI	0.5	1	0.1
	cPPI*	-	1.5	-
solution	WPI	-	1	-
	iePPI	0.5	1	0.0
	cPPI	0.5	1	0.1
	cPPI*	-	0.5	-

Table A7.6. The standard deviation (SD) of the interfacial composition reported in Figure 7.9

Compositional analysis SD		solution	serum	cream
WPI	BSA	0.3	0.1	0.5
	β-lg	0.7	0.1	1.2
	α-lac	1.0	0.2	0.7
iePPI	convicilin	0.0	1.1	0.2
	vicilin	0.1	0.9	2.3
	legumin	0.2	2.0	2.0
cPPI	convicilin	-	0.7	1.0
	vicilin	-	0.1	0.7
	legumin	-	0.7	0.3

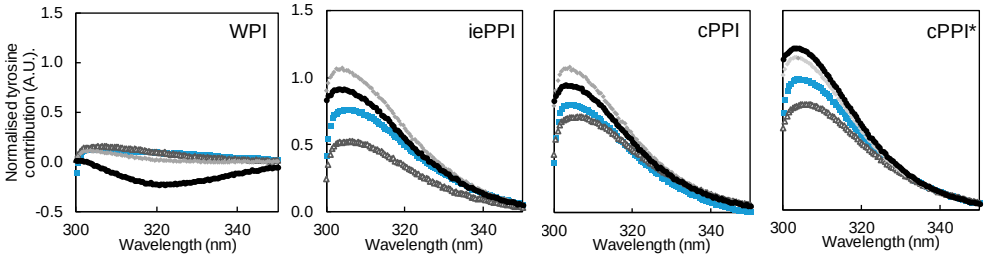

Table A7.1. Tyrosine contribution to the protein emission spectra recorded at an excitation wavelength of 275 nm for the emulsion (■), creamed (△) and serum (◆) phases, and initial solutions (●).

*Table A7.7. The ratio (*R*) between the intensity of the difference peak (Tyr) and of the total peak (Tyr + Trp) at 305 nm for the front-surface fluorescence emission recorded at an excitation wavelength of 275 nm.*

	average				SD			
	emulsion	cream	serum	solution	emulsion	cream	serum	solution
WPI	0.1	0.2	0.1	0.0	0.0	0.0	0.0	0.0
iePPI	0.4	0.4	0.4	0.4	0.0	0.0	0.0	0.0
cPPI	0.5	0.5	0.5	0.5	0.0	0.0	0.0	0.0
cPPI*	0.6	0.5	0.7	0.8	0.0	0.0	0.0	0.0

Appendix B

β-lactoglobulin sequence from UniProt (https://www.uniprot.org/uniprot/P02754):

LIVTQTMKGLDIQKVAGTWYSLAMAASDISLLDAQSAPLRVYVEELKPTPE
GDLEILLQKWENGECAQKKIIAEKTKIPAVFKIDALNENKVLVLDTDYKKY
LLFCMENSAEPEQSLACQCLVRTPEVDDEALEKFDKALKALPMHIRLSFNP
TQLEEQCHI

W = Tryptophan
Y = Tyrosine

Chapter 8

Stability of food emulsions prepared with pea protein fractions

This chapter is based on: Stability of food emulsions prepared with pea protein fractions, Hinderink, E.B.A., Schröder, A, Sagis, L., Schroën, K., Berton-Carabin, C.C, *submitted*.

8.1. *Abstract*

There is a growing interest in replacing dairy proteins with their plant-based counterparts in food emulsions which is also referred to as the protein transition. However, plant protein ingredients generally contain a substantial insoluble protein fraction, of which the properties may differ considerably from those of the soluble fraction. Here, we explore the use of pea proteins fractions for the production of oil-in-water (O/W) emulsions, and compare them to dairy proteins, which are fully soluble. Three types of emulsifiers were therefore used: commercial pea proteins isolate (full pea proteins), its insoluble fraction (insoluble pea proteins), and commercial whey proteins isolate (whey proteins).

In 10 wt.% O/W emulsions, the use of full pea proteins led to physically instable emulsions that showed droplet flocculation and coalescence, whereas the insoluble pea proteins and whey proteins formed physically stable emulsions. The insoluble pea proteins fraction was also able to physically stabilise high internal phase O/W emulsions (HIPEs) containing 70 wt.% oil, giving ~10 times higher viscosity than whey protein-based HIPEs. These results suggest that the different constituents of commercial pea proteins isolate have specific functionalities, which is important ground knowledge for the design of stable plant protein-based emulsions.

Graphical abstract

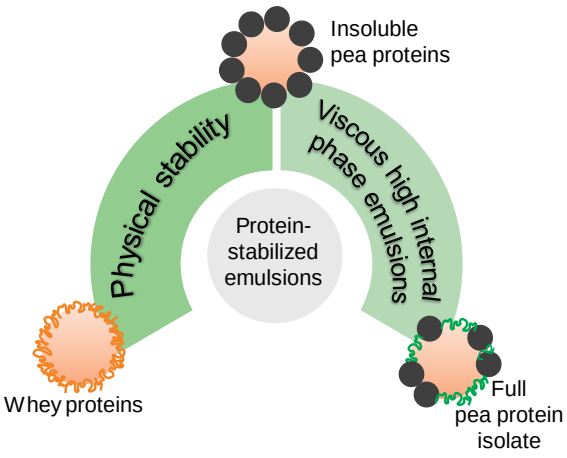

8.2. Introduction

Many food products comprise two immiscible phases, such as oil droplets dispersed in water, referred to as oil-in-water (O/W) emulsions. Their oil fraction may range from ~3 wt.% in beverages, to 10-30 wt.% in dressings, and up to 80 wt.% in mayonnaises (Jacobsen et al., 2013; McClements, 2005), resulting in increasingly densely packed droplets. This leads to a range of physical appearances, from low viscosity fluids to highly viscous systems, and even viscoelastic solids.

The interface between oil and water is physically stabilised by emulsifiers to prevent, or at least delay, phase separation (McClements, 2005). Dairy proteins (e.g., whey and casein fractions) are widely used for this purpose, and their emulsifying properties have been extensively studied and verified (Dickinson, 2001). The adsorbed protein interfacial layer provides electrostatic repulsion at pH away from the isoelectric point, as well as steric hindrance, preventing physical destabilisation of the droplets (McClements, 2005). Furthermore, certain proteins such as β-lactoglobulin, present in whey, are able to form a strong viscoelastic network at the oil-water interface, protecting the droplets against coalescence.

Over the past decade, plant proteins have attracted a lot of attention as more sustainable alternatives to animal-derived proteins. Substantial work has already been done at characterising the emulsifying properties of plant proteins; especially soy proteins have been widely studied (Tang, 2017). They have been shown to form stable emulsions at pH away from their isoelectric point (Xu et al., 2018), as well as during processing at high temperatures and pressures (Puppo et al., 2008). Mainly β-conglycinin contributes to their emulsifying properties, as demonstrated by its ability to form small and stable emulsion droplets (1 wt.% protein, 10 wt.% oil, average diameter around 0.4 μm) (Keerati-U-Rai et al., 2010). Yet, soy proteins have some drawbacks such as allergenicity risks, GMO origin, and limited production in Europe; therefore, other plant proteins such as pea proteins have gained attention lately. Pea proteins ingredients are commercially available at low cost, and have a well-balanced amino acid profile (containing notably a high amount of lysine; Roy, Boye, & Simpson, 2010). Without pre-treatment, commercial pea proteins isolate has limited solubility at neutral pH (40-60%) (Can Karaca et al., 2011) and forms polydisperse emulsions (Gumus et al., 2017a; McCarthy et al., 2016), whereas its soluble fraction can form monodisperse stable droplets (Gumus et al., 2017a, Ho et al., 2017, Hinderink et al., 2019).

In these studies, the soluble fraction represents only 25% of the proteins present in the pea proteins isolate, which leaves a large fraction unutilized, and limits the sustainability potential of this ingredient. Therefore, it is important to explore the functionality of insoluble pea proteins and identify conditions under which this fraction may effectively be used for emulsion stabilisation. The fact that this fraction is insoluble implies that it exists in a supramolecular, particulate form. If such particles are partly wetted by both liquid phases, they could be candidates for Pickering stabilisation (Sarkar et al., 2020).

Pickering emulsions, i.e., particle-stabilised emulsions, have garnered substantial interest for food applications lately, mainly due to their high physical stability (Berton-Carabin et al., 2015; Dickinson, 2020). Many food-grade Pickering particles have been studied for this purpose, i.e., modified starch particles (Timgren et al., 2013), lipid particles (Schröder, Sprakel, et al., 2017), and water-insoluble protein particles such as zein (i.e., corn protein) particles (de Folter et al., 2012). It is important to note that chemical modifications or additional processing steps (e.g., anti-solvent precipitation or heat treatment) are generally needed to tune particle wettability such that they strongly anchor at the oil-water interface, which is not optimal from sustainability and clean-label points of view.

In this context, it is important to understand the emulsifying properties of pea proteins isolate as a whole, and of its insoluble fraction. In the present work, we evaluate the physical stability of emulsions prepared with full pea proteins isolate, or with only the insoluble pea proteins fraction, and also characterise whey protein-stabilised emulsions for comparison purposes. To relate to a range of possible applications, we consider not only fluid emulsions with a relatively low oil fraction (10 wt.% oil), but also high internal phase emulsions (HIPEs, 70 wt.% oil).

8.3. Materials & methods

8.3.1. Materials

Sodium phosphate monobasic, sodium phosphate dibasic, sodium dodecyl sulfate (SDS), and a bicinchoninic acid (BCA) kit were purchased from Sigma-Aldrich (Sigma-Aldrich, Saint Louis, USA). Sunflower oil was purchased from a local supermarket, and stripped with alumina powder (MP EcoChrome™ ALUMINA N, Activity: Super I, Biomedicals, Eschwege, Germany) to remove impurities and tocopherols (Berton et al., 2011). All chemicals and solvents were of analytical grade. Pea proteins isolate (PPI) was purchased from Roquette, France (NUTRALYS s85F, Roquette, France; see Appendix Table A2.1, Chapter 2 for the amino acid composition and content, and protein content) and whey proteins isolate (WPI) from Davisco foods, Switzerland (BiPro®, purity 97.0-98.4%). Ultrapure water (18.2 MΩ) was used for all the experiments (Millipore Corporation, Billerica, MA, USA).

8.3.2. Preparation of the insoluble pea proteins fraction

A 5 wt.% PPI suspension was prepared in phosphate buffer (10 mM, pH 7.0), stirred overnight at 4 °C and subsequently centrifuged at 16,000 x *g* for 20 min at 20 °C. The supernatant, which contained soluble pea proteins, was removed and the pellet was re-suspended in the same amount of phosphate buffer. This centrifugation/resuspension procedure was repeated four times.

8.3.3. Emulsion preparation

Pea and whey proteins were dispersed in phosphate buffer (10 mM pH 7) at 2 wt.%, stirred for 2 h and stored in the fridge overnight. The insoluble pea proteins (2 wt.%) were dispersed in buffer 1 h before use. Stripped sunflower oil (10 or 70 wt.%) was added to an aqueous phase (90 wt.% or 30 wt.%, respectively) containing 0.5, 1.0 or 2 wt.% emulsifier (pea proteins, insoluble pea proteins, or whey proteins). A coarse emulsion was prepared using a rotor-stator homogeniser (Ultra-turrax IKA T18 basic, Germany) at 11,000 rpm for 1 min (10 wt.% oil), or at 6,000 rpm for 30 sec (70 wt.% oil). The obtained coarse emulsion was then processed through a lab scale colloid mill with gap width of 0.32 mm (IKA Magic Lab, Staufen, Germany) operating for one min at 15,000 rpm. The resulting emulsions were stored at 4 °C.

8.3.4. Physical characterisation of emulsifiers and O/W emulsions

Protein suspension and emulsion morphology

The morphology of insoluble pea proteins suspensions was visualised by transmission electron microscopy (TEM). Samples were deposited onto freshly glow discharged copper grids (400 mesh), excess solvent was blotted using standard filter paper, followed by staining with an aqueous 1 wt.% phosphotungstic acid solution. Images were recorded on a JEOL JEM 1400 plus transmission electron microscope (Peabody, USA) operating at 120 kV in combination with JEOL CCD camera Ruby (8 M pixel).

The morphology of the emulsions in terms of occurrence of flocculation was evaluated by light microscopy using a Carl Zeiss Axioscope A1 microscope equipped with a camera (AxioCam Mrc5).

Droplet size measurement

The droplet size distribution of fresh and incubated emulsions was measured by static light scattering using a Mastersizer 3000 (Malvern Instruments Ltd.; Worcestheshire, UK). The fresh emulsions were stored at 4 ºC, in the dark for 14 days. In order to assess whether the emulsions became subject to flocculation over time, 7-day and 14-day old emulsions were diluted in 1 wt.% SDS solution prior to the measurement. The following optical properties were used: refractive indices of 1.465 (stripped sunflower oil) and 1.330 (ultrapure water) with an absorption index of 0.01. Sizes are reported as $d_{3,2}$ and are the average of two independent samples of which each was measured five-fold.

ζ–Potential measurement

The ζ–potential of the emulsion droplets was determined by dynamic light scattering (Zetasizer Nano ZS, Malvern Instruments, Worcestershire, UK) using a Dip Cell (ZEN1002) at 25 ºC. Prior to the measurement, emulsions were diluted 200 times in phosphate buffer (10 mM, pH 7.0) to prevent multiple scattering. The ζ-potential was calculated using the Smoluchowski model and expressed as the mean of two independent samples, of which each was measured in triplicate.

Rheological characterisation

The rheological behaviour of the 70 wt.% oil emulsions was characterised at 25 °C in terms of dynamic viscoelastic properties and flow behaviour using a rheometer (Anton-Paar, mcr

502) with a parallel plate geometry (PP50, 50 mm diameter and 1 mm gap). The emulsions were pre-sheared at 10 s^{-1} for 1 min prior to the measurement. Amplitude sweeps were performed from 0.01-100% strain at a frequency of 1 Hz for all samples. Frequency sweeps were performed from 0.01 to 10 Hz within the identified linear viscoelastic regime at 1% strain for the pea protein- and insoluble pea protein-stabilised emulsions, and 0.1% strain for the WPI-stabilised emulsion. The flow behaviour was taken in a steady-state flow mode by increasing the shear rate from 0.01 to 100 s^{-1}. The viscoelastic properties were reported as elastic modulus (G') or loss modulus (G'') as a function of frequency or amplitude, and the flow behaviour as apparent viscosity as function of shear rate (γ). The data are presented as the average of the independent duplicates.

8.4. Results and discussion

8.4.1. Particle characterisation

We prepared the insoluble pea proteins fraction by removing the soluble fraction from commercial pea proteins isolate using multiple centrifugation and resuspension cycles. After 5 centrifugation and resuspension cycles, less than 0.1 wt.% soluble pea proteins were still present in the insoluble pea proteins fraction (referred to as 'insoluble pea proteins' in the following). The latter contained aggregates of various sizes, with a fractal morphology (Figure 1).

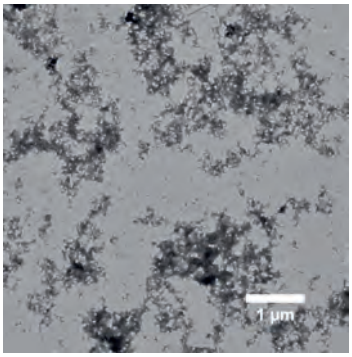

Figure 8.1. Transmission electron microscopy image of an aqueous suspension of the insoluble pea proteins fraction, showing aggregates.

8.4.2. Physical stabilisation

We prepared 10 wt.% O/W emulsions with full pea proteins, insoluble pea proteins, or whey proteins at initial concentrations of 0.5, 1.0 and 2.0 wt.% in the aqueous phase. All emulsions had a negative surface charge (Figure 2), with initial ζ–potentials of -25, ~-16 and ~-18 mV for whey protein-, full pea protein-, and insoluble pea protein-stabilised emulsions, respectively, and became more negatively charged over time (Figure 2). An increase in the net ζ– potential of protein-stabilised emulsions over time may be related to conformational rearrangements of proteins at the interface, exposing more charged groups (Wiacek et al., 2002).

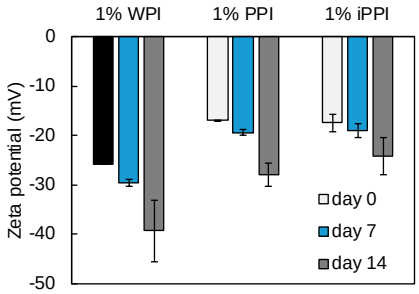

Figure 8.2. ζ–Potential of 1 wt.% whey protein-, full pea protein- and insoluble pea protein-stabilised emulsions at day 0, day 7 and day 14 of storage at 4 ℃ under non-oxidative conditions. Error bars represent the standard deviation of three measurements on two independent replicates.

All emulsions had comparable droplet sizes ($d_{3,2}$ around 3 to 4.6 µm) immediately after preparation. Whey protein- and insoluble pea protein-stabilised emulsions remained physically stable for 14 days at 4 °C, with no change in average diameter and droplet size distribution (Figure 8.3, data for 1 wt.%; data for other concentrations are shown in Appendix Figure A8.1 and Figure A8.2). The insoluble pea protein-stabilised emulsion was partly flocculated immediately after preparation, as could be concluded from the decrease in $d_{3,2}$ after dilution of the fresh emulsion in SDS solution (4.6 to 3.2 µm; droplet size distributions are shown in Figure A8.3 in Appendix), but the emulsion did not show further physical destabilisation upon storage. Full pea protein-stabilised emulsions showed an increase in droplet size after 7 days, caused by both flocculation and coalescence, as demonstrated by the fact that dilution of the emulsion in SDS solution prior to the measurement led to reduction in droplet size, but not to restoration of the initial droplet size.

To sum up, both insoluble pea proteins and whey proteins were able to physically stabilise O/W emulsions, whereas the full pea proteins isolate was not. Previous research showed that soluble pea protein-stabilised emulsions prepared in similar buffer conditions were susceptible to flocculation, but the interfacial layer was strong enough to protect the droplets against coalescence in the protein-rich regime (Hinderink et al., 2019).

In the emulsion stabilised by the full pea proteins isolate, the soluble proteins may have decreased the interfacial tension, or have adhered to the insoluble particles and influence their wettability, thus, in both cases reducing the Gibbs free energy of the system (Berton-Carabin et al., 2015) even prior to the particles nesting in the interface. This effect reduces the overall

energy gain that the system can achieve by having insoluble protein in the interface, and may reduce the stability of the emulsions.

Several authors have studied the combined use of particles and conventional emulsifiers, mostly in non-food emulsions, leading to various effects (Dickinson, 2013; Drelich et al., 2010; Pichot et al., 2012). Emulsifiers can adsorb onto Pickering particles and influence their wettability, and therewith emulsion stability, as reported for silica particle-stabilised emulsions with added cationic surfactants (Binks et al., 2007). In another example, a synergistic effect regarding the formation of small and stable emulsion droplets was found for silica particles and sodium caseinate. Sodium caseinate reduced the interfacial tension and promoted droplet break-up, and the particles and proteins coated the interface, preventing coalescence (Pichot, Spyropoulos, & Norton, 2010). However, particles and emulsifiers may also compete for adsorption when emulsifiers are present in excess, leading to phenomena comparable to the displacement of proteins by surfactants (Pichot et al., 2010; Vashisth et al., 2010).

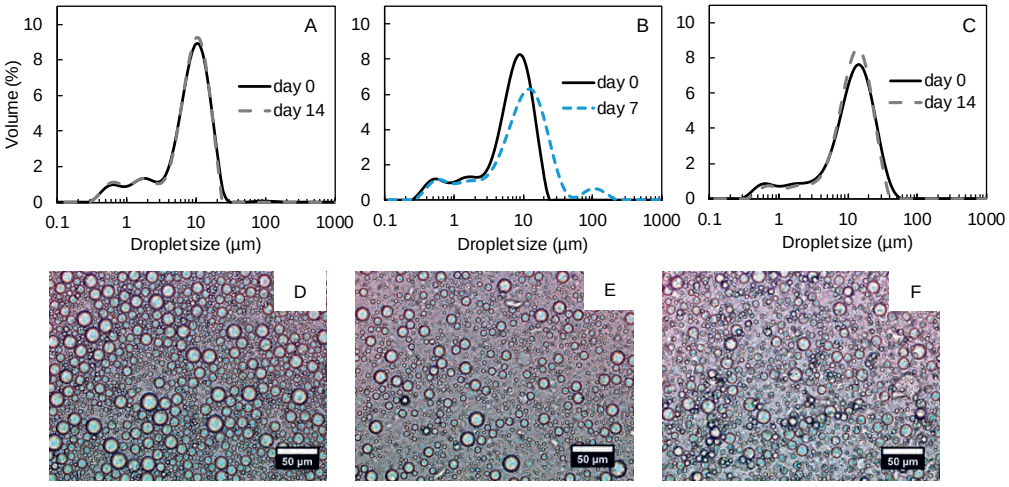

Figure 8.3. Droplet size distributions at different storage time, and microscopy images of the fresh 10% O/W emulsions prepared with 1 wt.% whey proteins (A and D), full pea proteins (B and E), or insoluble pea proteins (C and F).

Next to 10 wt.% O/W emulsions, we also prepared high internal phase emulsions (HIPEs) containing 70 wt.% oil, and 2 wt.% protein in the starting aqueous phase. Fresh whey protein-stabilised HIPEs had a droplet size comparable to that of 10 wt.% oil emulsions ($d_{3,2}$ around 4 µm), and were also physically stable over a period of 14 days at 4 °C (Figure 4). In contrast,

the fresh full pea protein- and insoluble pea protein-stabilised HIPEs exhibited larger average particle sizes ($d_{3,2}$ =10-12 µm) compared to those of the 10 wt.% O/W emulsions, which was due to flocculation, as could be concluded from the measurements after dilution in SDS solution, in line with what also occurred in the 10 wt.% insoluble pea protein-stabilised emulsions.

We experimentally determined that the surface-exposed hydrophobicity of pea proteins was substantially higher compared to that of whey proteins (Appendix, Figure A8.4). When hydrophobic interactions overcome electrostatic and steric repulsion, the resulting net droplet-droplet interaction forces are attractive, and droplets tend to flocculate (Berton-Carabin et al., 2018). This effect was reversible for insoluble pea proteins, as can be concluded from the particle size distributions at day 7 (Figure 8.4C). The increased net charge between the droplets over time (Figure 8.2) leads to stronger repulsions that may overcome attractive interactions, leading to reversible flocculation over the 7 days. In the full pea protein-stabilised emulsions, flocculation also occurred and over time the droplets coalesced (Figure 8.4B). Ultimately, a visible oil layer was observed after 14 days as well as for the insoluble pea proteins fraction (that did not coalesce over a 7 day storage period; Figure 8.4C).

The antagonistic effect of soluble and insoluble pea proteins fractions present in the full pea protein-stabilised emulsion, as described earlier, also holds for HIPEs; for the insoluble fraction, having solely particles at the interface may not be sufficient to provide stability in products containing tightly packed droplets, but did improve product stability considerably compared to the full pea proteins.

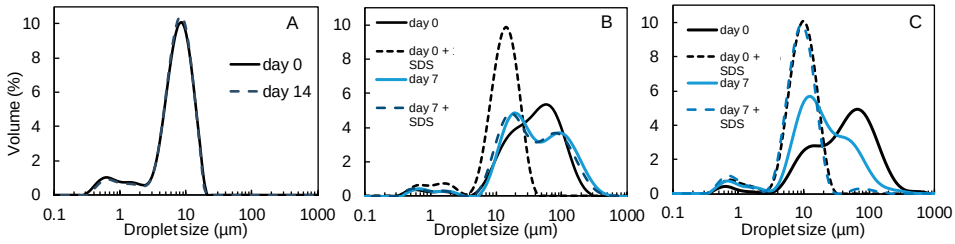

Figure 8.4. Droplet size distribution at different storage time of HIPEs stabilised by 2 wt.% whey proteins (A), full pea proteins (B), or insoluble pea proteins (C).

8.4.3. Rheological properties of high internal phase emulsions

HIPEs (70 wt.% oil) stabilised by whey proteins had a higher loss tangent, were relatively more liquid-like, and showed different rheological behaviour compared to full pea protein- or insoluble pea protein-stabilised HIPEs (Figure 8.5). In amplitude sweeps, all HIPEs showed a linear regime, in which the moduli were independent of the applied amplitude, after which strain softening occurred (Figure 8.5A). For whey protein-stabilised HIPEs, Type I nonlinear behaviour was observed (i.e., *G'* and *G"* are both decreasing), and the strain softening started at lower shear strains (around 0.1), whereas the full pea protein- and insoluble pea protein-stabilised HIPEs showed strain softening at higher strains (around 10). The latter two HIPEs showed type III nonlinear behaviour (Hyun et al., 2002), in which *G"* first shows shear thickening behaviour, until a maximum is reached, beyond which *G"* starts to decrease. The broader linear viscoelastic region of both pea protein-containing emulsions is expected to be related to attractive forces between the interfacial pea proteins, resulting in the highly flocculated state of the droplets as found by others (Guerrero et al., 1998; Yuan et al., 2017) and confirmed by our droplet size measurements (Figure 8.4). This can also explain the observed type III behaviour. In such emulsions, the oil droplet flocs resist deformation as they are jammed together, leading to an increase in *G*" with increasing shear strain, until the structure is destroyed and the loss modulus decreases. The crossover point (*G"*>*G'*) after the linear regime suggests yielding of the emulsion structure. Both the amplitude and frequency sweeps (Figure 8.5B) revealed a dominantly elastic behaviour (*G'*>*G''*) for the three HIPEs, although both pea protein-containing emulsions had an elastic modulus around 10-fold higher than that of the whey protein-stabilised emulsion. The flow curves for both pea protein-containing emulsions start at an apparent viscosity around 100 times higher compared to that of the whey protein-stabilised emulsion (Figure 8.5C). At increasing shear rates, the apparent viscosity decreased for all emulsions tested, albeit more strongly for pea protein-containing emulsions due to cluster breakdown, which occurred to a lesser extent in the whey protein-stabilised emulsion.

To put things into perspective, the initial *G'* values (10^3 Pa at 1 Hz), the shear thinning response, and the shear strain overshoot in *G*" in pea protein-containing emulsions were similar to values found for commercial mayonnaises (Duvarci et al., 2017). Compared to whey proteins, insoluble pea proteins were much more effective in increasing emulsion viscosity, which is an interesting lead for food product design.

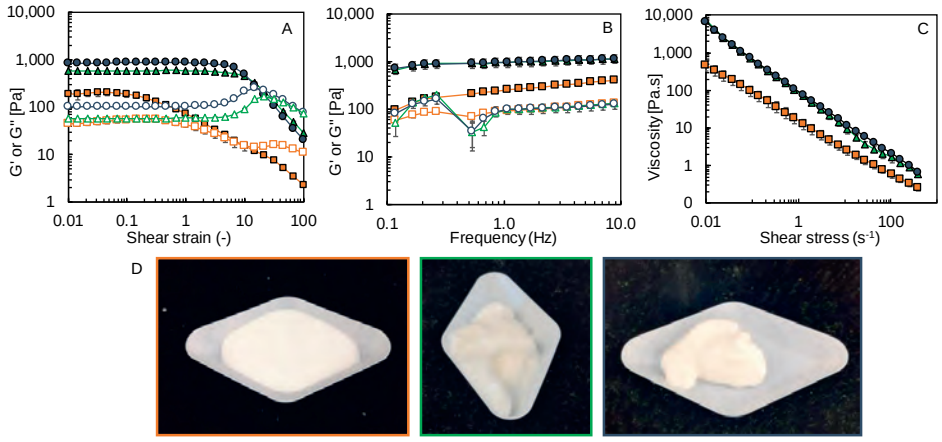

Figure 8.5. Rheological characterisation of whey protein- (orange), full pea protein- (green), and insoluble pea protein- (grey) stabilised HIPEs (70 wt.% oil): (A) amplitude sweep at constant frequency of 1.0 Hz, (B) frequency sweep at constant amplitude of 0.1% for the whey protein-stabilised emulsions, and 1% for pea containing emulsions, (C) flow curve and (D) pictures of the emulsions (from left to right: whey protein-, full pea protein- and insoluble pea protein-stabilised emulsion).

8.5. Conclusions

In this work, the physical stability of emulsions stabilised by pea proteins fractions (full fraction and insoluble fraction) was compared to that of emulsions stabilised by whey proteins isolate. Whey protein-stabilised emulsions formed physically stable 10 wt.% O/W emulsion over 14 days. The full pea protein-stabilised emulsions were physically unstable and coalesced within 7 days. In contrast, the insoluble pea protein-stabilised emulsions were initially flocculated but did not coalesce over the 14-day period. Apart from these results obtained on 10 wt.% emulsions, whey protein-stabilised HIPEs (70 wt.% oil) were physically stable, but had a substantially lower viscosity compared to pea protein-stabilised HIPEs (for both the full and insoluble pea fractions). The high viscosity of both pea protein-containing HIPEs was related to droplet flocculation by bridging of the pea proteins, as a consequence of the proteins' hydrophobic nature. The insoluble pea protein-stabilised HIPE was physically stable over a 7-day period but the full pea protein-stabilised HIPE showed coalescence, which reveals a possible antagonistic effect between the soluble and insoluble parts of pea proteins isolate, as also found in the 10 wt.% O/W emulsions. These findings show that understanding the functionality of pea proteins ingredients, and of

their components, is an important step towards the rational design of food systems suitable for industrial applications.

8.6. *Appendix*

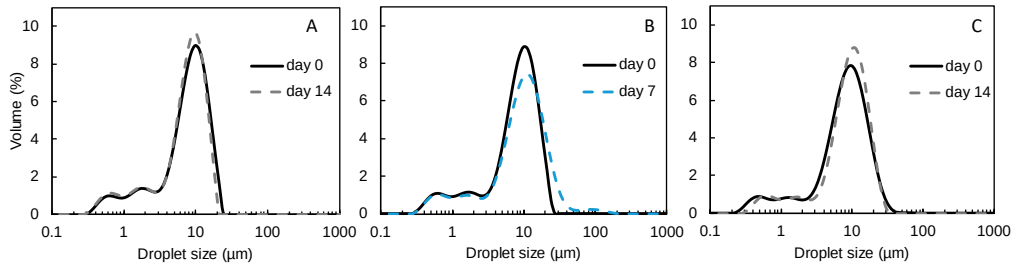

Figure A8.1. Droplet size distributions at different storage time of 0.5 wt.% whey proteins- (A), pea proteins- (B), and insoluble pea proteins-stabilised 10 wt.% O/W emulsions (C).

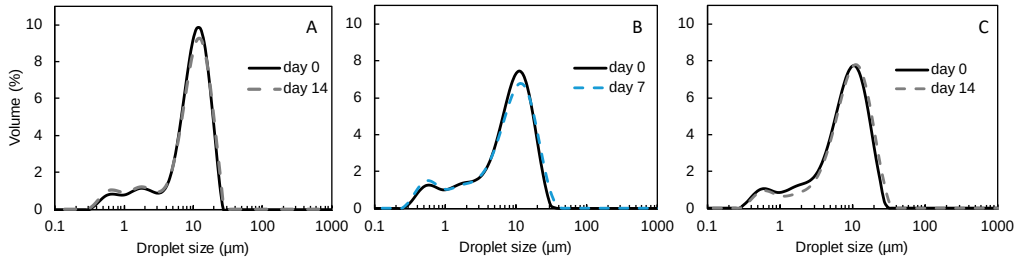

Figure A8.2. Droplet size distributions at different storage time of 2 wt.% whey proteins- (A), pea proteins- (B), and insoluble pea proteins-stabilised 10 wt.% O/W emulsions (C).

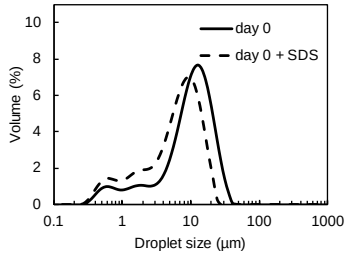

Figure A8.3. Droplet size distribution of 1 wt.% iPPI-stabilised emulsions with 10 wt.% oil at day 0.

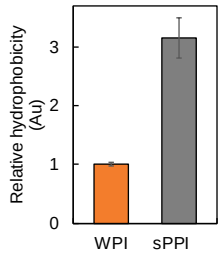

Figure A8.4. Protein surface hydrophobicity measured with ANSA (8-Anilino-1-naphthalenesulfonic acid ammonium salt) for whey proteins and soluble pea proteins at 0.12 g L^{-1} measured at emission spectrum between 400 and 650 nm, with an excitation wavelength of 385 nm and scan rate of 12 nm/min. Relative exposed hydrophobicity of the soluble pea proteins was expressed as increase in the integrated titration curve between 400 and 600 nm, after blank subtraction, with respect to the WPI protein sample. Errors bars represent the standard deviation of three independent replicates.

Chapter 9

General discussion

9.1. Introduction

This thesis focussed on the interfacial and emulsifying properties of plant-dairy protein blends. We used a multi-scale approach to gain understanding regarding their interfacial rheological behaviour, and how they are involved in the formation and physical stability of emulsions. We examined the stability of the formed droplets at short and long time scales, and related this to the proteins' molecular properties and interfacial rearrangements. To summarise, we aimed to connect emulsion stability to the composition and structure of the oil-water interfacial films, and link this to the molecular properties of the proteins.

Chapters 2-4 are dedicated to the characterisation of conventional model interfaces and of emulsions, in order to obtain insights in the long term processes relevant to emulsion properties (stability, interfacial protein rearrangements). In **Chapters 5 and 6**, we used microfluidic tools to probe interfacial properties at very short time scales (<1 s), which are relevant to understand emulsion formation in conventional homogenisation processes. Furthermore, we dove deeper into the functional properties of pea proteins at the molecular scale (**Chapter 7**), and investigated their emulsifying properties in different application-relevant systems (**Chapter 8**).

9.2. Main findings and conclusions

In **Chapter 2**, we highlighted a synergistic behaviour in the blend-stabilised emulsions (dairy and pea proteins), in terms of long term physical stability in the protein rich-regime. We confirmed that, in this regime, both proteins adsorbed at the interface and thus contributed to droplet stability. We observed that compositional rearrangements at the interface occurred over a time span of several days. More specifically, whey proteins were able to partly displace pea proteins from the interface, which were themselves able to displace caseins. Such rearrangements are important to consider, since the integrity of the interfacial network could be compromised after partial displacement, which may result in the physical destabilisation of emulsions. In parallel, we characterised the interfacial behaviour of the proteins using model air-water and oil-water interfaces (**Chapter 3**). It was clear that the WPI-stabilised interfaces had superior stiffness compared to the other systems tested. The layers' strength decreased when whey proteins were blended with pea proteins. Sodium caseinate formed the weakest interfacial layers, but blending it with pea proteins improved the mechanical strength

of the layer. Thus, in interface-dominated colloidal systems, blending sodium caseinate and pea protein isolate is favourable, and may increase droplet resistance against coalescence.

In **Chapter 4,** we combined the approaches used in Chapters 2 and 3 to mechanistically understand the interfacial rearrangements over time. Whey proteins, and more specifically β-lactoglobulin, were able to partly displace pre-adsorbed pea proteins from the oil-water interface when present in the continuous phase even at relatively low concentrations (at least 1 g/L). Displacement led to an increased interfacial elasticity, but was not driven by a decrease in interfacial tension. We hypothesise that the in-plane protein-protein interactions establishing upon the compositional modification of the layer are thermodynamically favourable for the overall system and therewith, the driving force for displacement. Addition of pea proteins to a pre-adsorbed whey protein layer led to an increase in surface load. The interfacial connectivity decreased, resulting in less stiff interfaces.

In **Chapter 5**, we used microfluidic tools to understand early film formation at the surface of protein (blend)-stabilised droplets. The rheological properties of the protein-based films covering the droplets, in response to a moderate deformation induced by passage of the droplets through a channel constriction, could be assessed from 0.16 to 1 second. These time scales cannot be captured with conventional characterisation methods, such as drop tensiometry, whereas they are highly relevant to understand the early interfacial film formation in emulsions. We found that rapid protein adsorption at the surface of freshly formed oil droplets was followed by slower network formation with an increased viscous contribution over time. The PPI-stabilised films had weaker in-plane interactions compared to WPI-stabilised films, which resulted in droplets that were less stable to coalescence. When a whey-pea protein blend was used, high interfacial connectivity was achieved, but this only took place at relatively long time scales (1 s), and thus could not prevent rapid droplet coalescence.

In **Chapter 6**, we oxidised commercial pea proteins to various levels, and determined the coalescence stability of emulsion droplets prepared with the resulting oxidised fractions. The low molecular weight, soluble protein oxidation products were able to form droplets that resisted coalescence well, probably as a result of the formation of structurally more homogenous films, as compared to the starting protein material. The down-side is that oxidation largely reduced the overall pea protein solubility, which reduced the amount of protein that can effectively be used. It is clear that the oxidative status is very relevant for

plant protein functionality, and should be considered when conducting protein fractionation and subsequent product design.

From the previous chapters, it was evident that the emulsifying and interfacial properties of the dairy and plant proteins were very different. In **Chapter 7**, we zoomed in further, and used right-angle and front surface fluorescence to gain insight in the tertiary structure of the proteins in solution and at the interface. The commercial pea proteins behaved as soluble aggregates, and thus as relatively rigid particles, whereas in the more mildly lab-purified isolates, proteins were less aggregated and were able to change their conformation upon adsorption at the oil-water interface. This highlights the effect of the conditions applied upon protein fractionation on the isolate's functionality.

In **Chapter 8**, we took a next step in assessing the functionality of the commercial pea protein isolate for application purposes. Contrarily to what was performed in the other chapters, where only the so-called "soluble fraction" of PPI was used (i.e., the fraction that remained in the supernatant of the PPI suspension), we attempted to make use of the full suspension, or even of the insoluble fraction only. We found that the insoluble fraction could physically stabilise 10 and 70 wt.% O/W emulsions in the protein-rich regime, probably due to the predominant presence of aggregates that could act as Pickering particles. When the full fraction was used, emulsions were physically unstable, probably due to competition between the soluble proteins and insoluble structures at the interface.

9.3. Main findings put into a wider perspective

9.3.1. Droplet formation and stabilisation

When emulsions are formed in high shear devices, so within milliseconds (Håkansson, 2016), as is customary in industry, the droplet size is a resultant of droplet break-up and rapid recoalescence if the droplets are not sufficiently stabilised (Walstra, 2003). Since conventional homogenisers do not allow for visual evaluation, the droplet size distribution is measured after leaving the homogeniser. For both droplet break-up and recoalescence, the interfacial tension and interfacial rheological properties play an important role; a low interfacial tension facilitates droplet break-up and reduces the total Gibbs free energy of the system and thus the driving force for coalescence. If droplets come into contact, a stiff interfacial layer can protect droplets against coalescence (Bos et al., 2001; Murray, 2011). Traditional methods to study interfacial tension and rheological properties (e.g., drop

tensiometer) cannot measure at typical time scales occurring in a high-pressure homogeniser. These methods typically have their first measurement point around one second and, therefore, the microfluidic techniques that we developed have great added value. In fact, they allow for characterising the formation of droplets at short time scales (<1 s) and within these devices, emulsifier transport towards the interface occurs by convection instead of diffusion, which is relevant to large scale emulsification processes. Using tailor-made microfluidic chips, droplet coalescence and interfacial rheology can effectively be measured and linked at short time scales (<1 s) (**Chapters 5 and 6**). Accessing such uncharted timescales was instrumental to determine that for certain protein compositions and/or concentrations, protein adsorption was not rapid and complete enough, which resulted in insufficient in-plane interactions between the adsorbed proteins and heterogenous interfaces, and subsequently in droplet coalescence (**Chapter 5**). In other words, we were able to unravel the sub-second cascade of interfacial phenomena that drive rapid droplet coalescence.

Interface stabilisation in the protein-rich regime

At high enough protein concentrations, high surface loads can be achieved and densely packed interfacial layers are formed with a high resistance against deformation, which thereby protect emulsion droplets against recoalescence. This is well in line with the properties of emulsions formed by high-pressure homogenisation (**Chapter 2**). In the protein-rich regime, all emulsions had a similar droplet size, which suggests that the droplets were sufficiently stabilised upon high-pressure homogenisation and re-coalescence hardly occurred – or if any, it is efficiently compensated by the five passages through the high-shear interaction chamber, which is common practice in high-pressure homogenisation (Jafari et al., 2008; Tcholakova et al., 2003).

The effect of protein aggregates in the protein-poor regime

At low protein concentrations, low surface loads are achieved, as well as larger droplet sizes due to recoalescence of the freshly formed droplets within the homogeniser (Tcholakova et al., 2003). Especially for pea proteins, a high level of recoalescence occurred (**Chapters 2 and 6**), which was explained by the presence of soluble aggerates in the soluble fraction (i.e., non-precipitated fraction) of the commercial isolate dispersion (**Chapters 6 and 7**). Next to process-induced aggregation, plant proteins have a complex quaternary structure and a strong tendency for aggregation and association with other components such as polyphenols (Amagliani & Schmitt, 2017; Sarkar et al., 2020). The plant proteins are thus present as

colloidal particles rather than molecularly dissolved (Velev et al., 1993). When such protein particles are used for emulsion stabilisation purposes, the interfacial phenomena become more complex. Particles can promote coalescence (i.e., act as active destabilisers), which has been well known and described for aqueous foams (Hunter et al., 2008) and recently also for emulsions (Nagarkar et al., 2012; Schröder et al., 2018). Active destabilisation may occur via two routes: in the first one, referred to as “bridging dewetting”, the particle is preferentially wetted by the dispersed phase and bridges two droplets, and the contact line recedes across the particle and promotes coalescence. The second one relates to a phenomenon occurring when particles are preferentially wetted by the continuous phase, but the drop surface is not completely covered. In that case, the particle free surface (the edge of the bridged monolayer) is perceptive for disturbances allowing the film to rupture and droplets to coalesce (Nagarkar et al., 2012; Schröder et al., 2018). Complete coverage of the interfacial layers immobilises the interfacial layer therewith supressing coalescence. The destabilising effect of particles is thus expected to play a major role when using plant proteins, and has to be taken into account in the design of plant protein-stabilised emulsions (Velev et al., 1993). Yet, the size of such protein structures can be reduced by different pre-treatments, which is discussed further in the next section.

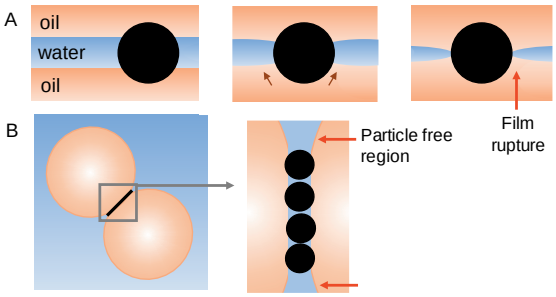

Figure 9.1. A) A Pickering particle adsorbed at two fluid-fluid interface. The formation of an oil bridge between the two films leads to dewetting of the Pickering particle and subsequent film rupture; adapted from Denkov, Cooper, & Martin, 1999 B). The structure of a bridging monolayer. The particle free region next to the monolayer are susceptible to coalescence under flow; adapted from Nagarkar & Velankar, 2012.

Plant protein modifications to enhance the early film formation

Subjecting proteins to oxidation led to a broadening of the structures and molecular sizes present: on the one hand, extensive aggregation occurred, leading to very large aggregates that were insoluble and could not even be used for emulsification purposes. On the other hand, the fraction that remained soluble contained peptides arising from protein hydrolysis,

which were able to rapidly adsorb at the interface and efficiently prevent re-coalescence (**Chapter 5**). This highlights the potential of limiting/reducing the size of the protein molecules and structures for yielding physically stable emulsions immediately after droplet formation. Yet, purposely performing oxidation is not relevant from a nutritional point of view (Estévez et al., 2019; Hellwig, 2020), and also because of the large loss in protein solubility (Hellwig, 2019). At first sight, performing mild protein hydrolysis could be another option to improve the emulsifying properties of pea proteins (Barać et al., 2011; García Arteaga et al., 2020; Klost et al., 2019); but at neutral pH values, a moderate degree of hydrolysis may decrease the protein solubility further (García Arteaga et al., 2020; Klost et al., 2019). Therefore, other routes to improve the interfacial and emulsifying properties should be considered. For instance, we applied high-pressure homogenisation to protein suspensions, which led to de-aggregation of the process-induced supramolecular structures, (Figure 9.2A and B), or salt addition (250 mM) to de-aggregate legumin (Gueguen et al., 1988). Both strategies improved the coalescence stability of emulsions as evaluated by microfluidics, with addition of salt being the most effective (Figure 9.2C). However, when applied in food emulsions, a high salt concentration may screen the interfacial charges leading to droplet flocculation and thus negatively affecting the long term stability of the emulsions (McClements, 2004b).

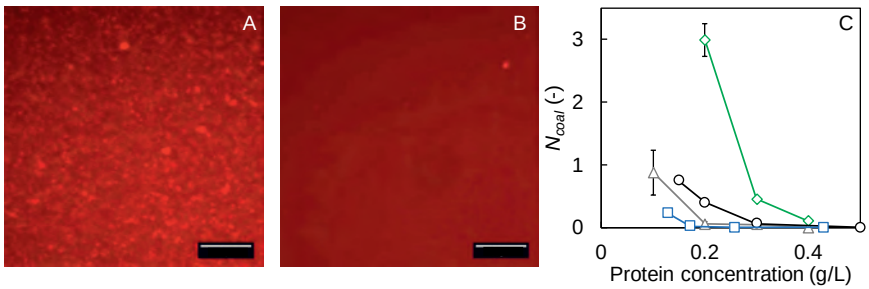

Figure 9.2. CLSM images of A) non-homogenised and B) homogenised pea protein 'soluble' fractions stained with rhodamine B. The samples were subjected to a high-pressure homogenisation (Microfluidizer) at 400 bars for 5 passes. The scale bar represents 25 μm; and C) mean number of droplet coalescence occurrences at the outlet of the coalescence channel (microfluidic chip with an adsorption time of 100 ms) for PPI (◊), homogenised PPI (○) and 24h-oxidised PPI (△) in 10 mM phosphate buffer, and PPI in 250 mM NaCl phosphate buffer (□) (pH = 7.0 in all cases). The lines between the markers guide the eye.

9.3.2. Long term physical stability

In the protein-rich regime, emulsions with similar droplet sizes were formed independently of the protein or protein blend used, suggesting that all droplets were efficiently stabilised

during the homogenisation process. However, over longer time scales, the PPI-stabilised emulsions showed substantial flocculation after 14 days, but not coalescence (**Chapter 2**). We interpret this as follows: attractive intermolecular interactions between the adsorbed pea proteins, due to their hydrophobic nature, overcome the electrostatic and steric repulsions, and therewith lead to droplet flocculation (Berton-Carabin et al., 2018). The fact that the droplets did not subsequently coalesce indicates that the interfacial film resists rupture, which could be due to the thick and stiff interfacial structure formed by pea proteins (**Chapter 3**). Emulsions stabilised with the protein blends showed excellent physical stability, probably due to weak attractive interactions and strong electrostatic repulsion, which prevented flocculation. For the SC-PPI protein blend, a stiffer interfacial network was formed compared to SC-stabilised interfaces (**Chapter 3**), which may also protect droplets against coalescence (**Chapter 2**). The rheological properties measured using model interfaces were therefore useful to explain the stability of the corresponding emulsion droplets. Dedicated microfluidic tools revealed that the onset of the formation of organised structures at the interface already occurs at very short times after droplet formation, which is an important step to unravelling the development of interfacial protein films.

Interfacial rearrangements

Understanding the interfacial displacement phenomena occurring with blends of plant and dairy proteins was an important milestone of this project. For instance, after highlighting that caseins were able to displace pea proteins when used concomitantly to fabricate an emulsion (**Chapter 2**), we showed that SC and PPI led to the same equilibrium interfacial tension at the oil-water interface. Pea proteins formed an interfacial film with higher interconnectivity and stiffness compared to caseinate (**Chapter 3**). This seems to indicate that in such systems, protein displacement is driven by differences in interfacial elasticity and the establishment of favourable inter-protein interactions, rather than by minimising interfacial tension, which will be discussed further in section 9.4. Furthermore, a prerequisite for interfacial displacement is the presence of the displacing protein in sufficient concentration in the continuous phase. This criterion is often met in studies dealing with food-relevant emulsions: for instance, a meta-analysis on 80 examples of emulsion formulations found in original research articles estimated that in 76% of the formulations, more than 50% of the emulsifier amount used were unabsorbed, and in 28% of the formulations the excess of emulsifiers was even more than 90% (Berton-Carabin et al., 2014). Furthermore, when looking at food

emulsion products (such as infant formulas and dressings), the protein concentration is always considerably higher than what is strictly needed to stabilise the oil-water interface – mostly to comply with product specifications. Interfacial rearrangements may thus be ubiquitous in most food emulsions, and also this aspect is hardly considered in related research and development, it may have an important role for product stability.

9.4. Important considerations for the analysis of protein blend-stabilised emulsions

Competitive adsorption and interfacial displacement with protein mixtures have been systematically studied in a number of studies, for binary protein mixtures (Dickinson, 2011; Fainerman et al., 2020). Since only a few proteins were considered per study, and the measurement techniques varied (Table 9.1, Table 9.2) it is difficult to draw generic conclusions and pinpoint the underlying mechanisms. For this, the use of theoretical models and simulations can be helpful. In the following section we will focus on the potential of Brownian dynamics (BD) simulations to describe the parameters that govern interfacial displacement. Such simulations describe very simple systems, whereas food emulsions are more complex both at a molecular level and at larger scales (Figure 9.3). To bridge this gap, we will describe the experimental techniques available to assess interfacial displacement using model interfaces or emulsions. We will emphasize the link between the model parameters and experimental results in order to provide a generic and fundamental understanding for displacement phenomena.

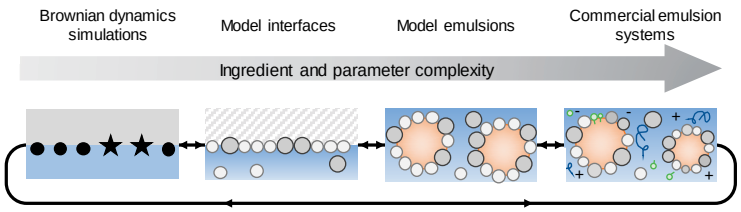

Figure 9.3. The system (i.e., ingredient and parameter) complexity in the techniques used to characterise interfacial displacement.

9.4.1. Brownian dynamics simulations

Interfacial displacement has been simulated using BD (Pugnaloni et al., 2003a, 2005; Wijmans et al., 1999b, 1999a), which provided useful information on the mechanisms involved. Wijmans and Dickinson simulated an adsorbed protein monolayer as bonded particles and introduced non-interacting displacer particles with a stronger affinity for the

interface. They showed that if the initially adsorbed particles form a strongly bonded network, very few displacer particles succeed in adsorbing at the interface. In case of less strong network interactions at the interface, the displacer particles could adsorb, when present in sufficiently large numbers, and produce a closely packed monolayer with a lower interfacial tension (Wijmans et al., 1999a, 1999b). A generic conclusion was drawn, according to which for displacement to occur in the BD simulations, three criteria need to be met:

1. The interfacial layer needs to be cross-linked with small holes through which the displacing molecules can penetrate.
2. The cross-linked film has to be flexible enough to allow compression prior to displacement.
3. Short-range repulsive interactions need to establish between the adsorbed and displacer components, which enhances local phase separation and subsequent growth of the areas occupied by displacer particles.

Repulsive interactions between displacer particles and bonded monolayer were investigated by Pugnaloni, Ettelaie, & Dickinson (2003b), and ultimately, the BD simulations were compared to experimental data on displacement of a protein layer by surfactants (Mackie et al., 2003). The comparison could only be done semi-quantitatively, because the interactions within the layers, which varied greatly between β-lactoglobulin and β-casein, could be taken into account only in a fairly simple coarse-grained manner.

The outcomes of BD simulations highlight the importance of the interfacial rheological properties of the pre-adsorbed monolayer and of the surface activity of the displacing particle, and thus represents the displacement of adsorbed proteins by low molecular weight emulsifiers (e.g., SDS, Tween 20). It is presumable that similar mechanisms play a role in displacement mechanisms in protein blends, although the interfacial tension differences are much smaller (as discussed in section 9.3 and Chapter 3). Furthermore, the nature and strength of in-plane protein interactions of the pre-adsorbed and displacing protein would need to be considered in order to conduct relevant BD simulations.

9.4.2. Sequential adsorption and interfacial displacement studied using model interfaces

As discussed extensively throughout this thesis, model interfaces are widely used to describe the rheological properties of interfacial layers, and have also been used for displacement studies, as summarised in Table 9.1. This summary highlights the variety of protocols applied for the preparation of the interfacial layers, studied time scales and subsequent measurements. Most of the studies only involve optical observations (e.g., ^{14}C surface radioactivity) and interfacial tension measurements (e.g., Wilhelmy plate). These are very useful to determine whether displacement occurs, but do not allow for mechanistical understanding; for this latter perspective, the determination of interfacial rheological properties is essential.

In this thesis, we used a drop tensiometer to characterise the dilatational rheological properties of protein interfacial layers by applying sinusoidal area deformation to a model droplet while recording the interfacial tension. Sequential introduction of another protein, post-formation of the initial protein layer, can be achieved by exchanging either the drop phase, or the bulk phase (Figure 9.4A and B). The interfacial rheological properties can be assessed using large amplitude oscillatory dilatational experiments (i.e., amplitude sweeps, Figure 9.4C, (Sagis & Fischer, 2014)). Expressing the results as Lissajous plots is especially useful, as it reveals the in-plane mechanical properties and highlight the non-linear response of the interface, such as strain softening or jamming, which are typical in structurally heterogeneous layers. Interfacial protein aggregation can also be characterised using step dilatational measurements (i.e., sudden extension or compression of the drop). The stress-relaxation can be analysed using a Kholrausch-Williams-Watt stretched exponential function (Equation, 9.1 (Sagis et al., 2019)).

$$\gamma(t) = ae^{-(t/\tau_1)^{\beta}} + be^{-t/\tau_2} + c \qquad 9.1$$

With γ the change in surface stress over time, τ_1 the relaxation time associated with stretched exponential behaviour, β the stretch exponent, and a, b and c constants. The second exponential, including τ_2, is added to correct for the regular ageing of the interface (i.e., decrease in interfacial tension that occurs independently of the step deformation), which is typically present in protein-stabilised interfaces, as for such systems interfacial tension does not reach true equilibrium in the probed time scales. Protein-stabilised interfaces typically have β-values of 0.4-0.6 in extension, and of 0.5-1 in compression. This implies two things: first, the fact that the values are different in compression and in extension indicates an

asymmetric behaviour. Second, the fact that the values are <0 indicates that there is not a single relaxation time that describes the response to sudden deformation, but rather a distribution of relaxation times, which is indicative of interfacial structural heterogeneity. The link between low β-values and heterogeneous structures at the interface has been experimentally validated by AFM images of LB films showing structural heterogeneity at the micrometer scale (Sagis et al., 2019; Yang et al., 2020, 2021).

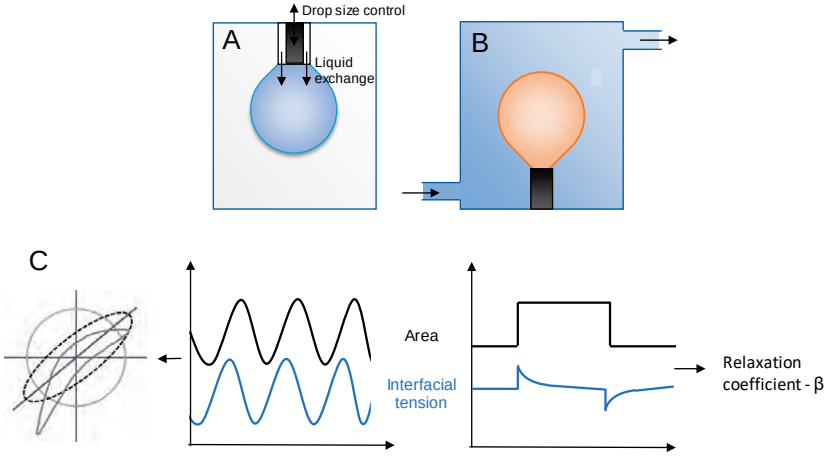

Figure 9.4 Schematic representation of two drop tensiometer set-ups that allow sequential introduction of proteins: A) using a double needle or B) using bulk phase exchange. C) Classical amplitude sweep and interfacial tension response (middle) and examples of Lissajous plots of various shapes (left) and step dilatational measurements (right).

Table 9.1 Examples of competitive adsorption and dynamic exchange experiments in model interfaces using binary mixtures of food proteins.

Proteins	*Primary layer*	*Second layer*	*Time*	*A-polar phase*	*Methods*	*Reference*
Lyophilized α_{s1}- and β-casein and 1:1 mixture	(Co-) adsorption	Injection (after 24h)	24 h	Air	^{14}C surface radioactivity, Langmuir trough, Wilhelmy plate	(Anand et al., 1996)
BSA, Lysozyme	(Co-) adsorption	Injection (after 24h)	24 h	Air	^{14}C surface radioactivity, Langmuir trough, Wilhelmy plate	(Anand et al., 1995)
BSA, β-casein	(Co-) adsorption	Injection		Air	^{14}C surface radioactivity, Langmuir trough, Wilhelmy plate	(Cao et al., 1995)
Lysozyme, β-casein	(Co-) adsorption	Injection (after 10 h)	14 h	Air	^{14}C surface radioactivity, Langmuir trough, Wilhelmy plate	(Hunter et al., 1991)
7S soy protein and β-casein Soy proteins, BSA, β-, α-casein, lysozyme, ovalbumin, β-lg, α-lac	(Co-) adsorption	Injection (after 20 min)	15 min – 30 h	Air	^{14}C surface radioactivity, Langmuir trough, Wilhelmy plate	(Razumovsky et al., 2001)
IgG (hydrophobized)	(Co-) adsorption	Injection (after 2 h)	18 h	Air	^{14}C surface radioactivity, glass container, Wilhelmy plate	(Baszkin et al., 2001)
BSA, β-casein	Co-adsorption	-	4 days	Air	Epifluorescence (LS-films), ^{14}C surface radioactivity, Langmuir trough, Wilhelmy plate	(Sengupta et al., 2000)
β-, α-casein and 1:1 mixture	Adsorption	Injection	20 h	Triolein	^{14}C surface radioactivity, Langmuir trough, Wilhelmy plate	(Damodaran et al., 2003)
ovalbumin, lysozyme and 1:1 mixture	Adsorption	Injection, washing and subsequent injection		Air	Langmuir sample trough + ellipsometry, surface shear rheometer	(Le Floch-Fouéré et al., 2010)

β- and α-casein	Adsorption	Injection		n-Tetradecane	Surface shear rheometer	(Dickinson, Rolfe, et al., 1988)
β-casein, α-lac, β-lg	Adsorption	Injection (after 24h)	24 h	n-Tetradecane	Surface shear rheometer	(Dickinson et al., 1990)
Casein, gelatin, α-lac and lyszoyme and 1:1 mixture	Adsorption	Injection (after 24h)		n-Hexadecane	Surface shear rheometer	(Castle et al., 1987)
β-lg and BSM and 1:1 mixtures	Co-adsorption	-	2.5 h	Air	Surface shear rheometer	(Çelebioğlu et al., 2017)
β-casein, β-lg and mixtures	Co-adsorption	-	3 h	Sunflower oil	Drop tensiometer	(Seta et al., 2014)
β-casein, β-lg and mixtures	Co-adsorption	-	2 h	Air	Drop tensiometer	(Fainerman et al., 2020)
WPI, PPI	Adsorption	Prefusion	1 h	Stripped sunflower oil	Drop tensiometer	(Hinderink et al., 2021)

igG, immunoglobulin; BSA, bovine serum albumin; β-lg, β-lactoglobulin; α-lac, α-lactalbumin; BSM, bovine submaxillary mucin; LS, Langmuir-Schaeffer.

9.4.3. Sequential adsorption and interfacial displacement studied in emulsion systems

Model interfaces give insight in the rheological properties of the interfacial layers, and can be used to visualise interfacial displacement; however, they are usually formed in different conditions than in actual emulsions, and do not allow for assessing inter-droplet interactions and related destabilisation phenomena. It is therefore useful to combine measurements performed on model interfaces and on emulsions.

When analysing possible competitive adsorption and displacement in protein-stabilised emulsions, the first step is to determine the surface load on the starting and final systems, to distinguish between additional adsorption and interfacial displacement. This is conventionally done by physically separating the aqueous and creamed phases of the emulsion, followed by analysis of the components present in both phases (Hunt et al., 1994). Subsequently, the surface load and interfacial composition are measured directly via the (washed) creamed phase, or indirectly via the serum phase and calculated by subtraction from the total protein present (as summarised in Table 9.2). In this project, we highlighted that the applied procedure can substantially alter the surface load measured (**Chapter 4**); for instance, washing the creamed phase reduced the measured surface load and may also affect the measured interfacial composition. Therefore, when comparing the outcomes of different displacement studies, it is important to consider the methods used.

Table 9.2. Examples of studies dealing with competitive adsorption and sequential protein introduction in emulsions prepared with mixtures of food proteins.

Proteins	*Pre-/post-emulsifying*	*Time scale*	*Phase*	*Concentration/ Surface load*	*Composition*	*Reference*
β-casein, α-casein	Post (washed cream)	1-24 h	Serum	FPLC	FPLC	(Dickinson, Rolfe, et al., 1988)
β-lg, α-lac	Post (washed cream)	1-32 h	Serum	FPLC	FPLC, electrophoretic mobilities	(Dickinson, Rolfe, et al., 1989)
SC and heated SPI	Pre and post	0	Washed cream	-	SDS-PAGE	(Aoki et al., 1984)
			Serum	Lowry method	SDS-PAGE	
β-lg in a 1:1 mixture with β-casein, α-lac or ovalbumin	Post (washed cream)	48 h	Serum	FPLC	FPLC	(Dalgleish et al., 1991)
WPI, SC	Post	10 min	Cream	SDS-PAGE	SDS-PAGE	(Dalgleish et al., 2002)
Phosvitin, β-casein	Post (washed cream)	48 h	Serum	FPLC	FPLC	(Hunt et al., 1993)
β-lg, α-lac in 1:1 mixture	Pre	1-18 h	Washed cream	SDS-PAGE	SDS-PAGE	(Matsumura et al., 1994)
β-lg, α-lac	Post (washed cream)	1-18 h	Serum	Lowry method	SDS-PAGE	
SC	Pre	1-24 h	Serum	FPLC	FPLC	(Robson et al., 1987)
WPI, egg yolk lipoproteins	Post (washed cream)	0-1 h	Cream		SDS-PAGE	(Aluko et al., 1998)
			Serum	Lowry method		
WPI, SC, PPI and 1:1 WPI-PPI or SC-PPI	Pre	0-72 h	Cream	-	SDS-PAGE	(Hinderink et al., 2019)
			Serum	BCA		
WPI, PPI and 1:1 mixture	Pre and post	0-72 h	(Washed) cream	BCA	SDS-PAGE	(Hinderink et al., 2021)
			Serum	BCA		

FPLC, fast protein liquid chromatography

From Table 9.1 and Table 9.2, it is clear that the techniques and approaches to study interfacial displacement vary greatly. The critical parameters that were determined to be critical by BD simulations are often not measured in displacement studies (e.g., the rheological properties of the primary monolayer and interfacial behaviour of the displacing protein). Furthermore, the available displacement studies have mostly focussed on proteins

of animal origin, e.g., gelatine or egg proteins combined with dairy proteins, and only one study considered a plant protein (7S soy protein) in combination with a dairy protein. Considering that plant protein isolates contain not only a broad variety of proteins (just like dairy ingredients do), but also a range of native and process-induced supramolecular structures, it seems relevant to continue the pioneering work of Dickinson and co-workers but now using plant proteins. Furthermore, determining the dynamic interfacial composition in protein-stabilised emulsions is relevant when soluble proteins and insoluble protein structures co-exist and may compete for adsorption (as in commercial plant protein isolates, Chapter 8) which leads to physically unstable emulsions.

There is thus a research gap that needs to be filled, and we suggest a multi-scale approach for this (Figure 9.3). By combining BD simulations, interfacial characterisation and measurements in model emulsion systems, a thorough understanding of the interfacial displacement can be obtained, which can be translated to real food emulsions. In particular, interfacial rheology measurements proved useful to explain the displacement phenomena. Furthermore, BD simulations can help pinpointing the important parameters involved, which is hardly possible in emulsions due to the high complexity of the systems.

9.5. Plant proteins as emulsifiers

Plant protein seeds (such as pea or soy) contain storage proteins which are synthesised and accumulated for reproduction purposes (i.e., ensuring that the seed will grow into a new plant (Gatehouse et al., 1984)) and stored in protein bodies (Spencer et al., 1984). Storage proteins are multimeric proteins and in general insoluble in aqueous solution (Gatehouse et al., 1984; Spencer et al., 1984), during germination, the proteins are broken down to their constituent amino acids that are used for the germination and early growth. In contrast, dairy proteins are water-soluble as milk contains a large fraction of water (~87 % (Kailasapathy, 2009)) and have to be easily digestible to provide the amino acid supply for growing calves (Argov et al., 2008). Based on the different physiological properties of plant and dairy proteins, it is logical that they largely differ in structure and techno-functional properties. It is actually surprising that this is not acknowledged much more broadly, and made better use of when coming to applications. To quote Albert Einstein:

> *"Everybody is a genius. But if you judge a fish by its ability to climb a tree, it will live its whole life believing that it is stupid."*

The low solubility of plant proteins has been considered a potentially valuable functional attribute only recently, due to the growing interest in colloidal emulsifiers able to form Pickering emulsions (Amagliani & Schmitt, 2017; Sarkar et al., 2020); a property of pea proteins that we also demonstrated in the present work (**Chapter 8**). It seems of high importance to continue this work, to make the best possible use of plant protein ingredients without further pre-treatments (e.g., hydrolysis, homogenisation).

In the current thesis, we mainly worked with a commercial pea protein isolate, but as discussed in **Chapter 7**, the use of plant protein concentrates obtained via mild processing could be of great relevance (Kornet et al., 2020; Ntone et al., 2020; Sridharan et al., 2020; Yang et al., 2021). Mild fractionation processes typically include fewer purification steps, which implies that the resulting ingredients are more complex, containing proteins and non-protein components such as carbohydrates, lipids and phenols. These components need to be taken into account in food design, although they do not necessarily affect stability negatively. For instance, the presence of lipids in mildly derived rapeseed protein isolate was shown to lower protein connectivity of the air-water interfacial layer, but did not affect foam stability (Yang et al., 2021). Pea flour (milled peas, 45-μm sieved) without further purification was able to physically stabilise oil-in-water emulsions and the authors showed that the starch granules did not have an impact on the physical stability of emulsions (Sridharan et al., 2020). These are good illustrations of the fact that despite their compositional complexity, mildly processed ingredients may contribute to a more sustainable food production, and open new perspectives for the design of plant-based food ingredients and food products.

9.6. Outlook

We discussed the use of interfacial rheology to understand emulsions' stability and interfacial rearrangements. In this thesis, we not only applied a conventional technique to measure interfacial rheology after hours, but we also developed a dedicated microfluidic tool to approach the rheology of the interfacial layer covering emulsion droplets within one second, under dynamic conditions. It would be relevant to tune the microfluidic chip design in order to extend analysis times, to also gain insights in processes that occur at intermediate timescales between these two extremes (>1 s). One could design new rheology chips, where droplets can be trapped, and re-measured at the desired time, which could be done by feedback tubing that would make emulsion droplets re-entering the observations area. Another route could be the use of droplet trapping platforms. Microfluidic droplet trapping

platforms have been used to characterise lipid digestion of emulsified oil (Marze, Algaba, & Marquis, 2014; Scheuble et al., 2017) (Figure 9.5) or to immobilise giant unilamellar vesicles to tune their composition and interfacial layers (Cochereau et al., 2020). Expanding the measurements to longer time scales would provide additional insight on the rheological properties of droplets formed under relevant conditions (i.e., convective mass transport).

The fact that the microfluidic tools operate under convective mass transfer conditions is a great benefit when studying the interfacial behaviour of plant proteins. In isolates such as PPI, a large fraction of proteins remains insoluble, which may act as Pickering particles (**Chapter 8**) that can only anchor at the interface when they have enough kinetic energy to exceed the adsorption energy barrier (which exceeds the energy associated with diffusion by orders of magnitude) (Tcholakova et al., 2008). The stability of emulsions stabilised by silica nanoparticles (Priest et al., 2011) or solid lipid particles (Schröder et al., 2018) has been studied using microfluidics, so the proof of principle has been delivered. As a next step, the interfacial rheological properties of such particle-stabilised droplets could be assessed with the microfluidic rheology chips (**Chapter 5**). This would open new perspectives to study the interfacial rheological properties of droplets stabilised by plant protein particles or other biobased particles. This would be a milestone for addressing the issues related to the insolubility of these proteins as it pertains to interfacial characterisation.

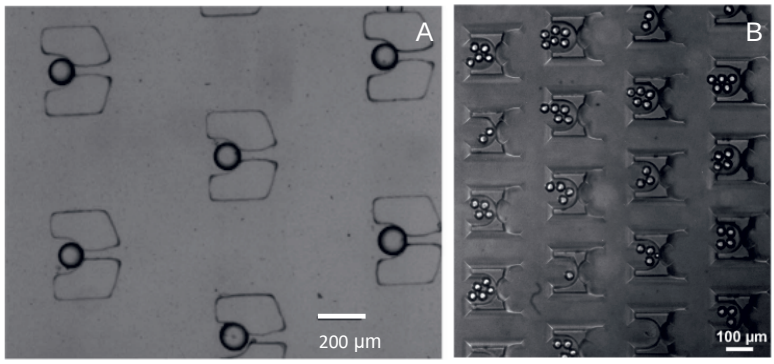

Figure 9.5. Examples of oil droplets immobilised in microfluidic traps. A) Olive oil droplets stabilised by β-lg. Reproduced from Marze et al., 2014, with permission from royal society of chemistry (RSC) and B) MCT oil droplets stabilised by β-lg. Reproduced from Scheuble et al., 2017, with permission from ACS publications.

R

References

Achouri, A., Zhang, W., & Shiying, X. (1998). Enzymatic hydrolysis of soy protein isolate and effect of succinylation on the functional properties of resulting protein hydrolysates. *Food Research International*, *31*(9), 617–623. https://doi.org/10.1016/S0963-9969(98)00104-5

Aluko, R. E., Keerati-U-Rai, M., & Mine, Y. (1998). Competitive adsorption between egg yolk lipoproteins and whey proteins on oil-in-water interfaces. *Colloids and Surfaces B: Biointerfaces*, *10*(6), 385–393. https://doi.org/10.1016/S0927-7765(98)00006-X

Amagliani, L., O'Regan, J., Kelly, A. L., & O'Mahony, J. A. (2017). Composition and protein profile analysis of rice protein ingredients. *Journal of Food Composition and Analysis*, *59*, 18–26. https://doi.org/10.1016/j.jfca.2016.12.026

Amagliani, L., & Schmitt, C. (2017). Globular plant protein aggregates for stabilization of food foams and emulsions. *Trends in Food Science and Technology*, *67*, 248–259. https://doi.org/10.1016/j.tifs.2017.07.013

Amine, C., Dreher, J., Helgason, T., & Tadros, T. (2014). Investigation of emulsifying properties and emulsion stability of plant and milk proteins using interfacial tension and interfacial elasticity. *Food Hydrocolloids*, *39*, 180–186. https://doi.org/10.1016/j.foodhyd.2014.01.001

Anand, K., & Damodaran, S. (1995). Kinetics of adsorption of lysozyme and bovine serum albumin at the air-water interface from a binary mixture. *Journal of Colloid And Interface Science*, *176*(1), 63–73. https://doi.org/10.1006/jcis.1995.0008

Anand, K., & Damodaran, S. (1996). Dynamics of Exchange between α S1 -Casein and β-Casein during Adsorption at Air−Water Interface. *Journal of Agricultural and Food Chemistry*, *44*(4), 1022–1028. https://doi.org/10.1021/jf950212t

Aoki, H., Shirase, J., Kato, J., & Wanabe, Y. (1984). Emulsion Stabilizing Properties of Soy Protein Isolates Mixed with Sodium Caseinates. *Journal of Food Science*, *49*(1), 212–216. https://doi.org/10.1111/j.1365-2621.1984.tb13710.x

Argov, N., Lemay, D. G., & German, J. B. (2008). Milk fat globule structure and function: nanoscience comes to milk production. *Trends in Food Science and Technology*, *19*(12), 617–623. https://doi.org/10.1016/j.tifs.2008.07.006

Barać, M., Čabrilo, S., Pešić, M., Stanojević, S., Pavlićević, M., Maćej, O., & Ristić, N. (2011). Functional properties of pea (Pisum sativum, L.) protein isolates modified with chymosin. *International Journal of Molecular Sciences*, *12*(12), 8372–8387. https://doi.org/10.3390/ijms12128372

Barac, M., Cabrilo, S., Pesic, M., Stanojevic, S., Zilic, S., Macej, O., & Ristic, N. (2010). Profile and functional properties of seed proteins from six pea (Pisum sativum) genotypes. *International Journal of Molecular Sciences*, *11*(12), 4973–4990. https://doi.org/10.3390/ijms11124973

Baret, J. C., Kleinschmidt, F., Harrak, A. El, & Griffiths, A. D. (2009). Kinetic aspects of emulsion stabilization by surfactants: A microfluidic analysis. *Langmuir*, *25*(11), 6088–6093. https://doi.org/10.1021/la9000472

Baroud, C. N., Wang, X. C., & Masson, J. B. (2008). Collective behavior during the exit of a wetting liquid through a network of channels. *Journal of Colloid and Interface Science*, *326*(2), 445–450. https://doi.org/10.1016/j.jcis.2008.06.040

Baszkin, A., Boissonnade, M. M., Kamyshny, A., & Magdassi, S. (2001). Native and hydrophobically modified human immunoglobulin G at the air/water interface: Sequential and competitive

adsorption. *Journal of Colloid and Interface Science*, *239*(1), 1–9. https://doi.org/10.1006/jcis.2001.7521

Benjamins, J. (2000). *Static and Dynamic Properties of Proteins Adsorbed at Liquid Interfaces* [Agricultural university]. https://doi.org/10.1039/9781847550835-00216

Benjamins, J., Cagna, A., & Lucassen-Reynders, E. H. (1996). Viscoelastic properties of triacylglycerol/water interfaces covered by proteins. *Colloids and Surfaces A: Physicochemical and Engineering Aspects*, *114*, 245–254. https://doi.org/10.1016/0927-7757(96)03533-9

Benjamins, J., Lyklema, J., & Lucassen-Reynders, E. H. (2006). Compression/expansion rheology of oil/water interfaces with adsorbed proteins. Comparison with the air/water surface. *Langmuir*, *22*(14), 6181–6188. https://doi.org/10.1021/la060441h

Bergfreund, J., Bertsch, P., Kuster, S., & Fischer, P. (2018). Effect of Oil Hydrophobicity on the Adsorption and Rheology of β-Lactoglobulin at Oil-Water Interfaces. *Langmuir*, *34*(16), 4929–4936. https://doi.org/10.1021/acs.langmuir.8b00458

Bernardini, C., Stoyanov, S. D., Arnaudov, L. N., & Cohen Stuart, M. A. (2013). Colloids in Flatland: a perspective on 2D phase-separated systems, characterisation methods, and lineactant design. *Chemical Society Reviews*, *42*(5), 2100–2129. https://doi.org/10.1039/c2cs35269a

Berton-Carabin, C. C., Genot, C., Gaillard, C., Guibert, D., & Ropers, M. H. (2013). Design of interfacial films to control lipid oxidation in oil-in-water emulsions. *Food Hydrocolloids*, *33*(1), 99–105. https://doi.org/10.1016/j.foodhyd.2013.02.021

Berton-Carabin, C. C., Ropers, M. H., & Genot, C. (2014). Lipid Oxidation in Oil-in-Water Emulsions: Involvement of the Interfacial Layer. *Comprehensive Reviews in Food Science and Food Safety*, *13*(5), 945–977. https://doi.org/10.1111/1541-4337.12097

Berton-Carabin, C. C., Sagis, L., & Schroën, K. (2018). Formation, Structure, and Functionality of Interfacial Layers in Food Emulsions. *Annual Review of Food Science and Technology*, *9*(1), 551–587. https://doi.org/10.1146/annurev-food-030117-012405

Berton-Carabin, C. C., Schröder, A., Rovalino-Cordova, A., Schroën, K., & Sagis, L. (2016). Protein and lipid oxidation affect the viscoelasticity of whey protein layers at the oil-water interface. *European Journal of Lipid Science and Technology*, *118*(11), 1630–1643. https://doi.org/10.1002/ejlt.201600066

Berton-Carabin, C. C., & Schroën, K. (2015). Pickering Emulsions for Food Applications: Background, Trends, and Challenges. *Annual Review of Food Science and Technology*, *6*(1), 263–297. https://doi.org/10.1146/annurev-food-081114-110822

Berton, C., Genot, C., Guibert, D., & Ropers, M. (2012). Effect of lateral heterogeneity in mixed surfactant-stabilized interfaces on the oxidation of unsaturated lipids in oil-in-water emulsions. *Journal of Colloid and Interface Science*, *377*, 244–250.

Berton, C., Genot, C., & Ropers, M. H. (2011). Quantification of unadsorbed protein and surfactant emulsifiers in oil-in-water emulsions. *Journal of Colloid and Interface Science*, *354*(2), 739–748. https://doi.org/10.1016/j.jcis.2010.11.055

Berton, C., Ropers, M. H., Guibert, D., Solé, V., & Genot, C. (2012). Modifications of interfacial proteins in oil-in-water emulsions prior to and during lipid oxidation. *Journal of Agricultural and Food Chemistry*, *60*(35), 8659–8671. https://doi.org/10.1021/jf300490w

Beverung, C. J., Radke, C. J., & Blanch, H. W. (1999). Protein adsorption at the oil/water interface: characterization of adsorption kinetics by dynamic interfacial tension measurements. *Biophysical Chemistry*, *81*(1), 59–80. http://www.ncbi.nlm.nih.gov/pubmed/10520251

Binks, B. P., Rodrigues, J. A., & Frith, W. J. (2007). Synergistic interaction in emulsions stabilized by a mixture of silica nanoparticles and cationic surfactant. *Langmuir*, *23*(7), 3626–3636. https://doi.org/10.1021/la0634600

Bos, M. A., & Van Vliet, T. (2001). Interfacial rheological properties of adsorbed protein layers and surfactants: A review. *Advances in Colloid and Interface Science*, *91*(3), 437–471. https://doi.org/10.1016/S0001-8686(00)00077-4

Britten, M., & Giroux, H. J. (1991). Emulsifying Properties of Whey-Protein and Casein Composite Blends. *Journal of Dairy Science*, *74*, 3318–3325. https://doi.org/10.3168/jds.S0022-0302(91)78519-6

Brösel, S., & Schubert, H. (1999). Investigations on the role of surfactants in mechanical emulsification using a high-pressure homogenizer with an orifice valve. *Chemical Engineering and Processing: Process Intensification*, *38*(4–6), 533–540. https://doi.org/10.1016/S0255-2701(99)00050-1

Brosseau, Q., Vrignon, J., & Baret, J. C. (2014). Microfluidic Dynamic Interfacial Tensiometry (μDIT). *Soft Matter*, *10*(17), 3066–3076. https://doi.org/10.1039/c3sm52543k

Burstein, E. A., Vedenkina, N. S., & Ivkovia, M. N. (1973). fluorescence and the location of trp residues in protein molecules. *Photochemistry and Photobiology*, *18*, 163–279.

Cabral, J. T., & Hudson, S. D. (2006). Microfluidic approach for rapid multicomponent interfacial tensiometry. *Lab on a Chip*, *6*(3), 427. https://doi.org/10.1039/b511976f

Can Karaca, A., Low, N. H., & Nickerson, M. (2011). Emulsifying properties of chickpea, faba bean, lentil and pea proteins produced by isoelectric precipitation and salt extraction. *Food Research International*, *44*(9), 2742–2750. https://doi.org/10.1016/j.foodres.2011.06.012

Can Karaca, A., Low, N. H., & Nickerson, M. T. (2015). Potential use of plant proteins in the microencapsulation of lipophilic materials in foods. *Trends in Food Science and Technology*, *42*(1), 5–12. https://doi.org/10.1016/j.tifs.2014.11.002

Cao, Y., & Damodaran, S. (1995). Coadsorption of β-Casein and Bovine Serum Albumin at the Air-Water Interface from a Binary Mixture. *Journal of Agricultural and Food Chemistry*, *43*(10), 2567–2573. https://doi.org/10.1021/jf00058a003

Castelain, C., & Genot, C. (1994). Conformational changes of bovine serum albumin upon its adsorption in dodecane-in-water emulsions as revealed by front-face steady-state fluorescence. *Biochimica et Biophysics Acta*, *1199*, 59–64.

Castle, J., Dickinson, E., Murray, B. S., & Stainsby, G. (1987). mixed-protein films adsorbed at the oil-water interface. In *Proteins at interfaces : physicochemical and biochemical studies* (pp. 118–134).

Çelebioğlu, H. Y., Kmiecik-Palczewska, J., Lee, S., & Chronakis, I. S. (2017). Interfacial shear rheology of β-lactoglobulin—Bovine submaxillary mucin layers adsorbed at air/water interface. *International Journal of Biological Macromolecules*, *102*, 857–867. https://doi.org/10.1016/j.ijbiomac.2017.04.063

Chao, C. C., & Stadtman, E. R. (1997). Modification of protein hydrophobicity by oxidative systems. *Proceedings of the National Academy of Sciences*, *94*(7), 2969–2974.

Chen, M., Lu, J., Liu, F., Nsor-Atindana, J., Xu, F., Goff, H. D., Ma, J., & Zhong, F. (2019). Study on the emulsifying stability and interfacial adsorption of pea proteins. *Food Hydrocolloids*, *88*(August 2018), 247–255. https://doi.org/10.1016/j.foodhyd.2018.09.003

Chen, N., Zhao, M., & Sun, W. (2013). Effect of protein oxidation on the in vitro digestibility of soy protein isolate. *Food Chemistry*, *141*(3), 3224–3229. https://doi.org/10.1016/j.foodchem.2013.05.113

Chen, N., Zhao, M., Sun, W., Ren, J., & Cui, C. (2013). Effect of oxidation on the emulsifying properties of soy protein isolate. *Food Research International*, *52*(1), 26–32. https://doi.org/10.1016/j.foodres.2013.02.028

Chevallier, M., Riaublanc, A., Cauty, C., Hamon, P., Rousseau, F., Thevenot, J., Lopez, C., & Croguennec, T. (2019). The repartition of whey protein microgels and caseins between fat droplet surface and the continuous phase governs the heat stability of emulsions. *Colloids and Surfaces A: Physicochemical and Engineering Aspects*, *563*, 217–225. https://doi.org/10.1016/j.colsurfa.2018.12.001

Chevallier, M., Riaublanc, A., Lopez, C., Hamon, P., Rousseau, F., & Croguennec, T. (2016). Aggregated whey proteins and trace of caseins synergistically improve the heat stability of whey protein-rich emulsions. *Food Hydrocolloids*, *61*, 487–495. https://doi.org/10.1016/j.foodhyd.2016.06.009

Cochereau, R., Renard, D., Noûs, C., & Boire, A. (2020). Semi-permeable vesicles produced by microfluidics to tune the phase behaviour of encapsulated macromolecules. *Journal of Colloid and Interface Science*, *580*, 709–719. https://doi.org/10.1016/j.jcis.2020.07.022

Croy, R. R., Gatehouse, J. A., Tyler, M., & Boulter, D. (1980). The purification and characterization of a third storage protein (convicilin) from the seeds of pea (Pisum sativum L.). *The Biochemical Journal*, *191*(2), 509–516. https://doi.org/10.1042/bj1910509

Cui, Z., Chen, Y., Kong, X., Zhang, C., & Hua, Y. (2014). Emulsifying properties and oil/water (O/W) interface adsorption behavior of heated soy proteins: Effects of heating concentration, homogenizer rotating speed, and salt addition level. *Journal of Agricultural and Food Chemistry*, *62*(7), 1634–1642. https://doi.org/10.1021/jf404464z

Dagorn-Scavinier, C., Gueguen, J., & Lefebvre, J. (1986). A comparison of interfacial behaviours of pea (Pisum sativum L.) legumin and vicilin at air/water interface. *Food / Nahrung*, *30*(3–4), 337–347. https://doi.org/10.1002/food.19860300332

Dagorn-Scavinier, C., Gueguen, J., & Lefebvre, J. (1987). Emulsifying Properties of Pea Globulins as Related to Their Adsorption Behaviors. *Journal of Food Science*, *52*(2), 335–341. https://doi.org/10.1111/j.1365-2621.1987.tb06607.x

Dalgleish, D. G. (1996). Conformations and structures of milk proteins adsorbed to oil-water interfaces. *Food Research International*, *29*, 541–547.

Dalgleish, D. G., Euston, S. E., Hunt, J. A., & Dickinson, E. (1991). Competitive adsorption of b-Lactoglobulin in Mixed Protein emulsions. In *Food Polymers, gels and colloids* (pp. 485–489).

Dalgleish, D. G., Goff, H. D., & Luan, B. (2002). Exchange reactions between whey proteins and caseins in heated soya oil-in-water emulsion systems - Behavior of individual proteins. *Food*

Hydrocolloids, *16*(4), 295–302. https://doi.org/10.1016/S0268-005X(01)00102-3

Damodaran, S. (2004). Adsorbed layers formed from mixtures of proteins. *Current Opinion in Colloid and Interface Science*, *9*(5), 328–339. https://doi.org/10.1016/j.cocis.2004.09.008

Damodaran, S., & Sengupta, T. (2003). Dynamics of competitive adsorption of αs-casein and β-casein at planar triolein-water interface: Evidence for incompatibility of mixing in the interfacial film. *Journal of Agricultural and Food Chemistry*, *51*(6), 1658–1665. https://doi.org/10.1021/jf020784v

de Folter, J. W. J., van Ruijven, M. W. M., & Velikov, K. P. (2012). Oil-in-water Pickering emulsions stabilized by colloidal particles from the water-insoluble protein zein. *Soft Matter*, *8*(25), 6807. https://doi.org/10.1039/c2sm07417f

Denkov, N. D., Cooper, P., & Martin, J. Y. (1999). Mechanisms of action of mixed solid-liquid antifoams. 1. Dynamics of foam film rupture. *Langmuir*, *15*(24), 8514–8529. https://doi.org/10.1021/la9902136

Derjaguin, B. V., & Landau, L. D. (1941). Theory of the stability of strongly charged lyophobic sols and the adhesion of strongly charged particles in solutions of electrolytes. *Acta Physiochimica URSS*, *14*, 633–662.

Dickinson, E. (1992). Structure and composition of adsorbed protein layers and the relationship to emulsion stability. *Journal of the Chemical Society, Faraday Transactions*, *88*(20), 2973. https://doi.org/10.1039/ft9928802973

Dickinson, E. (1994). Protein-Stabilized Emulsions. *Journal of Food Engineering*, *22*, 59–74. https://doi.org/10.1016/0260-8774(94)90025-6

Dickinson, E. (1997). Properties of Emulsions Stabilized with Milk Proteins: Overview of Some Recent Developments. *Journal of Dairy Science*, *80*(10), 2607–2619. https://doi.org/10.3168/jds.S0022-0302(97)76218-0

Dickinson, E. (1999). Adsorbed protein layers at fluid interfaces: interactions, structure and surface rheology. *Colloids and Surfaces B: Biointerfaces*, *15*(2), 161–176. https://doi.org/10.1016/S0927-7765(99)00042-9

Dickinson, E. (2001). Milk protein interfacial layers and the relationship to emulsion stability and rheology. *Colloids and Surfaces B: Biointerfaces*, *20*, 197–210. https://doi.org/10.1016/S0927-7765(00)00204-6

Dickinson, E. (2010). Flocculation of protein-stabilized oil-in-water emulsions. *Colloids and Surfaces B: Biointerfaces*, *81*(1), 130–140. https://doi.org/10.1016/j.colsurfb.2010.06.033

Dickinson, E. (2011). Mixed biopolymers at interfaces: Competitive adsorption and multilayer structures. *Food Hydrocolloids*, *25*(8), 1966–1983. https://doi.org/10.1016/j.foodhyd.2010.12.001

Dickinson, E. (2013). Stabilising emulsion-based colloidal structures with mixed food ingredients. *Journal of the Science of Food and Agriculture*, *93*(4), 710–721. https://doi.org/10.1002/jsfa.6013

Dickinson, E. (2020). Advances in food emulsions and foams: reflections on research in the neo-Pickering era. *Current Opinion in Food Science*, *33*, 52–60. https://doi.org/10.1016/j.cofs.2019.12.009

Dickinson, E., Flint, F. O., & Hunt, J. A. (1989). Bridging flocculation in binary protein stabilized emulsions. *Topics in Catalysis*, *3*(5), 389–397. https://doi.org/10.1016/S0268-005X(89)80013-X

Dickinson, E., & Golding, M. (1997). Depletion flocculation of emulsions containing unadsorbed sodium caseinate. *Food Hydrocolloids*, *11*(1), 13–18. https://doi.org/10.1016/S0268-005X(97)80005-7

Dickinson, E., Hunt, J. A., & Dalgleish, D. G. (1991). Competitive adsorption of phosvitin with milk proteins in oil-in-water emulsions. *Topics in Catalysis*, *4*(5), 403–414. https://doi.org/10.1016/S0268-005X(09)80135-5

Dickinson, E., & Matsumura, Y. (1991). Time-dependent polymerization of b-lactoglobulin through disulphide bonds at the oil-water interface in emulsions. *International Journal of Biological Macromolecules*, *13*(1), 26–30. https://doi.org/10.1016/0141-8130(91)90006-G

Dickinson, E., Murray, B. S., & Stainsby, G. (1988). Coalescence stability of emulsion-sized droplets at a planar oil-water interface and the relationship to protein film surface rheology. *Journal of the Chemical Society, Faraday Transactions 1*, *84*(3), 871. https://doi.org/10.1039/f19888400871

Dickinson, E., Rolfe, S. E., & Dalgleish, D. G. (1988). Competitive adsorption of αs1-casein and β-casein in oil-in-water emulsions. *Topics in Catalysis*, *2*(5), 397–405. https://doi.org/10.1016/S0268-005X(88)80004-3

Dickinson, E., Rolfe, S. E., & Dalgleish, D. G. (1989). Competitive adsorption in oil-in-water emulsions containing α-lactalbumin and β-lactoglobulin. *Topics in Catalysis*, *3*(3), 193–203. https://doi.org/10.1016/S0268-005X(89)80003-7

Dickinson, E., Rolfe, S. E., & Dalgleish, D. G. (1990). Surface shear viscometry as a probe of protein-protein interactions in mixed milk protein films adsorbed at the oil-water interface. *International Journal of Biological Macromolecules*, *12*(3), 189–194. https://doi.org/10.1016/0141-8130(90)90031-5

Drelich, A., Gomez, F., Clausse, D., & Pezron, I. (2010). Evolution of water-in-oil emulsions stabilized with solid particles. Influence of added emulsifier. *Colloids and Surfaces A: Physicochemical and Engineering Aspects*, *365*(1–3), 171–177. https://doi.org/10.1016/j.colsurfa.2010.01.042

Duque Estrada, P., Berton-Carabin, C. C., Schlangen, M., Haagsma, A., Pierucci, A. P. T. R., & Van Der Goot, A. J. (2018). Protein Oxidation in Plant Protein-Based Fibrous Products: Effects of Encapsulated Iron and Process Conditions. *Journal of Agricultural and Food Chemistry*, *66*(42), 11105–11112. https://doi.org/10.1021/acs.jafc.8b02844

Duvarci, O. C., Yazar, G., & Kokini, J. L. (2017). The comparison of LAOS behavior of structured food materials (suspensions, emulsions and elastic networks). *Trends in Food Science and Technology*, *60*, 2–11. https://doi.org/10.1016/j.tifs.2016.08.014

Erickson, H. P. (2009). Size and shape of protein molecules at the nanometer level determined by sedimentation, gel filtration, and electron microscopy. *Biological Procedures Online*, *11*(1), 32–51. https://doi.org/10.1007/s12575-009-9008-x

Erni, P., Fischer, P., & Windhab, E. J. (2005). Deformation of single emulsion drops covered with a viscoelastic adsorbed protein layer in simple shear flow. *Applied Physics Letters*, *87*(24), 1–3. https://doi.org/10.1063/1.2146068

Erni, P., Windhab, E. J., & Fischer, P. (2011). Emulsion drops with complex interfaces: Globular versus flexible proteins. *Macromolecular Materials and Engineering*, *296*(3–4), 249–262. https://doi.org/10.1002/mame.201000290

Estévez, M., Kylli, P., Puolanne, E., Kivikari, R., & Heinonen, M. (2008). Fluorescence spectroscopy as a novel approach for the assessment of myofibrillar protein oxidation in oil-in-water emulsions. *Meat Science*, *80*(4), 1290–1296. https://doi.org/10.1016/j.meatsci.2008.06.004

Estévez, M., & Xiong, Y. (2019). Intake of Oxidized Proteins and Amino Acids and Causative Oxidative Stress and Disease: Recent Scientific Evidences and Hypotheses. *Journal of Food Science*, *84*(3), 387–396. https://doi.org/10.1111/1750-3841.14460

Euston, S. E., Singh, H., Munro, P. a., & Dalgleish, D. G. (1996). Oil-in-Water Emulsions Stabilized by Sodium Caseinate or Whey Protein Isolate as influenced by Glycerol Monostearate. *Journal of Food Science*, *61*(5), 916–920. https://doi.org/10.1111/j.1365-2621.1996.tb10901.x

Fainerman, V. B., Aksenenko, E. V., Makievski, A. V., Trukhin, D. V., Yeganehzad, S., Gochev, G., & Miller, R. (2020). Surface tension and dilational rheology of mixed β-casein – β-lactoglobulin aqueous solutions at the water/air interface. *Food Hydrocolloids*, *106*(December 2019). https://doi.org/10.1016/j.foodhyd.2020.105883

Fernandez-Avila, C., & Trujillo, A. J. (2016). Ultra-High Pressure Homogenization improves oxidative stability and interfacial properties of soy protein isolate-stabilized emulsions. *Food Chemistry*, *209*, 104–113. https://doi.org/10.1016/j.foodchem.2016.04.019

Friedman, H. L., & Mills, R. (1986). Hydrodynamic approximation for distinct diffusion coefficients. *Journal of Solution Chemistry*, *15*(1), 69–80. https://doi.org/10.1007/BF00646311

García Arteaga, V., Apéstegui Guardia, M., Muranyi, I., Eisner, P., & Schweiggert-Weisz, U. (2020). Effect of enzymatic hydrolysis on molecular weight distribution, techno-functional properties and sensory perception of pea protein isolates. *Innovative Food Science and Emerging Technologies*, *65*, 102449. https://doi.org/10.1016/j.ifset.2020.102449

Gatehouse, J. A., Croy, R. R. D., Boulter, D., & Shewry, P. R. (1984). The synthesis and structure of pea storage proteins. *Critical Reviews in Plant Sciences*, *1*(4), 287–314. https://doi.org/10.1080/07352688409382182

Gatehouse, J. A., Lycett, G. W., Croy, R. R. D., & Boulter, D. (1982). The post-translational proteolysis of the subunits of vicilin from pea (Pisum sativum L.). *Biochemical Journal*, *207*(3), 629–632. https://doi.org/10.1042/bj2070629

Geerts, M. E. J., Nikiforidis, C. V., van der Goot, A. J., & van der Padt, A. (2017). Protein nativity explains emulsifying properties of aqueous extracted protein components from yellow pea. *Food Structure*, *14*(May), 104–111. https://doi.org/10.1016/j.foostr.2017.09.001

Genot, C., Montenay-Garestier, T., & Drapron, R. (1984). Intrinsic spectrofluorometry applied to soft wheat (Triticum aestivum) flour and gluten to study lipid-protein interactions. *LWT - Food Science and Technology*, *17*(3), 129–133.

Graham, D. E., & Phillips, M. C. (1979a). Proteins at Liquid Interfaces II adsorption isotherms. *Journal of Colloid and Interface Science*, *70*(3), 415–426.

Graham, D. E., & Phillips, M. C. (1979b). Proteins at Liquid Interfaces III molecular structures. *Journal of Colloid and Interface Science*, *70*(3), 427–439.

Graham, D. E., & Phillips, M. C. (1980). Proteins at Liquid Interfaces IV. Dilatational Properties. *Journal of Colloid and Interface Science*, *76*(1), 227–239.

Granger, C., Barey, P., Toutain, J., & Cansell, M. (2005). Direct quantification of protein partitioning in oil-in-water emulsion by front-face fluorescence: Avoiding the need for centrifugation. *Colloids and Surfaces B: Biointerfaces*, *43*(3–4), 158–162. https://doi.org/10.1016/j.colsurfb.2005.04.002

Gueguen, J., Chevalier, M., Barbot, J., & Schaeffer, F. (1988). Dissociation and aggregation of pea legumin induced by pH and ionic strength. *Journal of the Science of Food and Agriculture*, *44*(2), 167–182. https://doi.org/10.1002/jsfa.2740440208

Gueguen, J., Vu, A. T., & Schaeffer, F. (1984). Large-scale purification and characterisation of pea globulins. *Journal of the Science of Food and Agriculture*, *35*(9), 1024–1033. https://doi.org/10.1002/jsfa.2740350912

Guerrero, A., Partal, P., & Gallegos, C. (1998). Linear viscoelastic properties of sucrose ester-stabilized oil-in-water emulsions. *Journal of Rheology*, *42*(6), 1375–1388. https://doi.org/10.1122/1.550965

Gumus, C. E., Decker, E. A., & McClements, D. J. (2017a). Formation and Stability of ω-3 Oil Emulsion-Based Delivery Systems Using Plant Proteins as Emulsifiers: Lentil, Pea, and Faba Bean Proteins. *Food Biophysics*. https://doi.org/10.1007/s11483-017-9475-6

Gumus, C. E., Decker, E. A., & McClements, D. J. (2017b). Impact of legume protein type and location on lipid oxidation in fish oil-in-water emulsions: Lentil, pea, and faba bean proteins. *Food Research International*, *100*(August), 175–185. https://doi.org/10.1016/j.foodres.2017.08.029

Guzey, D., & McClements, D. J. (2006). Formation, stability and properties of multilayer emulsions for application in the food industry. *Advances in Colloid and Interface Science*, *128–130*(2006), 227–248. https://doi.org/10.1016/j.cis.2006.11.021

Håkansson, A. (2016). Experimental methods for measuring coalescence during emulsification - A critical review. *Journal of Food Engineering*, *178*, 47–59. https://doi.org/10.1016/j.jfoodeng.2016.01.006

Hellwig, M. (2019). The Chemistry of Protein Oxidation in Food. *Angewandte Chemie - International Edition*, *58*(47), 16742–16763. https://doi.org/10.1002/anie.201814144

Hellwig, M. (2020). Analysis of Protein Oxidation in Food and Feed Products. *Journal of Agricultural and Food Chemistry*. https://doi.org/10.1021/acs.jafc.0c00711

Hinderink, E. B. A., Kaade, W., Sagis, L., Schroën, K., & Berton-Carabin, C. C. (2020). Microfluidic investigation of the coalescence susceptibility of pea protein-stabilised emulsions : Effect of protein oxidation level. *Food Hydrocolloids*, *102*(102). https://doi.org/10.1016/j.foodhyd.2019.105610

Hinderink, E. B. A., Münch, K., Sagis, L., Schroën, K., & Berton-Carabin, C. C. (2019). Synergistic stabilisation of emulsions by blends of dairy and soluble pea proteins : Contribution of the interfacial composition. *Food Hydrocolloids*, *97*. https://doi.org/10.1016/j.foodhyd.2019.105206

Hinderink, E. B. A., Sagis, L., Schroën, K., & Berton-Carabin, C. C. (2020). Behavior of plant-dairy protein blends at air-water and oil-water interfaces. *Colloids and Surfaces B: Biointerfaces*,

192, 111015. https://doi.org/10.1016/j.colsurfb.2020.111015

Hinderink, E. B. A., Sagis, L., Schroën, K., & Berton-Carabin, C. C. (2021). Sequential adsorption and interfacial displacement in emulsions stabilized with plant-dairy protein blends. *Journal of Colloid and Interface Science*, *583*, 704–713. https://doi.org/10.1016/j.jcis.2020.09.066

Ho, K. K. H. Y., Schroën, K., Martín-González, F. M., & Berton-Carabin, C. C. (2018). Synergistic and antagonistic effects of plant and dairy protein blends on the physicochemical stability of lycopene-loaded emulsions. *Food Hydrocolloids*, *81*, 180–190. https://doi.org/10.1016/j.foodhyd.2018.02.033

Ho, K. K. H. Y., Schroën, K., Martín-González, M. F. S., & Berton-Carabin, C. C. (2017). Physicochemical stability of lycopene-loaded emulsions stabilized by plant or dairy proteins. *Food Structure*, *12*, 34–42. https://doi.org/10.1016/j.foostr.2016.12.001

Hunt, J. A., & Dalgleish, D. G. (1994). Adsorption behaviour of whey protein isolate and caseinate in soya oil-in-water emulsions. *Topics in Catalysis*, *8*(2), 175–187. https://doi.org/10.1016/S0268-005X(09)80042-8

Hunt, J. A., Dickinson, E., & Horne, D. S. (1993). Competitive displacement of proteins in oil-in-water emulsions containing calcium ions. *Colloids and Surfaces A: Physicochemical and Engineering Aspects*, *71*(2), 197–203. https://doi.org/10.1016/0927-7757(93)80344-E

Hunter, J. R., Carbonell, R. G., & Kilpatrick, P. K. (1991). Coadsorption and Exchange of Lysozyme / -Casein Mixtures at the Air / Water Interface. *Journal of Colloid and Interface Science*, *143*(1), 37–53.

Hunter, T. N., Pugh, R. J., Franks, G. V., & Jameson, G. J. (2008). The role of particles in stabilising foams and emulsions. *Advances in Colloid and Interface Science*, *137*(2), 57–81. https://doi.org/10.1016/j.cis.2007.07.007

Hyun, K., Kim, S. H., Ahn, K. H., & Lee, S. J. (2002). Large amplitude oscillatory shear as a way to classify the complex fluids. *Journal of Non-Newtonian Fluid Mech.*, *107*, 51–65. https://doi.org/10.1016/S0377-0257(02)00141-6

Jacobsen, C. (1999). Sensory impact of lipid oxidation in complex food systems. *Fett/Lipid*, *101*(12), 484–492. https://doi.org/https://doi.org/10.1002/(SICI)1521-4133(199912)101:12<484::AID-LIPI484>3.0.CO;2-H

Jacobsen, C., Sørensen, A. D. M., & Nielsen, N. S. (2013). Stabilization of omega-3 oils and enriched foods using antioxidants. In *Food Enrichment with Omega-3 Fatty Acids* (pp. 130–149). https://doi.org/10.1533/9780857098863.2.130

Jafari, S. M., Assadpoor, E., He, Y., & Bhandari, B. (2008). Re-coalescence of emulsion droplets during high-energy emulsification. *Food Hydrocolloids*, *22*(7), 1191–1202. https://doi.org/10.1016/j.foodhyd.2007.09.006

Ji, J., Zhang, J., Chen, J., Wang, Y., Dong, N., Hu, C., Chen, H., Li, G., Pan, X., & Wu, C. (2015). Preparation and stabilization of emulsions stabilized by mixed sodium caseinate and soy protein isolate. *Food Hydrocolloids*, *51*, 156–165. https://doi.org/10.1016/j.foodhyd.2015.05.013

Jones, D. B., & Middelberg, A. P. J. (2003). Interfacial protein networks and their impact on droplet breakup. *AIChE Journal*, *49*(6), 1533–1541. https://doi.org/10.1002/aic.690490617

Kailasapathy, K. (2009). Chemical Composition, Physical and Functional Properties of Milk and Milk Ingredients. *Dairy Processing and Quality Assurance*, 75–103. https://doi.org/10.1002/9780813804033.ch4

Karaca, A. C., Low, N. H., & Nickerson, M. (2011). Emulsifying properties of chickpea, faba bean, lentil and pea proteins produced by isoelectric precipitation and salt extraction. *Food Research International*, *44*(9), 2742–2750. https://doi.org/10.1016/j.foodres.2011.06.012

Keerati-U-Rai, M., & Corredig, M. (2009). Effect of dynamic high pressure homogenization on the aggregation state of soy protein. *Journal of Agricultural and Food Chemistry*, *57*(9), 3556–3562. https://doi.org/10.1021/jf803562q

Keerati-U-Rai, M., & Corredig, M. (2010). Heat-induced changes occurring in oil/water emulsions stabilized by soy glycinin and β-conglycinin. *Journal of Agricultural and Food Chemistry*, *58*(16), 9171–9180. https://doi.org/10.1021/jf101425j

Keerati-u-rai, M., Miriani, M., Iametti, S., Bonomi, F., & Corredig, M. (2012). Structural changes of soy proteins at the oil-water interface studied by fluorescence spectroscopy. *Colloids and Surfaces B: Biointerfaces*, *93*, 41–48. https://doi.org/10.1016/j.colsurfb.2011.12.002

Kimura, A., Takako, F., Meili, Z., Shiori, M., Maruyama, N., & Utsumi, S. (2008). Comparison of physicochemical properties of 7S and 11S globulins from pea, fava bean, cowpea, and French bean with those of soybean-french bean 7S globulin exhibits excellent properties. *Journal of Agricultural and Food Chemistry*, *56*(21), 10273–10279. https://doi.org/10.1021/jf801721b

Klost, M., & Drusch, S. (2019). Functionalisation of pea protein by tryptic hydrolysis – Characterisation of interfacial and functional properties. *Food Hydrocolloids*, *86*, 134–140. https://doi.org/10.1016/j.foodhyd.2018.03.013

Kong, B., Xiong, Y. L., Cui, X., & Zhao, X. (2013). Hydroxyl Radical-Stressed Whey Protein Isolate: Functional and Rheological Properties. *Food and Bioprocess Technology*, *6*(1), 169–176. https://doi.org/10.1007/s11947-011-0674-8

Kornet, C., Venema, P., Nijsse, J., van der Linden, E., van der Goot, A. J., & Meinders, M. (2020). Yellow pea aqueous fractionation increases the specific volume fraction and viscosity of its dispersions. *Food Hydrocolloids*, *99*, 105332. https://doi.org/10.1016/j.foodhyd.2019.105332

Kotsmar, C., Aksenenko, E. V., Fainerman, V. B., Pradines, V., Krägel, J., & Miller, R. (2010). Equilibrium and dynamics of adsorption of mixed β-casein/surfactant solutions at the water/hexane interface. *Colloids and Surfaces A: Physicochemical and Engineering Aspects*, *354*(1–3), 210–217. https://doi.org/10.1016/j.colsurfa.2009.04.025

Krägel, J., O'Neill, M., Makievski, A. V., Michel, M., Leser, M. E., & Miller, R. (2003). Dynamics of mixed protein-surfactant layers adsorbed at the water/air and water/oil interface. *Colloids and Surfaces B: Biointerfaces*, *31*(1–4), 107–114. https://doi.org/10.1016/S0927-7765(03)00047-X

Krebs, T., Schroën, K., & Boom, R. (2012). Coalescence dynamics of surfactant-stabilized emulsions studied with microfluidics. *Soft Matter*, *8*(41), 10650–10657. https://doi.org/10.1039/c2sm26122g

Krebs, T., Schroën, K., & Boom, R. M. (2013). Coalescence kinetics of oil-in-water emulsions studied with microfluidics. *Fuel*, *106*, 327–334. https://doi.org/10.1016/j.fuel.2012.10.067

Ladjal Ettoumi, Y., Berton-Carabin, C. C., Chibane, M., & Schroën, K. (2017). Legume Protein Isolates for Stable Acidic Emulsions Prepared by Premix Membrane Emulsification. *Food*

Biophysics, *12*(1), 119–128. https://doi.org/10.1007/s11483-017-9471-x

Lakowicz, J. R. (2007). Principles of Fluorescence Spectroscopy. In *Protein Fluorescence*. https://doi.org/10.1007/978-1-4615-7658-7_11

Lam, A. C. Y., Karaca, A. C., Tyler, R. T., & Nickerson, M. T. (2018). Pea protein isolates: Structure, extraction, and functionality. *Food Reviews International*, *34*(2), 126–147. https://doi.org/10.1080/87559129.2016.1242135

Layne, E. (1957). Spectrophotometric and turbidimetric methods for measuring proteins. *Methods in Enzymology*, *3*(C), 447–454. https://doi.org/10.1016/S0076-6879(57)03413-8

Le Floch-Fouéré, C., Beaufils, S., Lechevalier, V., Nau, F., Pézolet, M., Renault, A., & Pezennec, S. (2010). Sequential adsorption of egg-white proteins at the air-water interface suggests a stratified organization of the interfacial film. *Food Hydrocolloids*, *24*(4), 275–284. https://doi.org/10.1016/j.foodhyd.2009.10.006

Levich, V. G., & Krylov, V. S. (1969). Surface-tension-driven phenomena. *Annual Review of Fluid Mechanics*, *1*(1), 293–316.

Levin, R., Garland, D., Oliver, C., Amici, A., Climent, I., Lenz, A., Ahn, B., Shaltiel, S., & Stadtman, E. (1990). Determination of carbonyl content in oxidatively modified proteins. *Methods Enzymol*, *186*, 464–478. http://ci.nii.ac.jp/naid/10025826524/en/

Li, W., Wang, Y., Zhao, H., He, Z., Zeng, M., Qin, F., & Chen, J. (2016). Improvement of emulsifying properties of soy protein through selective hydrolysis: Interfacial shear rheology of adsorption layer. *Food Hydrocolloids*, *60*, 453–460. https://doi.org/10.1016/j.foodhyd.2016.04.019

Liang, H. N., & Tang, C. H. (2013). PH-dependent emulsifying properties of pea [Pisum sativum (L.)] proteins. *Food Hydrocolloids*, *33*(2), 309–319. https://doi.org/10.1016/j.foodhyd.2013.04.005

Liu, Q., Lu, Y., Han, J., Chen, Q., & Kong, B. (2015). Structure-modification by moderate oxidation in hydroxyl radical-generating systems promote the emulsifying properties of soy protein isolate. *Food Structure*, *6*, 21–28. https://doi.org/10.1016/j.foostr.2015.10.001

Lund, M. N., Heinonen, M., Baron, C. P., & Estévez, M. (2011). Protein oxidation in muscle foods: A review. *Molecular Nutrition and Food Research*, *55*(1), 83–95. https://doi.org/10.1002/mnfr.201000453

Mackie, A. R., Gunning, A. P., Pugnaloni, L. A., Dickinson, E., Wilde, P. J., & Morris, V. J. (2003). Growth of surfactant domains in protein films. *Langmuir*, *19*(15), 6032–6038. https://doi.org/10.1021/la034409o

Mackie, A. R., Gunning, A. P., Wilde, P. J., & Morris, V. J. (1999). Orogenic Displacement of Protein from the Air/Water Interface by Competitive Adsorption. *Journal of Colloid and Interface Science*, *210*(1), 157–166. https://doi.org/10.1006/jcis.1998.5941

Mackie, A. R., Gunning, P. A., Ridout, M. J., Wilde, P. J., & Morris, V. J. (2001). Orogenic displacement in mixed β-lactoglobulin/β-casein films at the air/water interface. *Langmuir*, *17*(21), 6593–6598. https://doi.org/10.1021/la010687g

MacRitchie, F. (1998). Reversibility of protein adsorption. *Studies in Interface Science*, *7*(C), 149–177. https://doi.org/10.1016/S1383-7303(98)80051-3

Malabat, C., Sánchez-Vioque, R., Rabiller, C., & Gueguen, J. (2001). Emulsifying and foaming properties of native and chemically modified peptides from the 2S and 12S proteins of rapeseed (Brassica napus L.). *Journal of the American Oil Chemists' Society*, *78*(3), 235–242. https://doi.org/10.1007/s11746-001-0251-x

Maldonado-Valderrama, J., Fainerman, V. B., Jose, M., Cabrerizo-vı, M. A., & Miller, R. (2005). *Dilatational Rheology of -Casein Adsorbed Layers at Liquid - Fluid Interfaces*. 17608–17616.

Martin, A. H., Meinders, M. B. J., Bos, M. A., Cohen Stuart, M. A., & Van Vliet, T. (2003). Conformational aspects of proteins at the air/water interface studied by infrared reflection-absorption spectroscopy. *Langmuir*, *19*(7), 2922–2928. https://doi.org/10.1021/la0208629

Marze, S., Algaba, H., & Marquis, M. (2014). A microfluidic device to study the digestion of trapped lipid droplets. *Food and Function*, *5*(7), 1481–1488. https://doi.org/10.1039/c4fo00010b

Mason, P. E., Neilson, G. W., Dempsey, C. E., Barnes, A. C., & Cruickshank, J. M. (2003). The hydration structure of guanidinium and thiocyanate ions: Implications for protein stability in aqueous solution. *Proceedings of the National Academy of Sciences of the United States of America*, *100*(8), 4557–4561. https://doi.org/10.1073/pnas.0735920100

Matsumura, Y., Mitsui, S., Dickinson, E., & Mori, T. (1994). Competitive adsorption of α-lactalbumin in the molten globule state. *Topics in Catalysis*, *8*(6), 555–566. https://doi.org/10.1016/S0268-005X(09)80065-9

McCarthy, N. A., Kennedy, D., Hogan, S. A., Kelly, P. M., Thapa, K., Murphy, K. M., & Fenelon, M. A. (2016). Emulsification properties of pea protein isolate using homogenization, microfluidization and ultrasonication. *Food Research International*, *89*, 415–421. https://doi.org/10.1016/j.foodres.2016.07.024

McClements, D. J. (2004a). Emulsion stability. In *Food Emulsions Principles, Practices, and Techniques* (pp. 1–71).

McClements, D. J. (2004b). Protein-stabilized emulsions. *Current Opinion in Colloid & Interface Science*, *9*(5), 305–313. https://doi.org/10.1016/j.cocis.2004.09.003

McClements, D. J. (2005). Food Emulsions Principles, Practices, and Techniques Second Edition. *Food Emulsions Principles, Practices, and Techniques*. https://doi.org/10.1093/acprof:oso/9780195383607.003.0002

McClements, D. J., & Jafari, S. M. (2018). Improving emulsion formation, stability and performance using mixed emulsifiers: A review. *Advances in Colloid and Interface Science*, *251*, 55–79. https://doi.org/10.1016/j.cis.2017.12.001

Meagher, J. L., Beechem, J. M., Olson, S. T., & Gettinst, P. G. W. (1998). Deconvolution of the fluorescence emission spectrum of human antithrombin and identification of the tryptophan residues that are responsive to heparin binding. *Journal of Biological Chemistry*, *273*(36), 23283–23289. https://doi.org/10.1074/jbc.273.36.23283

Mession, J. L., Chihi, M. L., Sok, N., & Saurel, R. (2015). Effect of globular pea proteins fractionation on their heat-induced aggregation and acid cold-set gelation. *Food Hydrocolloids*, *46*, 233–243. https://doi.org/10.1016/j.foodhyd.2014.11.025

Miller, R., Grigoriev, D. O., Krägel, J., Makievski, A. V., Maldonado-Valderrama, J., Leser, M., Michel, M., & Fainerman, V. B. (2005). Experimental studies on the desorption of adsorbed proteins from liquid interfaces. *Food Hydrocolloids*, *19*(3), 479–483.

https://doi.org/10.1016/j.foodhyd.2004.10.012

Miriani, M., Keerati-U-Rai, M., Corredig, M., Iametti, S., & Bonomi, F. (2011). Denaturation of soy proteins in solution and at the oil-water interface : A fluorescence study. *Food Hydrocolloidsydrocolloids*, *25*(4), 620–626. https://doi.org/10.1016/j.foodhyd.2010.07.020

Mitropoulos, V., Mütze, A., & Fischer, P. (2014). Mechanical properties of protein adsorption layers at the air / water and oil / water interface : A comparison in light of the thermodynamical stability of proteins. *Advances in Colloid and Interface Science*, *206*, 195–206. https://doi.org/10.1016/j.cis.2013.11.004

Möbius, D., & Miller, R. (1998). *Proteins at liquid interfaces* (D. Möbius & R. Miller (eds.); Vol. 7, Issue 1). https://doi.org/10.1016/0021-9797(79)90050-X

Monahan, F. J., McClements, D. J., & Kinsella, J. E. (1993). Polymerization of Whey Proteins in Whey Protein-Stabilized Emulsions. *Journal of Agricultural and Food Chemistry*, *41*, 1826–1829. https://doi.org/Doi 10.1021/Jf00035a004

Morris, V. J., & Gunning, A. P. (2008). Microscopy, microstructure and displacement of proteins from interfaces: implications for food quality and digestion. *Soft Matter*, *4*(6), 1147–1150. https://doi.org/10.1039/b800106e

Muijlwijk, K., Berton-Carabin, C. C., & Schroën, K. (2016). Cross-flow microfluidic emulsification from a food perspective. *Trends in Food Science and Technology*, *49*, 51–63. https://doi.org/10.1016/j.tifs.2016.01.004

Muijlwijk, K., Colijn, I., Harsono, H., Krebs, T., Berton-Carabin, C. C., & Schroën, K. (2017). Coalescence of protein-stabilised emulsions studied with microfluidics. *Food Hydrocolloids*, *70*, 96–104. https://doi.org/10.1016/j.foodhyd.2017.03.031

Muijlwijk, K., Hinderink, E. B. A., Ershov, D., Berton-Carabin, C. C., & Schroën, K. (2016). Interfacial tension measured at high expansion rates and within milliseconds using microfluidics. *Journal of Colloid and Interface Science*, *470*. https://doi.org/10.1016/j.jcis.2016.02.041

Muijlwijk, K., Huang, W., Vuist, J.-E., Berton-Carabin, C. C., & Schroën, K. (2016). Convective mass transport dominates surfactant adsorption in a microfluidic Y-junction. *Soft Matter*, *12*(44), 9025–9029. https://doi.org/10.1039/c6sm01677d

Mulvihill, D. M., & Murphy, P. C. (1991). Surface active and emulsifying properties of caseins/caseinates as influenced by state of aggregation. *International Dairy Journal*, *1*(1), 13–37. https://doi.org/10.1016/0958-6946(91)90025-4

Murray, B. S. (2011). Rheological properties of protein films. *Current Opinion in Colloid & Interface Science*, *16*(1), 27–35. https://doi.org/10.1016/j.cocis.2010.06.005

Murray, B. S. (2019). Pickering emulsions for food and drinks. *Current Opinion in Food Science*, *27*, 57–63. https://doi.org/10.1016/j.cofs.2019.05.004

Murray, B. S., & Nelson, P. V. (1996). A Novel Langmuir Trough for Equilibrium and Dynamic Measurements on Air−Water and Oil−Water Monolayers. *Langmuir*, *12*(25), 5973–5976. https://doi.org/10.1021/la960748o

Murray, B. S., Ventura, A., & Lallemant, C. (1998). Dilatational rheology of protein-non-ionic surfactant films at air-water and oil-water interfaces. *Colloids and Surfaces A:*

Physicochemical and Engineering Aspects, *143*(2–3), 211–219. https://doi.org/10.1016/S0927-7757(98)00256-8

Nagarkar, S. P., & Velankar, S. S. (2012). Morphology and rheology of ternary fluid-fluid-solid systems. *Soft Matter*, *8*(32), 8464–8477. https://doi.org/10.1039/c2sm25758k

Ntone, E., Bitter, J. H., & Nikiforidis, C. V. (2020). Not sequentially but simultaneously: Facile extraction of proteins and oleosomes from oilseeds. *Food Hydrocolloids*, *102*, 105598. https://doi.org/10.1016/j.foodhyd.2019.105598

Oreskes, I., & Mandel, D. (1979). Spectrophotometric assay with turbidity correction of sized immunoglobulin G aggregates. *Analytical Biochemistry*, *99*(2), 346–351. https://doi.org/10.1016/S0003-2697(79)80018-4

Pajot, P. (1976). Fluorescence of Proteins in 6-M Guanidine Hydrochloride. *European Journal of Biochemistry*, *269*, 263–269. https://doi.org/10.1111/j.1432-1033.1976.tb10228.x

Peng, W., Kong, X., Chen, Y., Zhang, C., Yang, Y., & Hua, Y. (2016). Effects of heat treatment on the emulsifying properties of pea proteins. *Food Hydrocolloids*, *52*, 301–310. https://doi.org/10.1016/j.foodhyd.2015.06.025

Pichot, R., Spyropoulos, F., & Norton, I. T. (2010). O/W emulsions stabilised by both low molecular weight surfactants and colloidal particles: The effect of surfactant type and concentration. *Journal of Colloid and Interface Science*, *352*(1), 128–135. https://doi.org/10.1016/j.jcis.2010.08.021

Pichot, R., Spyropoulos, F., & Norton, I. T. (2012). Competitive adsorption of surfactants and hydrophilic silica particles at the oil-water interface: Interfacial tension and contact angle studies. *Journal of Colloid and Interface Science*, *377*(1), 396–405. https://doi.org/10.1016/j.jcis.2012.01.065

Pipe, C. J., & McKinley, G. H. (2009). Microfluidic rheometry. *Mechanics Research Communications*, *36*(1), 110–120. https://doi.org/10.1016/j.mechrescom.2008.08.009

Prevc, T., Cigić, B., Vidrih, R., Poklar Ulrih, N., & Šegatin, N. (2013). Correlation of basic oil quality indices and electrical properties of model vegetable oil systems. *Journal of Agricultural and Food Chemistry*, *61*(47), 11355–11362. https://doi.org/10.1021/jf402943b

Priest, C., Reid, M. D., & Whitby, C. P. (2011). Formation and stability of nanoparticle-stabilised oil-in-water emulsions in a microfluidic chip. *Journal of Colloid and Interface Science*, *363*(1), 301–306. https://doi.org/10.1016/j.jcis.2011.07.060

Pugnaloni, L. A., Ettelaie, R., & Dickinson, E. (2003a). Do mixtures of proteins phase separate at interfaces? *Langmuir*, *19*(6), 1923–1926. https://doi.org/10.1021/la026874b

Pugnaloni, L. A., Ettelaie, R., & Dickinson, E. (2003b). Growth and aggregation of surfactant islands during the displacement of an adsorbed protein monolayer: A Brownian dynamics simulation study. *Colloids and Surfaces B: Biointerfaces*, *31*(1–4), 149–157. https://doi.org/10.1016/S0927-7765(03)00134-6

Pugnaloni, L. A., Ettelaie, R., & Dickinson, E. (2005). Brownian dynamics simulation of adsorbed layers of interacting particles subjected to large extensional deformation. *Journal of Colloid and Interface Science*, *287*(2), 401–414. https://doi.org/10.1016/j.jcis.2005.02.024

Puppo, M. C., Beaumal, V., Chapleau, N., Speroni, F., de Lamballerie, M., Añón, M. C., & Anton, M.

(2008). Physicochemical and rheological properties of soybean protein emulsions processed with a combined temperature/high-pressure treatment. *Food Hydrocolloids*, *22*(6), 1079–1089. https://doi.org/10.1016/j.foodhyd.2007.05.018

Qin, B. Y., Bewley, M. C., Creamer, L. K., Baker, H. M., Baker, E. N., & Jameson, G. B. (1998). Structural basis of the tanford transition of bovine β-lactoglobulin. *Biochemistry*, *37*(40), 14014–14023. https://doi.org/10.1021/bi981016t

Rampon, V., Brossard, C., Mouhous-Riou, N., Bousseau, B., Llamas, G., & Genot, C. (2004). The nature of the apolar phase influences the structure of the protein emulsifier in oil-in-water emulsions stabilized by bovine serum albumin. A front-surface fluorescence study. *Advances in Colloid and Interface Science*, *108–109*, 87–94. https://doi.org/10.1016/j.cis.2003.10.004

Rampon, V., Genot, C., Riaublanc, A., Anton, M., Axelos, M. A. V., & McClements, D. J. (2003). Front-face fluorescence spectroscopy study of globular proteins in emulsions: Displacement of BSA by a nonionic surfactant. *Journal of Agricultural and Food Chemistry*, *51*(9), 2482–2489. https://doi.org/10.1021/jf026168g

Rampon, V., Lethuaut, L., Mouhous-Riou, N., & Genot, C. (2001). Interface characterization and aging of bovine serum albumin stabilized oil-in-water emulsions as revealed by front-surface fluorescence. *Journal of Agricultural and Food Chemistry*, *49*(8), 4046–4051. https://doi.org/10.1021/jf001170y

Rampon, V., Riaublanc, A., Anton, M., Genot, C., & McClements, D. J. (2003). *Evidence that Homogenization of BSA-Stabilized Hexadecane-in-Water Emulsions Induces Structure Modification of the Nonadsorbed Protein*. 5900–5905. https://doi.org/10.1021/jf0342526

Rao, C. S., & Damodaran, S. (2000). Is surface pressure a measure of interfacial water activity? Evidence from protein adsorption behavior at interfaces. *Langmuir*, *16*(24), 9468–9477. https://doi.org/10.1021/la0007168

Rawel, H. M., Czajka, D., Rohn, S., & Kroll, J. (2002). Interactions of different phenolic acids and flavonoids with soy proteins. *International Journal of Biological Macromolecules*, *30*(3–4), 137–150. https://doi.org/10.1016/S0141-8130(02)00016-8

Razumovsky, L., & Damodaran, S. (2001). Incompatibility of mixing of proteins in adsorbed binary protein films at the air-water interface. *Journal of Agricultural and Food Chemistry*, *49*(6), 3080–3086. https://doi.org/10.1021/jf001112c

Robson, E. W., & Dalgleish, D. G. (1987). Interfacial Composition of Sodium Caseinate Emulsions. *Journal of Food Science*, *52*(6), 1694–1698. https://doi.org/10.1111/j.1365-2621.1987.tb05908.x

Roy, F., Boye, J. I., & Simpson, B. K. (2010). Bioactive proteins and peptides in pulse crops: Pea, chickpea and lentil. *Food Research International*, *43*(2), 432–442. https://doi.org/10.1016/j.foodres.2009.09.002

Rühs, P. A., Affolter, C., Windhab, E. J., & Fischer, P. (2013). Shear and dilatational linear and nonlinear subphase controlled interfacial rheology of β-lactoglobulin fibrils and their derivatives. *Journal of Rheology*, *57*(3), 1003–1022. https://doi.org/10.1122/1.4802051

Ruíz-Henestrosa, V. P., Sánchez, C. C., Escobar, M. del M. Y., Jiménez, J. J. P., Rodríguez, F. M., & Patino, J. M. R. (2007). Interfacial and foaming characteristics of soy globulins as a function of pH and ionic strength. *Colloids and Surfaces A: Physicochemical and Engineering Aspects*, *309*(1–3), 202–215. https://doi.org/10.1016/j.colsurfa.2007.01.030

Sagis, L. M. C. (2009). Dynamics of encapsulation and controlled release systems based on water-in-water emulsions: Liposomes and polymersomes. *Physica A: Statistical Mechanics and Its Applications*, *388*(13), 2579–2587. https://doi.org/10.1016/j.physa.2009.03.024

Sagis, L. M. C. (2011). Dynamic properties of interfaces in soft matter: Experiments and theory. *Reviews of Modern Physics*, *83*(4), 1367–1403. https://doi.org/10.1103/RevModPhys.83.1367

Sagis, L. M. C., & Fischer, P. (2014). Nonlinear rheology of complex fluid-fluid interfaces. *Current Opinion in Colloid and Interface Science*, *19*(6), 520–529. https://doi.org/10.1016/j.cocis.2014.09.003

Sagis, L. M. C., Liu, B., Li, Y., Essers, J., Yang, J., Moghimikheirabadi, A., Hinderink, E. B. A., Berton-Carabin, C. C., & Schroën, K. (2019). Dynamic heterogeneity in complex interfaces of soft interface-dominated materials. *Scientific Reports*, *9*(1), 2938. https://doi.org/10.1038/s41598-019-39761-7

Sagis, L. M. C., & Scholten, E. (2014). Complex interfaces in food: Structure and mechanical properties. *Trends in Food Science and Technology*, *37*(1), 59–71. https://doi.org/10.1016/j.tifs.2014.02.009

Sakuno, M. M., Matsumoto, S., Kawai, S., & Taihei, K. (2008). *Adsorption and Structural Change of -Lactoglobulin at the Diacylglycerol - Water Interface*. *11*, 11483–11488. https://doi.org/10.1021/la8018277

Santiago, L. G., Maldonado-Valderrama, J., Martín-Molina, A., Haro-Pérez, C., García-Martínez, J., Martín-Rodríguez, A., Cabrerizo-Vílchez, M. A., & Gálvez-Ruiz, M. J. (2008). Adsorption of soy protein isolate at air-water and oil-water interfaces. *Colloids and Surfaces A: Physicochemical and Engineering Aspects*, *323*(1–3), 155–162. https://doi.org/10.1016/j.colsurfa.2007.11.001

Sarkar, A., & Dickinson, E. (2020). Sustainable food-grade Pickering emulsions stabilized by plant-based particles. *Current Opinion in Colloid and Interface Science*, *49*, 69–81. https://doi.org/10.1016/j.cocis.2020.04.004

Scheuble, N., Iles, A., Wootton, R. C. R., Windhab, E. J., Fischer, P., & Elvira, K. S. (2017). Microfluidic Technique for the Simultaneous Quantification of Emulsion Instabilities and Lipid Digestion Kinetics. *Analytical Chemistry*, *89*(17), 9116–9123. https://doi.org/10.1021/acs.analchem.7b01853

Schröder, A., Berton-Carabin, C. C., Venema, P., & Cornacchia, L. (2017). Interfacial properties of whey protein and whey protein hydrolysates and their influence on O/W emulsion stability. *Food Hydrocolloids*, *73*, 129–140. https://doi.org/10.1016/j.foodhyd.2017.06.001

Schröder, A., Sprakel, J., Schroën, K., & Berton-Carabin, C. C. (2017). Tailored Microstructure of Colloidal Lipid Particles for Pickering Emulsions with Tunable Properties. *Soft Matter*, 3190–3198. https://doi.org/10.1039/C6SM02432G

Schröder, A., Sprakel, J., Schroën, K., Spaen, J. N., & Berton-Carabin, C. C. (2018). Coalescence stability of Pickering emulsions produced with lipid particles: A microfluidic study. *Journal of Food Engineering*, *234*, 63–72. https://doi.org/10.1016/j.jfoodeng.2018.04.007

Schroën, K., Bliznyuk, O., Muijlwijk, K., Sahin, S., & Berton-Carabin, C. C. (2015). Microfluidic emulsification devices: From micrometer insights to large-scale food emulsion production. *Current Opinion in Food Science*, *3*, 33–40. https://doi.org/10.1016/j.cofs.2014.11.009

Schroën, K., de Ruiter, J., & Berton-Carabin, C. (2020). The importance of interfacial tension in emulsification : Linking scaling relations used in large scale preparation with microfluidic measurement methods. *Chemical Engineering*, *4*(63), 1–38.

Sengupta, T., & Damodaran, S. (1998). Role of dispersion interactions in the adsorption of proteins at oil-water and air-water interfaces. *Langmuir*, *14*(22), 6457–6469. https://doi.org/10.1021/la980275g

Sengupta, T., & Damodaran, S. (2000). Incompatibility and Phase Separation in a Bovine Serum Albumin/beta-Casein/Water Ternary Film at the Air-Water Interface. *Journal of Colloid and Interface Science*, *229*(1), 21–28. https://doi.org/10.1006/jcis.2000.6992

Seta, L., Baldino, N., Gabriele, D., Lupi, F. R., & Cindio, B. de. (2014). Rheology and adsorption behaviour of β-casein and β-lactoglobulin mixed layers at the sunflower oil/water interface. *Colloids and Surfaces A: Physicochemical and Engineering Aspects*, *441*, 669–677. https://doi.org/10.1016/j.colsurfa.2013.10.041

Shao, Y., & Tang, C.-H. (2014). Characteristics and oxidative stability of soy protein-stabilized oil-in- water emulsions: Influence of ionic strength and heat pretreatment. *Food Hydrocolloids*, *37*, 149–158. https://doi.org/10.1016/j.foodhyd.2013.10.030

Smith, P. K., Krohn, R. I., Hermanson, G. T., Mallia, A. K., Gartner, F. H., Provenzano, M. D., Fujimoto, E. K., Goeke, N. M., Olson, B. J., & Klenk, D. C. (1985). Measurement of protein using bicinchoninic acid. *Analytical Biochemistry*, *150*(1), 76–85. https://doi.org/10.1016/0003-2697(85)90442-7

Spencer, D., & Boulter, D. (1984). The Physiological Role of Storage Proteins in Seeds. *Philosophical Transactions of the Royal Society of London. Series B, Biological Sciences*, *304*(1120), 275–285.

Sridharan, S., Meinders, M. B. J., Bitter, J. H., & Nikiforidis, C. V. (2020). Pea flour as stabilizer of oil-in-water emulsions: Protein purification unnecessary. *Food Hydrocolloids*, *101*, 105533. https://doi.org/10.1016/j.foodhyd.2019.105533

Stang, M., Karbstein, H., & Schubert, H. (1994). Adsorption kinetics of emulsifiers at oil—water interfaces and their effect on mechanical emulsification. *Chemical Engineering and Processing: Process Intensification*, *33*(5), 307–311. https://doi.org/10.1016/0255-2701(94)02000-0

Steegmans, M. L. J., Schroën, K., & Boom, R. M. (2009). Characterization of Emulsification at Flat Microchannel Y Junctions. *Langmuir*, *25*(6), 3396–3401. https://doi.org/10.1021/la8035852

Tamm, F., Herbst, S., Brodkorb, A., & Drusch, S. (2016). Functional properties of pea protein hydrolysates in emulsions and spray-dried microcapsules. *Food Hydrocolloids*, *58*, 204–214. https://doi.org/10.1016/j.foodhyd.2016.02.032

Tang, C.-H. (2017). Emulsifying properties of soy proteins: A critical review with emphasis on the role of conformational flexibility. *Critical Reviews in Food Science and Nutrition*, *57*(12), 2636–2679. https://doi.org/10.1080/10408398.2015.1067594

Taniguchi, M., Du, H., & Lindsey, J. S. (2018). PhotochemCAD 3: Diverse Modules for Photophysical Calculations with Multiple Spectral Databases. *Photochemistry and Photobiology*, *94*(2), 277–289. https://doi.org/10.1111/php.12862

Taniguchi, M., & Lindsey, J. S. (2018). Database of Absorption and Fluorescence Spectra of >300

Common Compounds for use in PhotochemCAD. *Photochemistry and Photobiology*, *94*(2), 290–327. https://doi.org/10.1111/php.12860

Tcholakova, S., Denkov, N. D., & Lips, A. (2008). Comparison of solid particles, globular proteins and surfactants as emulsifiers. In *Physical Chemistry Chemical Physics* (Vol. 10, Issue 12, pp. 1608–1627). The Royal Society of Chemistry. https://doi.org/10.1039/b715933c

Tcholakova, S., Denkov, N. D., Sidzhakova, D., Ivanov, I. B., & Campbell, B. (2003). Interrelation between drop size and protein adsorption at various emulsification conditions. *Langmuir*, *19*(14), 5640–5649. https://doi.org/10.1021/la034411f

Timgren, A., Rayner, M., Dejmek, P., & Marku, D. (2013). *Emulsion stabilizing capacity of intact starch granules modified by heat treatment or octenyl succinic anhydride*. https://doi.org/10.1002/fsn3.17

Trégouët, C., Salez, T., Monteux, C., & Reyssat, M. (2019). Microfluidic probing of the complex interfacial rheology of multilayer capsules. *Soft Matter*, 1–10. https://doi.org/10.1039/c8sm02507j

Uhrínová, S., Smith, M. H., Jameson, G. B., Uhrín, D., Sawyer, L., & Barlow, P. N. (2000). Structural changes accompanying pH-induced dissociation of the β- lactoglobulin dimer. *Biochemistry*, *39*(13), 3565–3574. https://doi.org/10.1021/bi992629o

Utrera, M., & Estévez, M. (2012). Analysis of tryptophan oxidation by fluorescence spectroscopy: Effect of metal-catalyzed oxidation and selected phenolic compounds. *Food Chemistry*, *135*(1), 88–93. https://doi.org/10.1016/j.foodchem.2012.04.101

Van Aken, G. A., & Zoet, F. D. (2000). Coalescence in highly concentrated coarse emulsions. *Langmuir*, *16*(18), 7131–7138. https://doi.org/10.1021/la0000419

van der Goot, A. J., Pelgrom, P. J. M., Berghout, J. A. M., Geerts, M. E. J., Jankowiak, L., Hardt, N. A., Keijer, J., Schutyser, M. A. I., Nikiforidis, C. V., & Boom, R. M. (2016). Concepts for further sustainable production of foods. *Journal of Food Engineering*, *168*, 42–51. https://doi.org/10.1016/j.jfoodeng.2015.07.010

van Kempen, S. E. H. J., Schols, H. A., van der Linden, E., & Sagis, L. (2013). Non-linear surface dilatational rheology as a tool for understanding microstructures of air/water interfaces stabilized by oligofructose fatty acid esters. *Soft Matter*, *9*(40), 9579. https://doi.org/10.1039/c3sm51770e

Vashisth, C., Whitby, C. P., Fornasiero, D., & Ralston, J. (2010). Journal of Colloid and Interface Science Interfacial displacement of nanoparticles by surfactant molecules in emulsions. *Journal of Colloid And Interface Science*, *349*(2), 537–543. https://doi.org/10.1016/j.jcis.2010.05.089

Velev, O. D., Nikolov, a. D., Denkov, N. D., Doxastakis, G., Kiosseoglu, V., & Stalidis, G. (1993). Investigation of the mechanisms of stabilization of food emulsions by vegetable proteins. *Food Hydrocolloids*, *7*(1), 55–71. https://doi.org/10.1016/S0268-005X(09)80024-6

Verwey, E. J., & Overbeek, J. T. (1955). Theory of the stability of lyophylic colloids. *Journal of Colloid Science*, *10*(2), 224–225.

Vioque, J., Sánchez-Vioque, R., Clemente, A., Pedroche, J., & Millán, F. (2000). Partially hydrolyzed rapeseed protein isolates with improved functional properties. *JAOCS, Journal of the American Oil Chemists' Society*, *77*(4), 447–450. https://doi.org/10.1007/s11746-000-0072-y

Vivian, J. T., & Callis, P. R. (2001). Mechanisms of tryptophan fluorescence shifts in proteins. *Biophysical Journal*, *80*(5), 2093–2109. https://doi.org/10.1016/S0006-3495(01)76183-8

Wagner, J. R., & Guéguen, J. (1999). Surface functional properties of native, acid-treated, and reduced soy glycinin. 2. Emulsifying properties. *Journal of Agricultural and Food Chemistry*, *47*(6), 2181–2187. https://doi.org/10.1021/jf9809784

Wagner, J. R., Sorgentini, D. A., & Anon, M. C. (2000). Relation between solubility and surface hydrophobicity as an indicator of modifications during preparation processes of commercial and laboratory-prepared soy protein isolates. *Journal of Agricultural and Food Chemistry*, *48*(8), 3159–3165. https://doi.org/10.1021/jf990823b

Walstra, P. (2003). *Physical Chemistry of Foods* (I. Marcel Dekker (ed.)). CRC Press.

Walstra, P., & de Roos, A. L. (1993). Proteins at Air-Water and Oil-Water Interfaces -- Static and Dynamic Aspects. *Food. Rev. Int.*, *9*(4), 503–525. https://doi.org/10.1080/87559129309540976

Wang, K., Lu, Y. C., Xu, J., & Luo, G. S. (2009). Determination of dynamic interfacial tension and its effect on droplet formation in the T-shaped microdispersion process. *Langmuir*, *25*(4), 2153–2158. https://doi.org/10.1021/la803049s

Wiacek, A. E., & Chibowski, E. (2002). Zeta potential and droplet size of n-tetradecane/ethanol (protein) emulsions. *Colloids and Surfaces B: Biointerfaces*, *25*(1), 55–67. https://doi.org/10.1016/S0927-7765(01)00304-6

Wierenga, P. A., Meinders, M. B. J., Egmond, M. R., Voragen, F. A. G. J., & De Jongh, H. H. J. (2003). Protein Exposed Hydrophobicity Reduces the Kinetic Barrier for Adsorption of Ovalbumin to the Air-Water Interface. *Langmuir*, *19*(21), 8964–8970. https://doi.org/10.1021/la034868p

Wijmans, C. M., & Dickinson, E. (1999a). Brownian dynamics simulation of a bonded network of reversibly adsorbed particles: Towards a model of protein adsorbed layers. *Physical Chemistry Chemical Physics*, *1*(9), 2141–2147. https://doi.org/10.1039/a808990f

Wijmans, C. M., & Dickinson, E. (1999b). Brownian dynamics simulation of the displacement of a protein monolayer by competitive adsorption. *Langmuir*, *15*(24), 8344–8348. https://doi.org/10.1021/la990812c

Wilde, P. J. (2000). Interfaces: Their role in foam and emulsion behaviour. *Current Opinion in Colloid and Interface Science*, *5*(3–4), 176–181. https://doi.org/10.1016/S1359-0294(00)00056-X

Wilde, P. J., Mackie, A., Husband, F., Gunning, P., & Morris, V. (2004). Proteins and emulsifiers at liquid interfaces. *Advances in Colloid and Interface Science*, *108–109*, 63–71. https://doi.org/10.1016/j.cis.2003.10.011

Williams, A., Janssen, J., & Prins, A. (1997). Behaviour of droplets in simple shear flow in the presence of a protein emulsifier. *Colloids and Surfaces*, *125*, 95–107.

Williams, A., & Prins, A. (1996). Comparison of the dilational behaviour of adsorbed milk proteins in the air-water and oil-water interfaces. *Colloids and Surfaces A: Physicochemical and Engineering Aspects*, *114*(1), 267–275. https://doi.org/10.1016/0927-7757(96)03534-0

Wouters, A. G. B., Rombouts, I., Fierens, E., Brijs, K., & Delcour, J. A. (2016). Relevance of the Functional Properties of Enzymatic Plant Protein Hydrolysates in Food Systems.

Comprehensive Reviews in Food Science and Food Safety, *15*(4), 786–800. https://doi.org/10.1111/1541-4337.12209

Wüstneck, R., Moser, B., & Muschiolik, G. (1999). Interfacial dilational behaviour of adsorbed β-lactoglobulin layers at the different fluid interfaces. *Colloids and Surfaces B: Biointerfaces*, *15*(3–4), 263–273. https://doi.org/10.1016/S0927-7765(99)00093-4

Xiang, B. Y., Ngadi, M. O., Ochoa-Martinez, L. A., & Simpson, M. V. (2011). Pulsed Electric Field-Induced Structural Modification of Whey Protein Isolate. *Food and Bioprocess Technology*, *4*(8), 1341–1348. https://doi.org/10.1007/s11947-009-0266-z

Xu, J., Dong, P. F., Zhao, H., Tostado, C. P., & Luo, G. S. (2012). The dynamic effects of surfactants on droplet formation in coaxial microfluidic devices. *Langmuir*, *28*(25), 9250–9258. https://doi.org/10.1021/la301363d

Xu, J., Mukherjee, D., & Chang, S. K. C. (2018). Physicochemical properties and storage stability of soybean protein nanoemulsions prepared by ultra-high pressure homogenization. *Food Chemistry*, *240*, 1005–1013. https://doi.org/10.1016/j.foodchem.2017.07.077

Yang, J., Faber, I., Berton-Carabin, C. C., Nikiforidis, C. V., van der Linden, E., & Sagis, L. M. C. (2021). Foams and air-water interfaces stabilised by mildly purified rapeseed proteins after defatting. *Food Hydrocolloids*, *112*, 106270. https://doi.org/10.1016/j.foodhyd.2020.106270

Yang, J., Liu, G., Zeng, H., & Chen, L. (2018). Effects of high pressure homogenization on faba bean protein aggregation in relation to solubility and interfacial properties. *Food Hydrocolloids*, *83*(May), 275–286. https://doi.org/10.1016/j.foodhyd.2018.05.020

Yang, J., Thielen, I., Berton-Carabin, C. C., van der Linden, E., & Sagis, L. M. C. (2020). Nonlinear interfacial rheology and atomic force microscopy of air-water interfaces stabilized by whey protein beads and their constituents. *Food Hydrocolloids*, *101*(May 2019), 105466. https://doi.org/10.1016/j.foodhyd.2019.105466

Ye, A. (2008). Interfacial composition and stability of emulsions made with mixtures of commercial sodium caseinate and whey protein concentrate. *Food Chemistry*, *110*(4), 946–952. https://doi.org/10.1016/j.foodchem.2008.02.091

Yerramilli, M., Longmore, N., & Ghosh, S. (2017). Improved stabilization of nanoemulsions by partial replacement of sodium caseinate with pea protein isolate. *Food Hydrocolloids*, *64*, 99–111. https://doi.org/10.1016/j.foodhyd.2016.10.027

Yuan, D. B., Hu, Y. Q., Zeng, T., Yin, S. W., Tang, C. H., & Yang, X. Q. (2017). Development of stable Pickering emulsions/oil powders and Pickering HIPEs stabilized by gliadin/chitosan complex particles. *Food and Function*, *8*(6), 2220–2230. https://doi.org/10.1039/c7fo00418d

Zhai, J., Hoffmann, S. V., Day, L., Lee, T., Augustin, M. A., Aguilar, M., & Wooster, T. J. (2012). *Conformational Changes of α -Lactalbumin Adsorbed at Oil − Water Interfaces: Interplay between Protein Structure and Emulsion Stability*. https://doi.org/10.1021/la203281c

Zhao, C. X., Rondeau, E., Cooper-White, J. J., & Middelberg, A. P. J. (2012). Microfluidic elucidation of the effects of interfacial rheology on droplet deformation. *Industrial and Engineering Chemistry Research*, *51*(4), 2021–2029. https://doi.org/10.1021/ie200631m

S

Summary & Samenvatting

Many food products contain oil-in-water (O/W) emulsions, i.e., droplets of oil in a water phase. Due to the thermodynamic incompatibility between the two liquids, the droplets need to be covered by emulsifiers to ensure physical stability. The most widely used food emulsifiers are dairy proteins which are present in e.g., beverages, infant formula or dressings. However, their production has a large impact on the environment, therefore, plant proteins are currently considered as promising alternatives. Yet, the full replacement of dairy proteins by plant proteins brings along a number of technological challenges (e.g., functionality, product taste, pre-treatments). It can therefore be advantageous to rather consider partial replacement, but the properties of dairy-plant protein blends with regard to food systems' stabilisation had been largely unexplored. In the present work, we aimed to achieve a rational compromise between technical functionality of such blends, and product quality. We investigated formation and stability of protein blend-stabilised emulsions and focussed on the relevant interfacial phenomena. To do so, we used a multi-scale approach based on characterisations at different length- and time scales.

In the first chapters (**Chapters 2-4**), we focussed on the long term interfacial phenomena when using protein blends to formulate emulsions. We assessed the related properties of blends of pea protein isolate (PPI) with either whey protein isolate (WPI) or with sodium caseinate (SC) in **Chapter 2**. We showed a synergistic behaviour in terms of physical stability of the emulsions, when the blends were used. The blend-stabilised emulsions had higher surface loads compared to the individual protein-stabilised emulsions, which showed that more proteins were needed to stabilise the interface. Furthermore, compositional rearrangements at the interface were observed over days. More specifically, after emulsion formation, whey proteins were able to partly displace pea proteins from the interface, which were themselves able to displace caseins. Such considerations are usually not considered in food emulsion formulation, even though they are very relevant, as the interfacial layer protects emulsions droplets against physical destabilisation.

As a next step, we studied the interfacial behaviour of the same proteins and their blends using model air-water and oil-water interfaces in **Chapter 3**. We showed that the rheological response of the blend-stabilised interfaces deviated from what could be expected from averaging those of the individual proteins. The layer's strength decreased when WPI was blended with PPI. SC formed the weakest interfacial layers, but blending it with PPI improved the mechanical strength of the layer at both the air-water and oil-water interface.

In general, higher elastic moduli and more rigid interfacial layers were formed at the air-water interface compared to the oil-water interface, except for pure PPI.

Even though the targeted applications of blends of proteins of different biological origins are still lacking, many traditional or emergent emulsion products contain mixtures of proteins (for example, caseins and whey proteins naturally co-exist in dairy products), resulting in complex, non-equilibrated interfacial structures (as discussed in **Chapter 2**). Therefore, in **Chapter 4**, we aimed to further evaluate and understand the interfacial rearrangements over time in plant-dairy protein blend-stabilised emulsions. We notably found that the whey proteins were able to displace pre-adsorbed pea proteins. Using model interfaces, we were able to determine that protein-protein interactions at the interface were the driving force for such a displacement, rather than a decrease in interfacial tension. These outcomes could be instrumental in defining new strategies for plant-animal protein "hybrid" products, but also for any protein blend-stabilised emulsion.

In **Chapters 5** and **6**, we focussed on the interfacial film formation at very short time scales (<1 s), which is relevant when considering the time scales involved in conventional emulsification processes. In **Chapter 5**, we used tailor-made microfluidic chips to probe the rheological properties of the interfacial films of freshly prepared droplets, and the stability of the droplets against coalescence under flow. We showed that these microfluidic tools are useful to assess the rheological properties of protein-stabilised droplet interfaces within 1 second after droplet formation. For instance, we determined that the PPI-stabilised interfaces had weaker in-plane interactions compared to WPI-stabilised ones, which resulted in less stable droplets. Although the blend-stabilised interfaces showed high connectivity between the adsorbed proteins, this could not prevent droplet coalescence probably due to structural heterogeneity of the droplet surface.

In **Chapter 6**, we proceeded with using PPI to stabilise emulsion droplets formed in a microfluidic device, and recorded coalescence stability after droplet formation for proteins exposed to metal-catalysed oxidation. Protein oxidation led to a strong loss in protein solubility, which damages the overall ingredient functionality. Yet, in the fraction that remained soluble, it led to the formation of low molecular weight fragments that were able to form more homogenous interfaces compared to the non-oxidised proteins (as confirmed by the Langmuir-Blodgett films), and increased coalescence stability. Interfacial films that were structurally more heterogeneous were therefore more prone to rupture, as was

hypothesised in **Chapter 5**. Furthermore, it became clear that the emulsifying properties of pea proteins are strongly dependent on their chemical status, and on the associated structural properties at the molecular and supramolecular levels.

In **Chapter 7**, we zoomed in further and used fluorescence spectroscopy to gain insight in the tertiary structure of the proteins in solution and at the interface during a secondment at INRAE (Nantes, France). It became evident that the 'soluble' fraction of the commercial pea proteins was present as 'soluble aggregates', which thus behave as small particles. This is probably a direct result of the harsh processing applied to obtain those ingredients. In contrast, the isolates purified in-house by a mild procedure contained proteins that were less aggregated, and able to rearrange at the oil-water interface.

Plant protein ingredients generally contain a substantial insoluble protein fraction, of which the properties necessarily differ from those of the soluble fraction (**Chapter 8**). We showed that when the full fraction was used to formulate emulsions, the soluble and insoluble parts competed for interfacial localisation, resulting in physically unstable emulsions. In contrast, when used solely, the insoluble fraction could physically stabilise the emulsions, and in case of a high internal phase emulsion, even led to around 10 times higher viscosity than their whey protein-based counterparts. These results confirm that the constituents of commercial pea protein isolates behave very differently, which should be used as a starting point for designing stable plant protein-based emulsion.

Finally, in **Chapter 9**, we extensively reviewed the established and developing methods to measure interfacial displacement, which, in our view, is paramount for the production of physically stable food emulsions. It is crucial to take this complex phenomenon into account when characterising the emulsifying and interfacial properties of protein blends, and also evaluate the various fractions, as done within this thesis for pea proteins. We expect that both soluble plant proteins and insoluble fractions can be used to stabilise food emulsions, albeit through different mechanisms: either via the classical mechanisms involving amphiphilic polymers, or via a Pickering stabilisation mechanism, respectively. To be able to probe protein functionality in conditions relevant to emulsion processing and subsequent storage, we recommend the development and use of tailor-made microfluidic tools to characterise in-depth the mechanical properties of interfacial films under flow over a broad range of time scales.

Veel levensmiddelen bestaan uit olie-in-water (O/W) emulsies, oftewel; oliedruppels in een waterfase. Vanwege de thermodynamische incompatibiliteit tussen de twee vloeistoffen, worden emulgatoren toegevoegd om de druppels te bedekken en fysieke stabiliteit te geven. De meest gebruikte emulgatoren in levensmiddelen zijn zuiveleiwitten, deze worden bijvoorbeeld gebruikt in dranken, babyvoeding en dressings. De productie van zuiveleiwitten heeft echter een grote impact op het milieu, daarom worden plantaardige eiwitten momenteel als veelbelovende alternatieven beschouwd. Toch brengt de volledige vervanging van zuiveleiwitten door plantaardige eiwitten een aantal technologische uitdagingen met zich mee (zoals ingrediënt functionaliteit en de productsmaak). Daarom kan het voordelig zijn om zuiveleiwitten *gedeeltelijk* te vervangen. In het huidige werk willen we een rationeel compromis bereiken tussen de technische functionaliteit van dergelijke eiwitmengsels en de productkwaliteit. Hoe zuivel- en planteneiwitmengsels emulsies stabiliseren is grotendeels onbekend. We onderzochten de productie en stabiliteit van emulsies die met eiwitmengsels zijn gestabiliseerd en hebben ons gericht op de relevante grensvlakverschijnselen. Hierbij hebben we gekozen om verschillende lengte- en tijdschalen die karakteristiek zijn voor het emulsievormingsproces in detail te bestuderen.

In de eerste hoofdstukken (**Hoofdstukken 2-4**) focussen we op verschijnselen die op langere termijn optreden in grensvlakken die bestaan uit eiwitmengsels. We hebben de fysische stabiliteit van emulsies gestabiliseerd met eiwitmengsels (erwten-eiwitisolaat (EEI) met wei-eiwitisolaat (WEI) of met natrium caseïnaat (Cas)) bestudeerd in Hoofdstuk 2. Het gebruik van eiwitmengsels leidde tot een synergetisch gedrag en hogere fysische stabiliteit van de emulsies. De eiwitmengsel-gestabiliseerde emulsies hadden een hogere oppervlaktebelading in vergelijking met de individuele eiwit-gestabiliseerde emulsies, wat aantoonde dat er meer eiwitten nodig waren om het grensvlak te stabiliseren. Bovendien werden over tijd veranderingen van de grensvlak compositie waargenomen. Om preciezer te zijn, de wei-eiwitten waren in staat om erwten-eiwitten gedeeltelijk van het grensvlak te verdringen na emulsievorming. De erwten-eiwitten konden de caseïne verdringen. Deze veranderingen worden vaak over het hoofd gezien in voedselemulsies, ondanks dat ze zeer relevant zijn omdat de grenslaag de emulsiedruppels beschermt tegen fysische destabilisatie.

Als een vervolgstap hebben we het grensvlakgedrag van dezelfde eiwitten en hun mengsels bestudeerd met behulp van model lucht-water en olie-water grensvlakken in **Hoofdstuk 3**. We toonden aan dat het reologische gedrag van de eiwitmengsel-gestabiliseerde

grensvlakken afweek van wat verwacht kon worden van de som van de individuele eiwitten. De sterkte van de laag nam af door het mengen van WEI met EEI. Cas vormde de zwakste grensvlaklagen, maar het mengen met EEI verbeterde de mechanische sterkte van de laag aan zowel het lucht-water- als het olie-water-grensvlak. Over het algemeen werden stijvere grensvlaklagen met een hogere elasticiteit gevormd bij het lucht-watergrensvlak in vergelijking met het olie-watergrensvlak, behalve voor erwten-eiwit.

Hoewel gerichte toepassingen van eiwitmengsels van verschillende biologische oorsprong nog steeds ontbreken, bevatten veel emulsieproducten mengsels van eiwitten (caseïne en wei-eiwitten komen bijvoorbeeld van nature samen voor in zuivelproducten), wat resulteert in complexe grensvlakstructuren die niet in evenwicht zijn (zoals besproken in hoofdstuk 2). Daarom hebben we in **Hoofdstuk 4** de grensvlakherschikkingen in emulsies gestabiliseerd met mengsels van plantaardige en zuiveleiwitten verder bestudeerd. We vonden dat de wei-eiwitten in staat waren om vooraf geadsorbeerde erwten-eiwitten te verdringen. Met behulp van modelgrensvlakken konden we vaststellen dat eiwit-eiwitinteracties aan het grensvlak de drijvende kracht waren voor een dergelijke verdringing, en niet een afname van de grensvlakspanning. Deze inzichten kunnen helpen bij het produceren van 'hybride' producten met plantaardige en dierlijke eiwitten, maar ook andere emulsies die door een eiwitmengsel gestabiliseerd worden.

In **Hoofdstuk 5 en 6** hebben we ons gericht op de filmvorming op het grensvlak op zeer korte tijdschalen (<1 seconde) die relevant zijn voor conventionele emulgeerprocessen. In Hoofdstuk 5 hebben we een nieuw microfluïdisch instrument gebruikt om de reologische eigenschappen van de grensvlaklaag van net gevormde druppels en de stabiliteit van de druppels tegen samenvoeging (i.e., coalescentie) onder stroming te onderzoeken. We hebben aangetoond dat deze microfluïdische instrumenten nuttig zijn om de reologische eigenschappen van eiwitgestabiliseerde druppelgrensvlakken binnen 1 seconde na druppelvorming te bestuderen. We hebben bijvoorbeeld vastgesteld dat de EEI-gestabiliseerde grensvlakken zwakkere laterale interacties hadden in vergelijking met WEI-gestabiliseerde grensvlakken, wat resulteerde in minder stabiele druppels. Hoewel de mengsel-gestabiliseerde grensvlakken een hoge connectiviteit tussen de geadsorbeerde eiwitten vertoonden, kon dit de coalescentie van druppels niet voorkomen, waarschijnlijk als gevolg van structurele heterogeniteit van het druppeloppervlak.

In **Hoofdstuk 6** hebben we ons gericht op het gebruik van EEI om emulsiedruppels gevormd in een microfluïdisch instrument te stabiliseren, en bestudeerden we de coalescentie-stabiliteit van druppels gevormd met eiwitten die waren blootgesteld aan door metaal gekatalyseerde oxidatie. Eiwitoxidatie leidde tot een sterk verlies in eiwitoplosbaarheid, wat de algehele functionaliteit van het ingrediënt aantastte. In de fractie die oplosbaar bleef, werden fragmenten met een laag molecuulgewicht gevormd die in staat waren om homogenere grensvlakken te vormen in vergelijking met de niet-geoxideerde eiwitten (bevestigd middels Langmuir-Blodgett-films), en verhoogden de coalescentie-stabiliteit. Grensvlakfilms die structureel heterogener waren, waren vatbaarder voor scheuren, en dus coalescentie, zoals werd verondersteld in Hoofdstuk 5. Bovendien werd het duidelijk dat de emulgerende eigenschappen van erwten-eiwitten sterk afhankelijk zijn van hun chemische staat, en van de bijbehorende structurele eigenschappen op supramoleculaire niveaus.

In **Hoofdstuk 7** hebben we verder ingezoomd en hebben we de tertiaire structuur van eiwitten in oplossing en aan het grensvlak bestudeerd met fluorescentiespectroscopie, tijdens een onderzoek bij INRAE (Nantes, Frankrijk). Het werd duidelijk dat de ‘oplosbare’ fractie van de commerciële erwteneiwitten aanwezig was als ‘oplosbare aggregaten’, die zich gedragen als kleine deeltjes. Dit is waarschijnlijk een direct gevolg van de zware behandeling die is toegepast in de industrie om die ingrediënten te verkrijgen. Daarentegen bevatten isolaten die in het lab werden gezuiverd middels een mildere procedure, eiwitten die minder geaggregeerd waren en in staat waren om te herschikken aan het olie-water-grensvlak.

Plantaardige eiwitisolaten bevatten over het algemeen een substantiële onoplosbare eiwitfractie, waarvan de eigenschappen inherent verschillen van die van de oplosbare fractie (**hoofdstuk 8**). We toonden aan dat wanneer de volledige fractie werd gebruikt om emulsies te formuleren, de oplosbare en onoplosbare delen concurreren om grensvlaklokalisatie, wat resulteerde in fysisch onstabiele emulsies. De onoplosbare fractie alleen daarentegen kon de emulsies fysisch stabiliseren, en in het geval van een emulsie met een hoge interne fase leidde dit tot een 10 keer hogere viscositeit dan in wei-eiwit gestabiliseerde emulsies. Deze resultaten bevestigen dat de bestanddelen van de commerciële erwten-eiwitisolaten zich heel anders gedragen. Dit gedrag moet als een uitgangspunt worden genomen voor het ontwerpen van stabiele emulsies die met plantaardig eiwit zijn gestabiliseerd.

Ten slotte hebben we in **Hoofdstuk 9** uitgebreid de klassieke en nieuwe methoden besproken om grensvlakverdringing te meten, wat naar onze mening van groot belang is voor de

productie van fysiek stabiele voedselemulsies. Het is cruciaal om rekening te houden met dit complexe fenomeen bij het karakteriseren van de emulgerende en grensvlakkenmerken van eiwitmengsels, en ook om de verschillende fracties te evalueren, zoals in dit proefschrift gedaan is voor erwteneiwitten. We verwachten dat zowel oplosbare planteneiwitten als onoplosbare fracties kunnen worden gebruikt om voedselemulsies te stabiliseren, zij het via verschillende klassieke mechanismen dus via amfifiele polymeren, of Pickering-stabilisatie. Om voor de emulsiefunctionaliteit te bepalen welke omstandigheden het beste gebruik kunnen worden voor emulsieproductie en daaropvolgende opslag, raden we de ontwikkeling en het gebruik van microfluïdische instrumenten aan. Deze kunnen worden gebruikt om de mechanische eigenschappen van grensvlakfilms onder stroming en over verschillende tijdschalen diepgaand te karakteriseren.

.

Appendices

Acknowledgments - Dankwoord

About the author

Publications

Overview of completed training activities

Acknowledgments

I feel very happy to write the acknowledgments of my PhD thesis. During the past four years I had the privilege to work with many amazing people.

To start with, I would like to express my gratitude to my supervisors: *Claire, Karin and Leonard* for their guidance through each stage of the process. *Claire*, you are very knowledgeable, have a great eye for detail and are very dedicated to your own, as well as mine, work. This, in combination with your endless positivity, humour, kindness and unconditional support made you the perfect supervisor. *Karin*, I am extremely grateful for all the talks we had; your door was always open, and we regularly had spontaneous chitchats and in-depth discussions in your office or the coffee corner. *Leonard*, it must have been hard to deal with three (very) talkative women at the same time. Luckily, you were always able to calm our discussions down and bring them back to the point. Your input was crucial for many interpretations and conclusions in my work, thank you.

Throughout my PhD period I received a great deal of support and assistance. *Jolet*, thank you for all the help with the microfluidic experiments and data analysis. *Maurice*, thank you for the technical support in the microfluidic lab and beyond. *Jos*, your practical insights often saved my experiments, many thanks. *Marjan and Ilona*, thank you for the administrative support, and especially for organising my immediate return from France just before the lockdowns started. Someone whose help cannot be overestimated; *Martin*, the administration was clearly not my forte, but you supported me (*and Floor*) whenever needed.

I had the privilege to perform part of my research at INRAE (Nantes, France) and work together with many researchers. *Alain*, thank you for welcoming me in your group, the scientific input and support for my project. *Bérènice*, you are great with R and I enjoyed our time at the computer a lot. Many thanks to *Adeline and Claude*, you are great researchers and I learned a lot from you about protein characterisation and spectroscopic techniques. My bonus PhD-colleagues; *Remy and Line*, it was nice having random chitchats during lunch or in the office. Lastly; *Claire, Steve, Louis and Anna*, 'merci' for the nice lunches and dinners at your home.

During the past 10 years, several people motivated me to develop my scientific career. *Marieke (Mevrouw Hogeboo*m), your chemistry lectures and our talks inspired me to choose a chemistry-related study. *Kelly*, you showed me that research is a lot of fun and *Igor and*

Shane, you learned me that I could be a researcher myself. I would not have been here without any of you, thank you!

I would like to acknowledge my colleagues and project partners from TiFN, our discussions were very inspiring and interesting to me. A special thanks to all involved PhD students; *1a, 1b, 2, 4 5a, 5b, 6* or in other words; *Eleni, Simha, Maud, Jack, Remco, Dana and Marius.* Let's keep saving the planet.

My talented MSc and BSc students; *Katharina, Regina, Mengqi, Stefan, Esther, Jaap, Niels, Phyline, Sandra and Ana,* thank you for your help to gather data and valuable insights needed for this thesis. I learned a lot from all of you.

I enjoyed my time at FPE very much! Many thanks to all PhD colleagues and friends for the relaxing coffee breaks, PhD-trip, borrels and other (sports) activities. It was great being part of the borrel committee; *Jan, Steven, Jan-Eise, Bijoy, Konstantina, Floor, Nynke* and the PhD-trip committee; *Zulhaj, Isabel, Floor, Maurice and Martin.* Even if the trip was cancelled last-minute, we still had fun preparing it. *Floor and Qinhui,* you were the best office-mates, we laughed, had chitchats and serious in depth discussions. *Sten, Katharina, Jilu and Anja,* thank you for sharing the emulsion love. I appreciate our joint time in the lab and the support we gave each other. Special thanks to my extra FPH colleagues; *Jack and Raisa*, I had so much fun with you during the past years, it was great having you around.

My acknowledgments would be incomplete without thanking all my friends and family. My dear friends, thank you for supporting me and distracting me from my project from time to time. Special thanks to *Linde* for the design of my thesis cover and *Camiel and Floor* for being my paranymphs. *Edith, Henk, Ko en Adri*, bedankt voor de ontspannen weekenden en heerlijke ontbijtjes in 'Zeeland'. *Pap en Mam*, bedankt voor jullie onvoorwaardelijke steun en vertrouwen in mij, door jullie kan ik alles aan. Al laatste; lieve *Jelle*, bedankt voor al je steun, liefde en gezelligheid, elke dag met jou is een groot feest.

About the author

Emma Hinderink was born on 11 March 1994 in Nijmegen, the Netherlands. She attended 'de Driemark' in Winterswijk, where she obtained her high school diploma in 2011.

In the same year, Emma started the study Food Technology at Wageningen University & Research. She conducted her BSc thesis in the Food Process Engineering group on *The dynamic interfacial tension of protein-stabilised emulsions*, and obtained her bachelor degree in 2014. Emma continued with the European Master in Food Studies, a master program of leading universities in four European countries. The first year she completed courses and studied at Wageningen University & Research, University College Cork (Ireland), AgroParisTech (France) and Lund University (Sweden). In the second year, she did a combined MSc thesis and internship project at Firmenich SA in Geneva (Switzerland). The project was entitled *Flavour release from chewing gum: Using an Artificial Mouth for quantitative prediction.*

Emma continued working as a PhD candidate at the Laboratory of Food Process Engineering group in close collaboration with the Laboratory of Physics and Physical Chemistry of Foods of Wageningen University & Research. She worked on the project *Food emulsions stabilised by blends of plant and dairy proteins.* The results of her PhD project are presented in this thesis. Emma will continue to work as post-doctoral researcher at the TU Delft (the Netherlands) on the project *Droplet microfluidics: Stability of emulsions in shear flows.*

Publications

This thesis

E.B.A. Hinderink, K. Münch, L. Sagis, K. Schroën, C.C. Berton-Carabin, Synergistic stabilisation of emulsions by blends of dairy and soluble pea proteins: Contribution of the interfacial composition, *Food Hydrocolloids*, 97, (2019). https://doi.org/10.1016/j.foodhyd.2019.105206.

E.B.A. Hinderink, W. Kaade, L. Sagis, K. Schroën, C.C. Berton-Carabin, Microfluidic investigation of the coalescence susceptibility of pea protein-stabilised emulsions: Effect of protein oxidation level, *Food Hydrocolloids*, 102, (2020). https://doi.org/10.1016/j.foodhyd.2019.105610.

E.B.A. Hinderink, L. Sagis, K. Schroën, C.C. Berton-Carabin, Behaviour of plant-dairy protein blends at air-water and oil-water interfaces, *Colloids Surfaces B Biointerfaces* 192, 111015 (2020). https://doi.org/10.1016/j.colsurfb.2020.111015.

E.B.A. Hinderink, L. Sagis, K. Schroën, C.C. Berton-Carabin, Sequential Adsorption and Interfacial Displacement in Emulsions Stabilised with Plant-Dairy Protein Blends. *Journal of Colloid and Interface Science*, 583, (2021**)**, 704–713. https://doi.org/10.1016/j.jcis.2020.09.066.

E.B.A. Hinderink[+], A. Schröder[+], L. Sagis, K. Schroën, C.C. Berton-Carabin, Stability of food emulsions prepared with pea protein fractions, *submitted.*

E.B.A. Hinderink, C.C Berton-Carabin, K. Schroën, A. Riaublanc, B. Houinsou-Houssou, A. Boire, C. Genot, Conformational changes of whey and pea proteins upon emulsification studied by front-surface fluorescence, *submitted*.

E.B.A. Hinderink, J. de Ruiter, J. de Leeuw, L. Sagis, K. Schroën, C.C. Berton-Carabin, Early film formation in emulsions stabilised by whey-pea protein blends: Insights from a microfluidic approach, *submitted.*

Other publications

L.M.C. Sagis, B. Liu, Y. Li, J. Essers, J. Yang, A. Moghimikheirabadi, **E. Hinderink**, C. Berton-Carabin, K. Schroën, Dynamic heterogeneity in complex interfaces of soft interface-dominated materials, *Scientific reports*, 9 (2019) 2938. https://doi.org/10.1038/s41598-019-39761-7.

E.B.A. Hinderink, S. Avison, R. Boom, I. Bodnár, Dynamic flavor release from chewing gum: Mechanisms of release, *Food Research International*, 116 (2019) 717–723. https://doi.org/10.1016/j.foodres.2018.09.002.

K. Muijlwijk, **E. Hinderink**, D. Ershov, C. Berton-Carabin, K. Schroën, Interfacial tension measured at high expansion rates and within milliseconds using microfluidics, *Journal of Colloid and Interface Science* 470 (2016). https://doi.org/10.1016/j.jcis.2016.02.041

Overview of completed training activities

Discipline specific activities

Courses

Masterclass “Dairy Protein Biochemistry” (VLAG, NL)	2018
Food proteins: functionality, modifications and analysis (VLAG, NL)	2018
Micro – nanofluidics (JM burgercentrum, NL)	2018
Han-Sur-Lesse physical chemical winterschool (WUR & TU delft, NL)	2019

Conferences

Microscale investigation of multiphase systems (FPE, NL)	2017
Food Colloids (Leeds University, UK)	2018
Edible Soft matter (Le Mans university, FR)	2019
International Symposium on Food Rheology and Structure (ETH-Zürich, CH)	2019
Plant-based & animal hybrid proteins: fake innovation or an ingenious idea for flexitarians? (IAR-Pôle, FR)	2020

Other

Visiting researcher (INRAE, FR)	2019-2020

General courses

VLAG PhD week (VLAG, NL)	2017
Competence Assesment (WGS, NL)	2017
Presenting with impact (In’to languages, NL)	2017
Teaching and supervising thesis students (ESD, NL)	2017
Scientific writing (WGS, NL)	2018
Carreer Orientation (WGS, NL)	2020

Other activities

Preparation of research proposal	2017
PhD study tour to Canada	2018
FPE weekly group meetings	2017-2021
TiFN retreat	2018-2019
TiFN biweekly team meetings	2017-2021

The studies presented in this thesis were performed within the framework of TiFN.

Cover design by Linde Elsinga

Printed by ProefschriftMaken || www.proefschriftmaken.nl